University of Nottingham
UK | CHINA | MALAYSIA

Novel micro/nano scale characterisation of interfaces in multi-material additive manufacturing (3D-printing)

Tien Thuy Quach

Thesis submitted to the University of Nottingham
for the degree of Doctor of Philosophy

November 2023

ABSTRACT

Additive manufacturing (AM) or 3D-printing has many applications in automotive, engineering, healthcare, aerospace, defence, and in the current work. Multi-material additive manufacturing is the combination of different materials within a print to enhance the performance of a component and/or final product. Although AM in its various forms allows for the use of a wide range of materials, not all of them are compatible with each other. This can be problematic when designing interfaces that need to connect or overlap parts in complex geometric products.

My PhD research **"Novel micro/nano scale characterisation of interfaces in multi-material additive manufacturing (3D printing)"** aims to understand, detect, and improve the interfaces and micro/nanostructures of AM printed from functional multi-materials. This will help to build and enhance reliable process workflows for next-generation additive manufacturing. To achieve this goal, different materials and methodologies were employed throughout. AM is a technology that enables multi-disciplinary applications, here I will focus on its use in the pharmaceutical and engineering fields.

Data collection and interpretation are explained and evaluated correspondingly to clarify the recent context of the data management and legislation transformation in terms of Point-of-Care (POC) manufacturing of medicines (Chapter 3). I then develop suitable techniques to verify the interfaces and micro/nano structures with case studies from analysing 3D-printed commercialised and lab-based electronics (Chapter 4). I continue examining the principal properties of new ink formulations to clarify the physiochemical compatibilities in AM (Chapter 5). I close by indicating key factors to effectively monitor the interfaces in multi-materials AM and specifying reliable processes for qualified co-printed products in pharmaceutical sector (Chapter 6).

In summary, findings from this study based on micro- and nanoscale characterisation of the interfaces of multi-materials show the potential of the UK and others to develop and trial novel medicines via POC manufacturing that can be safely regulated and monitored, particularly for additive manufacturing and lay the groundwork for optimal workflows for the analysis of interfaces in multi-material AM prints.

ACKNOWLEDGEMENTS

Since my BSc, I have devoted 12 years to learning and growing in pharmaceutical sciences. It includes both challenging and cheering time, so I am quite emotional writing these words, especially when the past few years are flooding my mind now. I just want to say it is my great pleasure to meet and work with diverse individuals and organisations that I admire not only for their lovely aptitudes but also for their great profession that can be spread out and make many positive changes. I would like to thank the following people who have lightened my life and helped me complete my PhD journey:

Firstly, I would like to express my great gratitude to my principal supervisor Professor Clive Roberts for all advice and support throughout my journey. I am deeply thankful to Clive for accepting me to do PhD research right after my MSc, for always assisting me to approach new opportunities of learning and development, and for always giving me the freedom to initiate and decide my PhD works as well as other collaborative projects. I also admire your leadership, management, and empathy in research, teaching, and all the commitments you have had. I often say/think that I wish I could be good enough, and that I could have made you proud of me more as your PhD student!

I would like to express my great thankfulness to my supervisor Professor Richard Hague for all the motivation and suggestions throughout my work. My sincere appreciation also goes to my supervisor, Dr. Gustavo Ferraz Trindade for all assistance and inspiration for my professional development bonding in and out of my PhD. I had invaluable discussions with Clive, Richard, and Gustavo, especially their trust and facilitation played an essential part in my contribution and achievement that I have had throughout my PhD journey. All I want to say is my willingness to nurture our mentorship for the rest of my life.

I would like to send special thanks to the professionals for training me on a variety of techniques: Nicola Weston (Ultramicrotome), Dr. Elisabeth Steer (SEM), Ms. Denise Mclean (TEM), Dr. Christopher Parmenter (FIB-SEM), Dr. Long Jiang (AFM), Dr. Thomas Booth (Profilometer), Christopher Strong (Droplet Shape Analysis), Joseph Lamb (OrbiSIMS), Fiqoh Eviana Putri and Dr. Yinfeng He (Inkjet 3D-printing). Many thanks for the insightful collaboration: Dr. Jisun Im for making the new gold inks; Nano Dimension Company for providing the DragonFly product; Dr. Ben Sheridan, and Emma Glass for supporting my research at the British Standard Institution; Dr. Geoffrey Rivers, Dr. Peng Zhao, and Dr. Feiran Wang for collaborating in my UNICAS project.

I am thankful for the Programme Grant “Enabling Next Generation Additive Manufacturing” (EP/P031684/1) for funding my PhD research; the School of Pharmacy (SoP), the Centre for Additive Manufacturing (CfAM), and the Nanoscale and Microscale Research Centre (nmRC) for offering me novel facilities and great workplaces. Many thanks to Nottingham academics and students for their great sharing, especially those at the Advanced Materials and Healthcare Division, B19 Group, and the Researcher Academy. Big thanks to all administration and technician staff for making paperwork and laboratory more accessible, especially for Rebecca, Maria, Gail, Esme, Amy at SoP; Mirela, Yuan, Harinee, Flavia, two Mark, Adam, Kerri at CfAM; Nathan at the Manufacturing Metrology; and other staff at the Analytical Services. My thankfulness is extended to my managers and fellows from my part-time job and volunteer. I couldn’t continue my passion for doing research, supporting the community, and motivating the young generation without all the great encouragement and facilitation!

An extraordinary thanks to the YES Girls who have stayed by my side in good and bad times: Krishna Patel, Shirin Fateh, Tejasvi Shivakumar. I am so lucky and thankful to have you in my life! Lots of thanks to Fiqoh Eviana Putri and Dr. Cordula Hege for understanding and cheering me! Many thanks to my flatmates, my Vietnamese friends Hương, Thảo, cLinh, cKim, and other friends across the world for their encouragement.

I really appreciate the trust and sacrifice from my mom and dad so I can become a better version of myself. Many thanks for always being there for me and with me! I am also grateful to those who have dedicatedly supported my parents and other members in Vietnam, especially during and after Covid-19. Words cannot express my gratitude for that extended family and the countless things I have learned from them. My thesis is in honour of my beloved people, particularly great grandma Lê Thị Nội, dear friend Nguyễn Thị Xuân Ngọc, and strong colleague Nguyễn Hữu Phước. You are always loved and forever in our hearts!

Once more time, I would like to express my sincere gratitude to my family members, my previous and current teachers-advisors, my work and study colleagues-friends, my old and new students-mentees, and all other facilitators for their amazing inputs to my life.

Finally, this great chapter of my life is closed now, and I am very excited to start the next one. I hope to update you with different wonderful things in the future.

Tien Thuy Quach (Quách Thủy Tiên)

--- Tâm bất biến giữa dòng đời vạn biến ---

ACHIEVEMENTS

A. PUBLICATION

Book chapter

● Quach, T. T., Sheridan, B., Glass, E. & Roberts, C. J. (2023). Effective transformations of sustainable pharmaceutical supply chains for point of care manufacture centred on consideration in the UK pharmaceutical sector, to appear in 3D Printing of Pharmaceuticals and Drug Delivery Devices, or the series of Advances in Pharmaceutical Technology eds. Sheng Qi, Dimitrios A. Lamprou & Dennis Douroumis, Wiley–Blackwell

Journal publication

● Quach, T. T., Trindade, G. F., He, Y., Zhao, P., Hague, R., & Roberts, C. J. Design of active workflow to investigate the interfaces of co-printed (bio)pharmaceutical products (in preparation).

● Quach, T. T., Trindade, G. F., Hague, R., & Roberts C. J. Development of practical guide to investigate the physiochemical compatibilities of new ink formulations in additive manufacturing (in preparation).

● Quach, T. T., Trindade, G. F., Hague, R., & Roberts C. J. Challenges and opportunities of sample preparation and examination of additively manufactured electronic products (in preparation).

● Im, J., Trindade, G. F., Quach, T. T., Sohaib, A., Wang, F., Austin, J., Turyanska, L., Roberts, C. J., Wildman, R., Hague, R., & Tuck, C. (2022). Functionalized Gold Nanoparticles with a Cohesion Enhancer for Robust Flexible Electrodes. ACS Applied Nano Materials, 5(5), 6708–6716. https://doi.org/10.1021/acsanm.2c00742

B. CONFERENCE PRESENTATIONS AND ABSTRACTS

Oral presentation

● UK Making Pharmaceuticals Conference 2023 (MP23), Coventry, the United Kingdom, 25-26.04.2023

Oral presentation: "Frameworks for enhanced analytics in the pharmaceutical industry in the United Kingdom"

Tien Thuy Quach[1,2], Ben Sheridan**, Emma Glass**, and Clive J Roberts[1]

● FORGE 2022 hosted by the Particle Characterisation Interest Group – Royal Society of Chemistry, Northern Ireland, the United Kingdom, 23-24.03.2022

Oral presentation: "Interface analysis of the new gold conductive ink formulation"

Tien Thuy Quach[1,2], Gustavo F. Trindade[2,3], Jisun Im[2], Richard JM Hague[2] and Clive J Roberts[1]

● European Advanced Materials Congress (EAMC 2021) (Stockholm, Sweden) **Onsite, Online & On-demand Hybrid Participation Setups*, 23-25.08.2021

Oral presentation: "Interface characterisation for the next generation of multi-materials additive manufacturing" – Best Oral Presentation Prize (25.08.2021)

Tien Thuy Quach[1,2], Gustavo F. Trindade[2,3], Richard JM Hague[2] and Clive J Roberts[1]

● 2021 Annual International Solid Freeform Fabrication Symposium (AISFFS), 02-04.08.2021. *Oral presentation: "Gold Conductive Ink Formulation with Enhanced Cohesion for Material Jetting"*

Jisun Im[2], Gustavo F. Trindade[2,3], Tien T. Quach[1,2], Ali Sohaib[2], Feiran Wang[2], Richard Hague[2] and Christopher Tuck[2]

Poster presentation

● The 52nd IUPAC General Assembly, 49th IUPAC World Chemistry Congress combined with the 11th edition of CHAINS, the largest chemistry congress from the Netherlands (20-25.08.2023) (IUPAC-CHAINS 2023) organized by the Royal Netherlands Chemical Society (KNCV) and the Dutch Research Council (NWO), Hague, Netherlands, 20-25.08.2023

Poster presentation: "Surface and interface study of 3D-printed biopharmaceutical products"

Tien Thuy Quach[1,2], Joseph Lamb[1], Gustavo F. Trindade[2,3], Yinfeng He[2], Peng Zhao[2], Richard Hague[2], Clive Roberts[4]

● EPSRC Next Generation of Additive Manufacturing – Annual meeting 2023 hosted by the Centre for Additive Manufacturing - University of Nottingham, the United Kingdom, 26.04.2023

Poster presentation: "Micro/nano scale characterisation of interfaces in next generation 3d-printed multi-functional multi-materials"

Tien Thuy Quach[1,2], Gustavo F. Trindade[2,3], Richard JM Hague[2] and Clive J Roberts[4]

● European Conference on Applications of Surface and Interface Analysis 2022 (ECASIA 22) with the theme “Surface Analyses for Advanced Manufacturing” hosted by the University of Limerick - Limerick, Ireland, 29.05-03.06.2022

Poster presentation 1: "Surface and interface study of the new gold conductive formulations in additive manufacturing"

Tien Thuy Quach[1,2], Gustavo F. Trindade[2,3], Jisun Im[2], Richard Hague[2], Clive J. Roberts[4]

● Connected Everything Annual Conference 2022 “Digital Manufacturing Research Collaboration and Innovation” hosted by the Connected Everything Network – Victoria Gallery & Museum, Liverpool, the United Kingdom, 18-19.05.2022

Poster presentation: "Enhanced data analytics for the pharmaceutical supply chain in the United Kingdom", https://doi.org/10.6084/m9.figshare.19802251.v1

Tien Thuy Quach[1,2], Ben Sheridan**, Emma Glass**, and Clive J Roberts[1]

● EPSRC Next Generation of Additive Manufacturing – Annual meeting 2022 hosted by the Centre for Additive Manufacturing - University of Nottingham, Nottingham, the United Kingdom, 28.04.2022

Poster presentation: "Micro/nano scale characterisation of interfaces in next generation multi-materials additive manufacturing (3D-printing)"

Tien Thuy Quach[1,2], Gustavo F. Trindade[2,3], Richard JM Hague[2] and Clive J Roberts[5]

● UK Surface Analysis Forum – Winter meeting 2022 hosted by the School of Physics - University of Bristol, Bristol, the United Kingdom, 13.04.2022

Poster presentation: "Developing the micro/nano scale characterisation of interfaces in multi-functional multi-materials additive manufacturing (3D-printing)"

Tien Thuy Quach[1,2], Gustavo F. Trindade[2,3], Laura Ruiz-Cantu[2,4], Richard JM Hague[2] and Clive J Roberts[5]

● Postgraduate Allied Health Research Conference (AHPGR) 2022 hosted by the University of Nottingham - Virtual session, the United Kingdom, 12-14.01.2022

Flash poster presentation: “Interface analysis of the new gold conductive ink formulation”

Tien Thuy Quach[1,2], Gustavo Trindade[2,3], Jisun Im[2], Richard JM Hague[2] and Clive J Roberts[1]

● Microscience Microscopy Congress (mmC) incorporating Electron Microscopy & Analysis Group (EMAG) 2021, 07.07.2021

Poster presentation: “Interface analysis for the next-generation of multi-materials additive manufacturing”

Tien Thuy Quach[1,2], Gustavo F. Trindade[2,3], Richard JM Hague[2] and Clive J Roberts[1]

- The FORGE: Characterization of Pharmaceutical Formulations, 25.03.2021:

Poster presentation: "Micro/nanoscale characterisation for the next-generation 3D-printed multi-materials"

– Best Interactive Researcher on 25.03.2021

Tien Thuy Quach[1,2], Gustavo F. Trindade[2,3], Jisun Im[2], Richard JM Hague[2] and Clive J Roberts[1]

- Formative Formulation 2 Conference, 12.03.2021

Poster presentation: "Micro/nanoscale analyses of the interfaces of the next-generation 3D-printed multi-materials"

Tien Thuy Quach[1,2], Gustavo F. Trindade[2,3], Richard JM Hague[2] and Clive J Roberts[1]

- Allied Health Professional Postgraduate Research Conference (AHPGR) 2021 hosted by the University of Nottingham - Virtual session, the United Kingdom, 13-15.01.2021

Flash poster presentation: "Developing micro/nanoscale analyses for the next-generation multi-functional 3D-printed products" – Best Flash Poster Prize on 15.01.2021

Tien Thuy Quach[1,2], Gustavo F. Trindade[2,3], Richard JM Hague[2] and Clive J Roberts[1]

- East Midlands Doctoral Network Postgraduate (EMDOC PGR) Research Conference 2020 with the theme "Sustainability", hosted by the University of Leicester and De Montford University - Virtual session, the United Kingdom, 9-10th September 2020

Poster presentation: "Designing and optimising micro/nanoscale characterisation methodologies for next-generation multi-functional 3D-printed products"

Tien Thuy Quach[1,2], Gustavo F. Trindade[2,3], Laura Ruiz-Cantu[2], Richard JM Hague[2] and Clive J Roberts[1]

C. OTHER

My contribution and accomplishment throughout my PhD journey can be summarised in the format of an academic CV in Appendix A1.

TABLE OF CONTENTS

LIST OF FIGURES

LIST OF TABLES

LIST OF ABBREVIATION

3D	Three Dimensional
ABS	Application-Based Software
Ace	Acetone
AC-TEM	Aberration Corrected Transmission Electron Microscopy
ADA Model	Advanced Drop Analysis Model
AE	Adverse Event
AEs	Auger Electrons
AFM	Atomic Force Microscopy
AGV	Automated Guided Vehicles
AI	Artificial Intelligence
AJP	Aerosol Jet Printing
AM	Additive Manufacturing
API for PMS	Application Programming Interface for Product Management Service
APIs	Active Pharmaceutical Ingredients
Ar	Argon
AR	Augmented Reality
ASTM	American Society for Testing and Materials
ATMPs	Advanced Therapy Medicinal Products
ATR	Attenuated Total Reflectance
AuNP	Gold NanoParticle
Au-TrisSH	New gold ink with cohesion enhancer* **trimethylolpropane tri(3-mercaptopropionate)*
BDA	Big Data Analytics
Bi	Bismuth
BJ	Binder Jetting
BSEs	Backscattered Electrons
CAD	Computer aided design
CAGR	Compound Annual Growth Rate
CAM	Contact Angle Measurement
CC	Cloud Computing
CCD	Charged-Couple Device
CMOS	Complementary Metal-Oxide Semiconductor
CNC	Computer Numerical Control
Cryo-SEM	Cryogenic Scanning Electron Microscopy
Cryo-TEM	Cryogenic Transmission Electron Microscopy
CSOM	Confocal Scanning Optical Microscopy
CTA	Clinical Trial Authorisation
Ctrl	Control sample
Ctrl-Au	Control gold ink *(without cohesion enhancer)*
TOM	Target Operating Model

DED	Directed Energy Deposition
DICM	Differential Interference Contrast Microscopy
DICOM	Digital Imaging and Communications in Medicine
DIW	Direct Ink Writing
DLP	Digital Light Processing
DMLS	Direct Metal Laser Sintering
DMP	Dimatix Materials Printer
DMPA	2,2-Dimethoxy-2-phenylacetophenone
DMSO	Dimethylsulfoxide
DMSO-d6	Deuterated Dimethylsulfoxide
DOD	Drop-On-Demand
DP	Depth profiling
DSA	Droplet Shape Analysis
eAFs	electronic Application Forms
EBM	Electron Beam Melting
EDS	Energy Dispersive Spectrometer
EDS-SEM	Energy Dispersion X-ray Spectroscopy - Scanning Electron Microscopy
EDS-TEM	Energy Dispersion X-ray Spectroscopy - Transmission Electron Microscopy
EDX	Energy Dispersive X-ray
EELS-TEM	Electron Energy Loss Spectroscopy - Scanning Transmission Electron Microscopy
EGDPEA	Ethylene glycol dicyclopentenyl ether acrylate
EMA	European Medicines Agency
EMP	Electron Microprobe
EMPA/ EPMA	Electron Microprobe Analysis/ Electron Probe Microanalysis
EPSRC	Engineering and Physical Sciences Research Council
Eq.	Equilibrium point
ESEM	Environmental Scanning Electron Microscopy
ET detector	Everhart–Thornley detector
ETEM	Environmental Transmission Electron Microscopy
EU	European Union
FBS	Functional Business System
FDA or US FDA	(United States) Food and Drug Administration
FDI	Direct Foreign Investment
FDM	Fused Deposition Modelling
FEG-SEM	Field Emission Gun - Scanning Electron Microscopy
FEG-TEM	Field Emission Gun - Transmission Electron Microscopy
FES	Field Emission Source
FFF	Fused Filament Fabrication
FHIR	Fast Healthcare Interoperability Resources
FIB-SEM	Focus Ion Beam - Scanning Electron Microscopy
FLM	Fused Layer Modelling

FM	Fluorescence Microscopy
FT-IR	Fourier Transform Infrared
GCIB	Gas Cluster Ion Beam
GCP	Good Clinical Practice
GDP	Good Distribution Practice
GIMP	GNU Image Manipulation Program
GIS	Gas Injection System
GLP	Good Laboratory Practice
GMP	Good Manufacturing Practice
GPs	Good Practices
GPvP	Good Pharmacovigilance Practice
GSDM	Ground State Depletion Microscopy
Hal	Halogen
He-cell mode	Helium-cell mode
HL7	Health Level Seven International
HME	Hot Melt Extrusion
HRTEM	High Resolution Transmission Electron Microscopy
ICCBBA	International Council for Commonality in Blood Banking Automation
ICH	International Council for Harmonization of Technical Requirements for Registration of Pharmaceuticals for Human Use
ICMRA	International Coalition of Medicines Regulatory Authorities
ICP-MS	Inductively Coupled Plasma Mass Spectroscopy
ICP-OES	Inductively Coupled Plasma Optical Emission Spectroscopy
IJP	Ink-Jet Printing
IMP	Investigational Medicinal Product
IoT	Internet of Things
IP	In-situ Photography
ISBT128	Global Information Standard for Medical Products of Human Origin
ISM	Image Scanning Microscopy
ISO	International Organization for Standardization
Iso	Isopropanol
ISO IDMP	ISO Identification of Medicinal Products
JSON	JavaScript Object Notation
LaB_6	Lanthanum hexaboride
LD	Laser deposition
LED	Light-Emitting Diodes
LENS	Laser Engineered NetShaping
LLEs	Low-Loss Electrons
LOINC	Logical Observation Identifiers Names and Codes
LOM	Laminated Object Manufacturing
LMIG	Liquid Metal Ion Gun
LPCVD	Low Pressure Chemical Vapor Deposition
MA	Microelemental Analysis

MA(A)	Marketing Authorisation (Application)
MAH	Marketing Authorisation Holder
MAM	Multi-material Additive Manufacturing
ME	Material Extrusion
MHRA	Medicines and Healthcare products Regulatory Agency
MJ	Material Jetting
MPID	Medicinal Product Identification
MRAs	Mutual Recognition Agreements
NA	Numerical Aperture
NHS	National Health Service
NMR	Nuclear Magnetic Resonance Spectroscopy
NSOM	Near-field Scanning Optical Microscopy
NUI model	Natural User Interface model
OECD	Organization for Economic Cooperation and Development
OM	Optical Microscopy
OMS	Organisation Management Service
orbiSIMS	A Time Of Flight - Secondary Ion Mass Spectrometer (ToF-SIMS) with hybrid OrbiTrap™ (hybrid SIMS)
OT-AuNPs	Octanelthiol-functionalised gold nanoparticles
PALM	Photoactivated Localization Microscopy
PBF	Powder Bed Fusion
PEN	Poly(Ethylene Naphthalate)
PEs	Primary Electrons
PFA	Perfluoroalkoxy
PhPID	Pharmaceutical Product Identification
PhSID	Substance Identifier
PLM	Polarized Light Microscopy
PMF system	Plasma Master File system
PMS	Product Management Service
POC	Point-Of-Care
POCT	Point-Of-Care Testing
ppm	Parts per million
PPR	Priority Research Programme
PSPD	Position-sensitive photodetector
PQS	Pharmacy Quality Scheme
PTFE	Polytetrafluoroethylene
PV	PharmacoVigilance
QP	Qualified Person
R&D	Research & Development
RESOLFT	REversible Saturable OpticaL Fluorescence Transitions
RFID	Radio-Frequency Identification
RiHN	Redistributed Manufacturing in Healthcare
RM	Rheology Measurement

RMS	Referentials Management Service
RT	Room Temperature
RTLS	Real-Time Location System
SEM	Scanning Electron Microscopy
SEs	Secondary Electrons
SI	Structural ink
SIM	Structured Illumination Microscopy
SL	Sheet Lamination
SLA	Stereolithography
SLS/SLM	Selective Laser Sintering/ Selective Laser Melting
SM	Stereo Microscopy
SMS	Substance Management Service
SNOMED	Systematized Nomenclature of Medicine
SPOR	Substance-Product-Orgnisation-Referentials
SROM	Super-Resolution Optical Microscopy
SSIM	Saturated Structured-Illumination Microscopy
STED(M)	Stimulated Emission Depletion Microscopy
STEM	Scanning Transmission Electron Microscopy
STL file	Standard Triangle Language file or Standard Tessellation Language file
STORM	Stochastic Optical Reconstruction Microscopy
SW	Silicon wafer
TCDMDA	Tricyclo decanedinmethanol diacrylate
TEM	Transmission Electron Microscopy
TIF or TIFF	Tagged Image Format or Tagged Image File Format
ToF-SIMS	Time Of Flight - Secondary Ion Mass Spectrometry
TrisSH	Trimethylolpropane tri(3-mercaptopropionate)
UC/UAM	Ultrasound Consolidation/ Ultrasound Additive Manufacturing
UV	Ultraviloet
VP	Vat Photopolymerization
VR	Virtual Reality
VRS	Verification Router Service
WDS	Wavelength-Dispersive Spectrometer
WHO	World Health Organisation
WI	Water-soluble ink
WS_2 nanotube	Tungsten disulfide nanotube
XEVPRM	eXtended EudraVigilance Product Report Message
XML	eXtensible Markup Language
ZrO_2	Zirconium dioxide

CHAPTER 1: INTRODUCTION

1.1. ADDITIVE MANUFACTURING

1.1.1. General principles

Additive Manufacturing (AM) or three-dimensional printing (3D-printing) is a computer-controlled technology used to produce solid objects, generally by laying down consecutive layers of material. Its advantages compared to traditional manufacturing include resource efficiency, production flexibility, shortened manufacturing times, and enhanced and potentially personalised product performance [1–3]. Overall, compositions for a 3D-printed multi-layered product aim to use the appropriate printing method or methods from the range available and select raw materials for potential property enhancements in industries such as automotive, electronics, pharmaceuticals, engineering, medical, aerospace, and defence (Figure 1.1) [4–6].

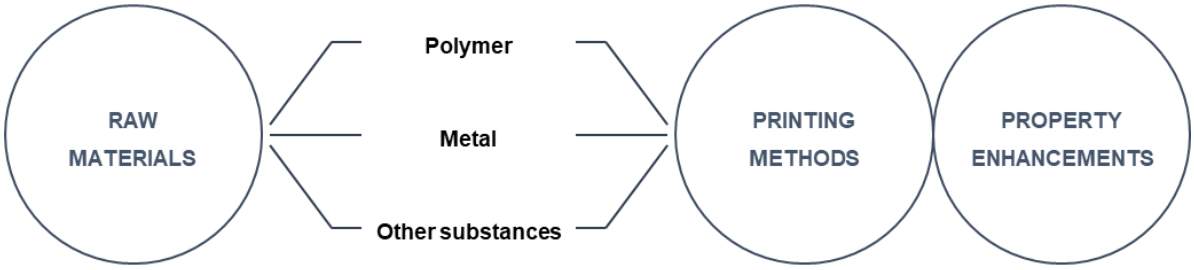

Figure 1.1. *Additive manufacturing with potential property enhancements*

1.1.2. Classification and features

In general, the standard production of a 3D-printed product follows a preliminary, main, and post stage process (Figure 1.2). Firstly, the preliminary stage includes the investigation of suitable materials, methods, and machines, based on fundamental knowledge and information from both research and industry. Secondly, the main stage includes five steps: 1) *Creating a 3D-model* of the targeted object by the computer-aided design (CAD) software or other engineering approaches, 2) *Converting the CAD file* to a standard additive manufacturing file format - usually a STL file (as "Standard Triangle Language" or "Standard Tessellation Language") which is then digitally assigned into multiple layers, 3) *Setting and checking the printing machine* (after inputting the STL file) for the most suitable

position and size to print object (along with the cost-saving and the residue reduction), 4) *Printing the targeted object* on the build platform, and 5) *Applying cooling and/or curing periods*. Finally, the post stage such as cleaning, polishing, painting, or finishing of the surface will be combined to improve the quality of the final product, which may require the use of other equipment [7–9].

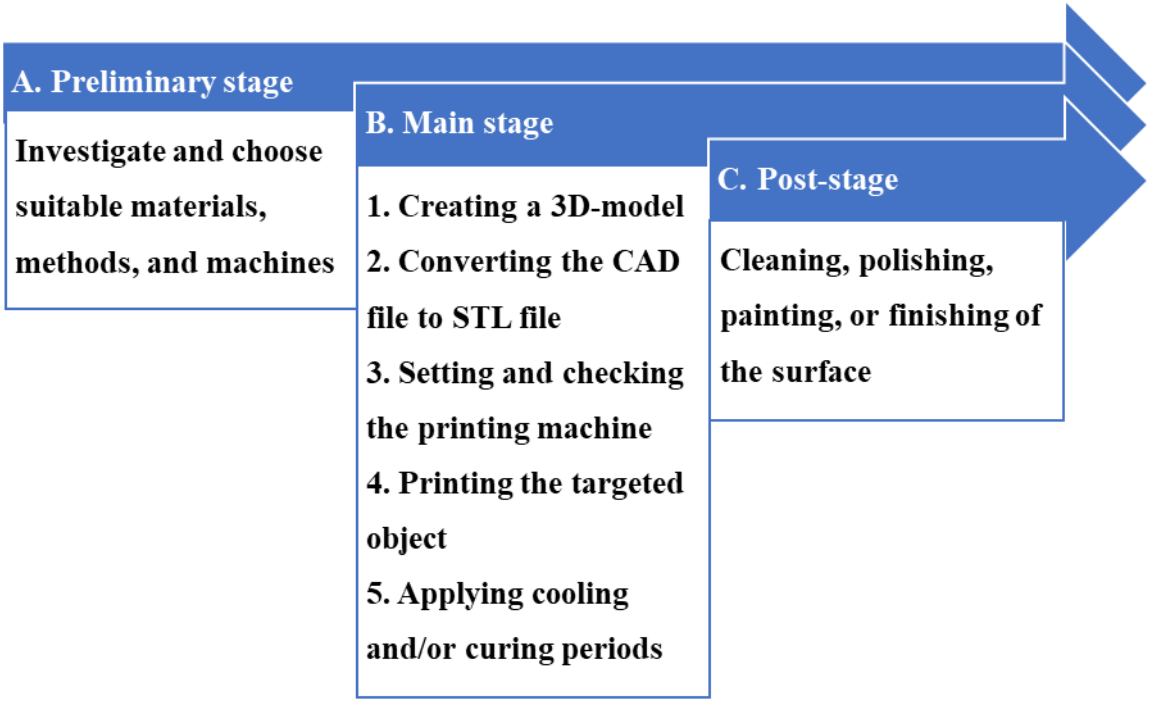

Figure 1.2. *Standard production of a 3D-printed product*

According to the International Organization for Standardization (ISO)/ American Society for Testing and Materials (ASTM), there are seven categories of additive manufacturing processes (Table 1.1) [7–9]:

1) binder jetting (BJ),
2) directed energy deposition (DED),
3) material extrusion (ME),
4) material jetting (MJ),
5) powder bed fusion (PBF),
6) sheet lamination (SL), and
7) vat photopolymerization (VP).

Table 1.1. Principle, technique, advantage, disadvantage, material, and manufacturer-country of seven ASTM categories (modified from [7–9])

ASTM category	Principle	Technique	Advantage	Disadvantage	Material	Manufacturer-country
Binder jetting (BJ)	Liquid binder/ jet printed onto thin layers of powder. The part is built up layer by layer by gluing the particles together	• 3D inkjet printing	• Free of support/substrate • Design freedom • Large build volume High print speed • Relatively low cost	• Fragile parts with limited mechanical properties • May require post processing	• Polymers • Ceramics • Composites • Metals • Hybrid	ExOne, USA PolyPico, Ireland
Directed energy deposition (DED)	Focused thermal energy melts materials *during* deposition	• Laser deposition (LD) • Laser Engineered NetShaping (LENS) • Electron beam • Plasma arc melting	• High degree control of grain structure • High quality parts • Excellent for repair applications	• Surface quality and speed requires a balance • Limited to metals/ metal based hybrids	• Metals • Hybrid	Optomec, USA InssTek, USA Sciaky, USA Irepa Laser, France Trumpf, Germany
Material extrusion (ME)	Material is selectively pushed out through a nozzle or orifice	• Fused Deposition Modelling (FDM)/Fused Filament Fabrication (FFF), Fused Layer Modelling (FLM)	• Widespread use • Inexpensive • Scalable • Can build fully functional parts	• Vertical anisotropy • Step-structured surface • Not amenable to fine details	• Polymers • Composites	Stratasys, USA
Material jetting (MJ)	Droplets of build materials	• Ink-jet Printing (IJP) • Direct Ink Writing (DIW)	• High accuracy of droplet deposition	• Support material is often required • Mainly	• Polymers • Ceramics • Composites	Stratasys, USA 3D Systems, USA PolyPico,

ASTM category	Principle	Technique	Advantage	Disadvantage	Material	Manufacturer -country
	are deposited		• Low waste • Multiple material parts • Multicolour	photopolymers and thermoset resins can be used	• Hybrid • Biologicals	Ireland 3Dinks, USA WASP, Italy
Powder bed fusion (PBF)	Thermal energy fuses a small region of the powder bed of the build material	• Electron beam melting (EBM) • Direct Metal Laser Sintering (DMLS) • Selective Laser Sintering/ Melting (SLS/SLM)	• Relatively inexpensive • Small footprint • Powder bed acts as an integrated support structure • Large range of material options	• Relatively slow • Lack of structural integrity • Size limitations • High power required • Finish depends on precursor powder size	• Metals • Ceramics • Polymers • Composites • Hybrid	ARCAM, Sweden; EOS, Germany; Concept Laser Cusing, Germany; MTT, Germany; Phoenix System Group, France; Renishaw, UK;Realizer, Germany; Matsuura, Japan, Voxeljet, 3Dsystems, USA
Sheet lamination (SL)	Sheets/foils of materials are bonded	• Laminated Object Manufacturing (LOM) • Ultrasound consolidation/ Ultrasound Additive Manufacturing (UC/UAM)	• High speed, • Low cost, • Ease of material handling	• Strength and integrity of parts depend on adhesive used • Finishes may require post processing • Limited material use	• Polymers • Metals • Ceramics • Hybrids	3D systems, USA MCor, Ireland
Vat photo-polymerization (VP)	Liquid polymer in a vat is light-cured	• Stereo Lithography (SLA) • Digital Light Processing (DLP)	• Large parts • Excellent accuracy • Excellent surface finish and details	• Limited to photopolymers only • Low shelf life, poor mechanical properties of	• Polymers • Ceramics	Lithoz, Austria 3D Ceram, France

ASTM category	Principle	Technique	Advantage	Disadvantage	Material	Manufacturer -country
				photopolymers • Expensive precursors/Slow build process		
Note: Materials are ranked in order of the most suitable and common use.						

1.2. MULTI-MATERIALS ADDITIVE MANUFACTURING

1.2.1. General principles

A variety of materials including polymers, metals, plastics, living cells and other substances in different forms (such as solids, liquids, or hydrogels) can be used separately or combined to formulate a 3D-printed product. Multi-material additive manufacturing (MAM) containing multiple materials with additional functionalities is a dominant trend for the next generation of 3D-printed systems [10,11]. MAM is not well established at present, in part due to challenges presented in the following sections. However, one of the greatest advantages of MAM is the flexible ability of controlling product properties such as stiffness, toughness, colour (changed on a voxel-by-voxel approach), or other properties when compared to conventional manufacturing in formulating the novel structures for many disciplines [12].

Shifting from single to multi materials can be achieved by two ways: 1) combining materials before or after the printing process (as a pre- or post-stage of manufacturing to help the rearrangement of separate counterparts), and 2) the material deposition [13–15]. In conventional manufacturing each part can be prepared separately and joined together (post-fabrication) to create multi-layered products in engineering sectors (Figure 1.3). This reveals the advantage of manufacturing multi materials such as reduced steps and time when the conventional manufacturing can complete in days to weeks (by a series of steps such as melt, cast, shape, finish, and join) and the additive manufacturing can complete in hours (by testing and joining the powder materials) [13]. Another approach to formulate multi materials is depositing the component gradient, for example, an AM functionally graded sample can be formed thanks to the gradient changes via varied densification of heterogeneous materials A and B at Figure 1.4 [14].

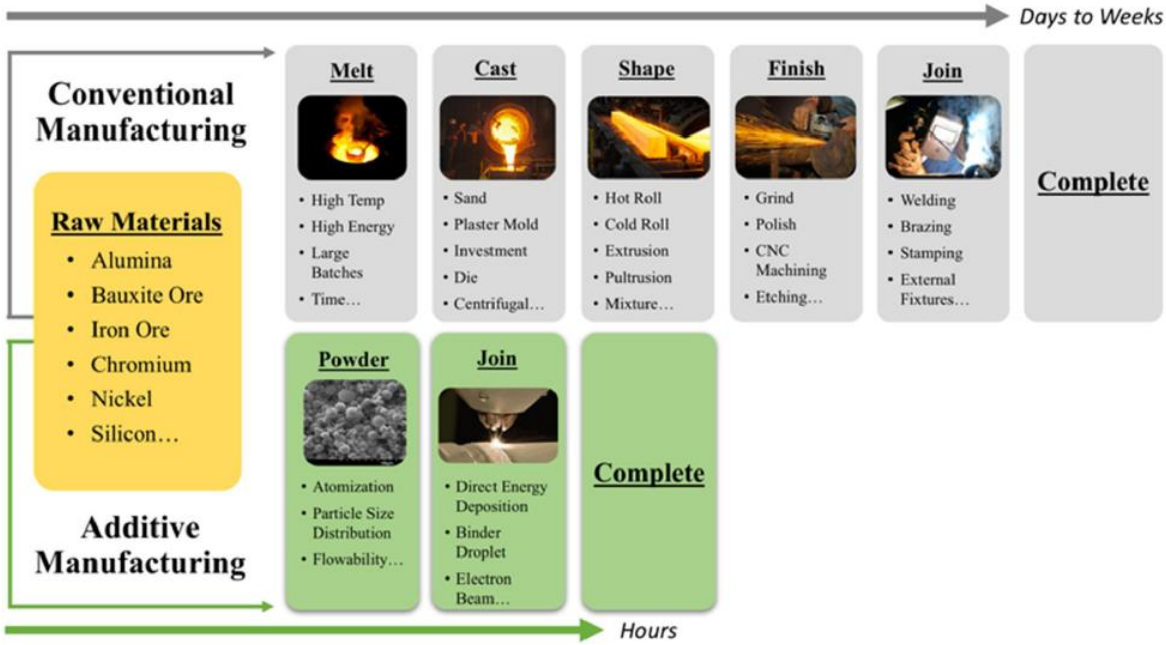

Figure 1.3. *Conventional manufacturing compared to additive manufacturing 1) conventional manufacturing can complete in days to weeks by a series of steps such as melt, cast, shape, finish, and join; and 2) additive manufacturing can complete in hours by lesser steps such as checking and joining the powders (modified from* [13]*)*

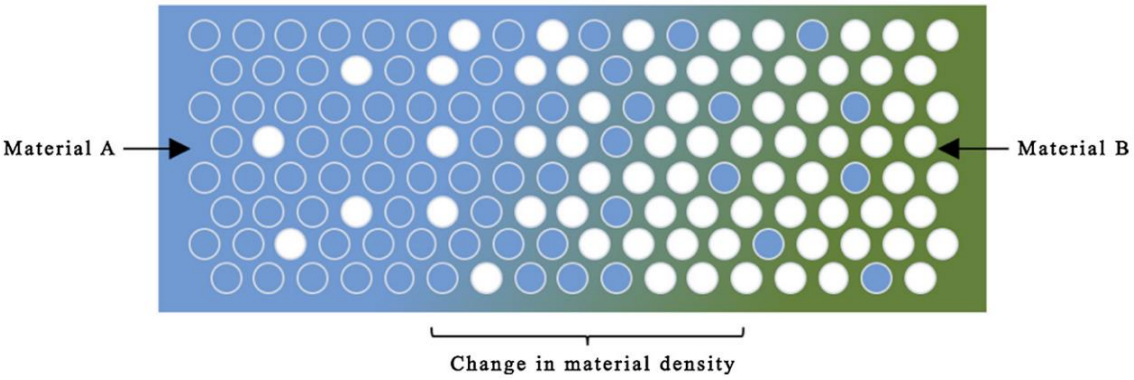

Figure 1.4. *The AM functionally graded materials can be formed by the gradient of varied densification for a heterogeneous composition (modified from* [14]*)*

1.2.2. Classification and features

Ranging from engineering to the medical sector, novel material synthesis and fabrication are essential to reduce the drawbacks of designing multi-materials in additive manufacturing so that the technology can spread (Figure 1.5) [16,17]. It is necessary to ensure the performance and reproducibility of the manufacturing for complete, reliable 3D-printed products. New

adaptable systems can be developed for novel materials with improved properties compared to conventional production methods in a single continuous manufacturing step [18,19]. Moreover, the specifically controlled 3D-printed multi-materials may require selective post-printing modification from the producers and the analysers to meet the requirements of the clients. To clarify the relationship among research endeavours and makers including designers, manufacturers, and end customers, it is necessary to consider four fundamental processes with key factors listed for each process (Figure 1.6): 1) Geometry design for AM; 2) Material design for AM; 3) Computational tools and interfaces development; and 4) Manufacturing tools and processes development [20].

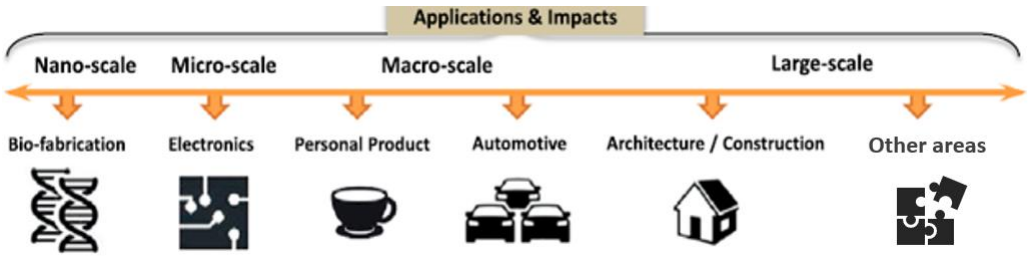

Figure 1.5. *Application and impacts of AM (modified from [16,1720])*

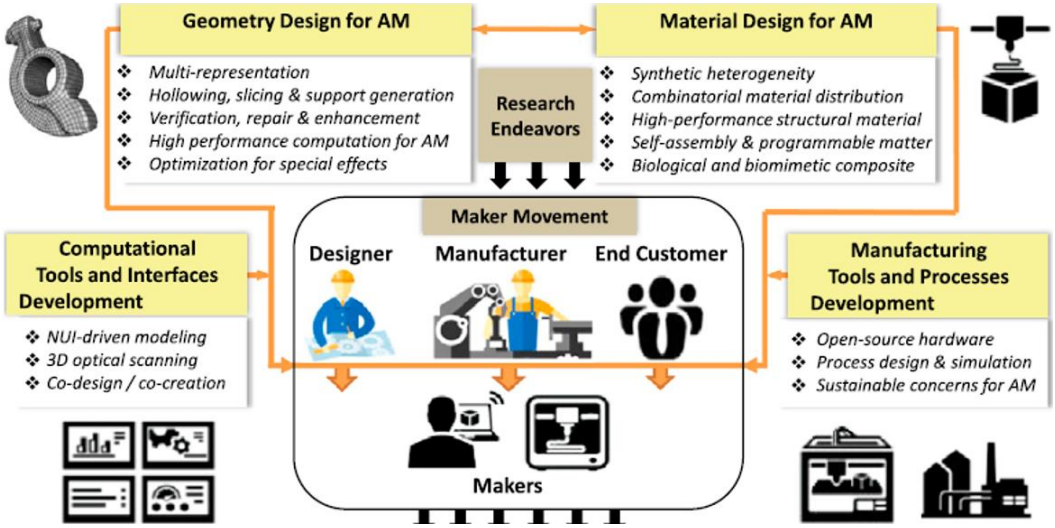

Figure 1.6. *A material-machine-process roadmap for AM and its maker movement reveals the relationship among research endeavours and makers including designers, manufacturers, and end customers). There are four primary processes with key points listed for each process: 1) Geometry design for AM; 2) Material design for AM; 3) Computational tools and interfaces development; and 4) Manufacturing tools and processes development (modified from [20])*

1.3. OPPORTUNITIES AND CHALLENGES OF INTERFACES IN MULTI-MATERIALS ADDITIVE MANUFACTURING

1.3.1. MAM applications in pharmacy/healthcare and engineering/electronic fields

There is recently a significant growth of applying 3D-printing with MAM in both pharmacy/healthcare and engineering/electronics due to several factors including: 1) to overcome the complexity of current products at reduced time and cost; 2) to target personalisation and hence improve the patient compliance or customer loyalty for using those personalised medicines or products; and 3) to enhance on-demand manufacture such as Point-Of-Care Manufacture (particularly when global pandemic such as Covid-19 limited the imports and exports from the conventional supply chains). The current global shortage of several medicines, inductors, and other goods during and after Covid-19 pandemic (due to the self-isolation and/or travel restriction regulations- rules) could lead to the increase of decentralised manufacture of those types of products (Table 1.2). For example, there are flexible fabrication of multi-active dosage forms and customised medical products for patient, but it takes certain time to prepare and formulate final products from different materials when using Fused Deposition Modelling (FDM) [21,22].

Among common AM techniques used in engineering/electronic fields, FDM and IJP also offer more advantages such as the ability to print thermoplastic materials, low-cost ink with suitable conductivity and printability, the compatibility with the desired substrates and less demanding post-processing. However, it also has few limitations such as unsuitable resolution to embed conductive ink materials or electronic devices [23,24], or the blocks/pauses in the poly-jet printing process [25,26].

Therefore, AM or 3D-printing has expanded in a variety of fields, particularly shifting its impacts towards pharmacy/healthcare (for 3D printing drug delivery systems, implants, and other surgical devices) and engineering/electronic fields (for 3D printing of dielectric materials, interconnectors conductive traces, and semiconductors) in the upcoming years.

Table 1.2. Different examples of MAM in pharmacy/healthcare and engineering/electronic fields

Application	Technique	Advantage (+) Disadvantage (-)	Example
Pharmacy/ healthcare field: printing drug delivery systems, implants, and other surgical devices	Fused Deposition Modelling (FDM)	+ Flexible fabrication of multi-active dosage forms + Customised medical products for patient - Take certain time to prepare and formulate final products from different materials [21,22]	FDM printer offered specific drug delivery system with different components [27] Capsular devices and scaffolds with hollow structures were manufactured by FDM [28,29]
	Ink-jet Printing (IJP), with the widely used method known as Drop-on-demand (DOD)	+ Ability to print different active components + Robust control of drop deposition dynamics - Only few affordable printers can inkjet printing multiple materials simultaneously [30,31]	Stimuli-responsive capsules including an aqueous core (of biomolecules) and polymeric shells were printed for the projected release [32] 3D-scaffolds were produced by low temperature additive manufacturing [33]
Engineering/ electronic field:	Fused Deposition Modelling (FDM)	+ Ability to print thermoplastic materials - Unsuitable resolution to embed conductive ink	Electrical traces were produced by the injection of low melting temperature metals [34] Multi-nozzle system was applied in the desired areas to print the electric interconnects [35]

printing dielectric materials, interconnectors conductive traces, and semiconductors		materials or electronic devices [23,24]	
	Ink-jet Printing (IJP)	+ Low-cost ink with suitable conductivity, printability + Compatibility with the desired substrates + Less demanding post-processing - The blocks/pauses in the poly-jet printing process [25,26]	IJP can be used to produce metal nanoparticles, metal-organic decompositions, and aqueous conductive solution [36] The poly-jet fabrication of multi-material embedded strain sensors [37]

1.3.2. The importance of interfaces in multi-materials additive manufacturing

An interface is the boundary between two spatial regions occupied by different materials, or by the same matter in a different physical state [38,39]. Figure 1.7 shows the interface examples (noticed as red areas) of several 3D-printed samples in the engineering/electronic and pharmacy/healthcare fields such as a) printed circuit board, b) artificial printed ear, c) semi-conductor, d) health patch, and e) finger prosthesis stent exemplar [20,38,39]. There are several reasons why AM formed interfaces are particularly challenging compared to those formed by more traditional approaches [40–46]: 1) Surface roughness: the micro-scale roughness of surfaces-interface from most 3D printing methods can affect the quality of final 3D-samples as they require additional post-processing steps to achieve the desired smoothness or a precision which can require more time and cost to the manufacturing process; 2) Material compatibility: AM allows for a wide range of materials, but not all of them are compatible with each other when used in a multi-material or multi-process design, which requires consideration in design and manufacturing to ensure the interlayer bonding or adhesion of dissimilar materials; and 3) Support structures: several 3D-printed products require the support structures to prevent overhangs and other geometric challenges during the printing

process. These support structures are usually removed after printing, which can leave behind residual marks or affect the quality of interfaces.

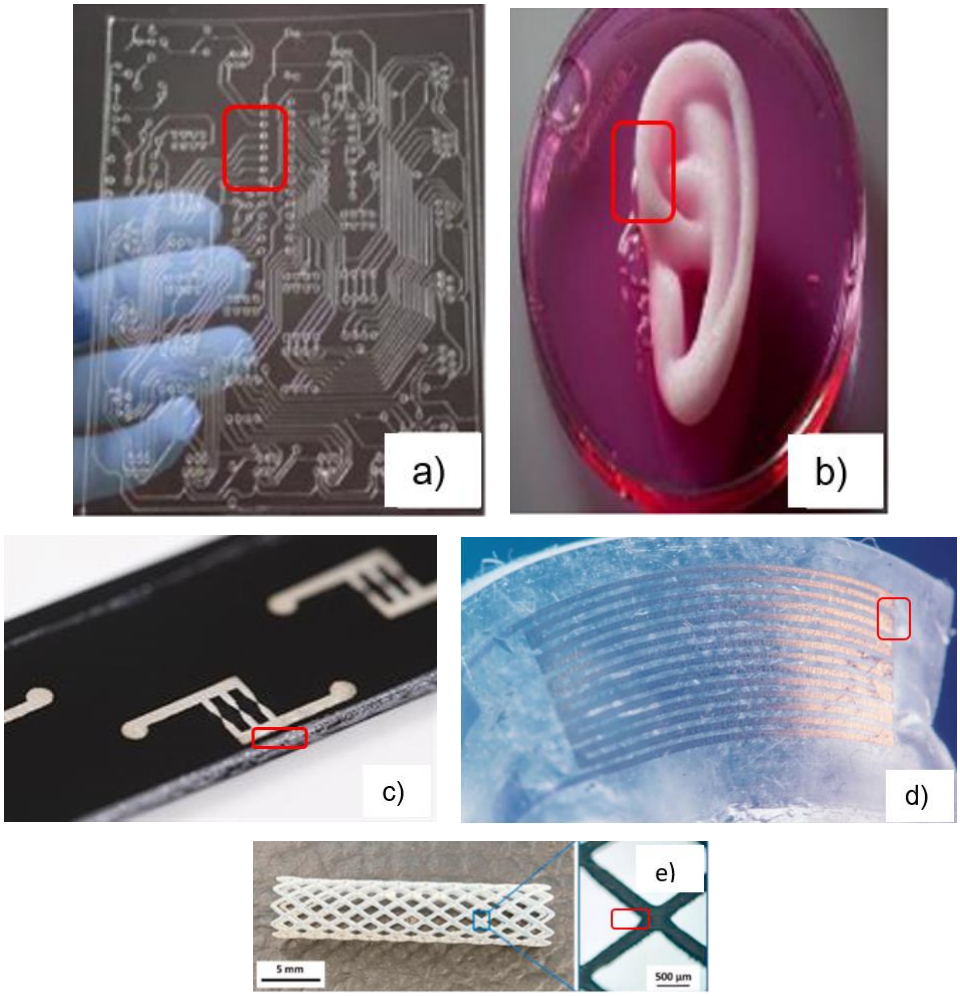

Figure 1.7. *Interface examples (noticed as red areas) of various samples with different 3D-printing techniques: a) printed circuit board, b) artificial printed ear, c) semi-conductor, d) health patch, and e) finger prosthesis stent exemplar* [20,38,39]

Although it is common to use polymer-type 3D-printers both at home and work nowadays, the customers have less accessibility to other types (as metal, ceramic, or composite) of 3D-printers [47,48]. Therefore, it is competitive between companies to not only improve structural design but also to expand performance and lessen cost and time of manufacturing for the next generation additive manufacturing by utilising the MAM [49]. Particularly, to overcome interface-related issues, it is necessary to have a good understanding of constraints and capabilities of specific AM technology. This requires a different approach compared to

traditional manufacturing methods, where such considerations may not be as critical, or the very well-defined interfaces are easier to characterise. Ongoing research and development in MAM are addressing some of the interface challenges to make it a more viable option for a wider range of applications [40–46].

1.4. THE SCOPE OF THIS THESIS

AM or 3D Printing is a promising approach with design flexibility and affordability to transform industries such as automotive, aerospace, electronics, biotechnology, and pharmaceuticals [1–6]. However, ensuring proper material compatibility at surfaces-interfaces can be complex and may require specific design considerations. AM formed interfaces are particularly challenging compared to those formed by more traditional approaches due to different reasons. For example, the adhesion or interlayer bonding can be weaker compared to the homogenous material structure of traditionally manufactured parts. This can cause reduced mechanical properties and may affect the integrity of the interfaces [40–46].

My PhD research **"Novel micro/nano scale characterisation of interfaces in multi-material additive manufacturing (3D printing)"** aims to develop robust methodologies to investigate interfaces and interphases at the micro and nanoscale of multi-material, multi-functional 3D printed products (Figure 1.8). The work forms part of the EPSRC Programme Grant "**Enabling Next Generation Additive Manufacturing**" (**EP/P031684/1**) that has the ambitious goal to control the manufacturing and characterising the new functional and structural multiple materials. There are four main challenges of developing the next generation AM, which includes analysing the interfaces of 3D-printed products, then modelling and simulating multi-material AM, and developing novel materials to produce the electronic and bio/pharmaceutical devices (Figure 1.9) [38,39].

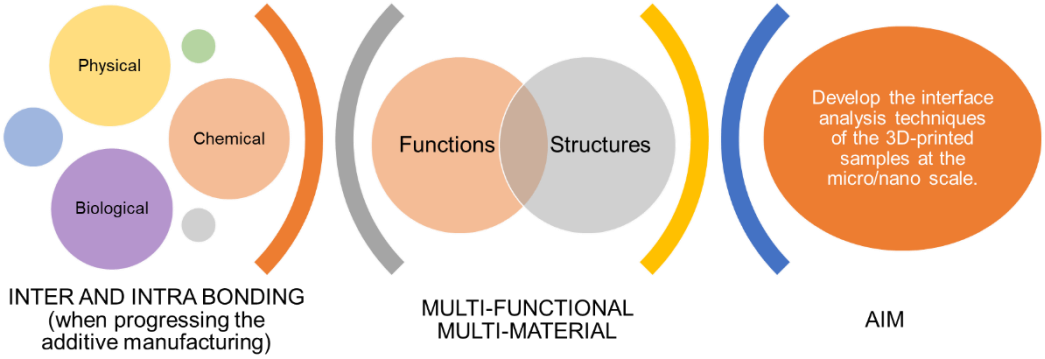

Figure 1.8. *The requirement to develop the interface analysis of 3D-printed samples at the micro/nano scale*

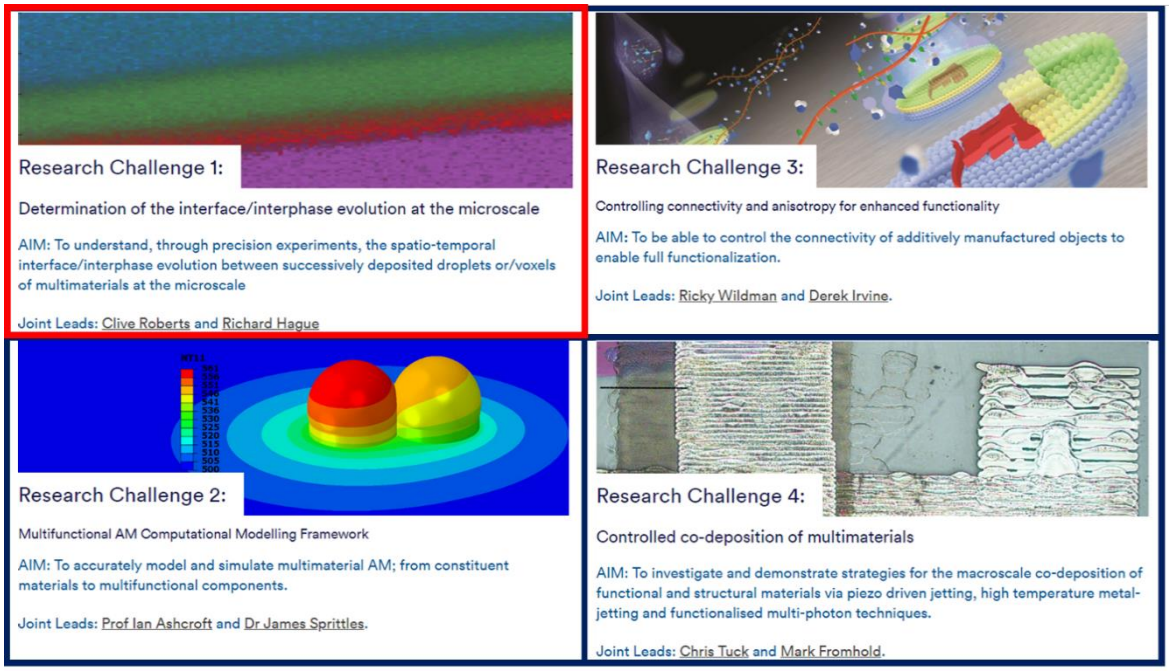

Figure 1.9. *Four main challenges in the Programme Grant "Enabling Next Generation Additive Manufacturing" (EP/P031684/1). This PhD is primarily in RC1* [38,39]

This thesis has the following objectives:

1) a literature review of the current additive manufacturing and characterisation techniques (Chapter 1 and 2).

2) consideration of the changing legal and regulatory framework around point of care manufacture of medicines as might be applicable to 3D printing (Chapter 3).

3) assessment of the commercialised and lab-based products for verifying the suitable metal nanostructures of 3D-printing of electronics (Chapter 4).

4) development of tailored analytical methodologies (with a range of sample preparation strategies, microscopy, spectroscopy, and related techniques) to investigate the physiochemical compatibilities of new ink formulations (Chapter 5).

5) creation of new design patterns and building the optimal workflows for reliable manufacturing of co-printed (bio)-pharmaceutical products (Chapter 6).

CHAPTER 2: MATERIALS AND METHODS

2.1. MATERIALS

Table 2.1. summarises the testing materials/3D-printed samples in this thesis, particularly in engineering/ electronic and pharmacy/ healthcare fields.

There are certain effort to understand and improve the structures of electronic devices in AM, and two testing samples (produced by ink-jetting technique) are presented at Section 4.2.1 - Chapter 4. The work aims to develop standard procedures to expose internal interfaces and acquire morphological/structural data of 3D-printed functional electronic materials including 3D-printed commercialised inductor (DragonFly product) and 3D-printed lab-based electrodes (flexible gold structures). More details will be illustrated in Chapter 4.

It is challenging to co-print and control the biopharmaceutical products as different functional formulations may interact differently at the interfacial areas, especially in context of dissimilar deposition and curing strategies. I investigate the interface/interphase between formulations-substrates and formulations-formulations from multi-functional multi-materials. Particularly, two materials were selected for investigation included water-soluble inks (WI) (having a support function) and structural ink (SI) (having a bacterial biofilm resistance function) and more details are illustrated at Section 5.2.1 - Chapter 5. Hence, the optimal co-printing workflow for water-soluble and structural inks will be built and developed (Chapter 5 and 6).

Table 2.1. List of testing materials/3D-printed samples in this thesis

Field	Samples	Chapter
Engineering/ electronic	3D-printed commercialised inductor (DragonFly product) 3D-printed lab-based electrodes (flexible gold inks)	Chapter 4
Pharmacy/ healthcare	Two ink formulations included water-soluble inks (WI) (having a support function) and structural ink (SI) (having a bacterial biofilm resistance function) 3D-printed patterns from single ink and co-printed inks	Chapter 5 Chapter 6

2.2. METHODS TO 3D-PRINTING MAM

MAM is a radical approach empowering the manipulation and development of numerous items that can be used in our everyday life [50,51]. Among the common AM techniques with process schematic diagrams (Figure 2.1), Material Jetting, or Ink-jet Printing (IJP) is the widely used method (also known as Drop-on-demand (DOD)) can offer the ability to print different active components and robust control of drop deposition dynamics (despite only few affordable printers can inkjet printing multiple materials simultaneously) [30,31]. Hence, I focused on evaluating the inkjet printing process with single and multiple printheads.

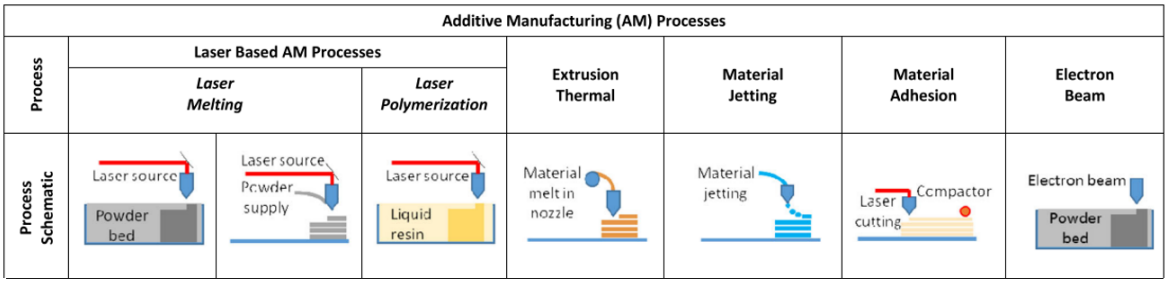

Figure 2.1. *Common AM techniques with process schematic diagrams* [7–9]

2.2.1. Inkjet printing MAM with single printhead

The inks are deposited using a Fujifilm Dimatix Materials Printer (DMP-2850) with a 10 pL cartridge (DMC-11610) (Figure 2.2) [52,53]. A nozzle temperature of 35 °C is used to generate a stable droplet. Different substrate temperatures ranging from 20 to 90 °C are used. For electrical property measurement, the inks are printed using one nozzle, with a droplet spacing of 30 μm, a jetting frequency of 1 kHz, a substrate temperature of 90 °C, and a sintering temperature of 150 °C (30 min, hot plate). The sintering temperature dependence of the electrical resistivity of a printed structure is studied by placing a sample on a hot plate at varying temperatures.

In this thesis, new gold nanoparticles are formulated and jetted using an inkjet printer with single printhead, which are completed with the support from Dr. Jisun Im (Chapter 4).

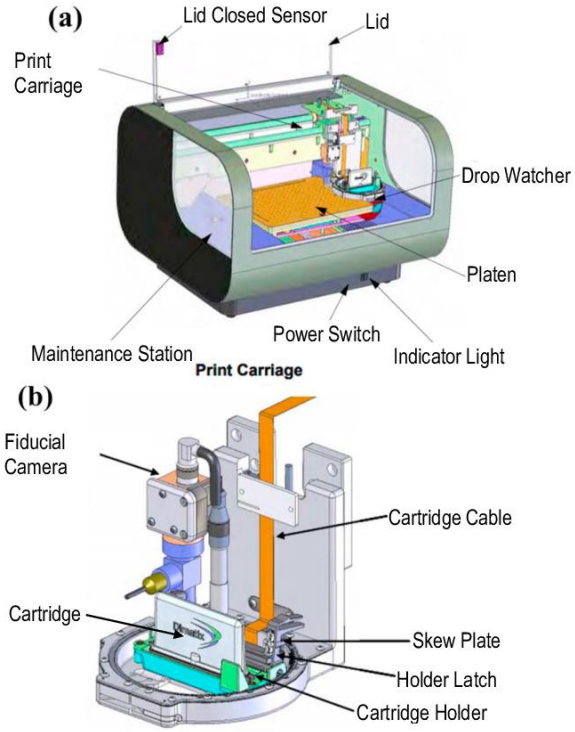

Figure 2.2. *Single printhead inkjet-printer: a) Schematic diagram of Dimatix-2850 inkjet printer, and b) Printer cartridge with single assembly* [52,53]

2.2.2. Inkjet printing MAM with multiple printheads

WI and SI inks are simultaneously printed by the SUSS LP50 Inkjet Printer (from PiXDRO 50 Ltd.) with a dual head assembly (Figure 2.3) [54–56]. Two printheads Spectra® SE-128 AA (from FUJIFILM Dimatix Inc.) are used. Each printhead has 128 nozzles (or maximum addressable jets) with nozzle diameter of 35 µm (and nozzle spacing of 508 µm). The Advanced Drop Analysis (ADA) Model is used to check and calibrate the active nozzles. The dual head assembly is equipped with the LED UV curing unit Phoseon Firefly™ (from Intertronics Co.) that can produce up to 4W/cm^2 peak irradiance at 395nm with the emission window of 25 x 10 mm [57].

To generate stable filming, the printhead 1 with the setting nozzle temperature of 85°C is used for WI, and the printhead 2 with the setting nozzle temperature of 55°C is used for SI (while the setting temperature was set of 25°C for all investigated substrates). The whole system is installed inside a glovebox maintaining low oxygen level (< 3%) at room temperature (20-25°C), and it is equipped with the Oxygen Analyser EC933 (from Systech Illinois Co.) to keep track of the set-up environmental parameters. This approach is applied

to help to reduce the inhibition effect caused by oxygen during the free radical photo-polymerization curing procedure.

In this thesis, the SUSS LP50 Inkjet Printer (having multiple printheads) was used to produce 3D-printed samples (Chapter 5 and 6).

Figure 2.3. *Multi-printheads inkjet-printer: a) Key features of SUSS LP50 Inkjet Printer* [54–56]*, and b) Dual assembly in LP50 Inkjet Printer*

2.3. METHODS TO EXPOSE SOLID-SOLID INTERFACES IN AM PRODUCTS

2.3.1. Sample preparation

Before trying to expose layers within a multi-material 3D printed specimen for analysis, it is important to understand primary bulk information, such as whether the original sample is dry or wet, small or big, thin or thick, soft or hard, ductile or brittle, conductible or not. Some prior steps such as drying or cutting may be required to expose the desired surfaces before

using specific preparation procedures [58,59]. Figure 2.4 shows potential sample preparation approaches including exposing the interfaces in samples (such as ultramicrotomy) and post-handling steps such as cleaning, marking, and storing the samples (if necessary). For example, samples that are wet in their normal state may need to be dried by gentle heating or special drying techniques which can help to remove the water from the frozen biological materials and limit the damage caused by the growth of ice crystals (after immersing in a liquid-cooled by liquid nitrogen) [60]. Moreover, some materials need cutting with a very thin sharp knife to produce different pieces in suitable sizes and shapes, which should be done as gently as possible because few damages can happen and possibly affect the partial or final samples. For example, a parallel-sided slice (typically a few millimetres thick) can be cut off and then trimmed to the required sections for the SEM or TEM [58].

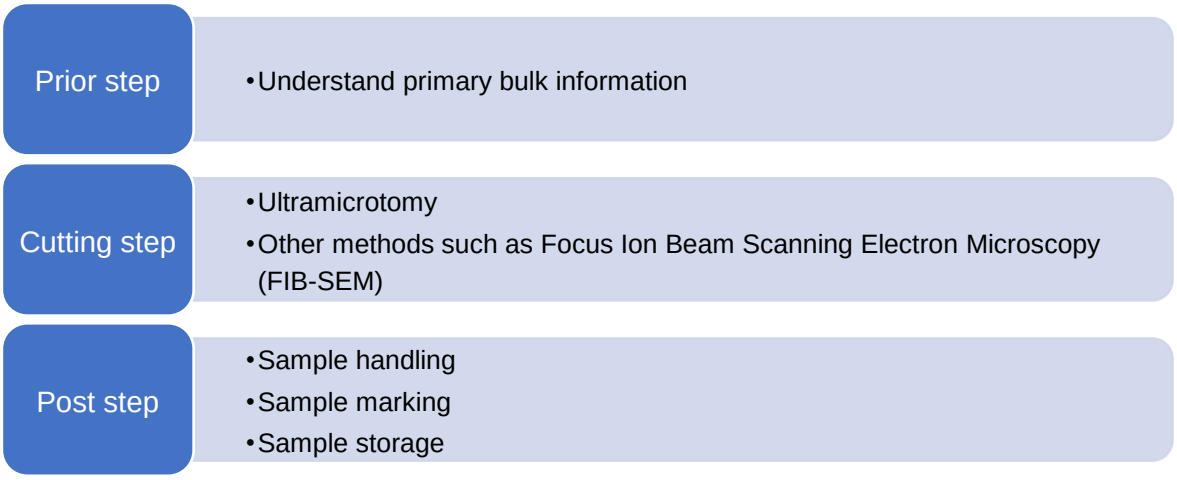

Figure 2.4. *Three main steps for exposing the surface-interface of 3D-printed samples at the micro/nanoscale*

2.3.2. Ultramicrotomy

Ultramicrotomy uses a mechanical glass or diamond knife to cut a sample to reveal a smooth surface and produce a series of sections (from a few tens to few hundred nanometres of thickness) at room temperature (RT-ultramicrotomy) or lower temperatures (Cryo-ultramicrotomy). RT-ultramicrotomy is used for brittle materials when their glass transition temperatures are higher than room temperature (T_g > RT), whereas cryo-ultramicrotomy is useful for softer or more sensitive (eg. hydrated) materials when their glass transition temperatures are lower than room temperature (T_g < RT). Some friable materials need to be

impregnated/supported within a suitable medium such as an epoxy resin to reinforce the necessary mechanical properties for cutting [61,62]

Generally, a ultramicrotome consists of 3 components (Figure 2.5): 1) The first part is the optical system to helps to observe and allocate the sample properly for cutting and obtaining the sections, 2) The second part is the cutting system including knife, knife holder and additional parts (such as water bath to contain sections for wet-capturing), 3) The third part is the sample holder which is the place embracing the sample at the suitable cutting site, and 4) The final part is the mechanical system including the drive wheel and the knife wheel to identify the sectioning interval and therefore control the thickness of the sections [58].

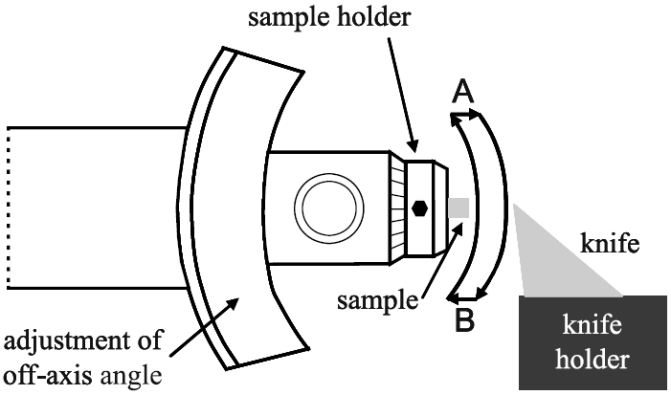

Figure 2.5. *Diagram of an ultramicrotome (modified from [58])*

Ultramicrotomy is used to control the thickness of section (such as semi-thin section with thickness 0.2–3 μm or ultrathin section with thickness lower than 0.2 μm) by precisely advancing the sample towards the knife. Therefore, the sample block and knife should be kept horizontally parallel within the proper distance to produce uniform sections. Each specimen thickness has a relative interference colour for direct observation or image-capturing [58]. Moreover, the quality of a section depends on numerous factors including material properties (such as the stiffness of the original sample or the thickness of the proposed section), cleanliness, pre-treatments (such as resin embedding), and cutting parameters (such as cutting speed, type of knife, or knife angle) [63,64].

Ultramicrotomy is a reliable and chemically benign technique to expose uniform cross-sections of materials such as polymers, biological tissues, metals, glasses, or

semiconductors. More importantly, it can be used for a variety of solid sample types that cannot be thinned by milling. Ultramicrotomy is extensively used to prepare samples for optical microscopy, scanning electron microscopy, transmission electron microscopy, atomic force microscopy, and other scanning probe techniques [58]. However, there are some challenges when using ultra-microtomy such as the mismatch of hardness between resin and sample materials and different physical or chemical artefacts caused by the sectioning process, such as high compression of sections, or striations [61]. Another example is a sample that is required to be cut below its glass temperatures, which means cryo-ultramicrotomy is appropriate. Cryo-dry sectioning usually takes place in the range of - 40ºC to - 150ºC, while cryo-wet sectioning is between -20ºC and -50ºC in different solvents (such as propanol - 90ºC) when using a glass knife or in a DMSO/water mixture when using a diamond knife. The reason for this is that the epoxy seal which is holding the diamond may be destroyed if a DMSO/water mixture is not used and the minimum temperature for using DMSO/water is - 45ºC [61].

In this thesis, Ultramicrotomy were used to expose interfaces and confirm nanostructures of 3D-printed samples (Chapter 4).

2.3.3. Focused Ion Beam Scanning Electron Microscopy

Focused ion beam (FIB) can be incorporated in a system such as scanning electron microscopy (SEM), allowing to expose the interfaces and obtain images simultaneously in a variety of areas across medicine and engineering research [65–67]. In the Focused Ion Beam Scanning Electron Microscopy (FIB-SEM), the primary ion beam such as the gallium (Ga^+) can hit the sample surface and sputter a small amount of material, resulting in a range of physical and chemical reactions. Then, it can leave the surface as either secondary ions, neutral atoms, or secondary electrons (Figure 2.6a). The primary beam rasters on the sample surface, the signals from the sputtered ions or secondary electrons are collected for primary imaging mode. Depending on the level of energy and the nature of materials, FIB-SEM can be used at other modes such as milling, deposition, or ion implantation (Figure 2.6b-d) [68].

Recently, there is an increase of FIB-SEM application in material sciences, but several points still need to be considered to obtain the consistent processing (e.g. sectioning and

imaging soft material without affecting its initial structures) [65,66]. Figure 2.7 shows a typical FIB-SEM dual beam system has two fundamental columns: a) SEM column including Electron Gun, Double condenser, Inlens EsB detector, Filter grid, Inlens SE detector, Objective, and Beam booster; and b) FIB column including Ga+ Reservoir, Suppressor, Extractor, Condenser, Differential Pumping Aperture, Beam Defining Apertures, Blanker Plates, Octopoles, and Objective [68,69].

In this thesis, FIB-SEM were used to confirm morphology (including layer thickness) of 3D-printed samples (Chapter 4).

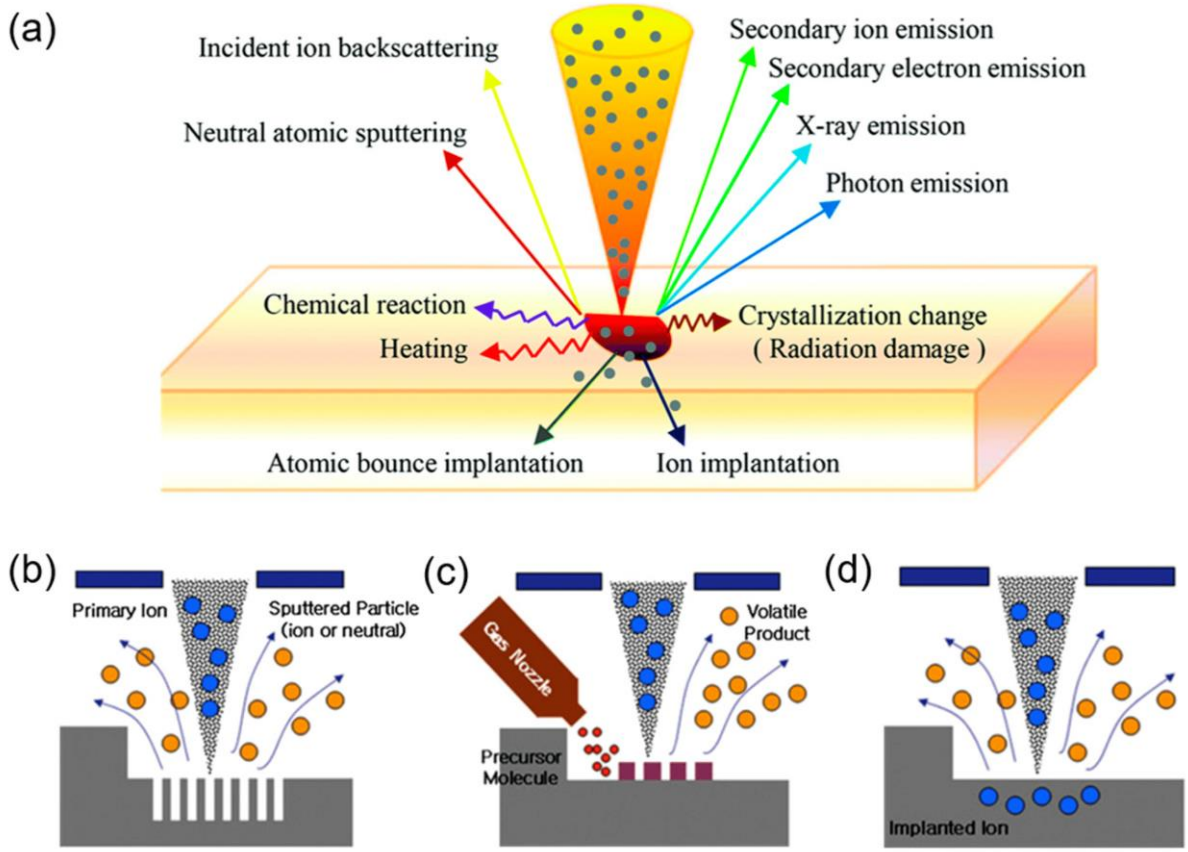

Figure 2.6. *Key features of FIB-SEM: a) A variety of signals on a specimen's surface from the incidence of primary ion beam; and the correlated modes (along with primary imaging mode): b) milling, c) deposition, and d) ion implantation (modified from [68])*

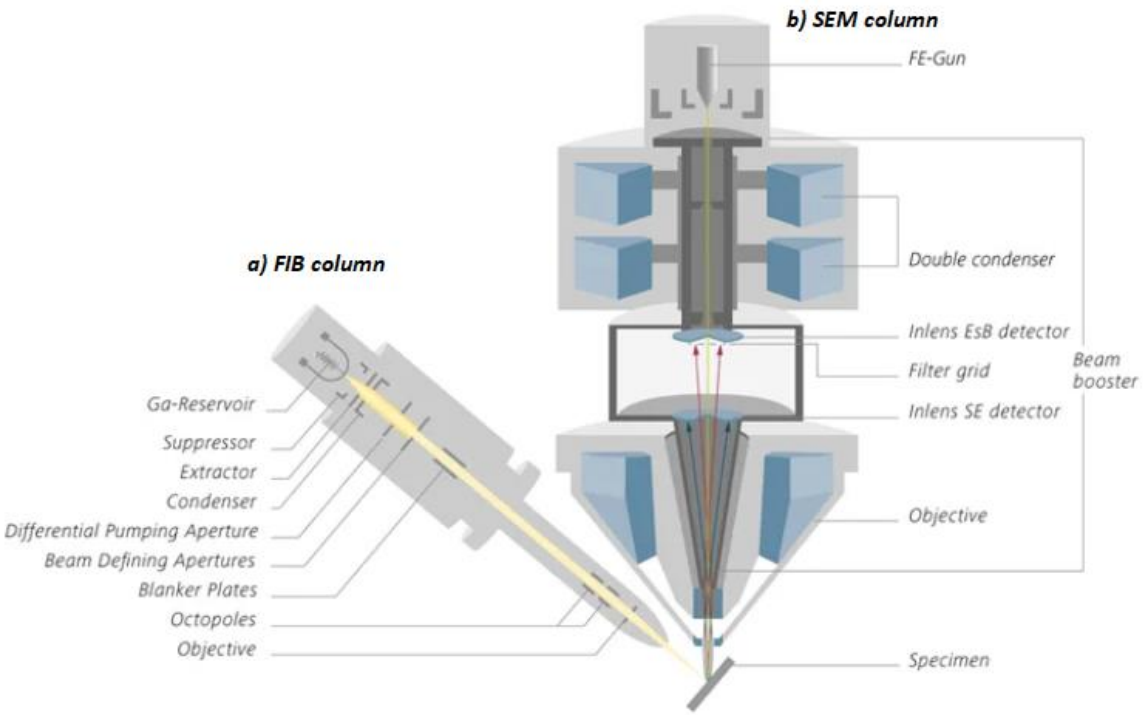

Figure 2.7. *Schematic diagram of FIB-SEM dual-beam system: a) FIB column; and b) SEM column (modified from* [68,69]*)*

2.3.4. Other techniques

Other physical sample-preparation methods are cutting sample thinning or cryo-vitrification for sensitive materials. For example, it is also useful to produce replicas or casts for the SEM investigation on the pore structures [70–72].

It is necessary to consider other sample handling needs before analysing the interfacial areas of the samples, as below.

- Sample cleaning

Firstly, samples can be polished to produce a flat ground surface by progressively cutting (with a glass or diamond knife in ultramicrotome) and then be carefully cleaned in a proper way. Cleanliness should be examined when handling samples to avoid degradation of the chamber vacuum and accumulation of the contamination such as using a compressed air-jet to remove dust. A standard cleaning method is washing the samples with a residue-free solvent such as water, ethanol, or ether (which will not damage the original or mounted samples) and then wiping with a lint free tissue. Moreover, samples can be coated to enhance

the conduction of electricity to prevent charging under electron bombardment. For example, carbon with its insignificant impact on the X-ray spectra is a common coating for X-ray analysis, while metal coating such as gold, copper, aluminium, or iridium is for minerals that may break down under the electron beam when being coated with carbon [73].

- Sample marking

Samples should be easily identified with certain symbols such as numbers at each stage of the preparation process. For example, a label can be embedded along with the specimen in each block of epoxy resin or a number can be scratched onto the back of every block. The specimen position can be more visible to view when choosing a suitable written ink (which is unaffected by the cleaning solvent) to mark SEM stubs. The areas of interest can be recognised through the scanned digital images of the whole specimen or the micrographs of the small regions by using optical microscopes or profilometers [58].

- Sample storage

The stability of sample structures should be considered, especially for long term storage. Samples are recommended to be kept in a low humidity- and dust-free environment such as desiccator. Besides, some samples (with or without the embedment in resin) are regularly glued to the SEM stub by using double-sided sticky tape or quick-setting glue before being saved in the plastic boxes for further analysis. In many cases, thin sections of samples are required to be done before saving them in a specialised sample holder (the TEM grid) [74].

2.4. METHODS TO INVESTIGATE THE MORPHOLOGY OF SURFACES-INTERFACES IN AM PRODUCTS

There is a variety of techniques available to characterise materials and gain access to internal layers and analyse solid interfaces between materials. The most widely used set of methods for the direct observation of external surfaces and the enhanced accessibility for internal structures is microscopy [75].

2.4.1. Optical Microscopy

Light Microscopy or Optical Microscopy (OM) is a method to capture images of materials by condensing the light reflected from or transmitted through objects with lenses as a “focal

point" to magnify and differentiate the details of the sample (Figure 2.8). The diameter of the condensed light at the focal point cannot be smaller than approximately half of a wavelength of the light used due to the wave nature of light (Rayleigh criteria). In addition, most current optical microscopes have an objective lens to produce a larger image of an object, and this image is then magnified by a second-lens system (the ocular or eyepiece) for clearer vision. Based on the light transmission or reflection on a sample, there are two fundamental modes to operate an optical microscope: 1) the light will transmit through a thin specimen, which is broadly used to investigate living creatures; and 2) the light will reflect from the surface of the sample and into the microscope objective, which is applied in analysing non-transparent materials or thicker sections [76–78].

In this thesis, optical microscopy was used to reveal preliminary morphology of 3D-printed samples (Chapter 5).

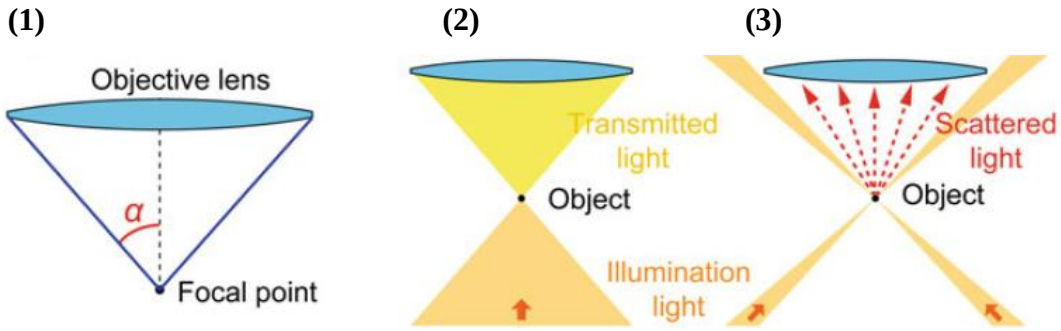

Figure 2.8. *Schematic of converging angle α (1) and the optical paths of a bright-field microscope (2) and a dark field microscope (3) in the upright microscope configuration (modified from [79])*

2.4.2. Electron Microscopy

Two main features are discussed in the following, namely sample properties, and machine settings. Sample properties such as size, conductivity, and environment compatibility will have a significant influence on analysis. For example, a sample needs to be conductive for SEM analysis, but in some cases, samples can be examined in their natural state with no requirement for a conductive coating layer in ESEM or low-vacuum SEM. ESEM can help to control the environmental conditions (selected from among water vapor, air, N_2, Ar, or

O_2) at certain pressures without surface charging, because the secondary electron detector is designed on the principle of gas ionization [80,81].

Among key features of machine settings, magnification is the ability to increase the visualised size of objects within an image. Resolution is the ability to recognise individual fine details when observing a sample. These both depend on the type of source being used and on the design of an instrument. For example, the spatial resolution of an SEM is strongly influenced by the size of the focused spot of the electron beam, and the volume of the material that interacts with the electron beam. A typical optical microscope (apart from a super-resolution microscope) has a resolution limit around 200 nm, while SEM can provide images with the resolution limit of 3-6 nm and TEM can offer a very high resolution, such as 0.2 nm. It should be noticed that higher magnification can result in an ill-defined blurry image (except for some cases equipped the high-resolution device) - so higher magnification does not necessarily lead to higher resolution [82,83].

Additionally, the contrast is the ratio between dark and light, so selectively staining a sample can be a way of increasing contrast, but this does increase sample preparation complexity (in the bright-field mode). The type and area of a surface exposed to the primary beam can also alter the effective brightness, because sloped and/or edges have a relatively larger surface compared to a flat sample, hence degrading resolution. Another essential parameter is the depth of field or depth of focus (which means the range of depth where a sample is at an acceptable focus). A microscope with a small depth of field will need focusing up or down continuously when observing a thick sample. It should be noticed that SEM has a high depth of field and hence can analyse samples in three-dimensional appearance while most TEM which have a very narrow depth of field can only provide two-dimensional images [84,85].

The potential applications of electron microscopy can be expanded after attaching different types of devices. For example, traditional SEM is restricted to only conductive samples, whereas environmental or low-vacuum SEM can analyse nonconductive (uncoated) samples in adjusted-pressure chambers. Both high-quality data of surfaces and elemental composition can be investigated at the same time with the energy dispersive spectroscopy (EDS) attached to SEM. Electron microscopy can also enhance knowledge in multi-

disciplines such as medical diagnostics, engineering, or materials sciences thanks to the larger magnification, higher resolution, greater depth of focus, and the ease of sample observation compared to the typical optical microscopy. For example, Environmental Transmission Electron Microscopy (ETEM) can offer a dynamic characterization of wetting, drying, absorption, melting, corrosion, and crystallization of the samples [86–88].

Although electron microscopy is a widely used analytical method, it still has certain constraints affecting the accuracy of the experimental results. For example, the sample can be damaged by the electron beam owing to ionisation effects. Another problem may be the data amount required to be representative of the materials.

i. Transmission Electron Microscopy (TEM)

Generally, TEM is an observation technique utilising a fine beam that passes through a thin specimen. Electromagnetic lenses collect the transmitted electrons in a range of modes including diffraction patterns and high-resolution images [89]. A transmission electron microscope primarily consists of five components (Figure 2.9): 1) The first component is an electron source (thermal filament) such as Lanthanum hexaboride (LaB_6) or a field emission gun; 2) The second part is an electromagnetic system including condenser lens, objective lens, internal lens or projector lens; 3) The third part is the detector system; 4) The fourth component is a sample chamber where the sample is loaded via a ring screwed into the well of the sample holder; 5) The final component is a display system which helps to present the magnified images on a fluorescent screen and record the results (from a digital camera). Additional parts are important in the TEM instrument such as a vacuum pump which is required to improve the evacuation of the electron path [90,91].

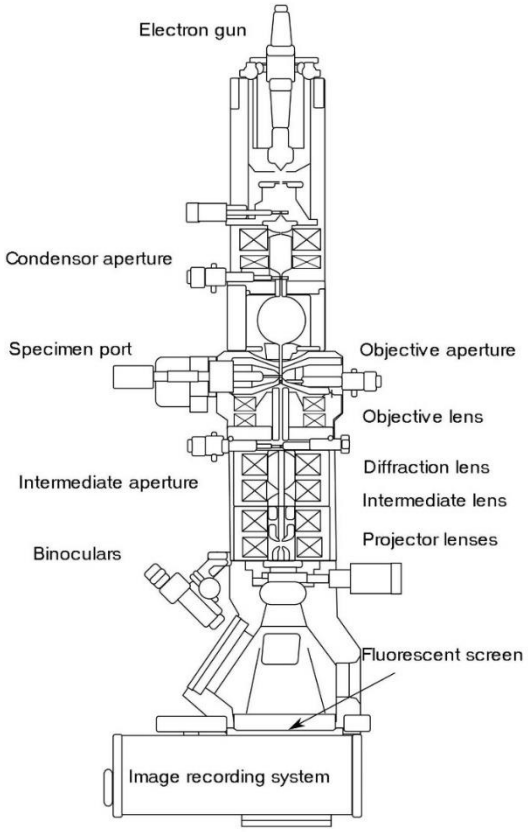

Figure 2.9. *Diagram of a transmission electron microscope* [91]

ii. Scanning Electron Microscopy (SEM)

Typically, there are six crucial components of a scanning electron microscope (Figure 2.10): 1) The first part is an electron source (with generally 10-30 kV) which can be a thermionic emitter with a tungsten filament, or a higher-intensity field emission source/gun (FES/G) that has a strong electrical field to increase the beam current; 2) The second component includes the condenser lens and the objective lens to help to focus electrons into a fine beam; 3) The third part is a vacuum scheme using different pumps and chambers to limit the damage of electron source; 4) The fourth component known as detection facilities can include the scanning coils (or the beam-deflection coils)X-ray spectrometers, and/or other accessories to record electrons or other signals emitted by the specimen; 5) The fifth component is a specimen stage with specific x-y-z directions that can be adjusted for desirable orientation of the specimen; 6) The final part is an output system with proper software to display the topographic, compositional or further types of images, and other supplementary results can be collected from the element mapping or X-ray analysis [92,93].

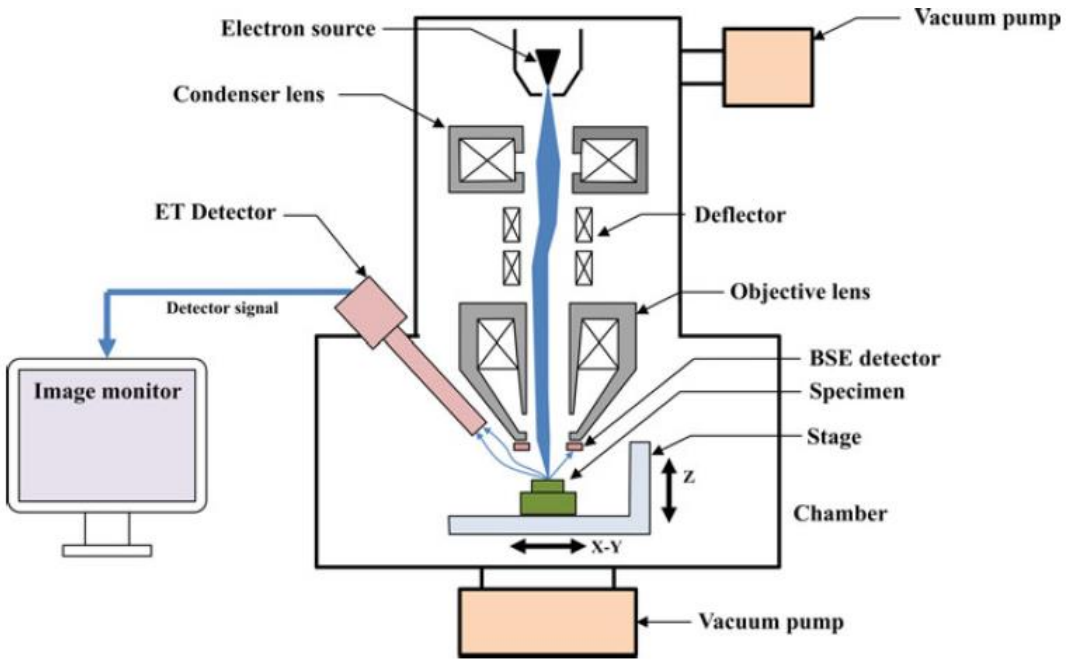

Figure 2.10. *Diagram of a scanning electron microscope* [93]

In the context of SEM, after being focused by the condenser lenses into a beam with a very fine spot size (usually about 5 nm), the electron beam of the scanning electron microscope will pass through the objective lens and scanning coils which can divert the allocated scanning pattern on the surface of an object. The focused electron beam (with energy usually less than 50 keV) irradiates a sample causing the interaction of the incident electron with atoms in the sample. A scintillator-photomultiplier monitors the resultant low energy secondary electrons to reveal topological aspects of the sample. Backscattered-electron (BSE) images are mainly used to reveal compositional variations owing to the atomic-number discrimination. Other signals (mostly X-ray signals) can be detected by the special attached detectors such as an energy-dispersive spectrometer (EDS) which records all X-ray energies simultaneously to deliver the output pulses related to different levels of photon energy [92,93].

An electron microscope utilises electrons instead of light as the illuminating source. This has a practical consequence of a larger depth of field than optical microscope and at the electron energies used their effective wavelength is much shorter than light, allowing a higher spatial resolution. For example, electrons usually have wavelengths in picometers (such as 6.98 pm at 30kV E beam and 2.51 pm at 200kV E beam) whereas light has

wavelengths in micrometers (such as 0.7 μm for red and 0.4 μm for violet). The electrons may be 'reflected' from a surface (SEM) or transmitted through (TEM). In SEM a variety of signals on the specimen's surface from a normal incidence of primary electrons (PEs) can be accessed (Figure 2.11) [93].

In this thesis, electron microscopy, particularly TEM, SEM, and FIB-SEM were evaluated to provide the morphological data of surfaces-interfaces of 3D-printed samples (Chapter 4 and 5).

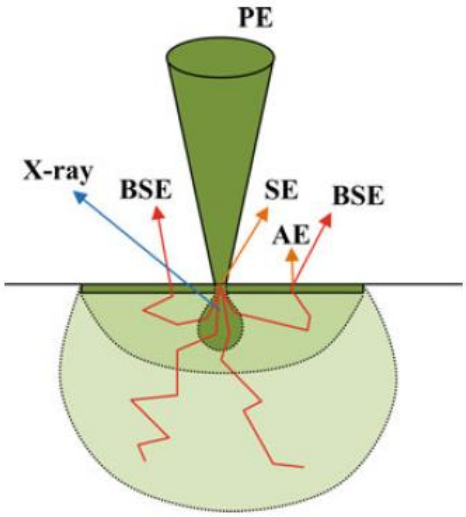

Figure 2.11. *A variety of signals on a specimen's surface: Secondary electrons (SEs), backscattered electrons (BSEs), Auger electrons (AEs), and X-rays from a normal incidence of primary electron (PE)* [93]

2.5. METHODS TO INVESTIGATE THE ROUGHNESS-THICKNESS OF SURFACES-INTERFACES IN AM PRODUCTS

Surface topography or surface finish is the nature of a surface as defined by the characteristics of surface roughness, lay, and waviness. Table 2.2 lists the common technologies for investigating surface topography in terms of non-contact (1) and contact methods (2) [94–98].

Table 2.2. Non-contact and contact methods with common technologies (including primary points) for investigating surface topography [94–98]

Method	Common technologies	Primary points
Non-Contact	a) Vertical scanning: Non-contact Profilometers; Coherence Scanning Interferometry (CSI); Confocal microscopy; Focus Variation; Confocal Chromatic Aberration. b) Horizontal scanning: Scanning Laser Microscope (SLM); Structured-Light Scanning c) Non-scanning: Digital Holographic Microscopy d) Atomic Force Microscope (with non-contact mode).	(+) No touching of the surface (the sample cannot be damaged) (+) The measurement speed is usually much higher (up to a million 3D points can be measured in a second) some of them are genuinely built for 3D surface topography rather than single traces of data
Contact	a) Contact Profilometer (that traditionally use a diamond stylus and work like a phonograph). b) Atomic Force Microscope (with contact or tapping mode).	(+) The system is very simple and sufficient for basic roughness, waviness or form measurement requiring only 2D profiles (e.g. calculation of the Ra value). (+) The system is never lured by the optical properties of a sample (e.g. highly reflective, transparent, micro-structured).

2.5.1. Atomic Force Microscopy

Atomic Force Microscopy (AFM) is one of the scanning probe microscopies, and is capable of high-resolution imaging of surfaces at the atomic and molecular levels in contact, intermittent and non-contact modes. By using a sharp tip that scans the sample surface, AFM can measure surface roughness and other physical properties at the atomic scale [99–101].

There are seven fundamental components of an atomic force microscope (Figure 2.12): 1) Cantilever is a flexible small beam typically made of silicon or silicon nitride; 2) Probe tip is attached to the free end of the cantilever, which interacts with the sample surface, sensing the forces and providing the resolution for imaging; 3) Laser diode provides a laser beam that is directed onto the back of the cantilever; 4) Position-sensitive photodetector (PSPD) monitors the reflected laser beam to detect the changes in the position of the cantilever (due to interactions with the sample); 5) Piezoelectric scanner is used to achieve precise and controlled movements (x, y, z) of AFM tip to scan the sample surface; 6) Feedback loop system adjusts the vertical direction (z) of the scanner to keep the cantilever deflection or another feedback parameter constant; and 7) Computer controls the operation and performs data and display the results (such as image visualisation). Some AFM instruments have additional accessories for specialised applications such as heating/cooling stages of sample holders, or environmental chambers for accommodating the liquid-cells experiment [99–101].

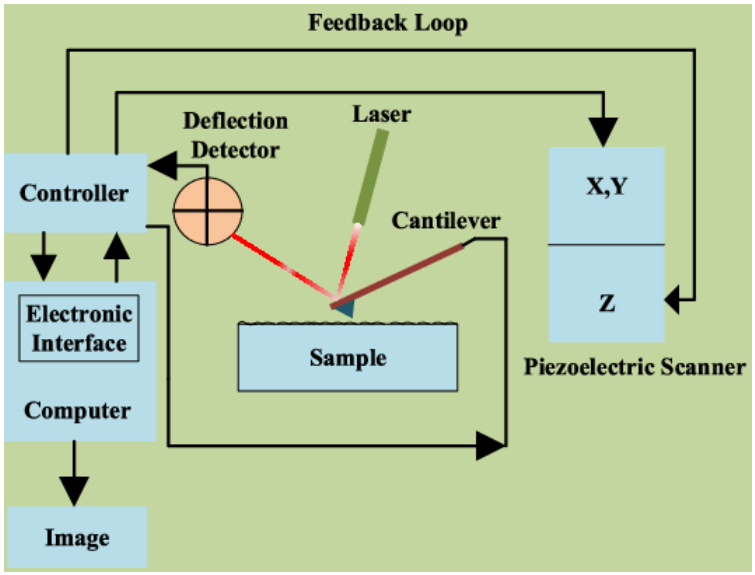

Figure 2.12. *Schematic diagram of the primary components of an Atomic Force Microscope* [102]

A wide range of cantilevers and tips are available for AFM, adapted for specific samples and modes. With samples that are harder to deform or have strong adhesive forces, either soft or stiff cantilevers can be used respectively for imaging. For example, softer cantilevers (with spring constants less than 5N/m) are more easily attracted to the surface and produce better, more reproducible images. Stiffer cantilevers give better contrast when mapping

surfaces with regions that differ in composition, such as magnetic recording heads or contaminant deposits [99–101].

Table 2.3 shows the principles, advantages (+), and disadvantages (-) of three primary imaging modes of AFM including: 1) Non-contact mode, 2) Contact mode, and 3) Tapping mode. Moreover, PeakForce Tapping mode is a proprietary Bruker imaging technique where the cantilever is actively oscillated well below its resonance (as is normal in Tapping mode). This oscillation results in a continuous series of force-distance curves being recorded at every imaging point, which makes PeakForce Tapping inherently stable and able to extract quantitative physical property maps [99–101].

Table 2.3. The principles, advantages (+), and disadvantages (-) of three primary imaging modes of AFM including: 1) Non-contact mode, 2) Contact mode, and 3) Tapping mode [99–101]

	Principles	**Advantages (+) and Disadvantages (-)**
Non-contact mode	The cantilever is set to vibrate at its resonant frequency. As the tip is brought close to the surface of the sample, the forces between the tip and the surface alter this resonant frequency. The size of these forces, and thus the distance between the tip and the surface, can be determined by this change in resonant frequency, without the tip actually coming into contact with the surface.	(+) No damage to sample (-) The slowest scan speeds (-) Lower resolution (-) It requires a stiffer cantilever than contact mode*. **The attractive forces that hold sway before the tip contacts the surface are smaller than the repulsive forces that hold sway when the tip contacts the surface.* (-) It produces a smaller signal than contact mode
Contact mode	The probe tip is in constant physical contact with the sample surface. While the tip scans along the surface, the sample topography induces a vertical deflection of the cantilever. A feedback loop maintains this deflection at a preset load force and uses the feedback response to generate a topographic image.	(+) High scan speeds (+) It is suitable for material science, biological, and basic research. (-) Damage to samples, particularly soft materials
Tapping mode	The technique maps topography by lightly tapping the surface with an oscillating probe tip. The cantilever's	(+) High resolution (+) Minimal damage to sample

	oscillation amplitude changes with sample surface topography, and the topography image is obtained by monitoring these changes and closing the z feedback loop to minimize them. It measures the average oscillatory amplitude while the tip is in contact with the surface.	**It is considered as the most popular AFM imaging mode.* (-) Slower scan speed (comparing to contact mode) (-) Can produce artifacts when imaging surfaces that possess peaks and troughs of a similar diameter to the tip.

Figure 2.13 shows the differences between PeakForce Tapping and other modes [99]. The probe periodically taps the sample, and the consequent pN-level interaction force can be measured directly by the effect on the cantilever oscillation. As the tip approaches the surface, long range attractive van der Waal forces increase until the tip jumps into contact. At this point, the tip experiences repulsive forces, which eventually dominate the attractive ones. PeakForce Tapping uses an intelligent algorithm to determine the peak force experienced by the tip in each oscillation cycle, which typically occurs at the point where the tip begins to withdraw from the surface. It can produce a quantifiable measurement of the peak force during each oscillatory cycle [103,104].

Along with the primary AFM modes, a wide range of secondary modes have been derived by employing functionalized tips or specialized cantilevers. While the principal modes focus on producing surface roughness that allows 3D images of surface topography, the other modes can probe various mechanical, chemical, and electrical features of the surface of materials. These include surface hardness, friction and elasticity, adhesion, permittivity, magnetism, conductivity, and temperature [105–107].
In this thesis, AFM were used to investigate the roughness-thickness of surfaces-interfaces of 3D-printed samples (Chapter 4).

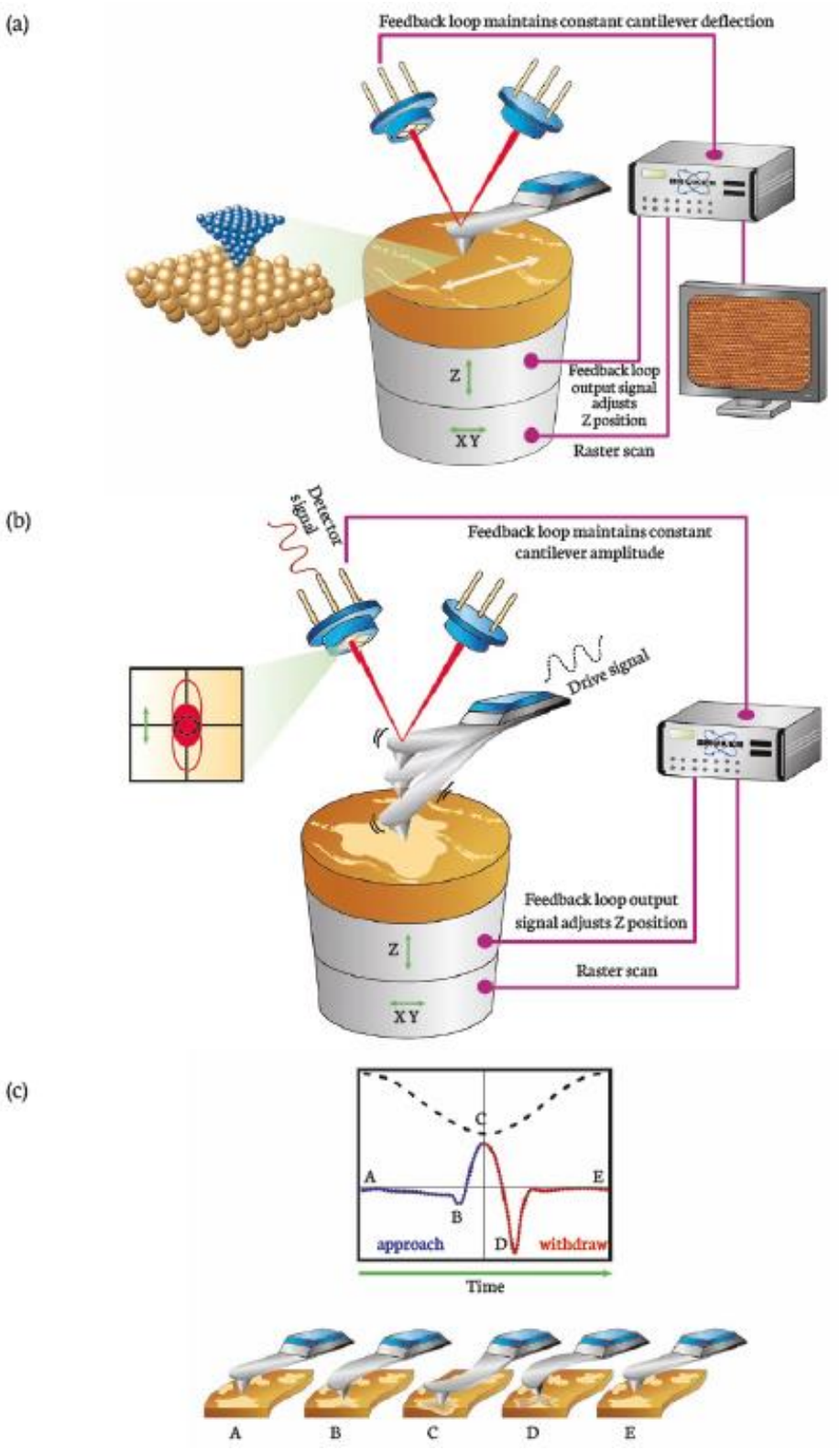

Figure 2.13. *Schematics of primary AFM modes (manufactured by Bruker): a) Contact mode; b) Tapping mode; and c) PeakForce Tapping mode* [99]

2.5.2. Profilometry and Interferometry

Profilometry is a technique used to extract topographical data (in the format of a single point, a line scan or even a full three-dimensional scan) by using a physical probe or a light source [108]. For example, Figure 2.14 represents an optical profilometer that directs the light source to detect the three-dimensional data of the surface. This example is a Zeta optical profiler that utilises a structured illumination technique (ZDot™ technology) to enhance the vertical resolution of the objective lens [109,110]: The ZDot grid, which is similar to an array of 1000s of pinholes, can enable simultaneous measurement of the entire field of view. Hence, there is no need to raster in lateral XY directions, but instead scan only in Z to determine where each individual grid point provides the optimum signal. As the ZDot grid is at the confocal focus plane, the true surface is determined because the grid is only in focus when the optics are in the correct position.

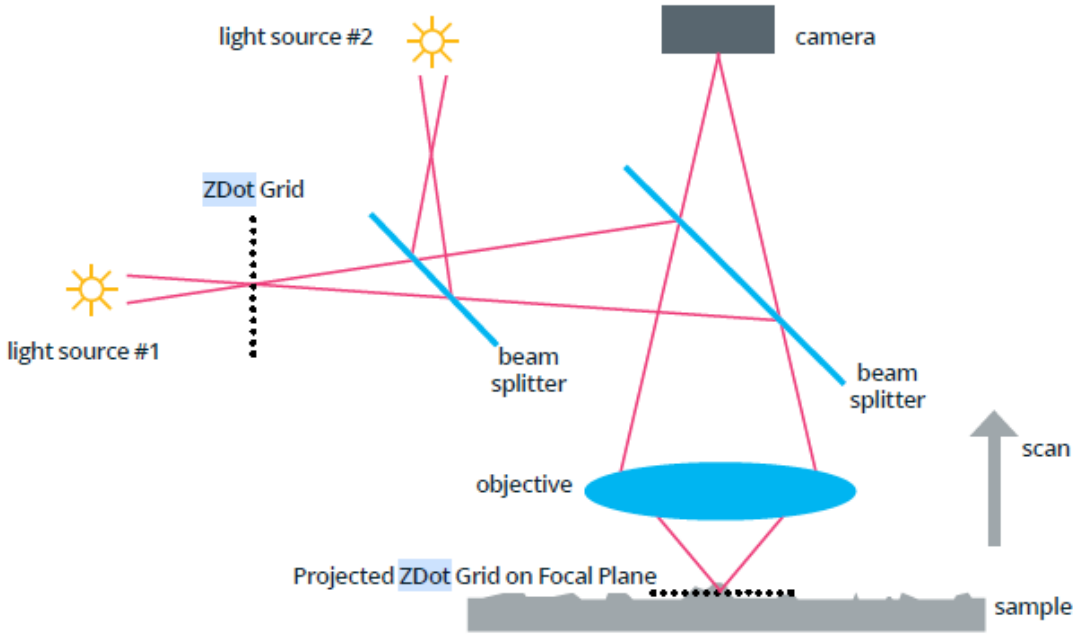

Figure 2.14. *Schematic diagram of a profilometer such as. Zeta-profilometer* [109,110]

Interferometry is a technique which uses the interference of electromagnetic waves to extract information for the measurement of microscopic displacements, refractive index changes and surface irregularities [95]. Figure 2.15 shows an example of a White Light Interferometry or Coherence Scanning Interferometry (CSI): Zygo NexView™ NX2 interferometer. The illumination is divided into two paths where one travels to a precision reference surface, and

the other travels to the test surface. The reflections from these two surfaces combine at a camera detector where they interfere with each other, and a pattern of light and dark intensities is created. That interference pattern represents the surface topography of the test surface [111–113].

Table 2.4 summarises key features and main applications of Optical Profilometry and Coherence Scanning Interferometer. Both optical profilometry (e.g. using Zeta-profilometer) and interferometry (e.g. using Zygo-interferometer) can be performed quickly and non-destructively *ex-situ* at any point in the manufacturing or development process [95,108–111].

In this thesis, Profilometry and Interferometry were evaluated to provide the roughness-thickness of surfaces-interfaces of 3D-printed samples (Chapter 5).

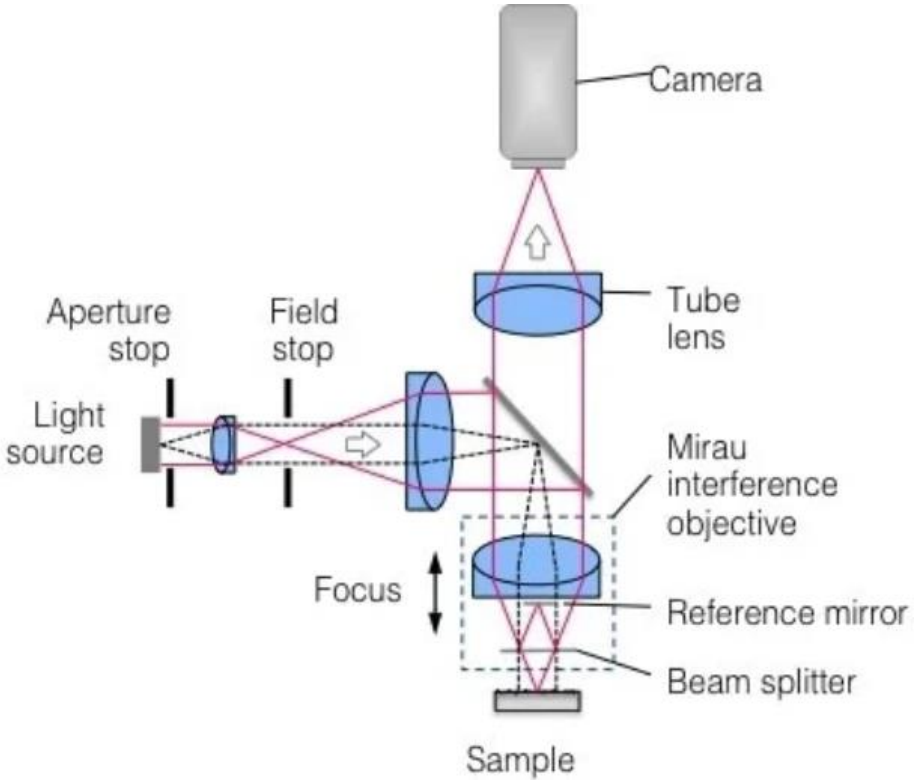

Figure 2.15. *Schematic diagram of an interferometer (e.g. CSI)* [95]

Table 2.4. Key features and main applications of Optical Profilometer (e.g. using Zeta-profilometer) and Coherence Scanning Interferometer (e.g. using Zygo-interferometer) [95,108–111]

Instrumentation	Key features	Main applications
Optical Profilometer	1) Improved optical resolution: The vertical resolution can be improved, for example, Zeta-profilometer can reach 0.013μm using the confocal ZDot™ grid (compared to 0.7 μm in typical optical microscopes); 2) True colour 3D imaging: The non-contact Zeta optical profiling combined with Å-level step height accuracy provide an infinite depth of focus, producing 3-dimensional images with all surfaces clearly displayed in sharp focus; 3) Multi-Mode Optics: ZDot technology can be enhanced further for better contrast imaging and film thickness measurement.	Zeta-profilometer can maximise the vertical resolution, so ZDot can help to achieve precise measurements of step height, film thickness, and roughness for use in materials development, device research, and manufacturing quality control.
Coherence Scanning Interferometer	1) High resolution with relatively large range: as an example, Zygo-interferometer can offer profile heights that vary from less than 1 nm up to 20000 μm; 2) High scanning speed with selectable monochrome and colour imaging mode: 1.9 million pixels are typically produced in a few seconds in this interferometer. 3) Consistent measurement: Sub-nanometre surface topography repeatability in Zygo-interferometer.	Zygo-interferometer can help to measure a wide range of surface types, including smooth, rough, flat, sloped, and stepped. Additional signal processing can be used to measure in the presence of transparent/ translucent optical films that confound other measurement methods (via ZYGO's Mx software).

2.6. METHODS TO INVESTIGATE THE ELEMENTS AND FUNCTIONAL GROUPS IN AM PRODUCTS

2.6.1. Infrared Spectroscopy

Among the widely molecular spectroscopic techniques (including ultra-visible, infrared, Raman), mid-infrared spectroscopy is based on the principle that the spectral frequencies are corresponding to the fundamental vibrations of the molecular bonds absorbing in the radiation region between 400 cm^{-1} and 4000 cm^{-1} (Figure 2.16). Changes in dipole moments yield qualitative and quantitative information of the samples and can be analysed by using functional group frequencies and the Beer-Lambert Law [114–117]

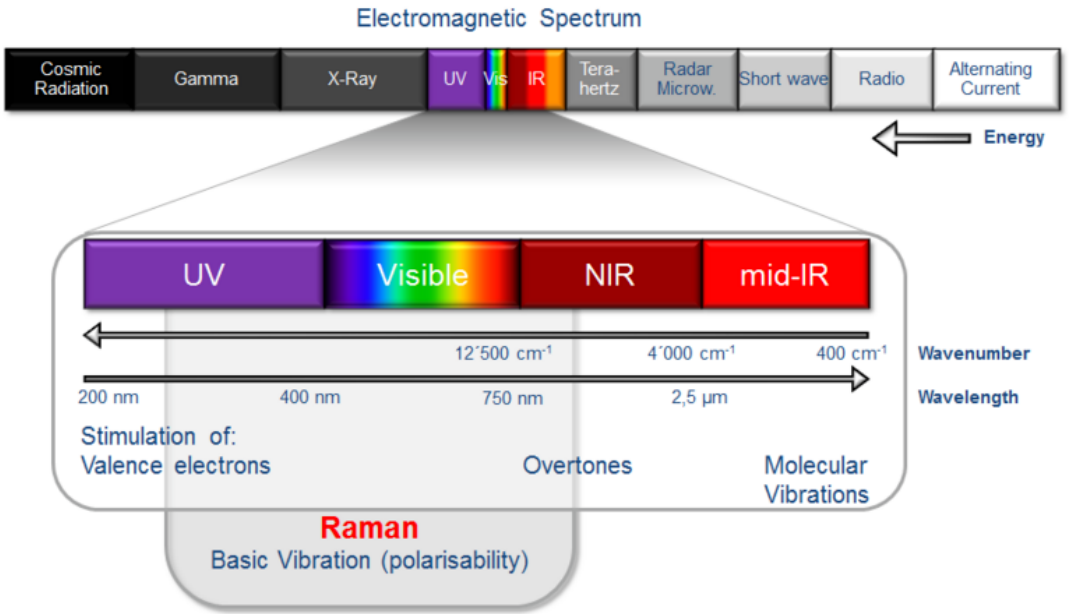

Figure 2.16. *Molecular spectroscopies at different wavelength including Ultraviolet (UV), Visible (vis), Near-infrared (NIR), Mid-infrared (mid-IR) and Raman spectroscopy* [117]

Although few Fourier-Transform Infrared (FT-IR) techniques have certain relative difficulties in sample preparation and interpretation of complex spectra, there are several advances in acquiring and processing data with the support of computer control. For example, FT-IR spectrometer having interchangeable sampling modules such as Transmission, DialPath, and Attenuated Total Reflectance (ATR) can enable high-throughput analyses (Figure 2.17).

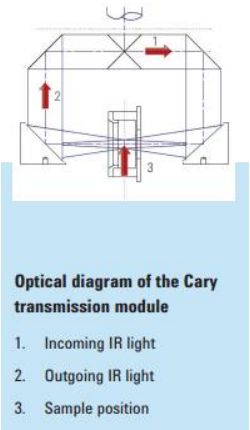

a) Transmission: allows for analysis using traditional techniques such as KBr pellets or salt discs (all required equipment and chemicals are available).

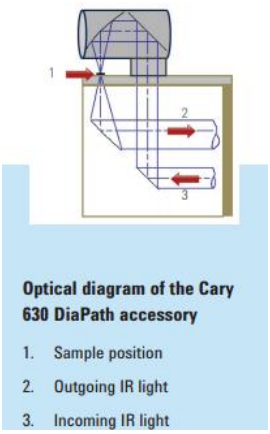

b) DialPath: for the analysis of liquid samples, even volatiles. Three switchable pathlengths means less time spent altering the concentration of samples.

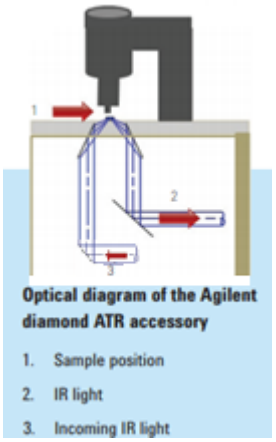

c) ATR: able to analyse most solids, powders and liquids with little to no sample preparation. Sample size needed is enough to cover a diamond window, approx. 2 mm.

Figure 2.17. *Agilent Cary 630 FT-IR spectrometer has interchangeable sampling modules: a) Transmission, b) DialPath, and c) ATR* [118–121]

Figure 2.18 illustrates basic components of one common FT-IR spectrometer, which include infrared (IR) source, polarizer, Attenuated Total Reflectance (ATR) crystal, and detector. The internal reflectance creates an evanescent wave protruding only few microns beyond the crystal surface, which means there must be good contact between sample and crystal surface. This technique requires little to no sample preparation, which is suitable for most solid and liquid materials [122]. Fourier-Transform Infrared (FT-IR) spectroscopy is generally used to analyse the chemical bonds in order to define the material structures (Figure 2.19). This technique can also help to compare samples, often to detect whether a bond is present in several samples [118–121].

In this thesis, FT-IR spectroscopy was used to reveal the potential chemical bondings in 3D-printed samples (Chapter 5).

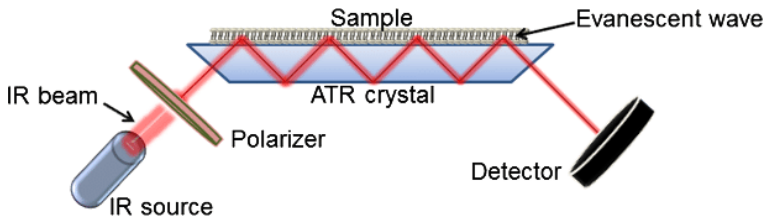

Figure 2.18. *Schematic diagram of ATR FT-IR spectrometer* [122]

a)

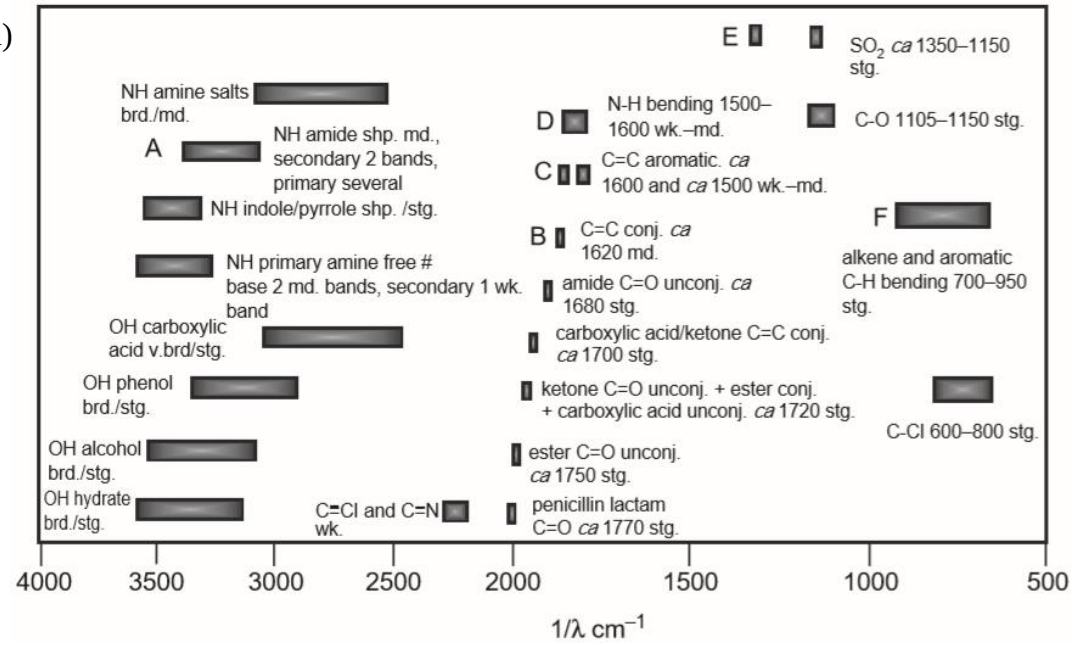

b)

Band	Comment
A	Restricted rotation about N–CO bond produces diastereomers, giving two bands in the case of secondary amides; see spectrum of phenoxymethyl penicillin
B	C=C unconjugated gives a very weak absorption but, when conjugated, the C=C bond gives a much stronger absorption, found typically in many steroids
C	C=C aromatic: the band at 1600 cm^{-1} may be weak unless the aromatic ring is substituted with polar substituents, e.g. a phenol, aromatic ether or aromatic amine free base
D	N–H bend is often obscured by stronger aromatic C=C stretching bands
E	SO_2 bands: although this absorption is in the fingerprint region, these bands are quite prominent in sulphonamides
F	C–H bending in many cases is not very distinctive in drug molecules because of the complexity of the fingerprint region

Figure 2.19. *FT-IR analysis with major bands (a) and data interpretation (b)* [114]

2.6.2. Secondary Ion Mass Spectrometry

Secondary Ion Mass Spectrometry (SIMS) is analytical technique using primary ion beam to remove parts of samples (typically under a high vacuum). The primary ion beam generates secondary ions, ionized atoms, and molecules (during sputtering process), which are then ejected from the chamber and conveyed into a mass spectrometer for analysis (Figure 2.20a-b) [123–127].

SIMS techniques can be categorised into two types: 1) "Static" SIMS: It uses a low primary ion dose (typically less than 10^{13} ions cm^{-2}) which removes only 1% of atomic sites from the sample surface; and 2) "Dynamic" SIMS: It removes relatively large amounts of material. At low primary ion doses, the chemical bonds (between molecular fragments) are more likely to be preserved, which enable "static" SIMS technique to obtain molecular data, especially mapping the distribution of elements, ions, and molecules in unknown samples [123]. "Dynamic" SIMS is ultilised to achieve high spatial resolution on distribution of element in the sample. One example of dynamic SIMS instruments is Nanoscale SIMS (NanoSIMS) with electrostatic and magnetic sector (as mass filter) that deflect ions into one stationary detector and six movable detectors (Figure 2.19c). This offers a total of seven species to be detected during each analysis, so it is necessary for NanoSIMS to decide a maximum of seven species for a single analysis time [123,126,128].

SIMS is commonly used in combination with a Time-of-Flight Secondary (ToF) analyser to achieve high spatial resolution and a fast acquisition rate [124–126]. Time-of-Flight Secondary Ion Mass Spectrometry (ToF-SIMS) comprises of the main components: 1) flood gun or gas cluster ion beam (GCIB column), 2) liquid metallic ion gun (LMIG column), 3) raster, 4) ToF analyser, 5) extractor, 6) reflector, and 7) detector (Figure 2.20c). In a typical dual-beam ToF-SIMS instrument, a primary ion gun is used to generate secondary ions for analysis, while a second "sputter" ion gun is used for depth profiling. Sputtering with the primary ion source yields charged secondary ions, which are then accelerated into the flight chamber [123,124].

In the ToF analyser, the mass of the secondary ions is determined by measuring their flight time to the detector after they are transferred to the mass spectrometer from point at the surface. After going through a mass analyser, the secondary ions will be separated towards

their mass-to-charge ratio (*m/z*) following their generation. Other types of mass analyser are magnetic sector and quadrupole; and each mass analyser has dissimilar benefits and drawbacks due to its mass resolving power, sensitivity, and duty cycle [126].

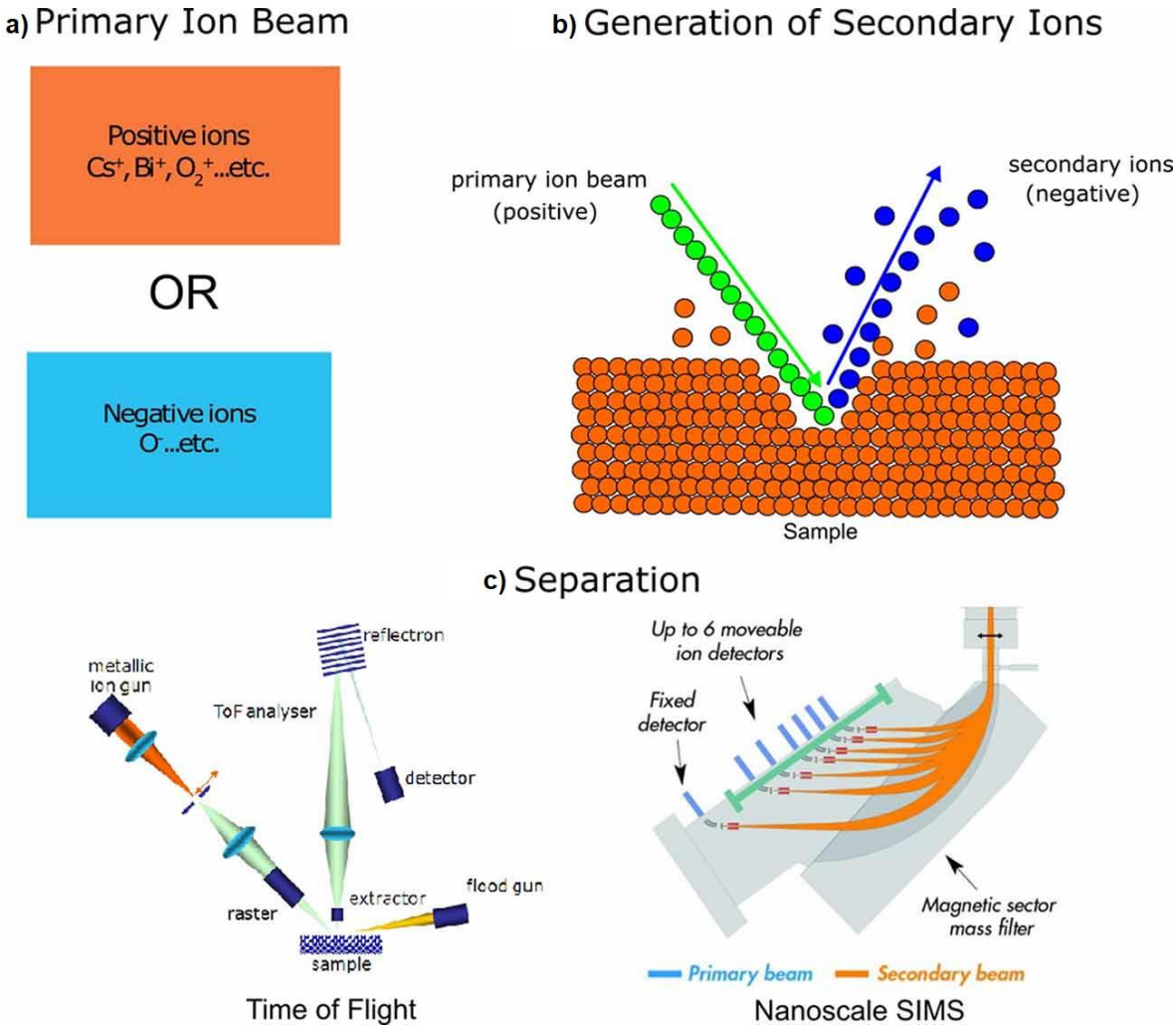

Figure 2.20. *Key features of Secondary Ion Mass Spectrometry (SIMS): a) Primary ion beam: It can made from either positive or negative ions; b) Generation of secondary ions: The primary ion beam strikes the analysis surface during sputtering, producing secondary ions; and c) Example of separation: Schematic diagram of ToF-SIMS and NanoSIMS instruments (modified from [123])*

The orbiSIMS is one of recent hybrid SIMS instruments that has an orbitrap™ analyser (Thermo Fisher Scientific, Germany) incorporating to a ToF-SIMS instrument (IONTOF GmbH, Germany). Figure 2.21a shows the usage of a focused dual beam and dual analyser

in orbiSIMS, which can implement MS on secondary ions by fragmenting them in a collision gas cell (MS/MS) to provide structural assignments. There are four main methods including Surface spectra, Depth profiling, 2D imaging, and 3D imaging (Figure 2.21b). Compared to conventional LMIG-ToF, the GCIB-Orbitrap can offer exceptionally accurate high-mass resolving power spectral analysis, which make it become more competitive for molecular technique [129].

More advances in SIMS will enable more promising methodologies for material and health sciences in terms of identifying and enhancing new structures and metabolism [125–127]. Table 2.5 summarises the key features of common SIMS techniques with specific primary ion source and the condition for acceleration of secondary ions, which result in differences in spatial resolution, mass resolution (or mass-resolving power), upper mass limit, and mass accuracy (or sensitivity) [123–127]. For example, ToF-SIMS and orbiSIMS can reveal distinct intensities for each material, which is useful in chemical identification. Although Matrix Assisted Laser Desorption/Ionisation combined with Mass Spectrometry (MALDI-MS) is not strictly a SIMS technique, it can be used for imaging and identifying chemical structures. Therefore, MALDI-MS will be included here in the comparison with NanoSIMS, ToF-SIM, and orbi-SIMS for imaging the targeted samples [126].

In this thesis, ToF-SIMS and OrbiSIMS were used to investigate the chemical changes of 3D-printed samples (Chapter 5 and 6).

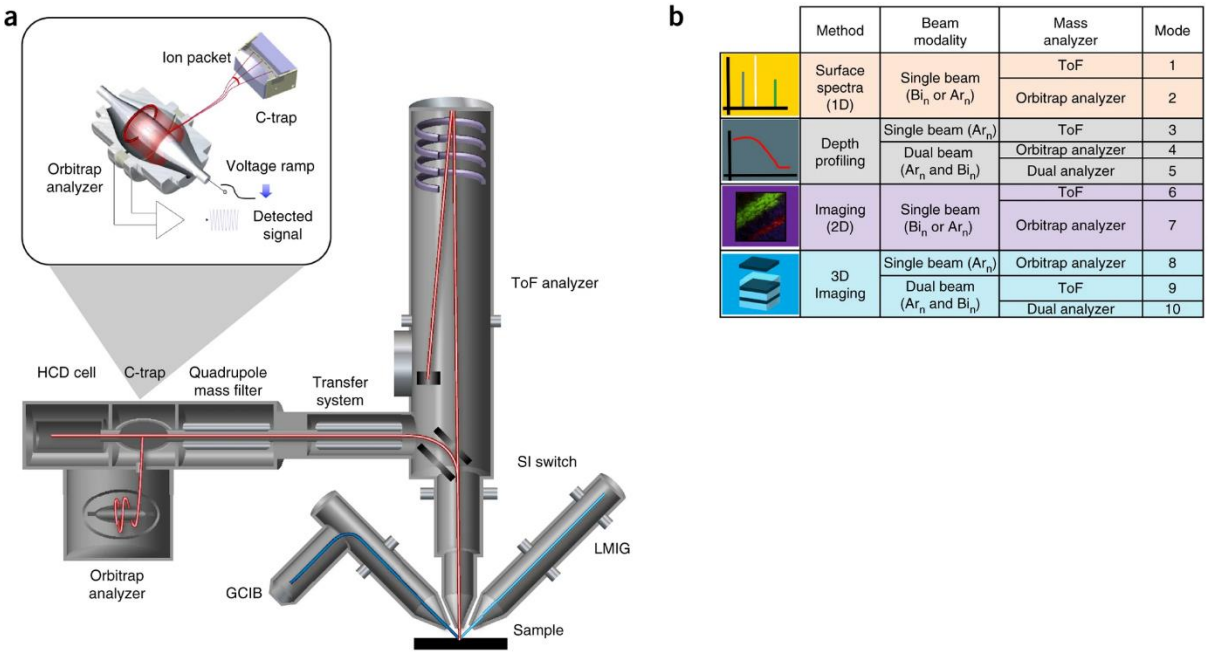

	Method	Beam modality	Mass analyzer	Mode
	Surface spectra (1D)	Single beam (Bi_n or Ar_n)	ToF	1
			Orbitrap analyzer	2
	Depth profiling	Single beam (Ar_n)	ToF	3
		Dual beam (Ar_n and Bi_n)	Orbitrap analyzer	4
			Dual analyzer	5
	Imaging (2D)	Single beam (Bi_n or Ar_n)	ToF	6
			Orbitrap analyzer	7
	3D Imaging	Single beam (Ar_n)	Orbitrap analyzer	8
		Dual beam (Ar_n and Bi_n)	ToF	9
			Dual analyzer	10

Figure 2.21. *Recent hybrid SIMS instrument: a) Schematic diagram of orbiSIMS instrusment, and b) Four main methods including Surface spectra, Depth profiling, 2D imaging, and 3D imaging (modified from* [129]*)*

Table 2.5. Comparison between several types of SIMS analyses including MALDI-MS, NanoSIMS, ToF-SIM, and orbiSIMS (modified from [123–127])

Technique	Primary ion source - The condition for acceleration of secondary ions	Spatial resolution	Mass resolution (M/ ΔM)	Mass accuracy (or sensitivity)	Note
Matrix Assisted Laser Desorption/ Ionisation, (MALDI) combined with Mass Spectrometry	Laser light - Matrix	1-150 µm (typically 10 µm)	>1000000 (using FT ion cyclotron resonance mass spectrometry)	Low sensitivity for those *m/z* < 200	Dynamic mode
Nanoscale Secondary Ion Mass Spectrometry (NanoSIMS)	Ion beam (Cs^+ or O^-) - A magnetic separation (using a quadrupole)	< 50nm (Cs^+) < 200nm (O^-)	10000	Medium sensitivity	Only dynamic mode
Time of Flight Secondary Ion Mass Spectrometry (ToF-SIMS)	Ion beam (Bi_n^+, Cs^+, C_{60}^+, Ar+, Ar_n^+, etc.) - A flight chamber	200nm-5µm High-speed ToF-imaging	>10000 Lower mass-resolving power	High sensitivity (20 ppm)	Static mode, Dynamic mode
orbiSIMS (which is the ToF-SIMS instrument combined with OrbiTrap™ analyser)	Ion beam (Bi_n^+, Cs^+, C_{60}^+, Ar+, Ar_n^+, etc.) - A flight chamber and Orbitrap™	Few nm to µm Lower-speed ToF-imaging	High mass-resolving power (>240000) for a peak of *m/z*=200	High sensitivity (ppm to ppb)	Static mode, Dynamic mode

2.7. METHODS TO INVESTIGATE THE PHYSIOCHEMICAL PROPERTIES OF INK FORMULATION (BEFORE INK-JETTING)

There are dissimilar physiochemical properties that can affect the droplet ejection in ink-jet 3D-printing, which needs a suitable analytical approach for clarification and optimisation.

2.7.1. Rheology Measurement including Surface Tension & Viscosity Measurements

Surface tension can be determined as the energy or work required to increase the surface area of a liquid due to intermolecular forces. For example, surface tension results from the greater attraction of liquid molecules to each other (due to cohesion) than to the molecules in the air (due to adhesion) at liquid–air interfaces. Figure 2.22 shows an example of surface tension in the complex of soil mineral-water-vapor [130]. The surface tension influences the liquids' behaviour in terms of wetting/wettability, dispersions/dispersibility, and droplet size [130–132].

Along with surface tension, viscosity is defined by the internal frictional force between adjacent layers of fluid that are in relative motion. The fluid's state such as its temperature, pressure, and rate of deformation can affect the viscosity. Rheology measurement is an identification of the fluid's resistance to deformation at a certain rate, and rheometer, viscometer, or other techniques can help to measure these parameters [133,134].

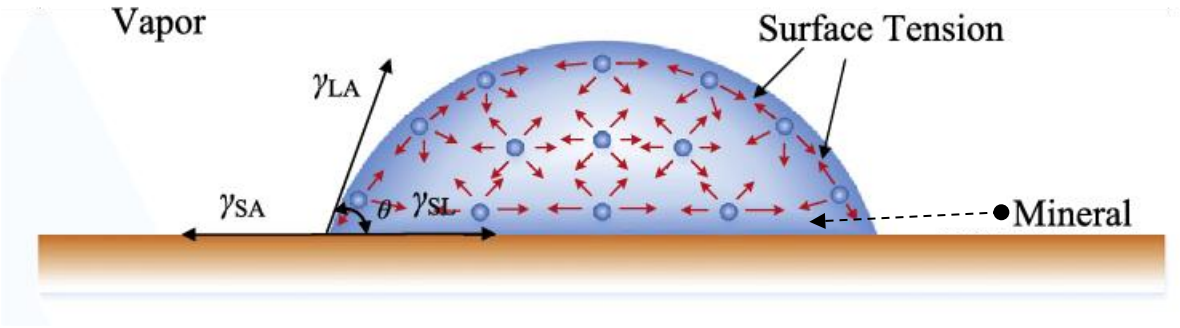

Figure 2.22. *An example of surface tension in the complex of mineral–water–vapor* [130]

The characterisation of these fluid properties can help to predict droplet ejection of ink formulations enabling high performance of inkjet printing [132]. For instance, Zhou *et al.* used the liquid handler instrumentation that comprised of eleven fundamental components [132,135]: A) Pipetting arm; B) Deck; C) Loading tray; D) Front cover; E) Waste slides for CO-RE head tips; F) Waste attachment for CO-RE head tips; G) Pipetting channel, CO-RE head; H)

Carrier for microplates, tips; I) Carrier for tubes; J) Autoload unit and barcode reader; and K) Waster container for pipetting channel tips (Figure 2.23).

In this thesis, rheology measurement including surface tension and viscosity measurements were used to investigate the printability of ink formulations (Chapter 5).

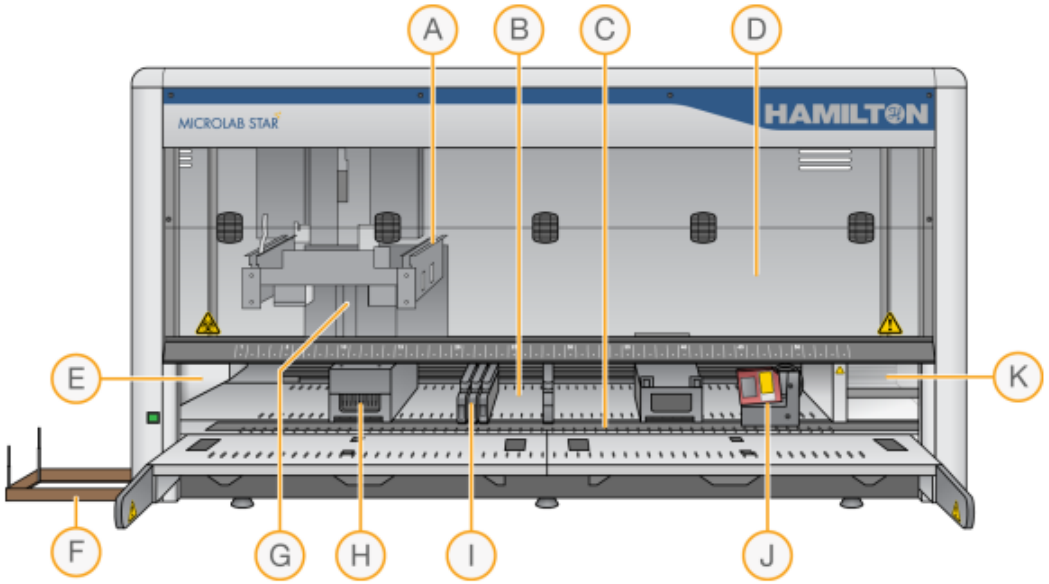

A Pipetting arm
B Deck
C Loading tray
D Front cover
E Waste slide for CO-RE head tips
F Waste attachment for CO-RE head tips
G Pipetting channel, CO-RE head
H Carrier for microplates, tips
I Carrier for tubes
J Autoload unit and barcode reader
K Waste container for pipetting channel tips

Figure 2.23. *Schematic diagram of a liquid handler* [135]

2.7.2. Contact Angle Measurement

The contact angle (θ) is the angle at which the solid–liquid interface meets liquid–vapor interface and Figure 2.21 also gives an example of contact angle. The Young's equation shows relationship between the contact angle and interfacial energy [136,137]:

$$\gamma_{SG} = \gamma_{SL} + \gamma_{LG} \cos(\theta)$$ Equation 2.2

where γ_{SG} is the interfacial energy between the solid and gas phases, γ_{SL} the interfacial energy between the substrate and the liquid, γ_{LG} is the interfacial energy between the liquid and gas phases, and θ is the contact angle between the solid–liquid and the liquid–gas interface.

According to Young's equation (Equation 2.2), the contact angle has an inverse correlation of wettability of a solid surface by a fluid. Particularly, a small contact angle (as $0° < \theta < 90°$) relates to high wetting of the surface, where the fluid will spread over a great area of the surface. Otherwise, a large contact angle (as $90° < \theta < 180°$) indicates low wetting of the surface, where the fluid will reduce contact with the surface and form a compact liquid droplet. The fluid will wet the substrate completely at $\theta = 0°$ and will not wet the substrate at all at $\theta = 180°$ [136,137].

At a given temperature and pressure, there is usually a unique equilibrium contact angle reflecting the relative strength of the liquid, solid, and vapour molecular interaction. It will depend on the nature of the liquid and solid in contact, particularly the changes of surface energy. In general, the major interactions holding the solid substrate together will imply the energy of the bulk component. For example, low-energy substrates are held together by forces (such as van der Waals and hydrogen bonding) whereas high-energy substrates are held together by bonds (such as covalent, ionic, and metallic bonds). Hence, compared to low-energy substrates, high-energy substrates can be wetted easily, which means more complete wetting will occur if the substrate has a much higher surface energy than the liquid [136,138].

There are divergent techniques to measure the contact angles, and one of them is Drop Shape Analysis (DSA) which is recently applied in the investigation of new ink formulation additive manufacturing [132,139]. Figure 2.24 shows Drop Shape Analysis instrumentation with eight basic components: 1) Light source, 2) Diffuser, 2) Syringe, 3) Motor, 4) Controller, 5) Microscope, 6) CCD Camera, 7) Host computer, and 8) Additional parts such as Inverted Cuvette for Sessile Drop and Temperature Cell for Pendant Drop [140].

DSA can identify the contact angle from the shadow image of a sessile drop and the surface tension or interfacial tension from the shadow image of a pendant drop. As an example, DSA instrument from KRÜSS GmbH has different operation methods (Figure 2.25): a) Sessile Drop, b) Advancing Angle, c) Receding Angle, d) Captive Bubble, e) Dynamic Contact Angle, and f) Pendant Drop [139–141].

In this thesis, contact angle measurement was used to investigate the wettability of ink formulations on tested substrates (Chapter 5).

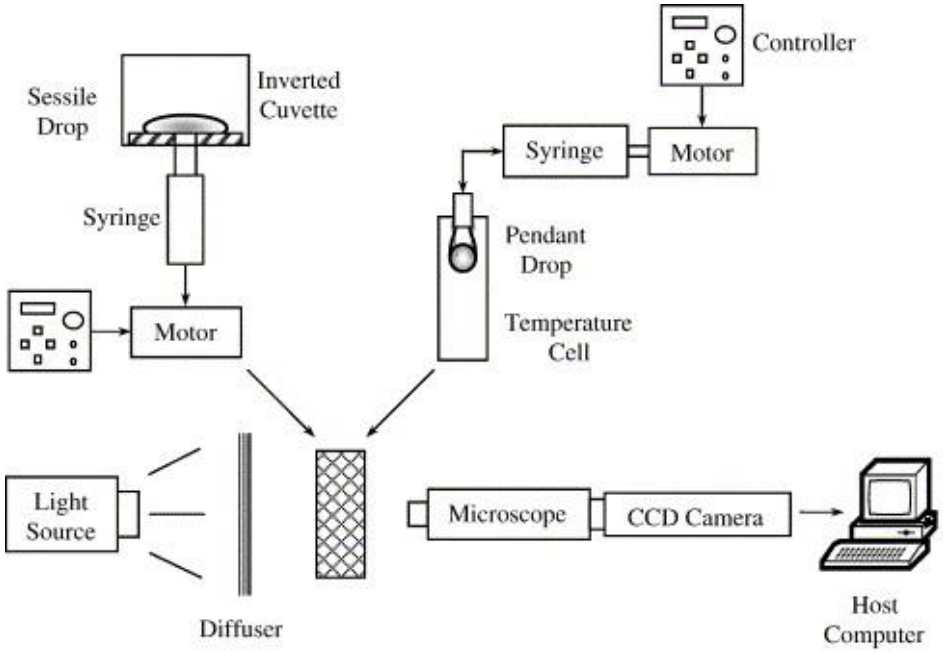

Figure 2.24. *Schematic diagram of Drop Shape Analysis instrumentation to measure the contact angles of sessile drop or pendant drop* [140]

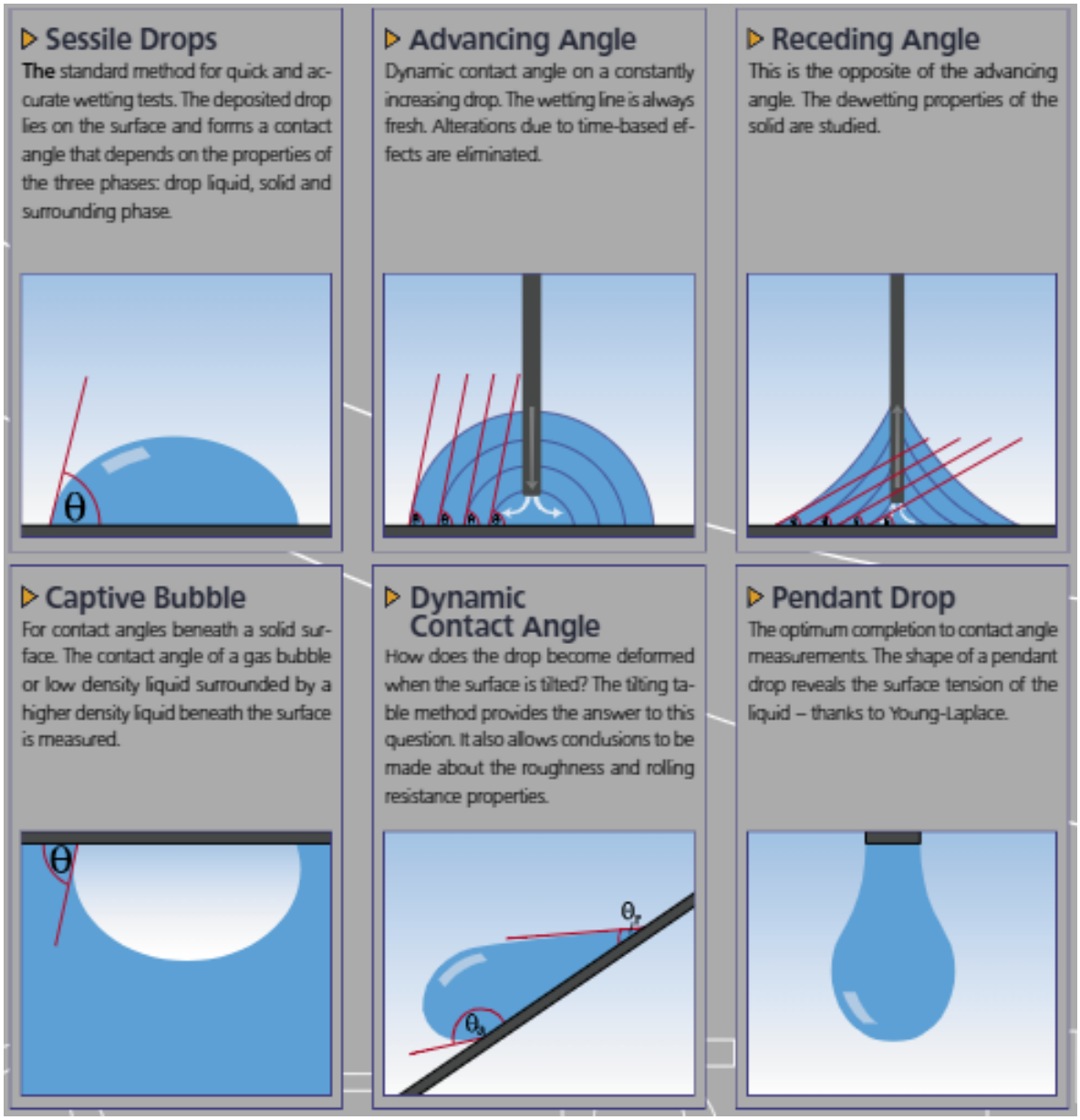

Figure 2.25. *Example of one DSA instrument (from KRÜSS GmbH) having different operation methods: a) Sessile Drop, b) Advancing Angle, c) Receding Angle, d) Captive Bubble, e) Dynamic Contact Angle, and f) Pendant Drop* [139]

2.7.3. Elemental analysis or CHNX analysis

The elemental analyser or CHNX analyser can be used to determine the mass fractions of carbon (C), hydrogen (H), nitrogen (N), and halogen (X) in the sample. Normally, a few milligrams of samples are requested but it can be adjusted according to the nature of sample and instrument, for example, larger amount will be useful for analysis due to the heterogeneity of the sample. A range of sample forms such as liquid, solid, or volatile

can be handled across the fields including pharmaceuticals, food, engineering, and energy [142,143].

The elemental analysis is commonly based on (flash) combustion of the sample that results in an instantaneous oxidisation into simple compounds. Then, those compounds will be detected by thermal conductivity detection or infrared spectroscopy [143,144]. As an example, Figure 2.26 illustrates CE-440 Elemental Analyser (from the manufacturer Exeter Analytical) that comprised of: 1) Scrubbers (for oxygen and helium), 2) Combustion, 3) Reduction, 4) Mixing volume, 5) Pressure Transducer, 6) Sample volume, 7) Traps (for CO_2, H_2O), 8) Detector Block (for C, H, N), and 9) Controller (PC and incorporated system) [145].

In this thesis, CHNX analysis were used to validate the fundamental elements (C, H, N) of the original inks before ink-jet 3D-printing (Chapter 5).

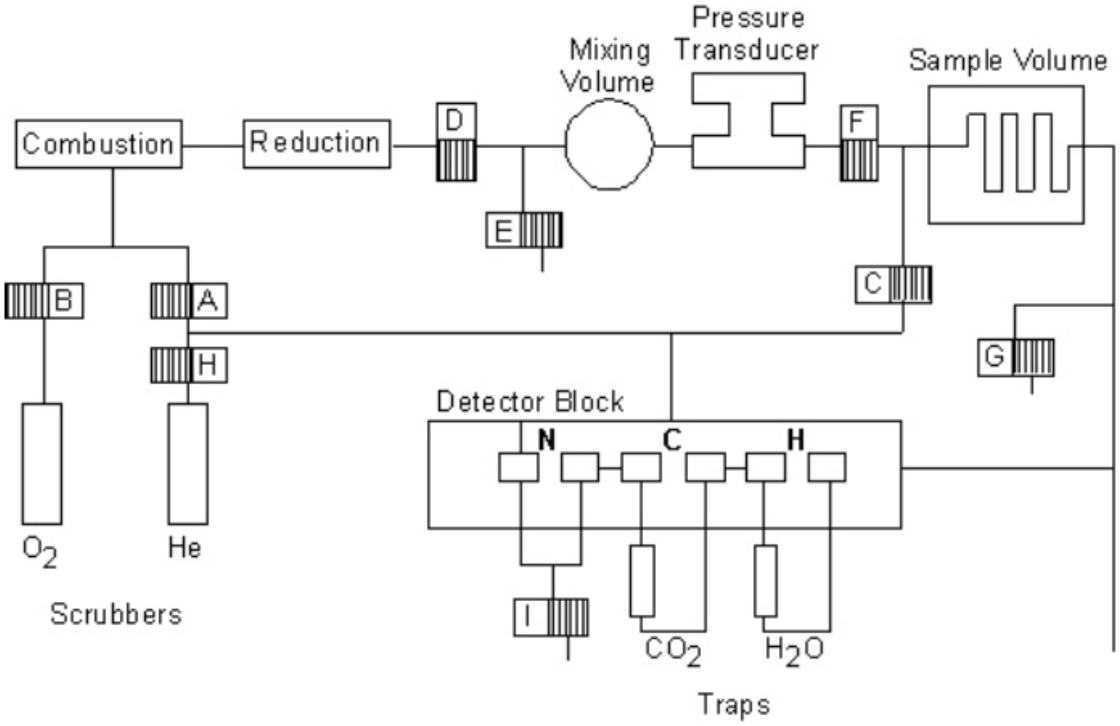

Figure 2.26. *Schematic diagram of CE-440 Elemental Analyser (Exeter Analytical)* [145]

2.7.4. Nuclear Magnetic Resonance Spectroscopy

Nuclear Magnetic Resonance (NMR) Spectroscopy is an analytical technique focusing on the interaction of an externally applied radiofrequency radiation with atomic nuclei. A net

exchange of energy will cause a change in an intrinsic property of the atomic nuclei (known as nuclear spin) during this interaction. A quantum number (I) will define the nuclear spin, which varies according to the isotope under consideration. Only atomic nuclei with I = 1,2,3... (NMR-active component such as ^{1}H, ^{13}C and ^{15}N) can be detected in NMR spectroscopy [146,147].

Nuclear spins of some NMR-active nuclei (also known as magnetic dipoles) can change into two different orientations, aligning with external magnetic fields (B_0). Figure 2.27a represented these two orientations: 1) The first orientation relates to the lowest energy level of the nucleus (which is parallel to the external magnetic field), and 2) The second orientation relates to the highest energy level of the nucleus (which is antiparallel to the external magnetic field). Figure 2.27b shows the tranisitions between energy levels (ΔE) is based on the magnetic field and the magnetogyric ratio, which can affect the sensitivity of NMR technique.

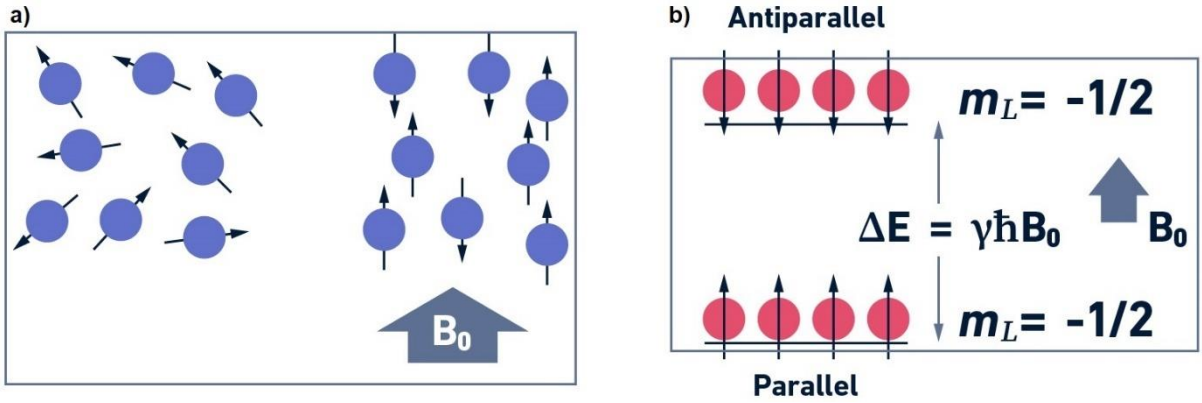

Figure 2.27. *Distribution of NMR-active nuclei: a) Two different orientations of nuclear spins (parallel and antiparallel to the external magnetic field B_0); and b) Nuclear spin transits to two possible energy levels (in nuclei with I = ½) (modified from* [148])

During the magnetic resonance (known as the irradiation process of nuclei with radiofrequency), these nuclear magnetic dipoles will not statically align with the magnetic field B_0. They will move like a spinning top around an axis that is parallel to the direction of the field (Figure 2.28a). The frequency of this precession movement, called Larmor frequency (vL) can be defined by the magnetogyric ratio and the magnetic field [146,147].

To achieve the resonance of nuclear spins, a magnetic pulse with frequencies close to the Larmor frequency can be applied perpendicular to B_0, generating a non-zero component (μ_{xy}). A relaxation process takes place after this pulse, and the μ_{xy} component gradually comes back to its net value of zero (Figure 2.28b). The energy will be emitted as radiofrequency due to this relaxation, offering a Free Induction Decay (FID) which is detectable. This distinctive signal FID is then converted into a plot of intensities versus frequencies, which is known as an NMR spectrum.

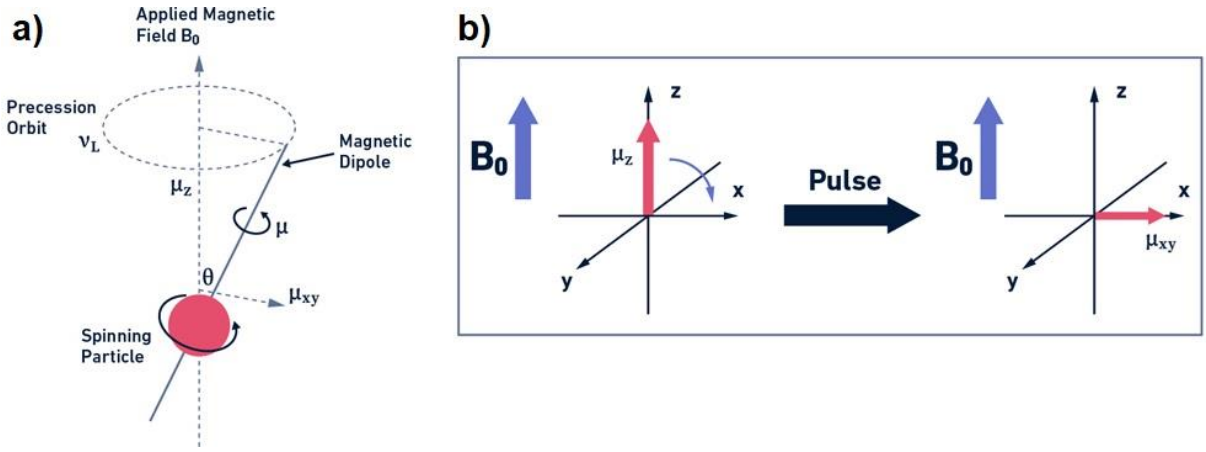

Figure 2.28. *Nuclear spin behavior: a) Under the influence of an external magnetic field; and b) Scheme of a basic NMR experiment in which the magnetization is transferred to the xy plane upon the application of a magnetic pulse (modified from* [148])

A typical NMR spectrometer will include the following fundamental parts [149]: 1) Vacuum Chamber, 2) Liquid Tanks such as Nitrogen Tank and Helium Tank, 3) Coil system including Radio Frequency Coils (Transmitter/Receiver), 4) Superconducting Solenoid, 5) Removable Probe, 6) Tuning Capacitors, 7) NMR Sample Tube, 8) Detector system including RF Detector, A/D Converter, and Preamplifier (PREAMP), and 9) Controller system including Computer, Pulse Programmer, and Pulse Amplifier (Figure 2.29). Because the Larmor frequency depends on the intensity of the magnetic field varying from instrument to instrument, so a mathematical transformation will be executed to provide a relative magnitude called chemical shift (δ) [150–152]. Figure 2.30 and 2.31 shows typical chemical shifts in ^{1}H NMR and ^{13}C NMR, which enable the NMR fingerprint analysis, the

determination of new compounds, and the investigation of dynamic interactions in multi-disciplinary sectors [148], [153].

In this thesis, NMR spectroscopy (with ^{1}H NMR and ^{13}C NMR) were used to reveal the chemical compositions of the original inks before ink-jet 3D-printing (Chapter 5).

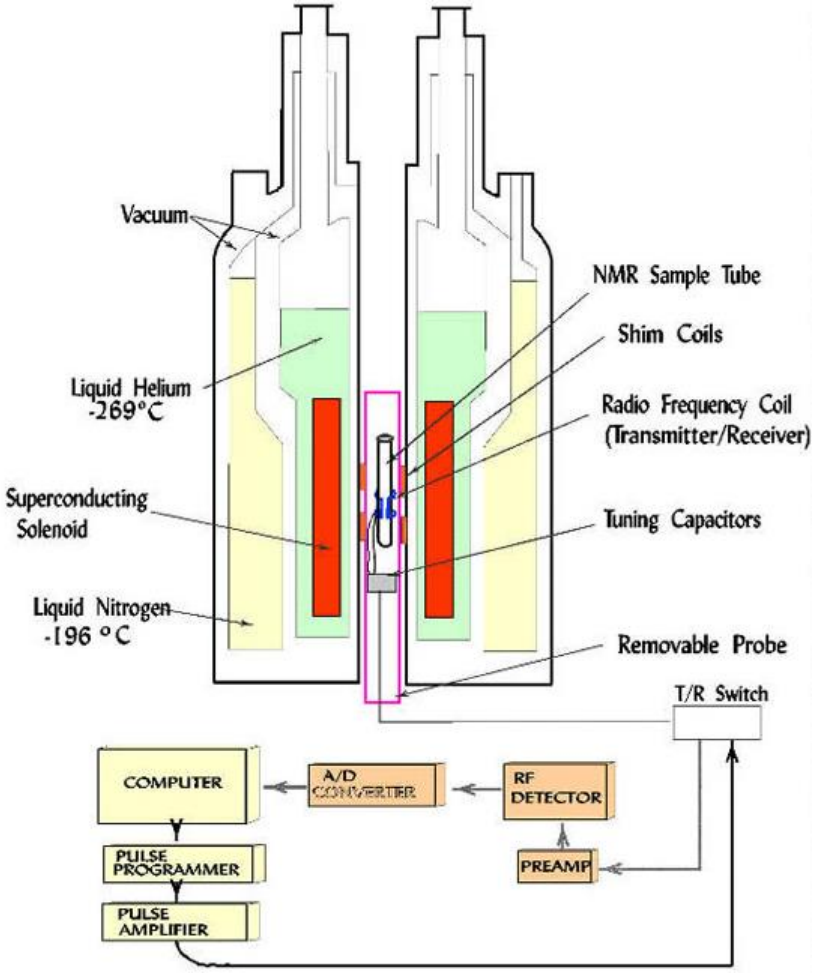

Figure 2.29. *Schematic diagram of an NMR spectrometer* [149]

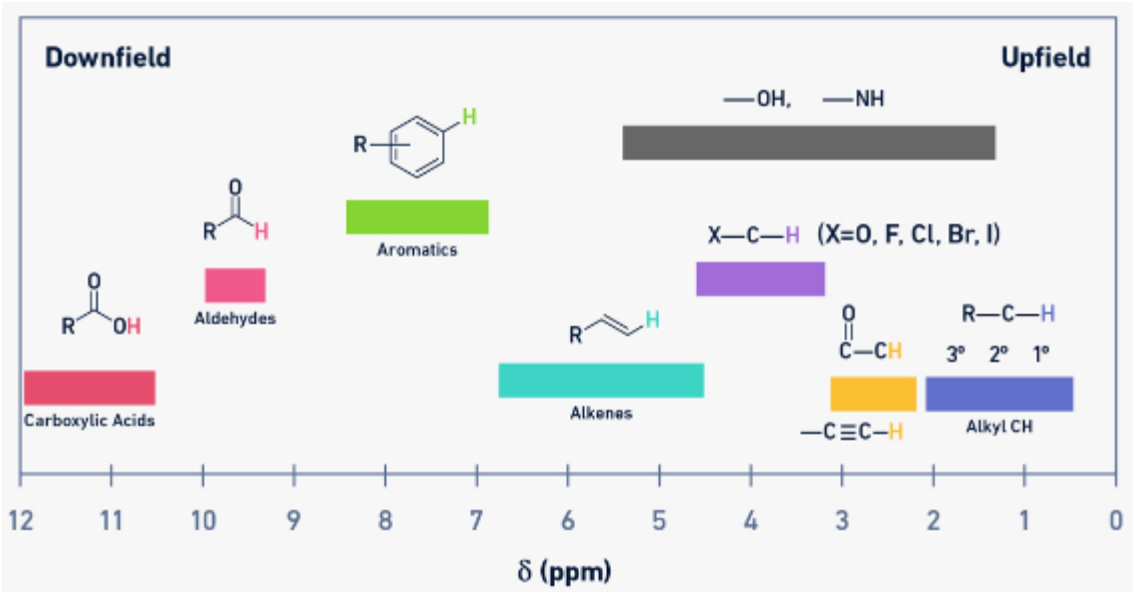

Figure 2.30. *Typical chemical shifts in ^{1}H-NMR* [148]

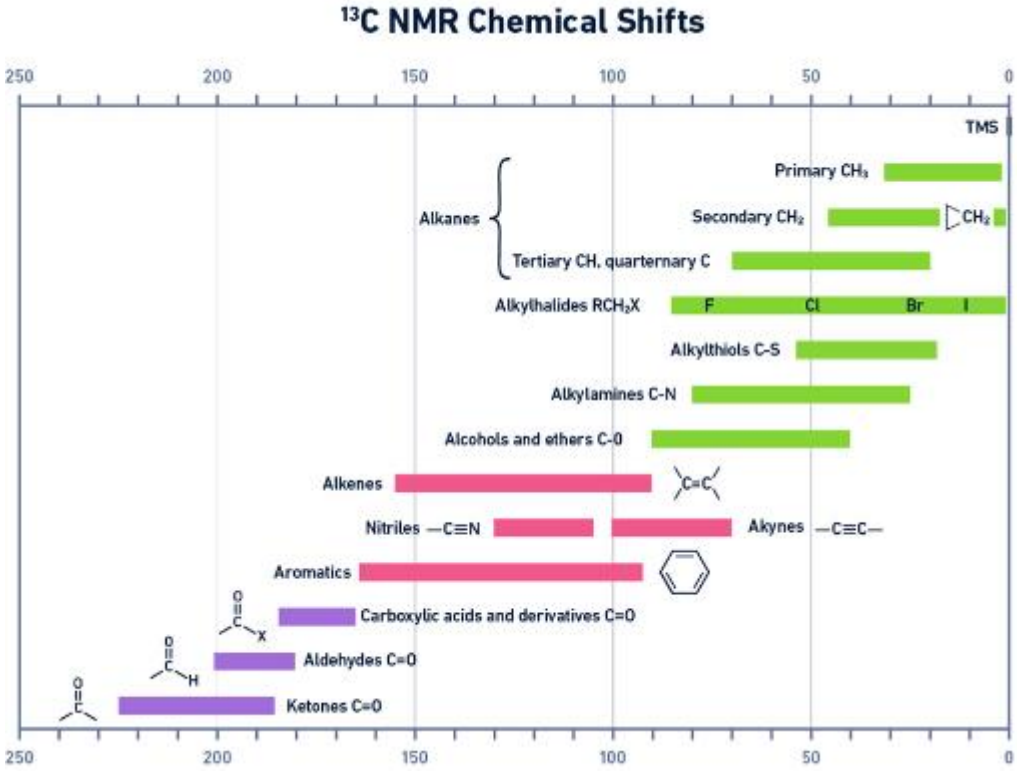

Figure 2.31. *Typical chemical shifts in ^{13}C-NMR* [148]

2.7.5. Inductively Coupled Plasma Optical Emission Spectroscopy

Atomic Emission Spectroscopy (AES) is a chemical analysis using the intensity of light emitted from a flame, plasma, or spark at a specific wavelength for the quantification of an element in a sample. Particularly, Inductively Coupled Plasma Atomic Emission Spectroscopy (ICP-AES) or Inductively Coupled Plasma Optical Emission Spectroscopy (ICP-OES) uses the inductively coupled plasma to produce excited atoms and ions, which can emit electromagnetic radiation respectively. The plasma is a high temperature source (from 6000 to 10000 K) of ionised source (Argon) that offer the complete atomisation of the elements in a sample and minimise the potential chemical interferences. The plasma is maintained by inductive coupling from electrical coils at megahertz frequencies [154,155].

Figure 2.32a demonstrates the plasma generation in the ICP torch [156,157]: 1) The injector tube (with typical aperture of 1–2 mm) introduces the sample into the plasma, and the sample aerosol can be emitted and strike a hole into the centre of the plasma; 2) The auxiliary tube provides gas flow elevating the bottom of the plasma from the injector tube; and 3) A tangential cool gas flow will be introduced between the auxiliary tube and the outer tube, which contains the plasma and keeps it away from the outer torch tube, protecting it from melting down.

After the sample is introduced into the plasma, the spectrometer (typically optical system in ICP-OES) will be used to separate specific wavelengths and direct the resolved light towards the detector. The spectrometer includes two sections: 1) the fore-optics, and 2) a mono- or polychromator. When the light exits the mono- or polychromator, it is focused onto the detector and the resulting signals are administered to quantify the elemental composition (Figure 2.32b) [156,157].

The principle of ICP-OES is each element emits energy at certain wavelengths (peculiar to its atomic characteristics). The concentration of targeted element is proportional to the intensity of the energy emitted at the chosen wavelength. It is common to select a single or a very few wavelength(s) for a given element although each element emits energy at multiple wavelengths in ICP-OES. Therefore, the determination of the intensities (of the emissions at those wavelengths) can clarify the elements in the testing samples (if there is an appropriate reference standard) [154–158].

In this thesis, ICP-OES were used to identify the additional elements (if existed) of the original inks before ink-jet 3D-printing (Chapter 5).

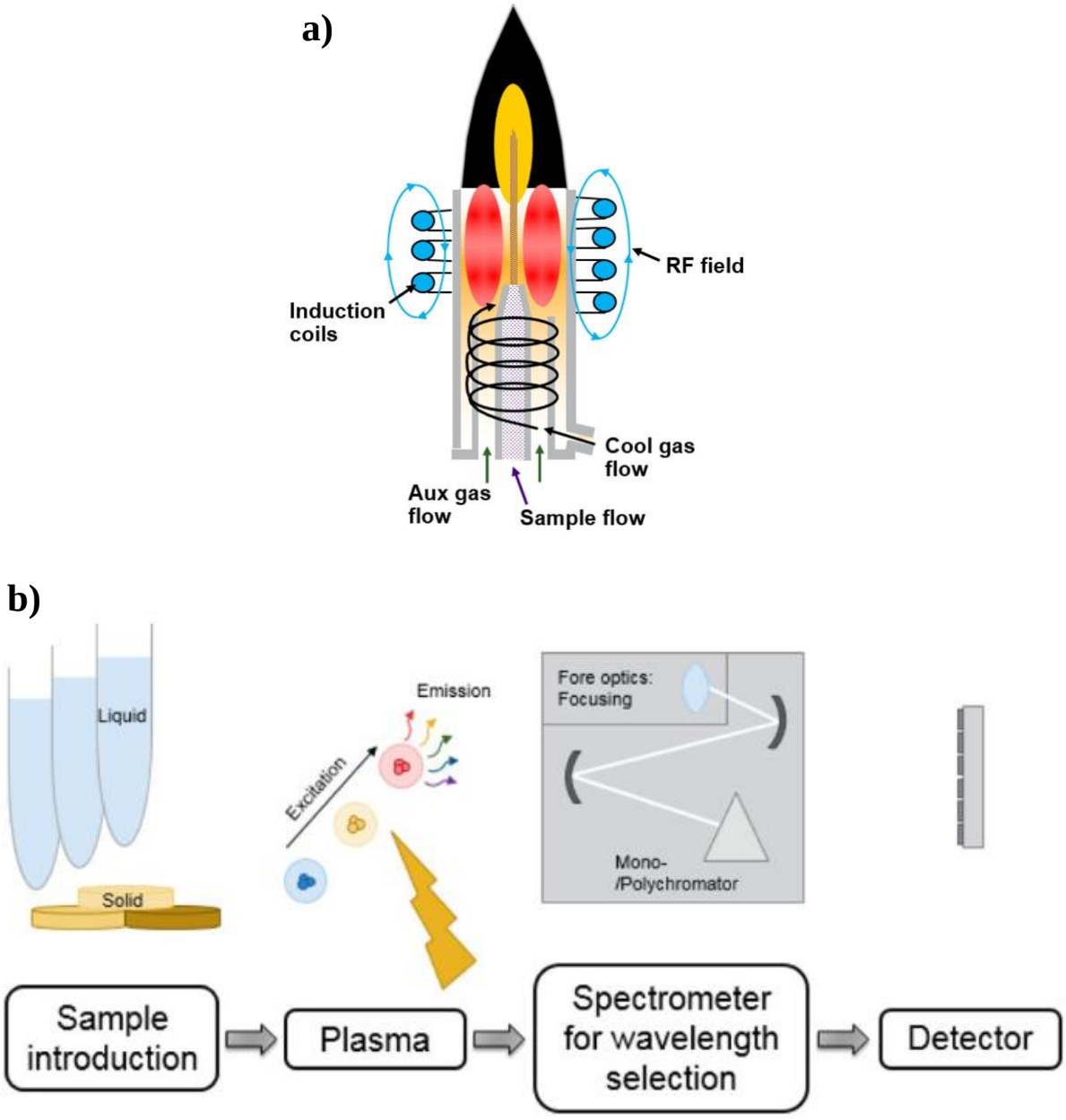

Figure 2.32. *The principle of Inductively Coupled Plasma: a) Generation of the plasma in ICP torch; and b) Schematic diagram of ab ICP-OES spectrometer* [156,157]

2.7.6. Inductively Coupled Plasma Mass Spectroscopy

Among elemental analysis technologies, Inductively Coupled Plasma Mass Spectroscopy (ICP-MS) can detect most of elements in the periodic table by using very small amounts of samples (such as milligram to nanogram per litter) [159–161].

The Inductively Coupled Plasma (ICP) is an ionisation source that can fully decompose a testing sample into the constituent elements before transforming those elements into ions. Argon gas is usually applied to generate the plasma, and the energy can be "coupled" to it via an induction coil or load coil. By a Radio Frequency (RF) generator, the plasma is sustained throughout very high-temperature plasma (up to 10000 K). At this high temperature, most elements of the sample can easily change from atoms to ions, which are then transferred to the mass analyser via a vacuum interface. After being separated, the ions are detected by the detection system (which will be either Faraday Cups or Electron Multipliers) [159–161]. Figure 2.33 shows the typical ICP-MS spectrometer with seven principal components: 1) Sample Introduction System; 2) Plasma (via Concentric Torch and RF Coil), 3) Vacuum Interface; 4) Ion optics (with photo stop), 5) Collision/ Reaction Cell (CRC), 6) Mass Analyser (as quadrupole type), and 7) Ion detection system (such as Scanning Electron Multiplier as detector) [161]. ICP-MS instrumentation can vary in design because of its exclusive applications in terms of chemical purities, material analysis, and clinical research. For instance, ICP-MS can be used in recent research in medical and electrochemical sciences [162,163].

Table 2.6 represents the advantages and disadvantages of using ICP-OES compared to ICP-MS [157]. For example, both ICP-OES and ICP-MS have the sample introduction system and plasma in atmospheric pressure, but ICP-MS requires the operation of the ion optics, ion separation, and ion detection in high vacuum. Therefore, running samples in ICP-MS can be more expensive than ICP-OES [160–163].

In this thesis, ICP-MS were used to identify the additional elements (if existed) of the original inks before ink-jet 3D-printing, particularly when the element concentration was very small and could be out of the detection limit of the ICP-OES (Chapter 5).

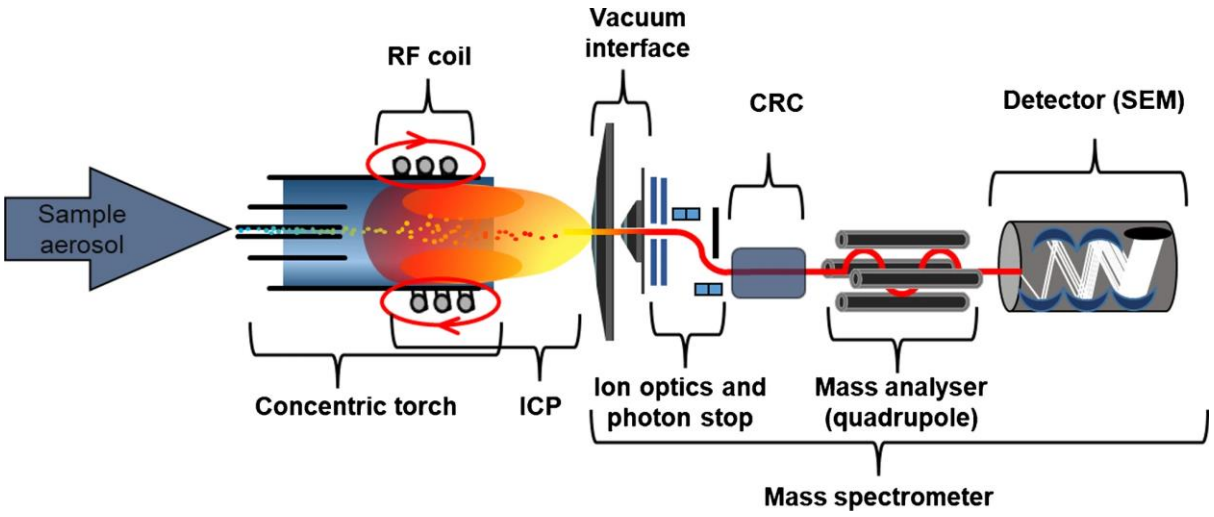

Figure 2.33. *Schematic diagram of ICP-MS spectrometer* [163]

Table 2.6. Comparison between ICP-OES and ICP-MS [157,160–163]

System	Benefits	Drawbacks
ICP-OES	• Sample throughput (can run over night, simultaneous measurement of all elements at all wavelengths • Good detection limits (especially when considering speed compared to Furnace AA) • Excellent precision • Excellent LDR • Can handle complex matrices (e.g., high TDS) • Uses inert gas (AR) • Easy routine operation	• Sample introduction techniques can add to analysis time (and cost). • Requires large amounts of sample • Prone to interferences (Physical and Spectral) • Correction can get complex • Requires ventilation • Plasma must be optimized for organics/petrochemical products • Can be difficult to maintain
System	**Benefits**	**Drawbacks**
ICP-MS	• Excellent detection limits • Sample throughput (Can run overnight, Simultaneous measurement of all elements • Excellent LDR • Capable of isotopic analysis • Uses small amounts of sample • Uses inert gas	• Cost • Environmental considerations (Clean lab)

CHAPTER 3: INVESTIGATION OF THE ENHANCED ANALYTICS IN SUSTAINABLE PHARMACEUTICAL SUPPLY CHAINS FOR POINT OF CARE MANUFACTURE CENTRED ON CONSIDERATION IN THE UK PHARMACEUTICAL SECTOR

3.1. INTRODUCTION

The first 3D-printed object was a tiny cup for eye wash (invented by Chuck Hill, US patent 4575330 in 1984) and after 10 years, 3D-printed human skull was implanted in a 22-years woman in Netherlands in 2014. However, only until 2015, the United States Food and Drug Administration (US FDA) approved the first 3D-printed medicine Spritam® for the treatment of epilepsy. The main advantages of new printed formulation are to enable the large dose of active pharmaceutical ingredient (such as 1000 mg levetiracetam in Spritam®) and/or to improve the drug disintegration within few seconds [164]. As more polypills have been under investigation for 3D-printing with multiple active components, it is necessary to understand the relevant international and national regulations for manufacturing 3D-printed (bio)pharmaceutical products, particularly on safety and authenticity for data sharing and collaboration [165–167].

Although many data analyses can be used to support and maintain the interests and trust in UK's consumers, it is hard to monitor the efficiency of their translation into good practices due to different concerns. For example, missing explanation or poorly defined procedures after the Covid-19 pandemic can confuse both public and private pharmaceutical organisations. Another issue is sharing sensitive data while preserving privacy demands, which may depend on technical advances as well as agreements between stakeholders and governance [165–167].

Therefore, it is beneficial to investigate available enhanced data analytics along with legal and regulatory frameworks to support supply chain innovation and new product development, particularly in pharmacy/healthcare field. This chapter aims to provide a better understanding of data and regulation management, and major prospects that should be focused on and thus worth considering further investigation (Figure 3.1).

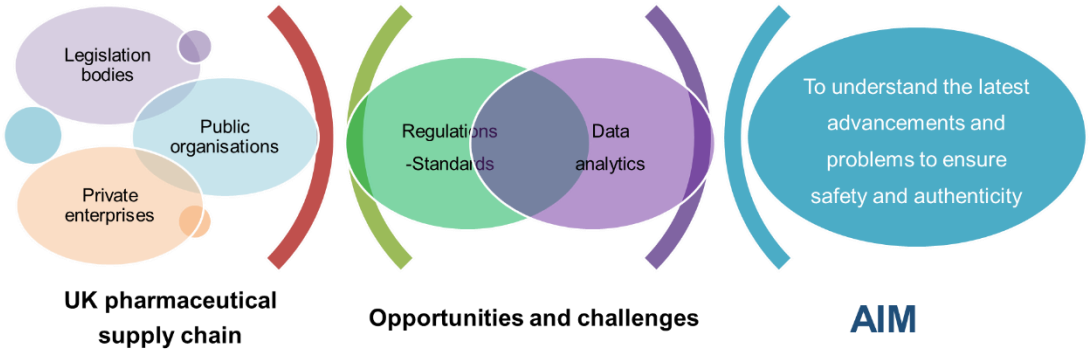

Figure 3.1. *The aim of chapter 3*

3.2. METHODS

I aim to describe and inform upcoming international regulations and innovative standards development to further establish good practice of data sharing and collaboration for sustainable pharmaceutical supply chains post the COVID-19 pandemic. I have reviewed and commented on the most updated regulation-standard documents and have evaluated specific case studies and evidence examples. The potential of the latest opportunities and challenges of applying enhanced data analytics and new legal-regulatory frameworks for sustainable pharmaceutical supply are highlighted.

The research consisted of following activities (Figure 3.2): 1) Understand the context of recent data, legal-regulation issues related to safety and authenticity in pharmaceutical industry via case studies; 2) Summarise major shifts into POC Manufacturing with(out) the support of enhanced data analytics with practical evidence examples, and 3) Recommend the strategy proposals as the suggested policy consultancy after evaluating current opportunities and difficulties for the sustainable pharmaceutical supply chain after Covid-19 pandemic.

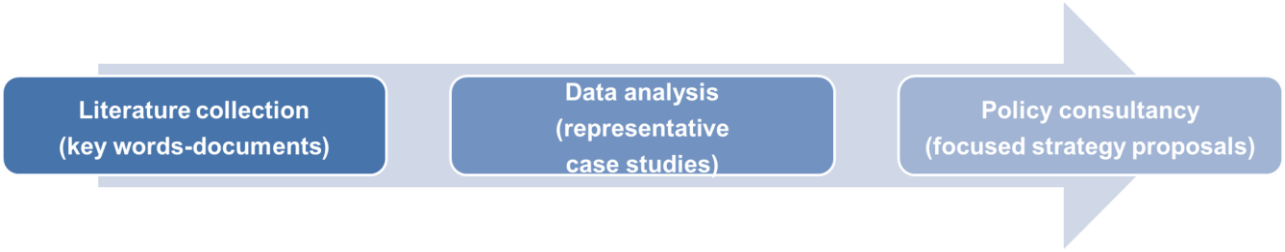

Figure 3.2. *Workflow to achieve the aim of Chapter 3*

3.2.1. Literature collection

Literature collection was carried out by searching key words from the documents related to relevant legislation public bodies. Key words included “pharmaceutical supply chain”, “data analytic(s)”, “legal/regulation document(s)” for acquiring updated information on the legislation bodies with relevant regulations-standards related to pharmaceutical supply chain.

3.2.2. Data analysis

The data analytics and their applications in legal frameworks were evaluated via representative case studies and evidence examples, focusing on the strategies for maintaining safety and authenticity.

3.2.3. Recommendation for policy consultancy

Recommendations for addressing the challenges and transforming the opportunities are introduced in the regards of policy consultancy for advancing Point-Of-Care (POC) Manufacture.

3.3. RESULTS AND DISCUSSION

3.3.1. Overview of the UK pharmaceutical manufacturing and digital technologies used in supply chains

Of the top 13 countries in pharmaceutical manufacturing ranked by value in 2018, only the UK decreased its productivity considerably: by -7.9% per year from 2008 to 2018 (Figure 3.3). There are a range of different indicators that affected the UK pharmaceutical manufacturing from 2008 to 2020. For example, CAGR is the Compound Annual Growth Rate, which is typical index for calculating and communicating the average returns of investment funds. Comparing the trade balance of pharmaceutical products between 2010 and 2020, the UK had an annual 1% increase in imports (CAGR) and an annual 2.8% decrease in exports (CAGR), leading to its trade balance declining to $1 billion in 2020 [168,169].

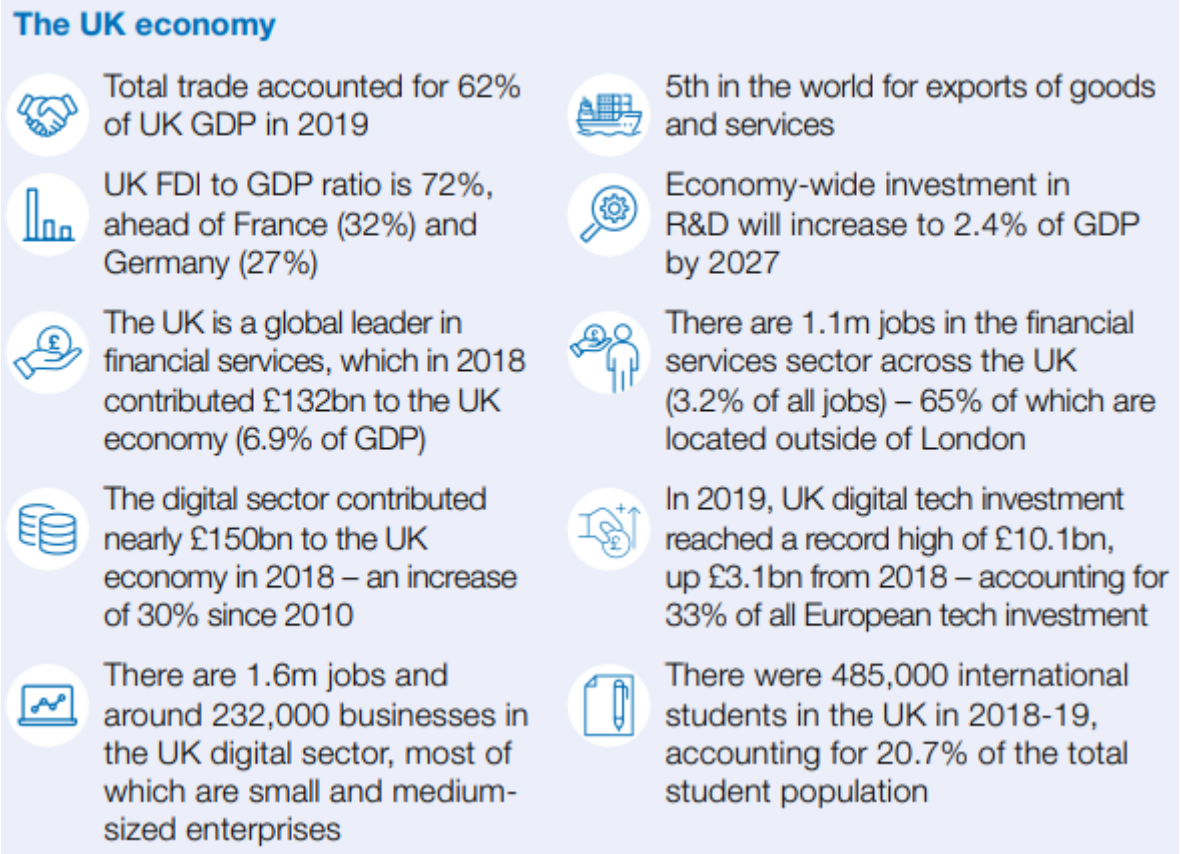

Figure 3.3. *The UK economy before Covid-19* [170]

R&D pharmaceutical manufacturing can be navigated according to different elements, which were listed in Table 3.1 [171–173]. The UK top 10 R&D investing companies (which have subsidiaries around the world) invested more than €17.4 billion in pharmaceutical manufacturing, and the top two UK-based firms belong to the pharmaceuticals sector, with GlaxoSmithKline (GSK) and AstraZeneca (AZ) respectively ranking 29 and 31 worldwide in 2020.

Figure 3.4 shows the UK Industrial Strategy Challenge Fund focused on improving healthcare as "By 2035, people enjoy five more years of healthy, independent living while narrowing the gap between the experience of the richest and the poorest" [173].

Table 3.1. Trending of the UK pharmaceutical manufacturing [171–173]

a. Indicators affeting the majority of UK pharmaceutical industry								
Company restructuring and site closures, including those by major sector employers	Increased offshoring of pharmaceutical manufacturing, including a large share of APIs	UK's inability to capture the "second wave" of international manufacturing investments	Greater incentives (e.g. tax) offered by other countries to attract manufacturing	New entrants focusing on early-stage drug discovery and non-manufacturing activities	Inability to commercialise and scale up manufacture of technologies developed in the UK	Caps on drug spending having an impact on the perception of the UK by investors	Increased use of generics pushing prices downwards and driving imports upwards	2016 EU membership referendum adding uncertainty to investment decisions

b. Elements navigating the pharmaceutical R&D in the UK				
Large share of domestic business R&D expenditure decisions taken abroad	Competitor countries having greater incentives to attract R&D investment	Difficulties to access scale-up funding locally leading to firm decisions to migrate UK companies may struggle to access scale-up funding locally and decide to migrate, impacting R&D expenditure	UK companies reducing in-house R&D investment in favour of acquiring small firms	Smaller innovative companies tend to outsource R&D

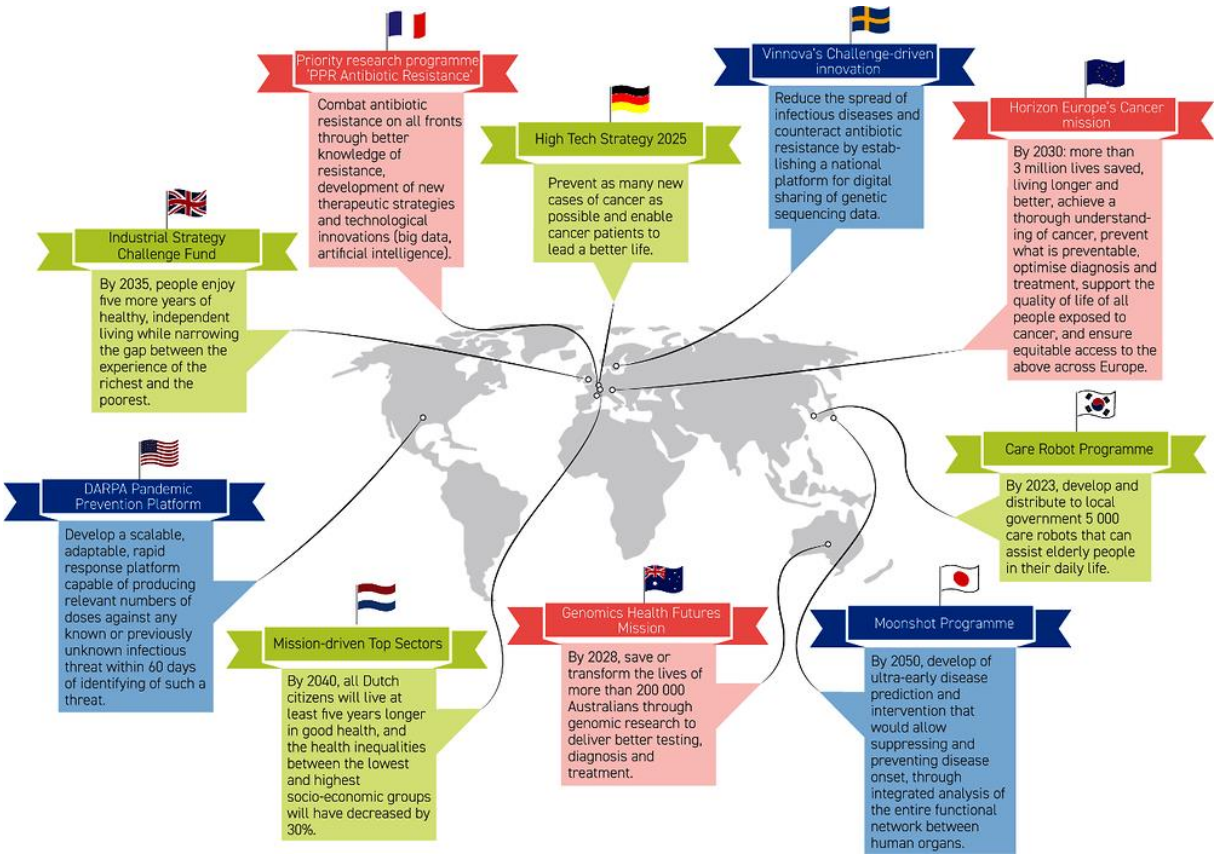

Figure 3.4. *Investment focus of major fund in the UK compared to other countries* [173]

Digital technologies and data analytics can be used to enhance and promote co-operation among the stakeholders including both individuals, public institutions, private companies and (non-)governmental organisations for data management. Figure 3.5 illustrates different types of digital technologies such as: 1) Information Flows (or Real Time Data Analytics) including Application-Based Software (ABS), Artificial Intelligence (AI), Big Data Analytics (BDA), Cloud Computing (CC), Functional Business System (FBS), and Internet of Things (IoT); 2) Material Flows (or Robotic and Automation) including 3D-printing or Additive Manufacturing (AM), Automated Guided Vehicles (AGV), Drones, and Robotic; 3) Combination between Information and Material Flow including Real-Time Location System (RTLS) (with Radio-frequency Identification (RFID) and Bluetooth), Augmented Reality (AR) and Virtual Reality (VR). Moreover, there are other areas where enhanced data analytics could have significant impact: Improving quality, improving yield, improving warranty & customer services, increasing production throughput, speeding up time to launch, predicting &/or preventing maintenance, improving or maintain supply chain operations [167,174].

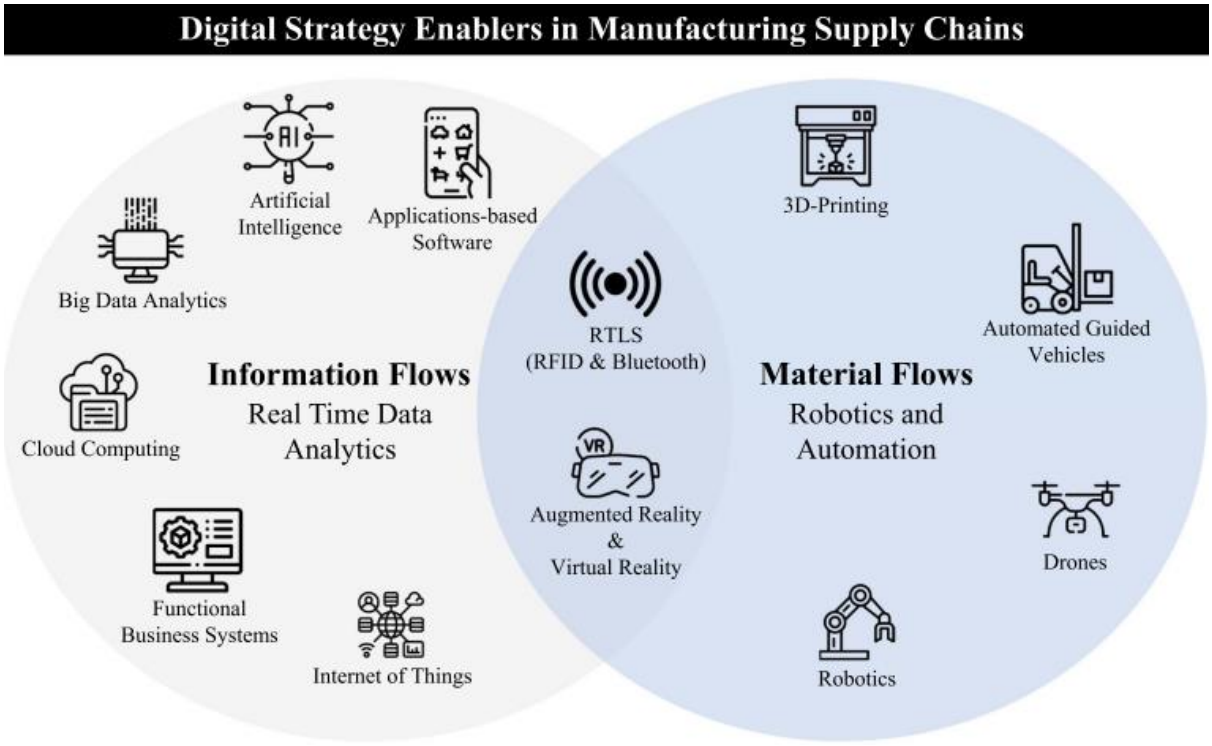

Figure 3.5. *Summary of current digital technologies used in supply chain* [174]

With such digital technologies, data can be monitored under a safe and ethical framework. However, it is necessary to understand the latest advancements and problems when ulilising these enhanced data analytics in pharmaceutical safety and authenticity in order to optimise the system operation and consumer trust. Enhanced data analytics methods and their current applications in the UK pharmaceutical industry should be evaluated to establish an initial approachable framework. Data analytics are progressing quickly, so it's useful for continuous assessment of their applications and impacts for effective framework. From comparison with other sectors in digitalisation of supply chains, the pharmaceutical industry can learn from these areas as specific positive/negative examples can provide learning points. Realizing how to reduce fake/faulty data in pharmaceutical industry could also be beneficial for other sectors such as consumer goods and food and drink.

3.3.2. Legislation bodies with representative case studies affecting the UK pharmaceutical supply chain after Covid-19 pandemic

The main legislation bodies that affect the UK pharmaceutical supply chain in terms of data and legal management can be categorized into internal and external types with representative case studies: 1) National body - Medicines and Healthcare products Regulatory Agency

(MHRA); 2) European Union regulatory body such as European Medicines Agency (EMA) and United States regulatory body such as United States Food and Drug Administration (FDA or USFDA); and 3) International bodies such as International Organization for Standardization (ISO) and World Health Organisation (WHO). Table 3.2 summarised the most recent resources (which were published and/or updated in 2021 and 2022) from the mentioned legislation bodies including plans, guidelines, proposals, webinars, etc. After reviewing the relevant information in those resources, five representative case studies were selected to illustrate the impact of data, legal and regulation management in the UK pharmaceutical supply chain in the following sections [175–186].

Table 3.2. Summary of main resources of legislation bodies affected the UK pharmaceutical supply chain after Covid-19 pandemic

NATIONAL BODY	**Medicines and Healthcare products Regulatory Agency (MHRA)** *Documents: British Pharmacopoeia, 2022; Consultation on Point of Care Manufacturing, 2021; Horizon Scanning Case Study: Point of Care manufacture - Case study, 2022; Medicines and Healthcare products Regulatory Agency, 2022* [165,187–189]
EUROPEAN REGULATORY BODY	**European Medicines Agency (EMA)** *Documents: European Commission, 2020; European Medicines Agency, 2022a, 2022b; European Pharmacopoeia (Ph. Eur.) 11th Edition, 2022* [190–194]
UNITED STATES REGULATORY BODY	**United States Food and Drug Administration (FDA or USFDA)** *Documents: ECFR :: Title 21 of the CFR -- Food and Drugs, n.d.; FDA Releases Update of 2022 Priority Guidance Topics for Foods Program | FDA, n.d.; Good Review Practices | GRPs | FDA, n.d.; Mutual Recognition Agreement (MRA) | FDA, n.d.; Regulations: Good Clinical Practice and Clinical Trials | FDA, n.d.; Training for Pharmaceutical Companies in Leadership & Soft Skills - Good Behavioural Practice (GBP) Pharma, n.d.* [195–200]
INTERNATIONAL BODIES	**International Organization for Standardization (ISO)** *Documents: IDMP Standards - IDMP1 Free Information Brochure Download, n.d.; ISO 14971:2019(En), Medical Devices — Application of Risk Management to Medical Devices,*

	n.d.; ISO 22870:2016, Point-of-Care Testing (POCT) — Requirements for Quality and Competence, n.d.; ISO 13485:2016(En), Medical Devices — Quality Management Systems — Requirements for Regulatory Purposes, n.d.; ISO 15190:2003(En), Medical Laboratories — Requirements for Safety, n.d.; ISO/IEC 17025:2017(En), General Requirements for the Competence of Testing and Calibration Laboratories, n.d. [182,185,201–204] **World Health Organisation (WHO)** *Documents: WHO Collaborative Centres, n.d.; World Health Organisation, n.d.* [205] **Other organisations:** **International Coalition of Medicines Regulatory Authorities (ICMRA)** *Documents: International Coalition of Medicines Regulatory Authorities (ICMRA), n.d.* [206] **International Council for Commonality in Blood Banking Automation (ICCBBA)** *Documents: International Council for Commonality in Blood Banking Automation (ICCBBA), n.d.*[207] **International Council for Harmonization of Technical Requirements for Registration of Pharmaceuticals for Human Use (ICH)** *Documents: International Council for Harmonization of Technical Requirements for Registration of Pharmaceuticals for Human Use (ICH), 2022* [208]

a. National body - Medicines and Healthcare products Regulatory Agency (MHRA)

Case study 1: Point-Of-Care (POC) Manufacturing with POC Master File

New technologies can offer the next generation of medicinal products that may have limited shelf lives (such as a few seconds to several hours), which facilitates manufacturing at the Point-Of-Care (Figure 3.6). Several examples include personalised dosage forms produced via 3D-(bio)printing, gaseous products, blood products, and Advanced Therapy Medicinal Products (ATMPs). Although they have a large variety in doses, forms, administration routes, etc, these have similarity of personalisation or on-demand purposes, which may be difficult to progress at the conventional manufacturing sites (such as the specific large factories producing the steady shelf-life products) [165]. The POC structures were followed to the previous and recent guidelines-regulations of the manufacturing of medicinal products including blood/tissue/cells processing. These measures include adaption of concepts in Good Manufacturing Practice (GMP) (e.g. those used in limited shelf life products including Real-Time or Control Release Test, Product Quality Reviews), the master file systems (e.g. those used for plasma and active pharmaceutical ingredients), and also the hub and spoke model for controlling the tissue and cells collection and processing (Figure 3.7) [165,209]

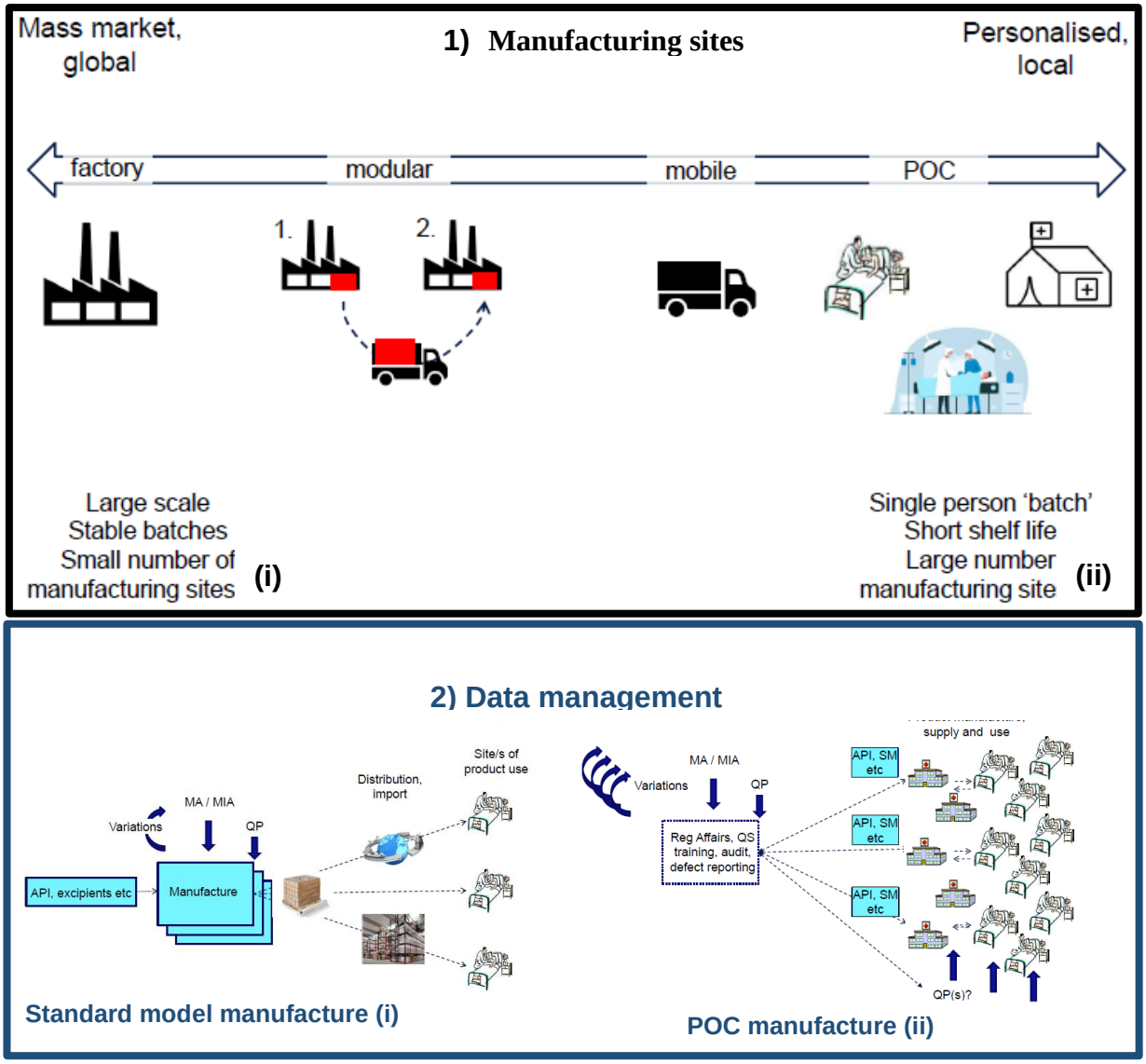

Figure 3.6. *Changing spectrum of manufacturing activities from standard model into Point-Of-Care Manufacture: 1) Manufacturing sites (varied from factory, modular, mobile, and POC) result in either (i) Large scale-Stable batches-Small number of manufacturing sites or (ii) Single person 'batch'-Short shelf life-Large number manufacturing sites; 2) Data management offer more control/authority at single site unit, which cause difference between (i) Standard model manufacture and (ii) POC manufacture* [165,209]

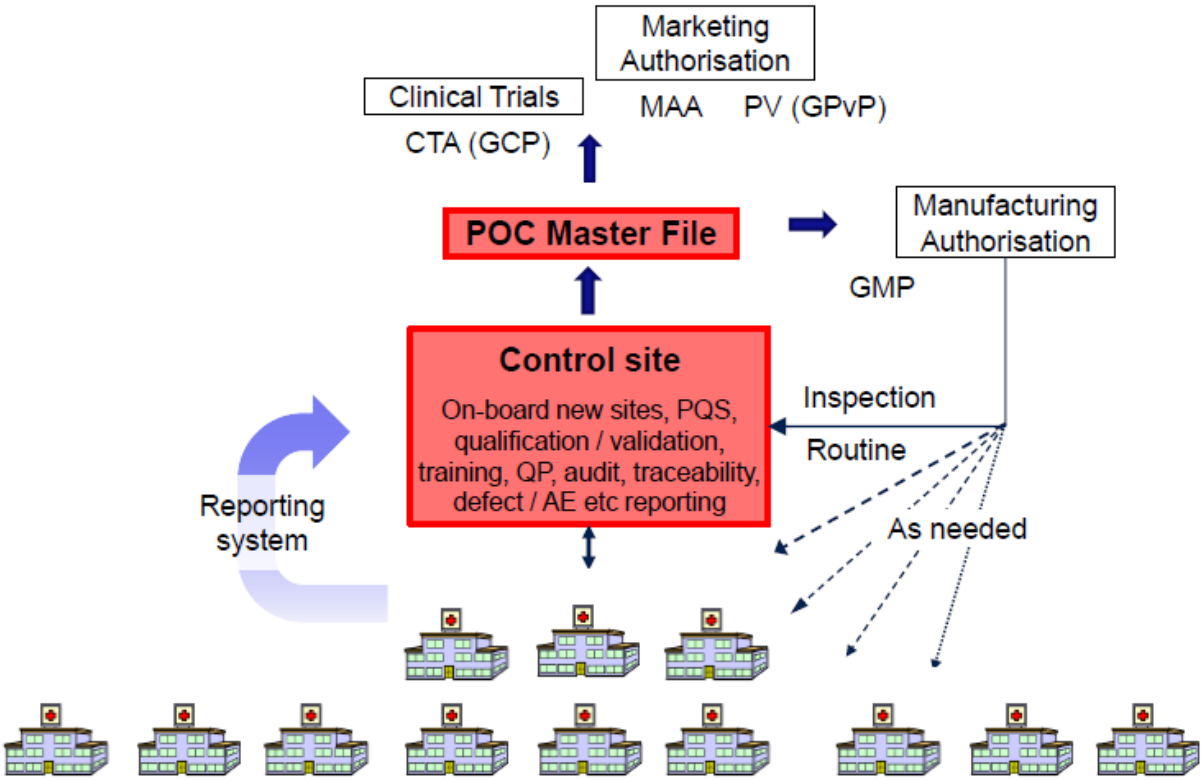

Figure 3.7. *Proposal for the new regulatory framework using plasma master file (PMF) in the UK POC Manufacturing* [209]

b. European Union regulatory bodies such as European Medicines Agency (EMA) and United States Food and Drug Administration (FDA or USFDA)

Case study 2: Data-centric Target Operating Model (TOM) with the electronic application forms (eAF) from the European Medicines Agency (EMA)

In order to apply the Data-centric Target Operating Model (TOM), EMA has highlighted the significant change from the current data platform (which are pdf-based forms) into new electronic applications (web-based forms**)** since 2022. The main advantage of TOM is the capability for reusing the product data for progressing regulatory documents (Figure 3.8) [186].

The business strategies along with scientific-technical elements should be reviewed to match the most updated regulation in terms of reliability, quality, and quantity of data management. Figure 3.9 showed that the electronic application forms (eAFs) can support data procurement of EMA under the several phases of reviews and reusages [186]. The Product Management Service (PMS) can provide detailed information of previous approved products, and the product data can be acquired and stored as specific application forms in

the correlation with the medicinal regulation. The PMS will extract all information of the products and related legal documents after full implementation. Hence, it requires signficant efforts at different stages for building, optimising, and applying the data-centric TOM effectively due to its complication in terms of specialised features and legal documents [186].

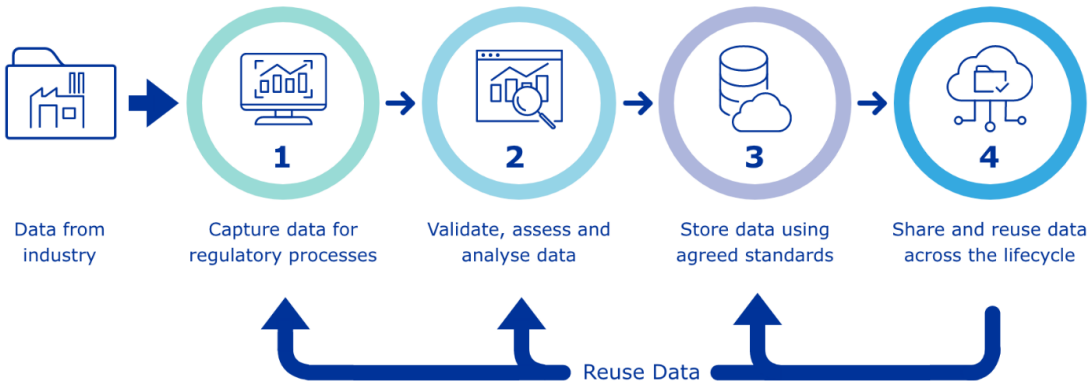

Figure 3.8. *Data-centric Target Operating Model (TOM)* [166]

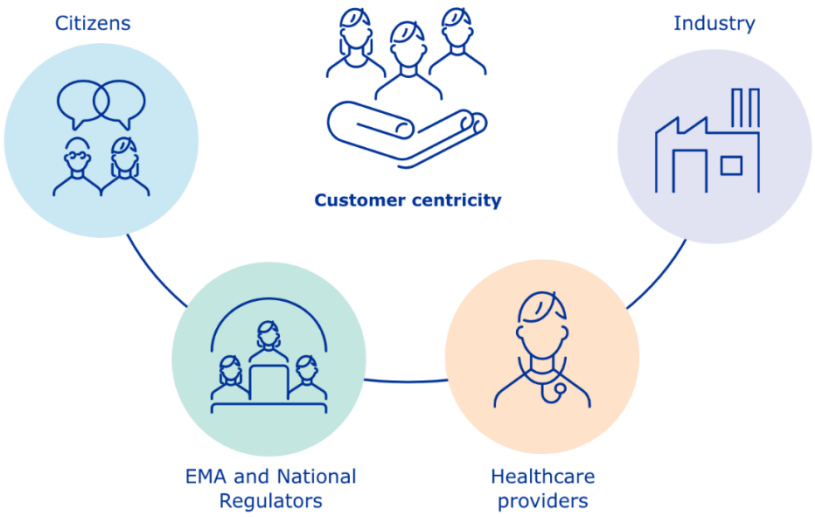

Figure 3.9. *EMA's electronic application forms (eAF)* [166]

Case study 3: Collaboration between FDA and EMA in issuing the guidance-regulation in pharmaceutical supply chain, particularly during Covid-19 pandemic

Mutual Recognition Agreements (MRAs) between the FDA and foreign regulatory authorities facilitate the drug inspectors to rely upon information from drug inspections conducted within each other's borders. Under the Food and Drug Administration Safety and

Innovation Act, enacted in 2012, the FDA has the authority to enter into agreements to recognize drug inspections conducted by foreign regulatory authorities if the FDA determined those authorities are capable of conducting inspections that meet U.S. requirements. MRAs yield greater efficiencies for U.S. and foreign regulatory systems by avoiding duplication of inspections; and enable reallocation of resources towards inspection of drug manufacturing facilities with potentially higher public health risks across the globe [167].

Although the UK left the European Union (EU) in 2021, the FDA still works together with the UK to ensure the safety and authenticity of medicinal-pharmaceutical products. MRAs based on the collaboration between the FDA, EMA and MHRA can help to ensure the updated regulations in practice (Figure 3.10). For example, both FDA and EMA investigated several guidelines-inspections affecting the manufacture and supply to utilise the benefits and reduce the threats of this mutual recognition during the Covid-19 pandemic [167].

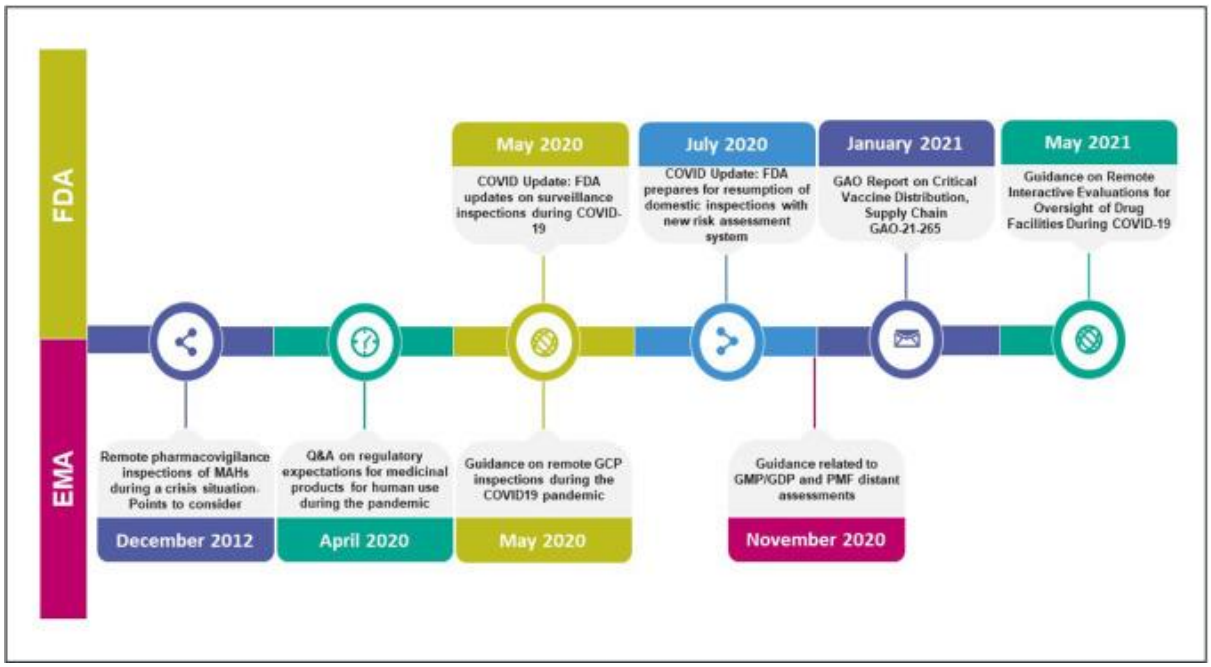

Figure 3.10. *Key positions and communications on remote inspections issued by the European Medicine Agency (EMA) and the US Food and Drug Administration (FDA) during Covid-19 pandemic* [167]

c. International bodies such as International Organization for Standardization (ISO) and World Health Organisation (WHO)

Case study 4: The new compatible data submission format - HL7 FHIR for implementing ISO IDMP

Identification of Medicinal Products (IDMP) is a suite of five standards established by the International Organization for Standardization (ISO) to facilitate the production and supply of medicinal products in the context of pharmacovigilance and the safety of medications throughout the world (Figure 3.11 and 3.12). The global framework can be facilitated by the ISO IDMP for producing and assessing the medicinal product data consistently. It can also enhance the international knowledge exchange among manufacturers, distributors, and regulators [201].

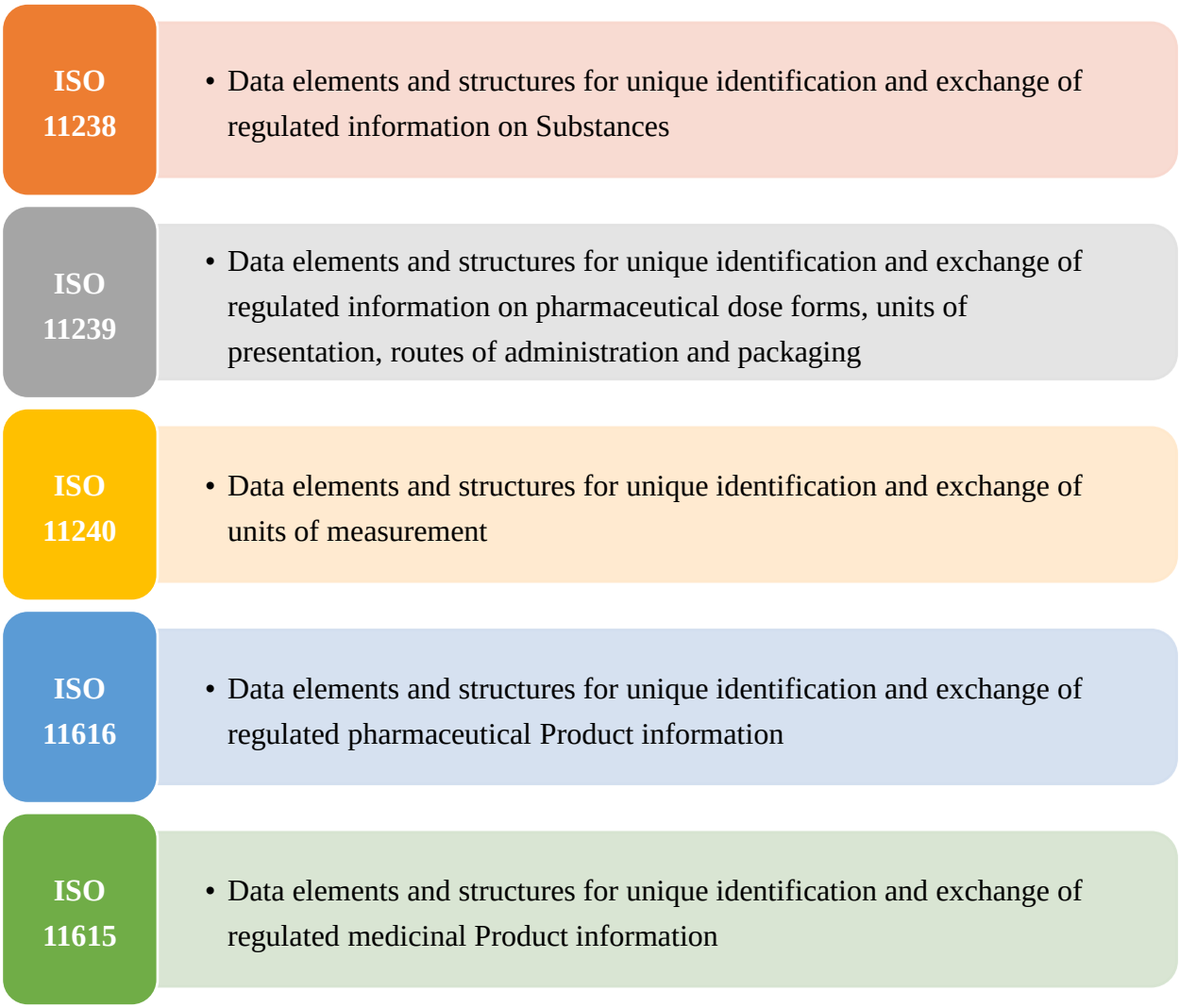

Figure 3.11. *Description of ISO Identification of Medicinal Products (IDMP)* [201]

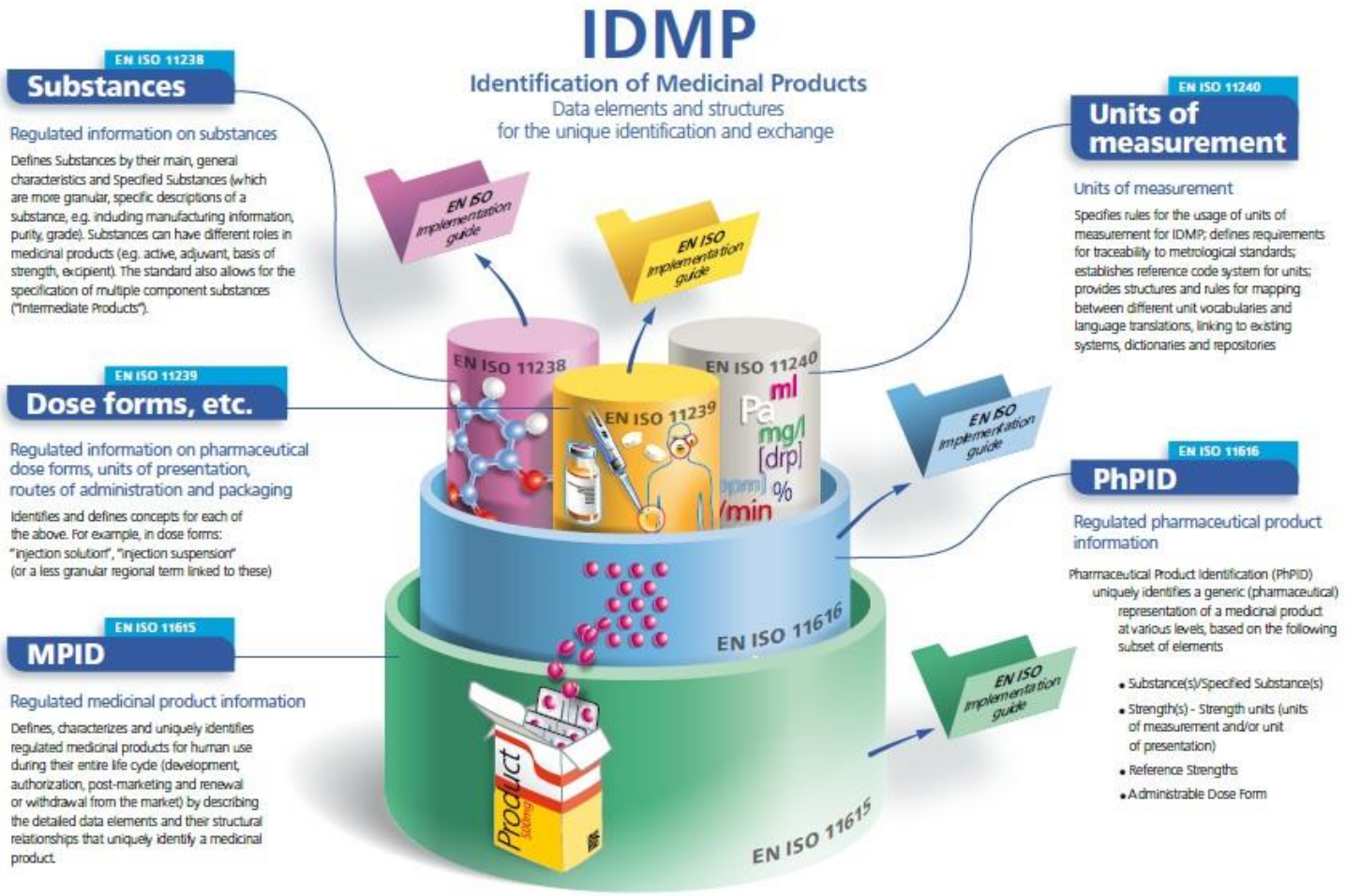

Figure 3.12. *ISO Identification of Medicinal Products (IDMP) including ISO 11238, ISO 11239, ISO 11240, ISO 11616, and ISO 11615* [201]

From the white paper "The Market Authorisation Holder (MAH) Guide to Preparing for IDMP" (23.07.2021), considerable progression of active pharmacovigilance matching the EMA's requirements can be illustrated via different aspects of ISO IDMP. The Health Level Seven (HL7) organisation and the European regulatory networks have been trying to integrate the ISO IDMP standards into the specific specification worldwide. The Application Programming Interface (API) for PMS has been developed from the Fast Healthcare Interoperability Resources (FHIR) offering the standards for data transformation in the European medicinal regulatory networks (mainly with EMA and FDA) [167]. Figure 3.13 shows that medicinal product data can be exchanged steadily via the Substance-Product-Orgnisation-Referentials (SPOR) Data Management Services which include the Substance Management Service (SMS), Product Management Service (PMS), Organisation Management Service (OMS), and Referentials Management Service (RMS). Figure 3.14 illustrates that during the IDMP implementation, the new platform of data acquisition - Health Level Seven Fast Healthcare Interoperability Resources 1 (HL7 FHIR 1) will replace the current platform - the eXtended EudraVigilance Product Report Message (XEVPRM) [210].

Figure 3.13. *Four domains of substance, product, organisation and referential (SPOR) master data in pharmaceutical regulatory processes* [186]

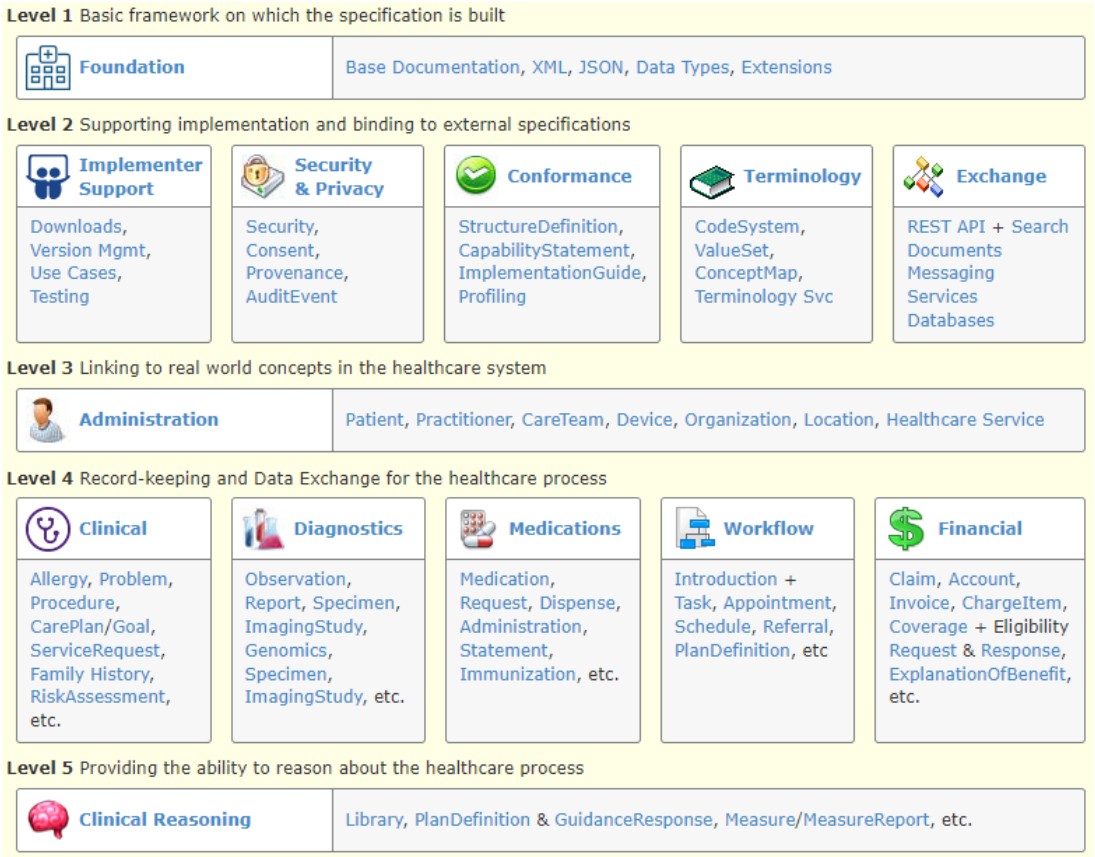

Figure 3.14. *HL7 FHIR replaces the current data submission format - the eXtended EudraVigilance Product Report Message (XEPRM) in implementing ISO IDMP* [210]

Case study 5: Standards cooperating in clinical treatment scenarios

The World Health Organisation (WHO) has a Global IDMP Working Group which will continue to collaborate with FDA and other regulatory agencies in order to implement regulations-standards. For example, the distinctive codes can be designed and optimised as a substitute for generating the global Pharmaceutical Product Identifier (PhPID), and Substance Identifier (PhSID). Along with ISOs, there are other standards that have been used such as Systematized Nomenclature of Medicine (SNOMED), Digital Imaging and Communications in Medicine (DICOM), The Global Information Standard for Medical Products of Human Origin (ISBT128), or Health Level Seven International (HL7), etc. They have strong focus on interoperability between heterogeneous IT systems for promoting and supporting the integration of systems in the healthcare enterprise. For example, HL7 showed significant advantage to manage data in the whole clinical treatment in all places such as ambulance, emergency room, X-ray, admission, consultation, operating room, recovery, and re-education after that (Figure 3.15) [211,212].

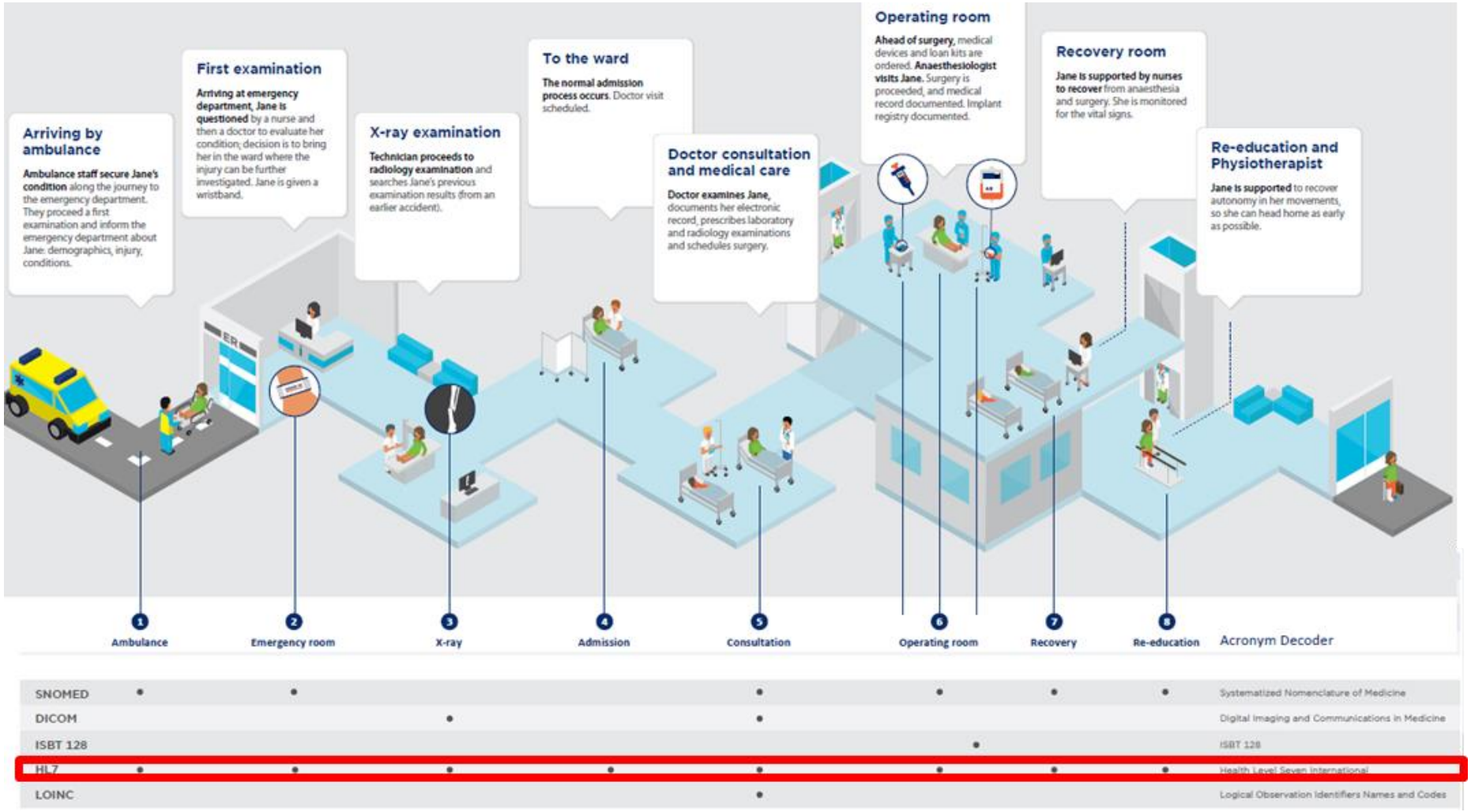

Figure 3.15. *Standards cooperating in clinical treatment scenarios* [211,212]

3.3.3. Evidence examples of major shifts in the global pharmaceutical supply chain

There is further evidence of major shifts in the global pharmaceutical supply chain: POC Manufacturing with(out) the support of enhanced data analytics has been universally evolving. Some recent examples are discussed.

Example 1 – The increase of central-cloud and edge facilities for centralised and decentralised manufacturing all over the world

On-premises and cell site edge nodes are not included in the deployment estimate below as it is considered that they will be implemented on demand. Data associated with any packaging of a medicinal product are to be accessed or queried by all the actors in the supply chain, the distributed databases option needs development of mechanisms for access to data and/or querying the databases, which can be rather complex. [190,206,213]. Hence, the three main available types of architecture for collecting and reporting of data are briefly described below:

1. Centralised: Centralised registration of entities and reporting of traceability data to a single (usually managed by a government agency) database or repository. This has been adopted, with different specificities, by most countries with traceability systems, including Turkey, the EU, Russian Federation and Brazil. The two main variations are the 'hub and spoke' architecture of the EU and the single central repository used elsewhere: a-EU model, central hub, multiple national repositories, not full track and trace; b- Track and trace model with a national repository.

2. Semi-centralised (Cumulative): In this model, there is no central repository of data but rather a linear and cumulative flow of information. Each supply chain entity is legally responsible for confirming receipt of accurate data from its upstream business partner, adding its own data, and transmitting the full chain of custody data downstream to the next recipient. In this way, the downstream partners have visibility of previous history. This system is adopted by China and the USA.

3. Distributed: Copies of compliance data are shared with other supply chain partners on a request basis, to verify product, but are not stored in a central place. This mechanism is used for management of USA saleable returns, via a verification router service (VRS).

Example 2 – Opportunity for accredited Point of Care Testing (POCT) in Spain

POCT can offer several instruments to use throughout 24 hours/day with different analytical mechanism (including clinical services) carried out inside and outside the hospital. For the optimal POCT, there are key principles should be frequently reviewed such as the methodology proof, quality assurance, competent workers, and continuous development [214]. One example was the La Paz University Hospital, Spain could utilise the ISO 22870 and ISO 15189 to enhance different features of the test processing. Particularly, ISO 22870 instructing the ambulatory care and ISO 15189 indicating the proficiency criteria in the medical laboratories, which helped to strongly boost the quality assessment and system management in the hospital [181].

Example 3 – Cell and gene therapy in Point of Care Manufacturing (POCM) in the UK

Autologous therapies can be produced consistently as small-sized batches (e.g. single product for an individual) to meet on-demand purposes. As the starting material is extracted directly from a patient, the shelf lives of products are (very) short (e.g. seconds to hours), which made it unfeasible to establish the POC manufacturing sites in the far distance from the patient or produce the POC products in advance before distribution [215,216]. In other words, the POC manufacturing comprises of various divisions including medicinal laboratories, clinics, hospitals, customised (mobile) units, which may represent many challenges in inspection-authorisation comparing to the conventional manufacturing. Therefore, different divisions in the same POC manufacturing site can be required and therefore has a need to enhance the separate training/competency of specialised knowledge and skills depending on the currently available facilities and software packages [217,218].

3.3.4. Current opportunities, challenges, and potential suggestions for the sustainable pharmaceutical supply chain in the UK after Covid-19 pandemic

a. Opportunities and challenges

Considering the representative case studies and examples in previous sections, I can understand the current opportunities and challenges (Figure 3.16) when developing the sustainable pharmaceutical supply chain with POC manufacturing centred on: i) POC Products, ii) POC Processes, iii) POC Premises, iv) POC Procedures, v) POC Personnel, and vi) POC Provision, which will be explained in detail in the following sections.

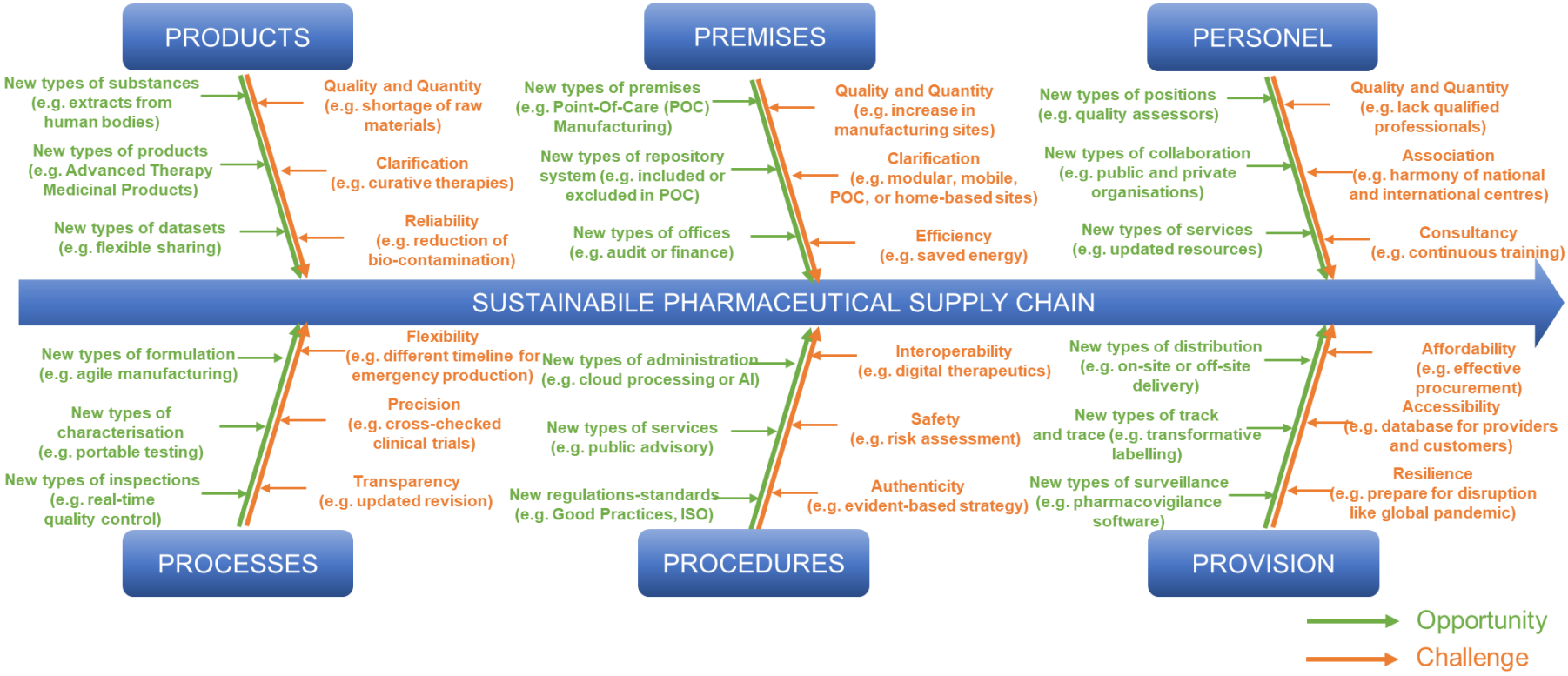

Figure 3.16. *Fish-bone diagram represents the current opportunities and challenges when developing the sustainable pharmaceutical supply chain in six aspects: Products, Processes, Premises, Procedures, Personnel, and Provision*

i) Products

POC products will be an important market segment in future medicinal-pharmaceutical industry with a range of new types of substances such as extracts from human bodies, new products like Advanced Therapy Medicinal Products (ATMPs) (e.g. gene/cell/tissue therapy-products) and new forms of datasets of potential therapeutics for flexible sharing. For example, certain final products with limited shelf lives will need to be produced only at local sites much closer to patients. This presents difficulties in maintaining the product quality and quantity (due to limited sources of raw materials), the clarification in relevant terminology (in new curative therapies), and the reliability of the products (due to potential bio-contamination). POC manufacture can employ terminologies such as GMP-in-a-box, decentralised manufacture or redistributed manufacture, which may result in confusion. Other examples are multi-functional multi-materials additive manufacturing (or 3D-printing) incorporating single or multiple Active Pharmaceutical Ingredients (APIs); or ATMPs manufacturing (or bio-printing) with specialised genes/tissues/cells. It will lead to the necessity for classifying these products into correct medicinal-pharmaceutical products (rather than devices).

ii) Processes

With the diversity of products, POC will require and expand to new types of formulation, agile manufacturing, new types of characterisation (e.g. portable testing) and new types of inspections (e.g. real-time quality control). Some of the POC manufactured products are autologous so they will have different life cycle demands (e.g. extracting from and being returned to the same patient). This will result in shorter time of management in terms of quality assurance and control when producing and delivering these products locally.

Moreover, current limitations for practical POC processes need to be considered in terms of flexibility (e.g. different timeline for emergency production), precision (e.g. cross-checked clinical trials), and transparency (e.g. updated revision). For instance, a larger number of POC products can be generated by the increase of the manufacturing sites with the clinical testing units. Hence, the assessment for the products' approval needs to be optimised so single POC product may not need to wait for longer time (to receive sufficient authorised signatures) before being delivered to the patients or launched on the market.

iii) Premises

To provide these and further products and processes, it's necessary for changes in our thinking of manufacturing sites and premises to enable POC manufacturing, new types of repository system (e.g. included or excluded in POC), and new types of offices (e.g. audit or finance). For example, traditional pharmaceutics are usually manufactured at massive globally distributed factories focusing full-time on a single product whereas POC products need to be manufactured at smaller scales closer to the patient (such as public or private clinics, hospital emergency units, pharmacies, etc).

Hence, there are challenges in developing the new range of POC premises such as quality and quantity (e.g. increase in manufacturing sites), clarification (e.g. modular, mobile, POC, or home-based sites), and efficiency (e.g. saved energy).

iv) Procedures

Thanks to the advanced science and technology, it is important for the optimisation of the POC procedures in comparison to the development of further POC products, processes, and premisses. There will be new types of administration (e.g. cloud processing or AI), new types of services (e.g. public advisory), and new regulations-standards (e.g. Good Practices, ISOs). For example, the MHRA is involved in an Engineering and Physical Sciences Research Council (EPSRC) funded project to investigate Redistributed Manufacturing in Healthcare (RiHN). Previous and current medicinal legislation will be reviewed and updated, which will result in the new platforms of data management - the Plasma Master File (PMF) system.

To accommodate further product types, POC procedures will require a specific degree of interoperability of the digital therapeutics, safety with risk assessment, and authenticity with evident-based strategy, which are also our major problems. For example, centralised sites conventionally require a series of legal documents and processes for approving the release of products onto the market. This can cause certain difficulties in shifting into the decentralised sites because it may be impossible to have all authorisation for very short shelf live POC products, particularly when delivering to an individual or a small group of individuals.

v) Personnel

It is a necessity to ensure accurate authorised signatures on product records, which highlights the importance of personnel in the pharmaceutical manufacturing. This works well for traditional pharmaceutical products (with typical shelf life between 1 and 5 years) whereas for POC products this same chain of authorisation may not be possible. Hence, there will be new positions (e.g. quality assessors), new types of collaboration (e.g. public and private organisations), and new types of services (e.g. updated resources) in POC personnel.

With the different approach for POC manufacturing which mainly prioritises on-demand purposes processes will be managed and scrutinised by fewer competent specialists in a short time. Hence, the personnel certifications should be reviewed properly as both production and characterisation are usually carried out at the same time following to the specific circumstances of single or multiple individuals.

vi) Provision

As POC manufacture applies advanced knowledge, skills and instruments for generating products, there will be a need for new types of distribution (e.g. on-site or off-site delivery), new types of track and trace (e.g. transformative labelling), and new types of surveillance (e.g. pharmacovigilance software). For example, the control, consistency and availability of product that complies with manufacturing and Clinical Trial Authorisation (CTA) and Marketing Authorisation (MA) requirements across a large number of POC sites. Marketing Authorisation (MA)s currently name each site of manufacture and the MA is varied when a new site is added, or an existing site withdrawn. However, for POC this requirement will be a heavy administrative burden and costly, potentially prohibitively, given that site changes are anticipated to be relatively frequent. A similar requirement exists for CTA, where the finished Investigational Medicinal Product (IMP) manufacturing site is named in the CTA. Each new manufacturing site will also need to be inspected, authorised and comparability demonstrated.

Moreover, a further consequence of a short shelf life with the requirement for proximity to the patient is challenges to manufacture at commercial scale, so will be by ‘scale out’ rather than the conventional approach of ‘scale up’. Depending on the product type, the ability of patients to travel, availability of specialist clinical expertise and clinical facilities, there may be some concentration or focal points in the provision of such products. The current scale

up manufacturing models include places where a product is typically manufactured in a few global locations, usually in the range of one to three sites, each at large scale. As mentioned before, there are also specific regulatory challenges that arise from manufacture at many manufacturing sites. Therefore, certain barriers in POC provision should be recognised including affordability (e.g. effective procurement), accessibility (e.g. database for providers and customers), and resilience (e.g. prepare for disruption like global pandemic).

b. Suggestions for future actions and review

After analysing the similarities and differences across six aspects of POC Manufacturing (including products, processes, premises, procedures, personnel, and provision), three main strategies for effective transformation of the current pharmaceutical supply chain can be offered as follows.

i) Recent prospects of implementing the POC Manufacturing should be understood and clarified when developing the sustainable pharmaceutical supply chain in the UK

Table 3.3 summarised the recent prospect of implementing the Point-of-Care Manufacturing, which should be understood and considered for future action plan. The major challenges include transparency and efficiency (e.g. differences in products and processes, real-time quality control); quality and quantity (e.g. insufficient qualified professionals, increase in control sites); and interoperability and pharmacovigilance (e.g. ineffective track-trace system, broaden database for administration). The major opportunities include accessibility and affordability (e.g. agile manufacturing like 3D-printing or curative therapeutics); resilience and harmony (e.g. preparation for disruption from global pandemic like Covid-19); regulations-standards (e.g. new GPs and ISO to facilitate the authority and responsibility of POC).

Besides, pharmaceutical supply chains include both upstream of the manufacturer, downstream of the manufacturer, inclusive of the NHS and/or patient (Figure 3.17). If data could be shared in a trusted environment, private, public and legal sectors as well as end-users will achieve a range of benefits. For example, patients increase trust in commercial products that can help to expand the business from the manufacturers and distributors. Another point is that the harmony/agreement between manufacturers and governance parties

can have optimal performance of quantity, quality, time, and cost. When submitting data to the Medicines and Healthcare Products Regulatory Agency (MHRA) and European Medicines Agency (EMA), there are different legal forms need to be considered such as Good Practices (GPs) with Good Manufacturing Practice (GMP), Good Clinical Practice (GCP), Good Distribution Practice (GDP). Other informative guidelines such as CTA/MAA and ISOs should also be studied and updated for manufacturing the POC products. In other words, there is a need for understand the recent situation and relevant regulation, which is current rather than at a future point.

Table 3.3. Key challenges and opportunities of the implementation of Point-Of-Care Manufacturing

Challenges	Opportunities
• Transparency and efficiency (e.g. differences in products and processes, real-time quality control) • Quality and quantity (e.g. insufficient qualified professionals, increase in control sites) • Interoperability and pharmacovigilance (e.g. ineffective track-trace system, broaden database for administration)	• Accessibility and affordability (e.g. agile manufacturing like 3D-printing or curative therapeutics) • Resilience and harmony (e.g. preparation for disruption from global pandemic like Covid-19) • Regulations-standards (e.g. new GPs and ISO to facilitate the authority and responsibility of POC)

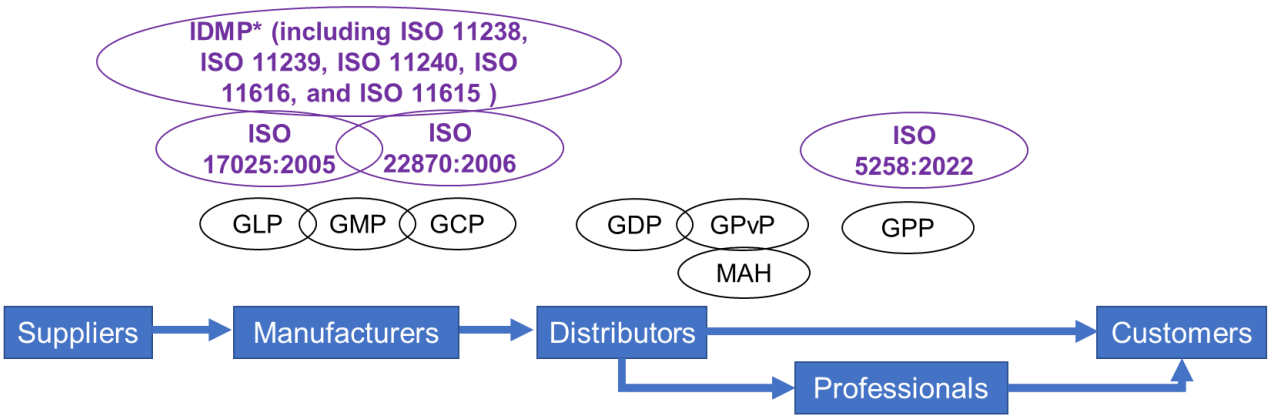

Figure 3.17. *Current regulation framework applying in the pharmaceutical supply chain*

ii) New frameworks of pharmaceutical supply chain should be considered focusing on review-update of ISOs and renewal-revision of GPs with the support of enhanced data analytics

MHRA perspective indicated that POC products should be produced in the close accessibility to the patients and emphasized the suitable alteration for ensuring the safety development (including both non-clinical and clinical tests) at larger number of manufacturing sites. Although MHRA showed the necessity of new regulatory framework for POC, the development of POC Master File was followed only on the GMP, GCP, and GPvP inspections along with the CTA/MAA guidance. Besides, there was no reviews from the perspectives of GLP, GDP, and GPP inspections which will be considerably different in POC Manufacturing.

Besides, the ISO IDMP is a good starting point to help clarify the opportunities and challenges because it enhances the safety and authenticity with visible risk management and pharmacovigilance. Focusing on systematic data-centric structures, the hazards can be detected and disseminated easily and quickly for both national and international context. For example, the medicinal information related to new vaccines could be acquired and shared worldwide to support the local shortages in the fight against of the Covid-19 pandemic. Hence, other relevant guidance for new regulations-standards should be considered for implementing the POC Manufacturing in the UK (Figure 3.18):

+ From suppliers to manufacturers, the renewal of GPs can be considered to form the enhanced GMP in terms of GLP, GMP, GCP, GDP along with ISO IDMP (including ISO 11238, ISO 11239, ISO 11240, ISO 11616, and ISO 11615), ISO 17025:2005, ISO 22870:2006.

+ From manufacturers to customers (not matter via professionals or not), the revision of GPs should be updated frequently to issue the updated GPP in terms of CGvP and GPP along with MAH, ISO 5258:2022, etc.

In other words, it is important for a new legal framework for guiding and managing the POC manufacture, which links to the existing regulatory controls and helps to ensure the safety, quality, quantity and productivity in the pharmaceutical industry.

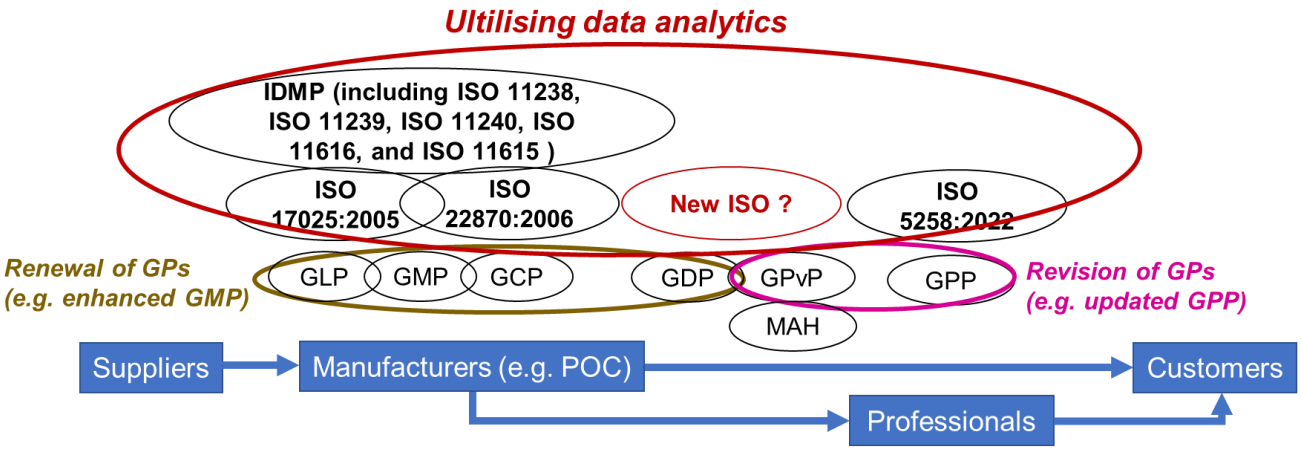

Figure 3.18. *New regulation framework for implementing the POC Manufacturing in the pharmaceutical supply chain*

iii) Government, public and private parties should co-operate for successful planning and effective performance within current and future regulation-standards

ISO IDMP is one of the systematic data-centric approaches that can cover a multi-disciplinary data set of manufacture, supply, regulation, and other relevant aspects. The implementation of ISO IDMP with full features of the future products will require the good co-operation from multiple Government, public and private parties. POC products have to date focused on immunology and/or pharmacology targets and belong to medicinal products (instead of medical devices). The official authorisation method should be established and augmented to investigate the reliability, quality, and quantity of the POC products, particularly those do not have clear boundaries compared to the current medical devices.

Moreover, to utilise opportunities (e.g. collaboration from multiple legislation bodies) and overcome the challenges (e.g. data management in the new situation), certain prioritised activities should be considered within the next 5 years as below:

+ Reviewing and updating the successful case studies-examples of implementing the guidelines and applying the enhanced data analytics in the pharmaceutical industry.

+ Comparing and ultilising the core elements where pharmaceutics and other sectors (e.g. food, engineering, automotive, defence, aerospace, etc) could learn from each other.

+ Clarifying and improving the current and future guidelines such as GPs, ISOs, MRA, etc about the changes of POC Manufacturing in the six aspects of Products, Processes, Premises, Procedures, Personnel, and Provision.

+ Building and employing the supports from national and international Assembles, Corresponding Boards and other Scientific and Regulatory communications.

+ Assuring and expanding the international collaboration in the response for global pandemic (e.g. Covid-19), and other urgent issues (e.g. nitrosamines crises) that can affect the pharmaceutical supply chain.

3.4. CONCLUSIONS

3.4.1. Summary

POC manufacturing will continuously change with advancing technology and data management, offering new opportunities for improved healthcare. This requires the current regulatory frameworks and documents to keep evolving to enable manufacture compliance and realise patient safety and benefits. There will be inevitable transformation of supply chains with embedded enhanced analytics in pharmaceutics and other disciplines (inter)nationally. From the representative case studies – evidence examples about the current opportunities and challenges of the UK pharmaceutical supply chain in terms of six core keys (including i) POC Products, ii) POC Processes, iii) POC Premises, iv) POC Procedures, v) POC Personnel, and vi) POC Provision), it is necessary for changes in this area, particularly for the official regulatory practices.

Recommendations for advancing POC Manufacturing are also considered, and specifically: i) Recent prospects of implementing POC Manufacturing within a sustainable pharmaceutical supply chain; ii) New frameworks of pharmaceutical supply chain considered in the context of the update of ISOs and renewal-revision of GPs with the support of enhanced data analytics; and iii) Government, public and private parties cooperation for successful planning and effective performance of current and future regulation-standards.

The suggested actions from this work include a proposed framework that will help the UK and other areas to become favourable locations to develop and trial novel medicines via POC manufacturing that is safely regulated and monitored, particularly after Covid-19 pandemic. This helps to build the corner stones for navigating the future progression by assessing the regulation-standards with data analytics to control the quality of emerging pharmaceutical supply chain in the future.

3.4.2. Outputs related to Chapter 3

a. Publication

- Quach, T. T., Sheridan, B., Glass, E. & Roberts, C. J. (2023). Effective transformations of sustainable pharmaceutical supply chains for point of care manufacture centred on consideration in the UK pharmaceutical sector, to appear in 3D Printing of Pharmaceuticals and Drug Delivery Devices, or the series of Advances in Pharmaceutical Technology eds. Sheng Qi, Dimitrios A. Lamprou & Dennis Douroumis, Wiley–Blackwell

b. Conference

- UK Making Pharmaceuticals Conference 2023 (MP23), Coventry, the United Kingdom, 25-26.04.2023

Oral presentation: "Frameworks for enhanced analytics in the pharmaceutical industry in the United Kingdom"

Tien Thuy Quach[1,2], Ben Sheridan**, Emma Glass**, and Clive J Roberts[1]

- Connected Everything Annual Conference 2022 “Digital Manufacturing Research Collaboration and Innovation” hosted by the Connected Everything Network – Victoria Gallery & Museum, Liverpool, the United Kingdom, 18-19.05.2022

Poster presentation: "Enhanced data analytics for the pharmaceutical supply chain in the United Kingdom", https://doi.org/10.6084/m9.figshare.19802251.v1

Tien Thuy Quach[1,2], Ben Sheridan**, Emma Glass**, and Clive J Roberts[1]

CHAPTER 4: DEVELOPMENT OF ADAPTIVE PROCEDURES FOR EXAMINING INTERFACES AND NANOSTRUCTURES OF ADDITIVELY MANUFACTURED ELECTRONIC PRODUCTS

4.1. INTRODUCTION

Due to the global shortage during and after Covid-19 pandemic, there is an increase of manufacturing new inductors, sensors, and relevant electronic products for electromagnetic and/or medical purposes. For example, connection pins or other conductive vias could be printed for vertical interconnections in electronics [219]. Another example was silver nanoparticle suspensions could be used for 3D-printing the conductive interconnectors in electronic chips [220].

In electronic materials and devices, the functionalities of the 3D-printed products will be affected due to the original designs, for example, the conductivity of final products will significantly reduce when having discontinuous structures. Several approaches were considered to improve the heterogenous distribution such as aerosol jet printing can deposit a focused gaseous stream of aerosolized ink (with different materials) at room temperature. However, this approach may require a thermal sintering as a post-processing step to increase the incorporation of deposited particles and enhance the conductivity [221]. Another example was multi-materials of metal nanoparticles on UV curable dielectric materials produced 3D sub-millimetre structures [222]. The existence of microcracks/pores after sintering can still limit the functionalities of final products, and it is also challenging to detect and overcome those microcracks/pores due to the variations of different manufacturing process (Figure 4.1) [223–226].

Therefore, Chapter 4 aims to show adaptive frameworks to understand and improve the cohesion among metal-metal and metal-polymer materials by investigating both commercialised and lab-based electronic printed products at the micro- and nano-scale.

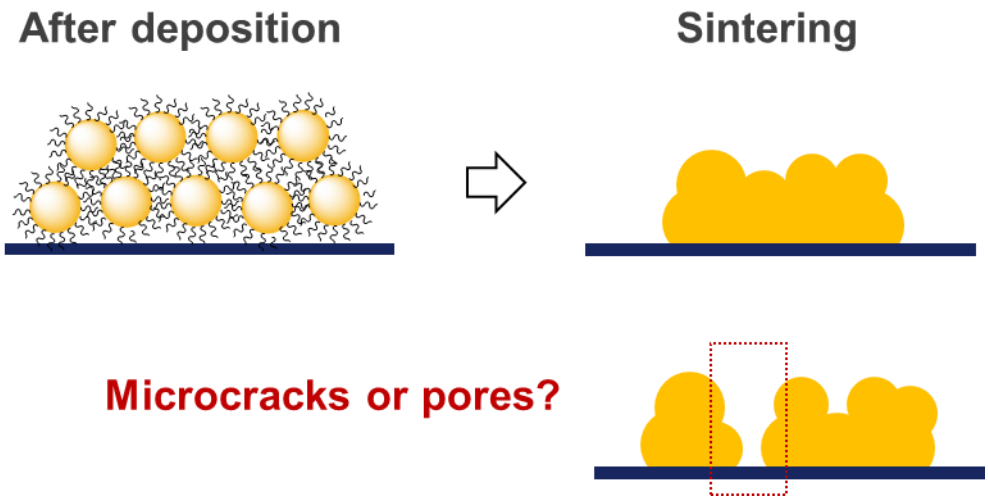

Figure 4.1. *Potential microcracks/pores existed when 3D-printing metal nanoparticles could limit the functionalities (e.g. reduced conductivity of the final products)* [223–226]

4.2. MATERIALS-METHODS

4.2.1. Materials

The work aims to develop standard procedures to expose internal interfaces and acquire morphological/structural data of 3D-printed functional electronic materials including 3D-printed commercialised inductor (DragonFly Product) and 3D-printed lab-based electrodes (flexible gold structures).

a. 3D-printed commercialised inductor (DragonFly Product)

The DragonFly™ systems makes it possible to 3D print electromagnetic coils, enabling product designers to vary physical shape and size for optimized application fit. By enabling increased Z direction tolerance, 3D printing can deliver significant improvements in electromagnet coil resolution. This also allows for lighter and more compact end products to be produced with lower time and costs [223–226].

The DragonFly is a commercialised product (manufactured by Nano Dimension Company), so some aspects of its formulation and production process are confidential. The applications of DragonFly products cover a diverse range of industries such as contributing to several medical devices and electromagnetic treatments. It has an insulated wire wound into a coil

around a core made of dielectric material. The coil is assigned with different circular connected layers in a 3D file such as a CAD model (Figure 4.2) [227].

The study aimed to investigate the printed metal-polymer interfaces and the distribution of different elements. The results could open new circuitry and cognitive-connected products for future healthcare applications.

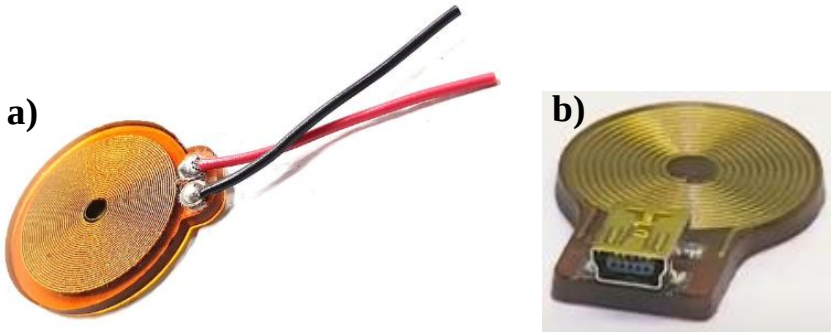

Figure 4.2. *Examples of the DragonFly™ systems include: a) 3D-printed inductor; and b) 3D-printed electromagnet connector* [227,228]

b. 3D-printed lab-based electrodes (flexible gold structures)

There are different fabrications of multi-material embedded electrodes and sensors in pharmacy/healthcare purposes. However, not all formulation and 3D-printing techniques can help achieve reliable conductivity and high resistance to oxidation (against external stimuli), particularly when printing electrochemical and/or electromagnetic devices [37229,219]. For example, Ink-jet Printing (IJP) has been used to produce metal nanoparticles, metal-organic decompositions, and aqueous conductive solution [36]. Therefore, as part of a wider project, Dr. Jisun Im was developing the most appropriate flexible gold structures for printing novel lab-based electrodes, and my novel analyses were conducted as part of this thesis supported this goal.

Two gold inks, termed Au-TrisSH and Ctrl-Au, were formulated with and without trimethylolpropane tri(3-mercaptopropionate), as cohesion enhancer, respectively. 25 wt% (1.59 vol%) of Octanethiol-functionalised gold nanoparticles (or OT-AuNPs) was dispersed in terpineol (mixture of isomers). 0.125 wt% of Trimethylolpropopane tri(3-mercaptopropionate) (or TrisSH) was added to produce Au-TrisSH ink formulation. The

particles were dispersed using a bath sonicator for 30 min and stored in the dark at ambient temperature before use. A single layer was sintered at 150°C on poly(ethylene naphthalate) (PEN) or silicon wafer (SW) substrate (Figure 4.3) [230].

The study aimed to identify the continuity and thickness of gold layer and analyse the interfaces between the ink and the substrate. The results could offer the fundamentals of manufacturing new electrodes and the correlation with the nanostructures of final products.

a)

Components	Ink formulation (wt%)	
	Ctrl-Au	Au-TrisSH
OT-AuNPs*	25	25
TrisSH**	0	0.125
Terpineol	75	74.875

*Octanethiol-functionalised gold nanoparticles
**Trimethylolpropane tri(3-mercaptopropionate)

b)

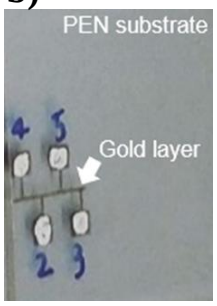

c)

Figure 4.3. *Flexible gold structures were developed in lab provided by Dr. Jisun Im: a) Ink formulation of Ctrl-Au and Au-TriSH; b) 3D-printed electrodes on PEN substrate; and c) 3D-printed electrodes on SW substrate*

4.2.2. Methods

a. Exposing interfaces

Due to the large size and high stiffness of the original DragonFly design which limited the immediate use of ultramicrotomy, it was useful to prepare the sample by applying mechanical force to form smaller fragmented parts to allow positions of interest to be studied. Direct visual observation was useful to choose suitable pieces such as having specified shapes or locating at the certain position for embedding the sample in the resin.

Figure 4.4 shows examples of the interfaces of interest in the DragonFly product and the gold conductive inks. Two specific positions were chosen for physical cross-sectioning to expose the interfaces of interest of the two different systems: metal-polymer at the central part and polymer only at the edge part of the DragonFly product and a single part (with central and sub line) of the gold conductive ink.

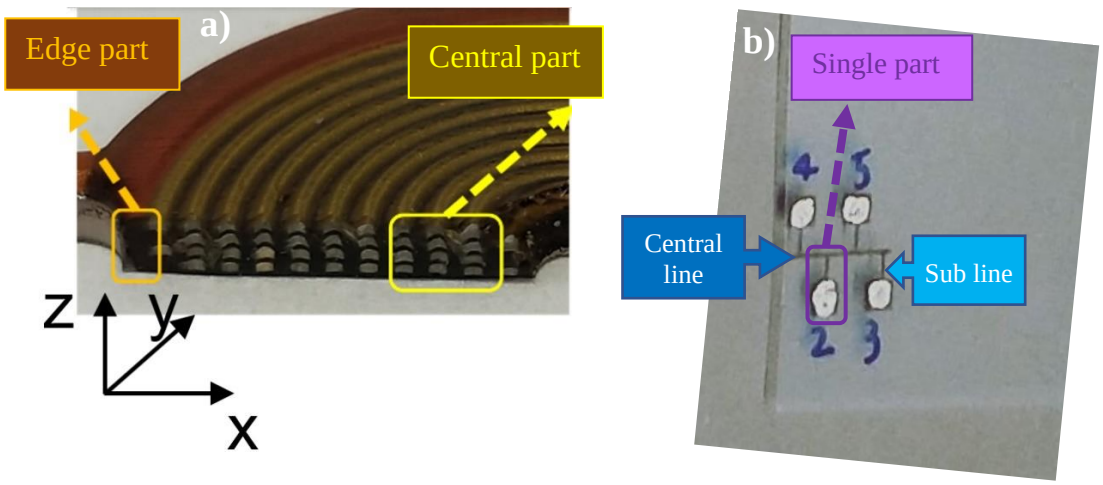

Figure 4.4. *Identifying the interfaces of interest: a) DragonFly product with central and edge parts, and b) gold formulation having central and sub lines*

i. Ultramicrotomy

A PowerTome PC (RMC Company) was used to expose the cross-sections before applying analysis. Each sample is embedded in Agar100 resin (Agar Scientific Company) before treating with DOW CORNING® Z-6040 Silane (Dow Company) to form a hard block. After 48h-drying in the vacuum oven at 60-70^{o}C for the polymerisation, the block face was trimmed and cut into different thicknesses by using the glass knife (Leica Knifemaker, Leica Microsystems Company) and a diamond knife (DiATOME Company) to create several trapezoidal shaped sections (with a typical size 0.1-0.2 mm, thickness 100-200 nm). Sections were dried at room temperature on filter paper (after wet sectioning with water) to deposit onto copper sample grids for later analyses with Scanning Electron Microscopy (SEM) and/or Transmission Electron Microscopy (TEM).

ii. Focused-Ion-Beam Scanning Electron Microscopy (FIB-SEM)

Focused-Ion-Beam Scanning Electron Microscopy (Zeiss Crossbeam XB550) was used to expose and analyse the interface-surface for combined purposes. For imaging, a secondary electron (SESI) microscope is operated at 2 kV and 100 pA to acquire original and cross-sectional images of the samples* (with SmartSEM software, Zeiss). For chemical testing, the gallium-FIB milling was used to expose the interfaces of 3D-printed samples before applying the Energy-Dispersive Spectrometer (EDS) (Oxford Instruments Company) to

capture elemental images at various magnifications. For thickness measurement, a gas injection system in Crossbeam 550 was used to deposit a carbon layer onto the targeted position to differentiate the sample's layer in the top view and side view.

b. Analysing interfaces

i. Scanning Electron Microscopy (SEM) characterisation

The morphology of block-faces and cross-sections were analysed by Scanning Electron Microscopy (SEM). Specimens are mounted onto aluminium stubs (using conductive carbon adhesive tape for the block). The sample surfaces were sputter-coated with a 14-nm thickness of carbon under argon using a Q150R Plus-Rotary Pumped Coater (Quorum Company). A SEM Quanta600 (FEI Company) with an Energy-Dispersive Spectrometer (EDS) (Bruker Company) were operated to capture images at various magnifications (as TIF files) in Quantax200 software.

ii. Transmission Electron Microscopy (TEM) characterisation

The surface topography of very thin cross-sections is identified by a Tecnai Biotwin TEM (FEI Company). Sections were placed onto the standard copper grid and kept dry at room temperature. Images were recorded as TIF files at high resolution and different magnification from TECNAI G2 software.

iii. Atomic Force Microscopy (AFM) characterisation

Atomic Force Microscopy (Dimension Icon, Bruker) with NanoScope Analysis software were used at two modes: 1) PeakForce Mapping in air with a scan size of 20 μm, scan rate of 0.2 Hz (512 lines), a PeakForce setpoint of 3.3 nN, and a PeakForce amplitude of 50 nm; and 2) Tapping in air with a scan size of 1 μm, a scan rate of 2 Hz (256 lines), an amplitude set point of 10 mV, and a drive amplitude of 50 mV. The two AFM tips (from Bruker), RTESPA 150 (with a medium force measurement of 6 N/m and a tip radius of 8 nm) and RTESPA 300 (with a high force measurement of 40 N/m and a tip radius of 8 nm), were used for PeakForce and Tapping mode imaging in air, respectively.

4.3. RESULTS AND DISCUSSION

4.3.1. Challenges and improvement in revealing the interfaces of the 3D-printed samples

The most common issue (when embedding the samples in resin) was the presence of bubbles in the resin block. The voids could be a result of air bubbles forming after embedding the sample in the resin (Figure 4.5). The resin blocks of the edge part in the brown colour region had many small voids (highlighted by the red circle in Figure 4.5a) compared to those of the central part. The bubbles might have formed from the quick mixing process (when making the liquid resin) and/ or the fast-pouring step that trapped air in the set resin.

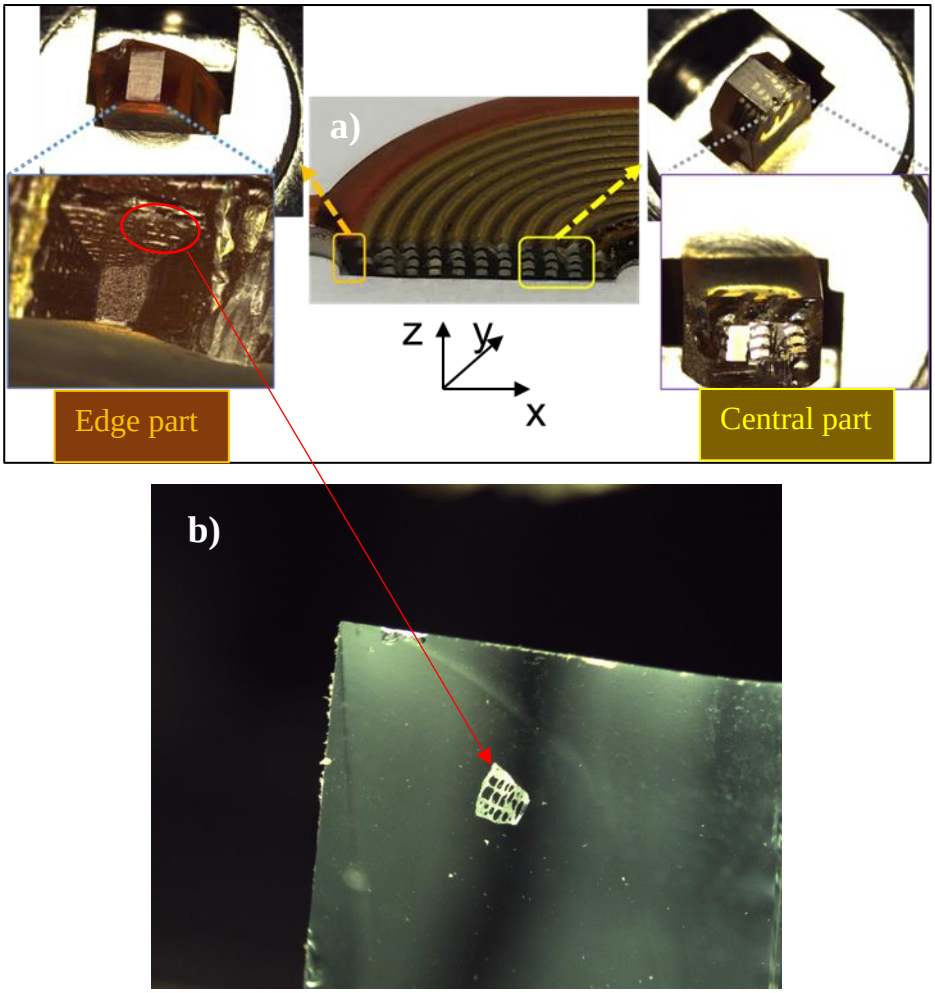

Figure 4.5. *General observation of the DragonFly products (after resin embedding): a) Overview of edge part and central part of the sample (with many small voids that were highlighted by the red circle) and b) An example of the cross-section had multiple holes from bubbles (after cutting a resin block of edge part by ultramicrotome)*

The sample position was adjusted to near the top of the resin mould to make post processing (such as trimming and cutting) more convenient. For example, the central line of the golden conductive ink that was of interest for the research was positioned near the top (Figure 4.6). However, the sample could not be fixed at that position, which was supposed to be parallel to the wall of the resin since for samples with a lower density than the liquid resin that tend to float freely in the liquid resin and then change their position in an uncontrolled fashion. Figure 4.6 also shows that the trimmed block could reveal an issue related to the embedding of the gold conductive ink: If the sample surface of the central line was not correctly assigned as parallel as expected (in red circle) to the surface of the resin block it caused inaccuracies when investigating the cross-sections with further imaging analysis such as the thickness measurements of different layers in the gold conductive ink. Therefore, it is recommended to observe and re-check the position of the samples in the liquid resin before drying step.

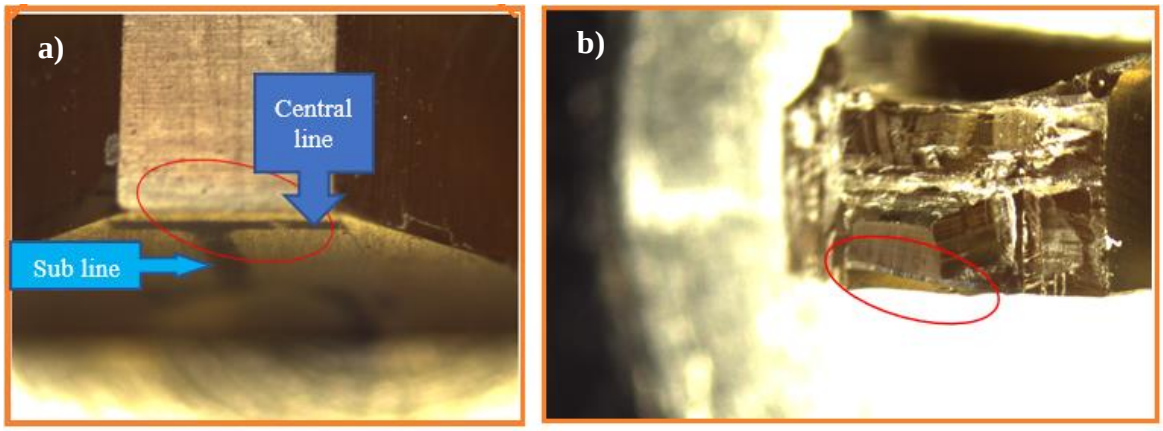

Figure 4.6. *Issue of allocating and ensuring the sample at the proposed position in the resin: a) Original block , b)Trimmed block. The surface of the central line of the golden conductive ink was not correctly assigned as parallel as expected (in red circle) to the surface of the resin block*

Figure 4.7a shows that the resin and the substrate (as PEN film) of the gold conductive ink were not closely attached, which resulted in the resin peeling off (as red circle in trimmed block) when trimming the sample because of different material properties (e.g. hardness) of the resin and the material. A potential solution for this issue was treating the sample with an epoxy primer before embedding it in resin to enhance the adhesion between resin and sample

substrate (as green circle in trimmed block) (Figure 4.7b). Also, sample sections could also curl over after trimming, again likely related to the variation of hardness among different material layers. The curling issue of new cross-sections from trimming the resin block of the gold conductive ink whereas this was not observed in the trimming process for the DragonFly product. It was because the gold electrodes (that was 3D-printed on PEN substrate) had more flexible structures which led to a lower level of hardness compared to the materials that were 3D-printed in the DragonFly product. It is therefore recommended to understand the difference in hardness between the resin and the sample, and the hardness of all materials should be tested and recorded as the reference benchmark before the sample embedment. Then, the suitable formula of resin could be selected for a specific material that has a relatively similar hardness. In addition, some parts of the resin layer of the sample were easily torn away when cutting (Figure 4.8) owing to the same reason - the weak bonding between the resin and the sample. This could be reduced by preparing new liquid resin for immediate usage and only kept under proper condition with high temperature (e.g. the oven 60-70^{o}C) and certain time (e.g. 48h) to restrict the contamination (such as dust or air bubbles) and preserve the initial properties (such as the hardness and viscosity).

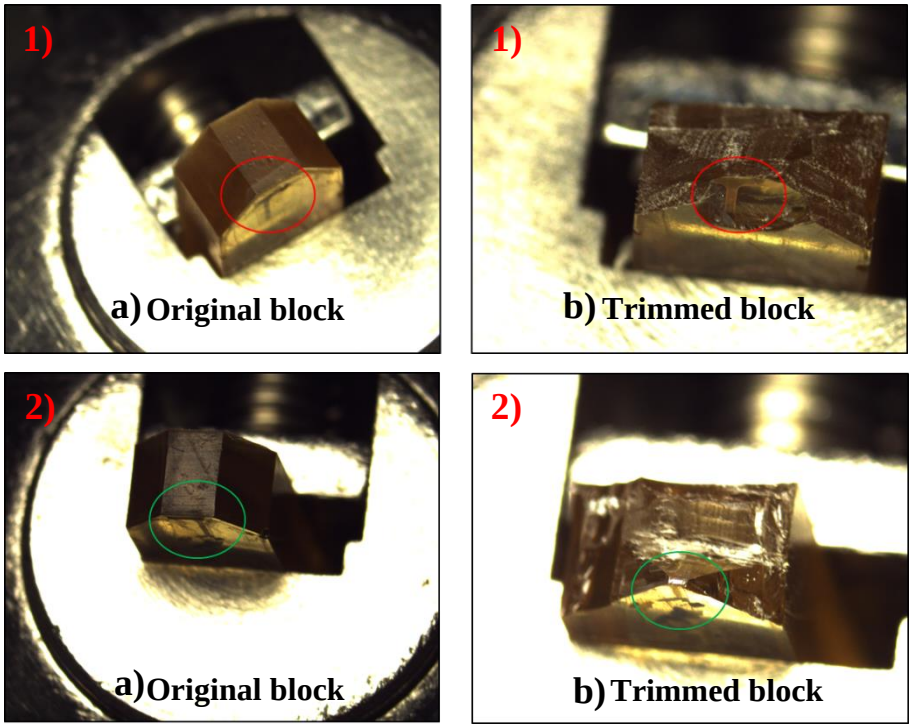

Figure 4.7. *Two approaches: 1) Directly embedding in resin (with red circle for the position where the resin peeling off), and 2) Treating with epoxy primer before embedding in the resin (with green circle for the position where resin still connecting). Each approach was illustrated via a) Original block, and b) Trimmed block.*

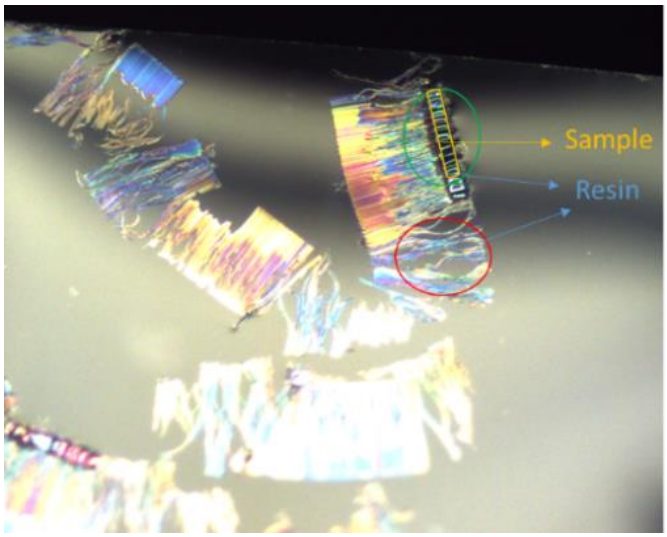

Figure 4.8. *Thin sections of the flexible gold structure (after cutting by a ultramicrotome) showed the part with normal adhesion (in green circle) and the parts were separated or easily torn away (in red circle)*

Compared to the diamond knife, the glass knife will be produced manually via the glass-cutting machine and the glass knife has lower stiffness, which could result in difference in the quality of the cross-sections of the samples. For example, it was difficult to expose the smooth surface of thin sections with the glass knife compared to the diamond knife (Figure 4.9). The reason for the uneven surface might be from the unqualified and/or unsharp surface after splitting the glass bar to make a knife [231]. The ultramicrotome can be used for dry or wet sectioning/ obtaining the sections for SEM or TEM (Figure 4.10): the wet-sectioning (or wet-obtaining) can help to acquire a ribbon of sections more easily owing to knife-friendly usage, low electrostatic charging and low compression, while the dry-sectioning (or dry-obtaining) does not need to deal with effects from the section floating in the liquid [58]. Each individual section of either the DragonFly product or the gold conductive ink could be separated and transferred onto a mesh grid with the support of a water bath (Figure 4.11). Another reason for preferring the wet sectioning was that the knife in water could help reducing the friction (between the knife and material) which can cause damage on the samples.

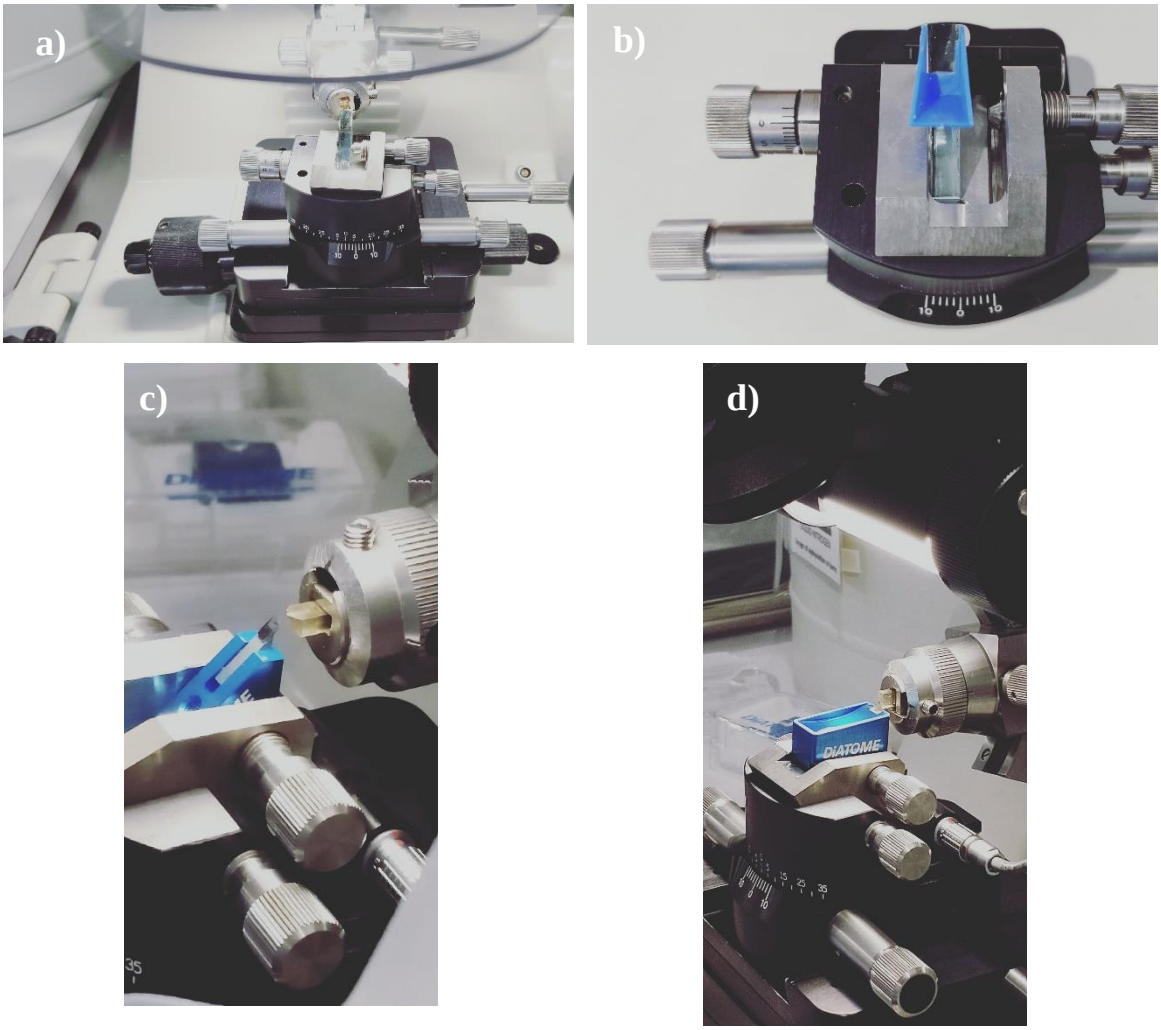

Figure 4.9. *Comparison between manually made glass knife and commercialised diamond knife showed the higher level for controlling the accurate and repeated ultra-thin sections of diamond knife (rather than glass knife) for wet-sectioning (rather than trimming or dry-sectioning): a) Glass knife set-up for trimming or dry-sectioning; b) Glass knife set-up for wet-sectioning; c) Diamond knife set-up for trimming or dry-sectioning; and d) Diamond knife set-up for wet-sectioning*

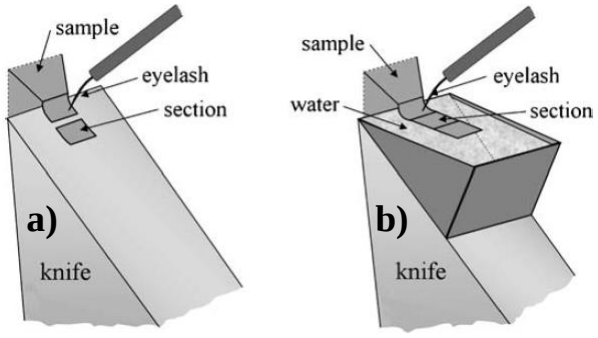

Figure 4.10. *Comparison between a) dry sectioning (when obtaining the sections directly in the air) and b) wet sectioning (when collecting the sections from the water surface onto a grid)* [58]

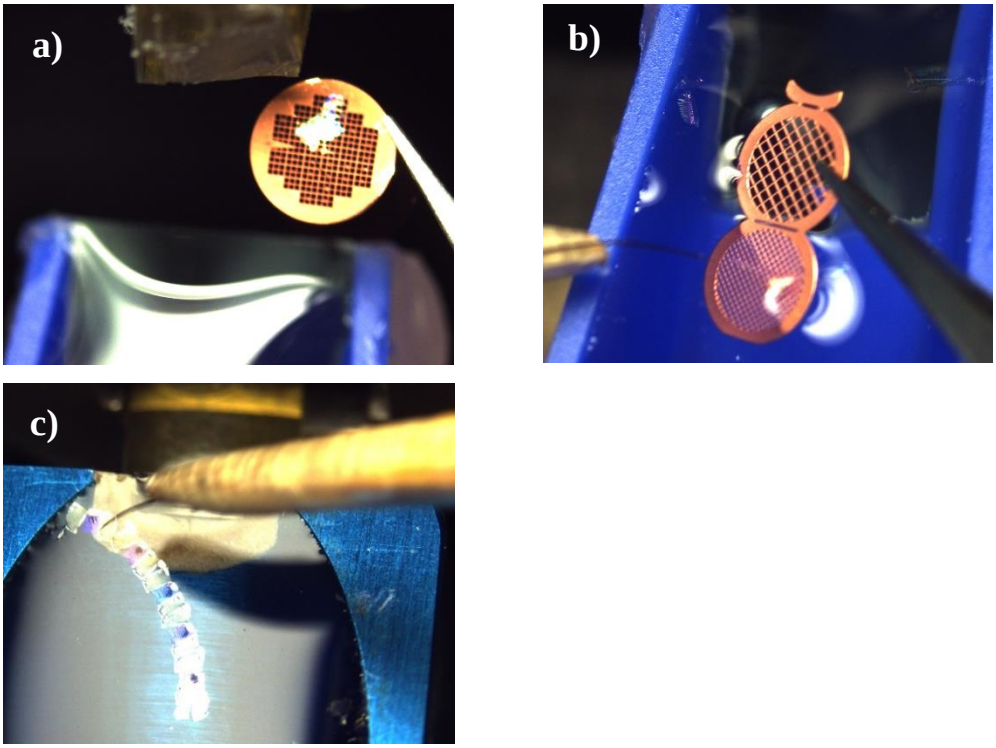

Figure 4.11. *Comparison of the cutting process: a) Cutting and collecting the sections of the DragonFly product; b) Cutting and collecting the sections of the gold conductive ink; and c) Series of ultra-thin cross-sections*

The important finding here was the need for compatibility (similarity) of the hardness between the resin and the 3D-printed multi-material. The sample could fall out if the resin is too hard to be attached firmly to the sample, or it will not support the sample when the

resin is too soft. Due to this adhesion issue, the resin should be selected and prepared to have the same hardness as the materials for the latter embedment [232]. The components and mixing process were presented in Figure A2.1 and A2.2 in Appendix A2. Besides, some porous substances (such as polymer) might need extra support to produce thin films, such as treating them with epoxy primers before sample embedment to promote adhesion between samples and resin.

In summary, I successfully developed an adapted standard procedure of ultramicrotomy for 3D-printed electronics to reveal the interfaces of 3D-printed electronics, which includes six main steps (Figure 4.12): 1) *Identifying* the positions of interest and applying mechanical forces (if necessary) to build; 2) *Embedding* small samples inside an epoxy resin after preparing the liquid monomeric plastic resin and treating with epoxy primer (if necessary); 3) *Polymerizing* the plastic resin to form a hard block by drying in an oven at 60-70^{o}; 4) *Trimming* the block face by using a trimming (diamond) knife to create a trapezoidal shape; 5) *Cutting* the small trapezoid with the glass knife (made by splitting a glass bar) or a diamond knife for wet-sectioning; 6) *Obtaining* the sections for further imaging analysis with a support, such as the TEM grid.

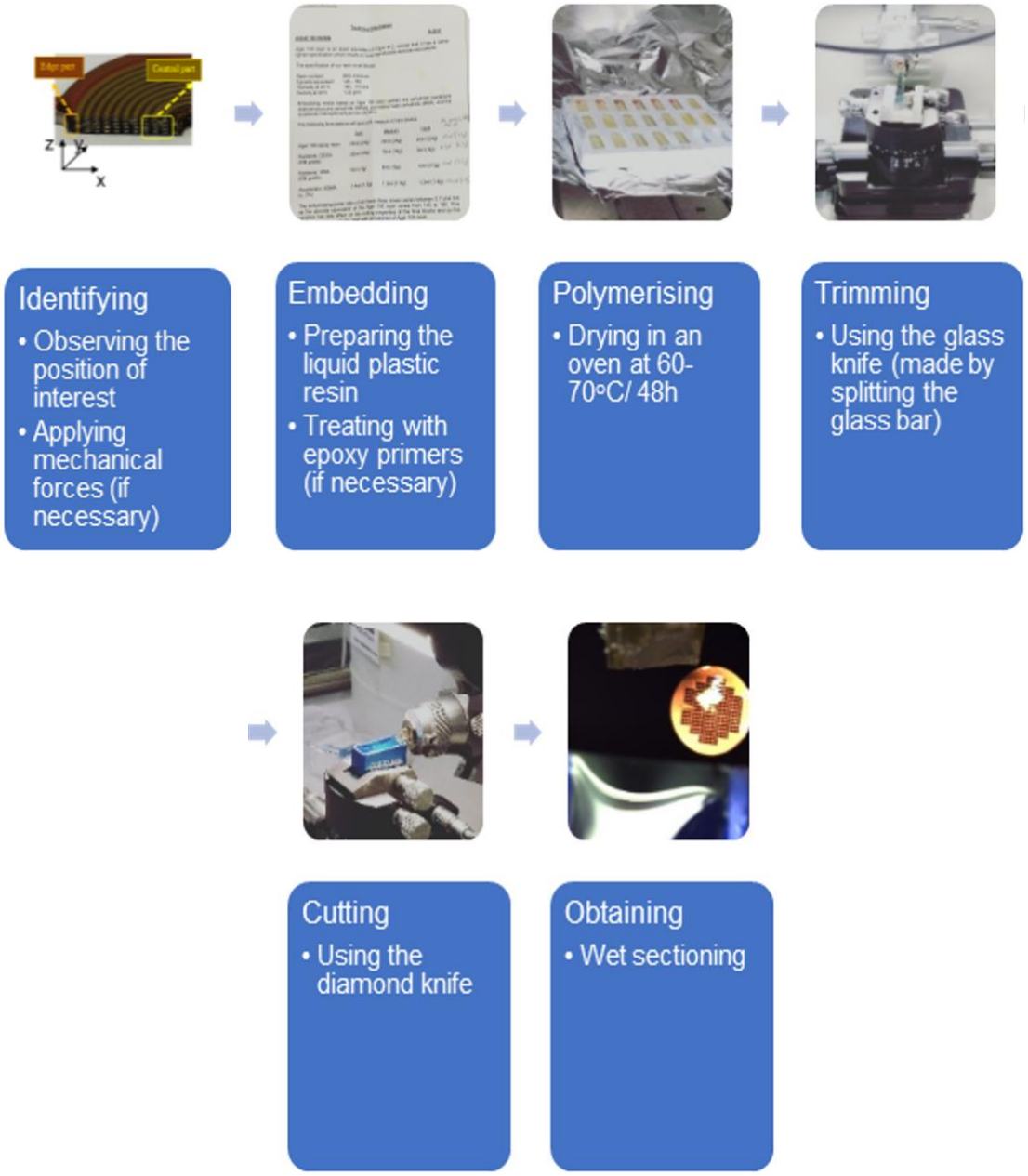

Figure 4.12. *Adapted standard procedure of ultramicrotomy for 3D-printed electronics consisted of six main stages such as Identifying, Embedding, Polymerising, Trimming, Cutting, and Obtaining*

4.3.2. Challenges and improvement in examining morphology and nanostructures of the 3D-printed samples

a. 3D-printed commercialised inductor (DragonFly Product)

There was an obvious difference between edge and central parts of the DragonFly product when observing the internal surfaces (Figure 4.13a). Moreover, different areas of metal and polymer were found at Figure 4.13b: dissimilar structures existed at the left/right direction compared to the top/bottom direction, which might be due to the initial 3D-printing design when metal droplets were spreading on the polymer base. Particularly, the left/right side had the tail structures, the final bottom layer was a straight line, but the top and another bottom layer had curved features.

The presence of metal (observed as light blue in Figure 4.13c) was confirmed with the most intense EDX peak (Figure 4.13d) being for silver in the sample whereas the remaining region was designated as the polymer. Hence, from SEM images (Figure 4.13b), the main distribution of silver was a well-aligned range of single metal units. Each unit had the same 'tail-like' structure at their edge (marked by red circles for the bottom left metal unit in Figure 4.13b). There were the same intervals of distance between each single metal unit, at approximately 200 μm (as yellow arrow in Figure 4.13b).

Information of the formulation and printing process of DragonFly product is confidential, but the reason might be due to that conventional thermal sintering caused deformation of the deposited silver ink droplet, which caused the effect on stretching the top and other bottom line [233]. The sintering process referred to surfactants' removal to promote the agglomeration of particles and the particle growth in the ink [234].

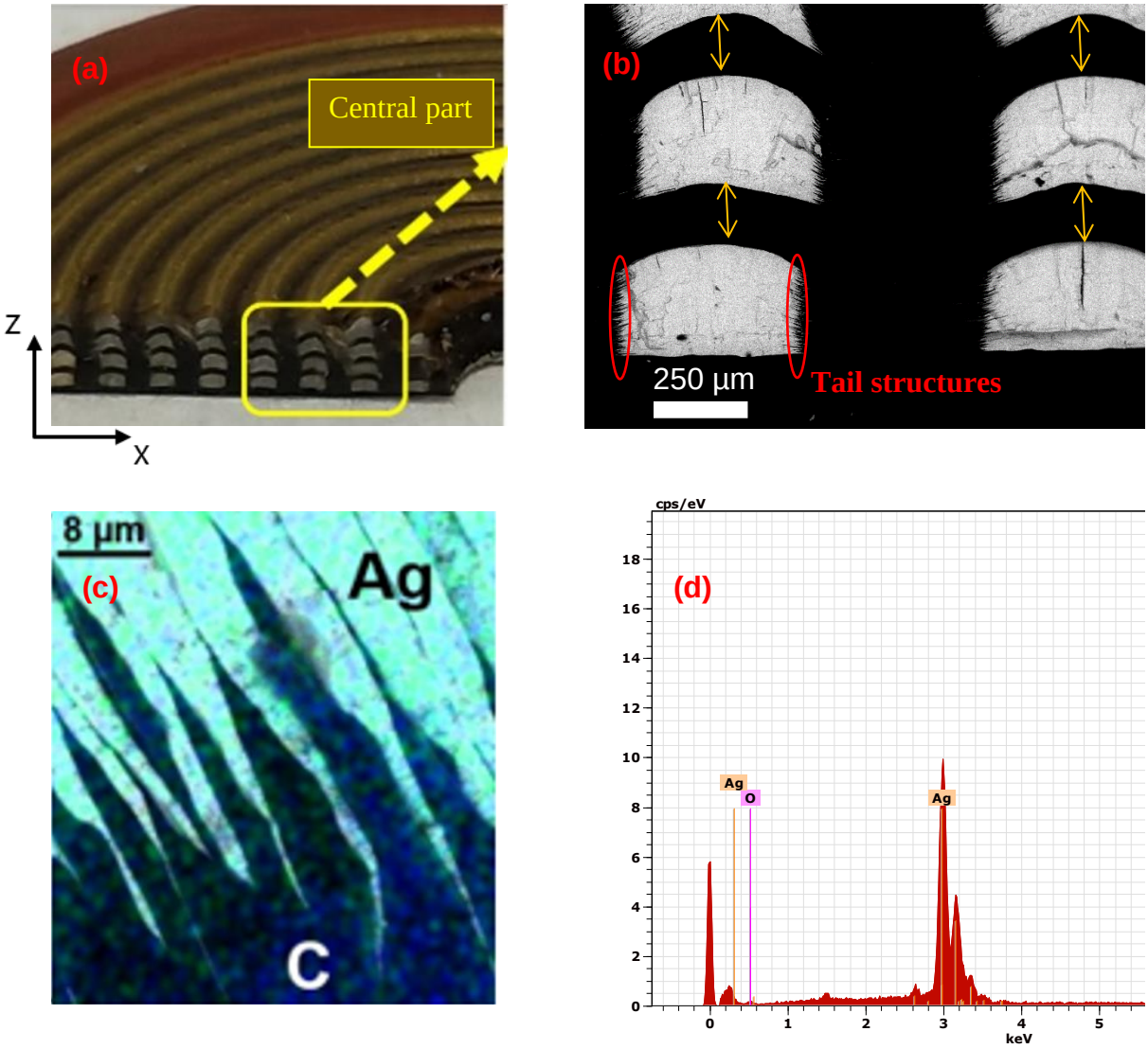

Figure 4.13. *Morphology and nanostructures of DragonFly product: (a) Image of original 3D-printed sample (showed obvious difference between edge and central part), (b) SEM image (revealed different areas of metal and polymer), (c) EDX mapping image (revealed the distribution of Ag and C), and (d) EDX elemental spectra confirmed the presence of Ag*

Furthermore, TEM images from Figures 4.14 shows the metal as dark (i.e. low electron transmission) regions and the polymer as lighter regions (more electron transparent) [84]. Several white grains associated with the silvers which were not completely fused due to the initial printing process. The cross-sections showed the tendency of direct attachment between metal layers and polymer layers, and the metal tail structures had different shapes and sizes compared to the polymer parts at this edge part of the DragonFly product. The

accumulation of silver nanoparticles was illustrated in the tail structure at the central part of the DragonFly product. TEM data confirmed the tail structure made of metal nanoparticles, which was consistent with the SEM results.

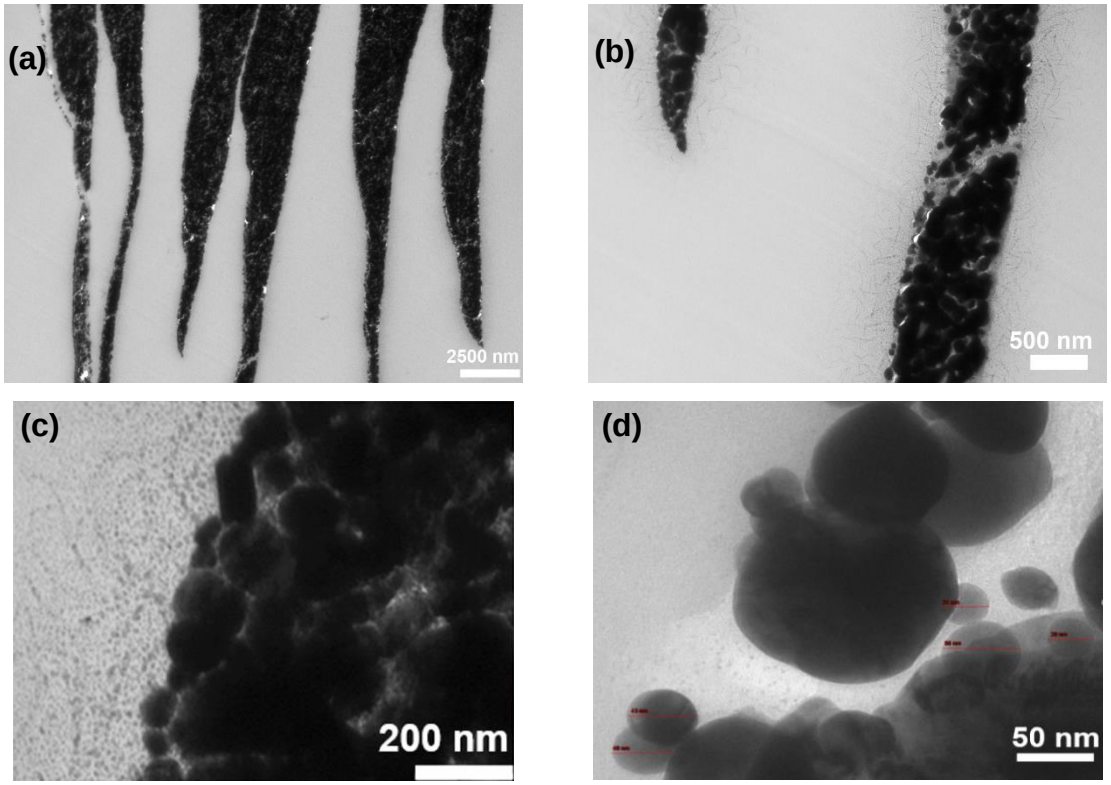

Figure 4.14. *TEM images of the tail structures (founded mainly at the central part) of the DragonFly product at different magnifications: (a) x4.2k, (b) x20.5k, (c) x87k, and (d) x220k. The results confirmed silver nanoparticles distributed unevenly that formed metal layer.*

b. 3D-printed lab-based electrodes (Flexible Gold Structures)

There were some scratches and curled/ folded areas of a single section of the gold conductive ink, which made it difficult to interpret the morphological data. This happened because the sections of the gold did not attach strongly to the resin layers during cutting process. Hence, a more suitable resin should be selected based on the compatibility of the material's hardness and surface properties, and the analytical process (particularly trimming and cutting) optimised to reduce the occurrence of scratches and scrolled/ folded areas.

However, it was challenging to use ultramicrotomy for sectioning the 3D-printed materials on the stiffer substrates (such as silicon wafer) due to inability of cutting and/or damages of

the original structures during cutting. Therefore, I proposed and validated a new approach of using FIB-SEM with four main steps (Figure 4.15): a) Deposition with Carbon; b) Milling with Gallium; c) Imaging for preliminary morphology; and d) Analysing to acquire thickness data. This approach was tested and developed by utilising innovative FIB-SEM which has a focused ion beam and gas injection system for sample sectioning along with the detecting functions to take images at high resolution with very low voltage. Therefore, I could successfully prepare and investigate samples effectively at once, which could help to reduce the time and cost of analysis. As a result, a single layer printed gold structure on a PEN substrate (Ctrl-Au) had the layer thickness confirmed as 163 ± 24 nm from FIB-SEM analyses.

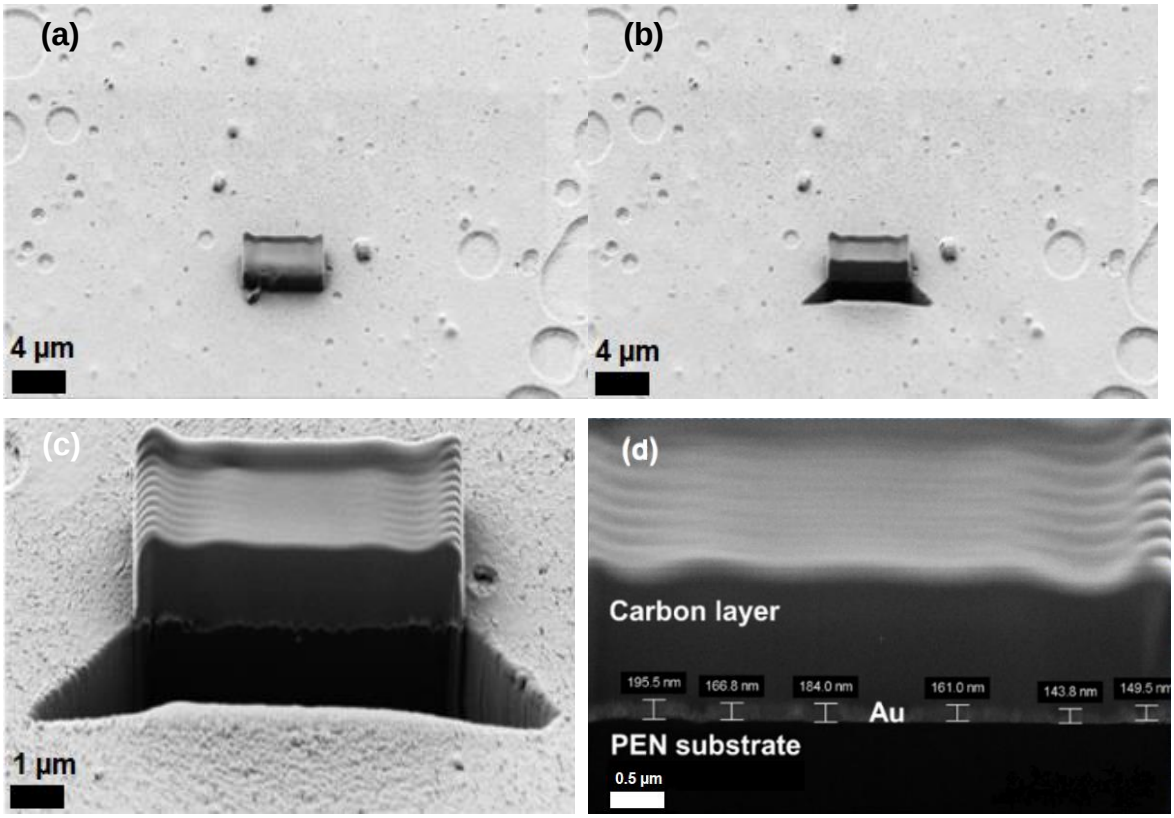

Figure 4.15. *New approach using FIB-SEM to identify morphology and thickness of printed gold formulation as a case study (e.g. single layer of Ctrl-Au) via four main steps: (a) Deposition with Carbon; (b) Milling with Gallium; (c) Imaging for preliminary morphology; and (d) Analysing to acquire thickness data*

To elucidate the role of a cohesion enhancer in improved electrical and mechanical properties, the chemical composition and presence of microstructures were investigated when being compared between the inkjet printed Au-TrisSH and the Ctrl-Au. Atomic force microscopy (AFM) was chosen for investigating the surface roughness because it could provide different standard roughness parameters with shorter time and lower cost. AFM images of the Ctrl-Au (with single layer on Si/SiO_2 substrate, sintering temperature is 150ºC) (Figure 4.16a) revealed a porous structure with pore diameters in the range of 1-2 µm and an average surface roughness R_a = 14.1 nm, root mean squared surface roughness R_q = 18.5 nm, and surface area roughness R_{sa} = 9.6 nm (estimated from 1 µm × 1 µm AFM images). R_q is the square root of the distribution of surface height and is considered to be more sensitive than R_a which is the average roughness for large deviations from the mean line/plane, and R_q is also used in computing other amplitude average parameters (according to ISO Standard [235]).

The formation of the pores was driven by coalescence of NPs at high T_{sint} to reduce their surface energy and decrease surface area during sintering. In contrast, the surface of the Au-TrisSH layer was found to be more continuous and denser compared to Ctrl-Au with reduced roughness values of R_a = 7.1 nm, R_q = 10.5 nm, and R_{sa} = 3.0 nm (Figure 4.16b). These results indicate that TrisSH helps to produce a more uniform and smooth printed gold layer. A considerable difference in grain microstructures of the printed layers was also noted, where non-uniform large grains were observed in Ctrl-Au layer compared to Au-TrisSH. The more uniform smaller grains observed for Au-TrisSH can be attributed to the role of TrisSH bound to neighboring NPs, which results in denser NP packing and enhanced cohesion. AuNPs without TrisSH are likely to have increased mobility on the substrate during sintering, leading to the formation of larger grains and pores within the printed structure. The universality of the ink formulation whereby the roughness of the Au layers are comparable when deposited on a polished Si/SiO_2 substrate (surface roughness typically < 1 nm) and on a PEN film. This result strengthened the previous FIB-SEM results that the existence of cohesion enhancer (TrisSH) could help to create a more uniform and smoother surface of a printed gold layer.

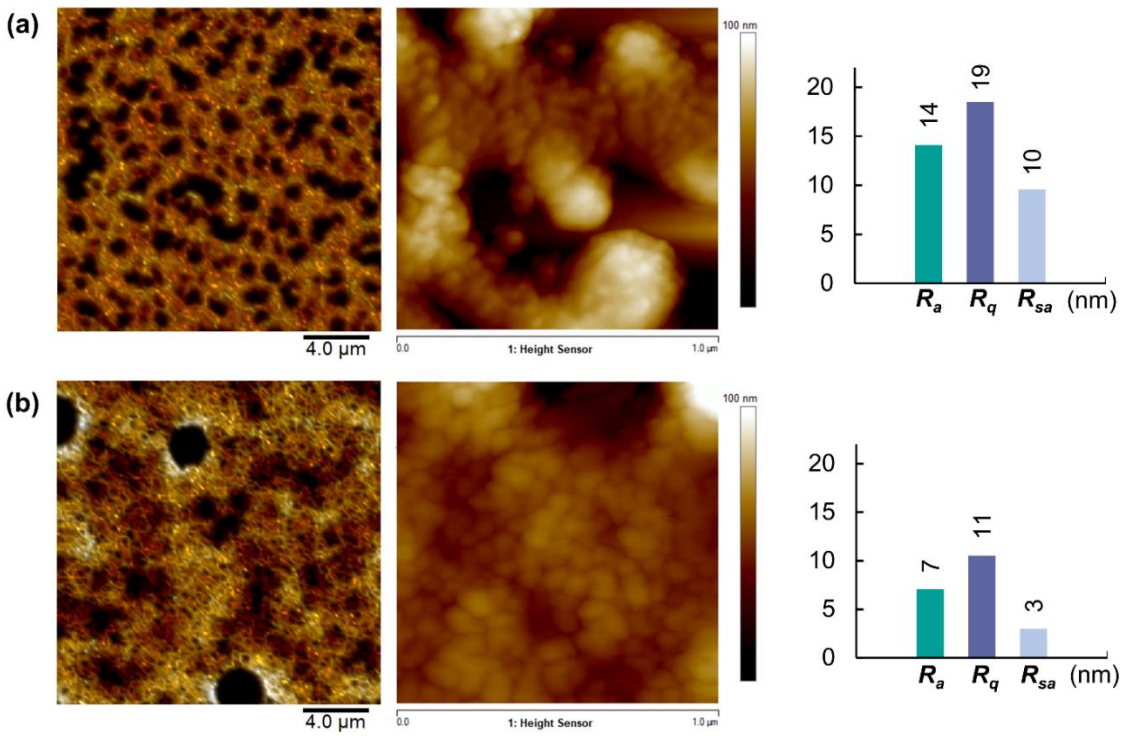

Figure 4.16. *Representative AFM images of surface morphology and microstructure characterization of single layer printed gold structures (Si/SiO_2 substrate, T_{sint} = 150°C) of (a) Ctrl-Au and (b) Au-TrisSH. The left images were acquired using PeakForce tapping mode (20 µm × 20 µm); the middle images show high resolution images over 1 µm × 1 µm (tapping mode); the right graphs show surface roughness values, R_a, R_q, and R_{sa}, estimated from 1 µm × 1 µm images*

4.4. CONCLUSIONS

4.4.1. Summary

From investigating the DragonFly product, the interfaces of cross-sections showed different features across the device due to the initial 3D-printing design or artifacts of analysing process, with a consistent interval of distance between single metal units. This difference could be due to the material properties (when printing to design the product) and/or the sample preparation (when picking the specific pieces of original products to embed in resin). The results showed each metal unit had tail-like structures associated with them. The silver nanoparticles were mainly at the central part of the DragonFly product. The number of pores observed at the edge regions should be decreased by optimising the 3D-printing process.

The production of DragonFly product could be modified for better performance of inductance when designing different layers of metals and polymers.

The uniform layer thickness of the 3D-printed lab-based electrodes was confirmed which played important part for the measurement of electrical properties of the flexible gold structures. Focused ion beam-scanning electron microscopy (FIB-SEM) was proven as the powerful preparation technique for sectioning and imaging of a single layer printed gold structure revealed the layer thickness of 163 ± 24 nm. These initial analytical results were helpful to improve the electrical conductivity measurements (related to the metal nanostructures and distribution), and to develop the most appropriate 3D-printed formulations for printing electrodes. Among different elements, gold is a suitable material due to its high conductivity, high resistance to oxidation, and stability when manufacturing at high temperature; and the cohesion enhancer offered more continuous and denser microstructures for new flexible gold electrodes. Ultramicrotomy and FIB-SEM were developed for sectioning samples. SEM, TEM, and AFM was ultilised to investigate morphology of a printed gold structure.

Two sample preparation and investigation processes were successfully optimised for confirming the interfaces and nanostructures of the additively manufactured electronic products as below: i) First approach: Using Scanning Electron Microscopy (SEM)/ Transmission Electron Microscopy (TEM) after applying adapted ultramicrotomy with six main steps including 1) Identifying, 2) Embedding, 2) Polymerising, 4) Trimming, 5) Cutting, and 6) Obtaining (as in Figure 4.13); ii)Second approach: Using Atomic Force Microscopy (AFM) and Focused-Ion-Beam Scanning Electron Microscopy (FIB-SEM) with three main steps including 1) Deposition with Carbon, 2) Milling with Gallium, and 3) Imaging/Analysing. Therefore, the findings from this study revealed the benchmark of cross-sectioning and analysing of the 3D-printed metal nanoparticles in electronics.

4.4.2. Outputs related to Chapter 4

a. Publication

- Quach, T. T., Trindade, G. F., Hague, R., Roberts C. J. Challenges and opportunities of sample preparation and examination of additively manufactured electronic products (in preparation).

● Im, J., Trindade, G. F., Quach, T. T., Sohaib, A., Wang, F., Austin, J., Turyanska, L., Roberts, C. J., Wildman, R., Hague, R., & Tuck, C. (2022). Functionalized Gold Nanoparticles with a Cohesion Enhancer for Robust Flexible Electrodes. ACS Applied Nano Materials, 5(5), 6708–6716. https://doi.org/10.1021/acsanm.2c00742

ACS APPLIED NANO MATERIALS

www.acsanm.org Article

Functionalized Gold Nanoparticles with a Cohesion Enhancer for Robust Flexible Electrodes

Jisun Im,* Gustavo F. Trindade, Tien Thuy Quach, Ali Sohaib, Feiran Wang, Jonathan Austin, Lyudmila Turyanska, Clive J. Roberts, Ricky Wildman, Richard Hague, and Christopher Tuck*

Cite This: ACS Appl. Nano Mater. 2022, 5, 6708–6716 Read Online

ACCESS | Metrics & More | Article Recommendations | Supporting Information

ABSTRACT: The development of conductive inks is required to enable additive manufacturing of electronic components and devices. A gold nanoparticle (AuNP) ink is of particular interest due to its high electrical conductivity, chemical stability, and biocompatibility. However, a printed AuNP film suffers from thermally induced microcracks and pores that lead to the poor integrity of a printed electronic component and electrical failure under external mechanical deformation, hence limiting its application for flexible electronics. Here, we employ a multifunctional thiol as a cohesion enhancer in the AuNP ink to prevent the formation of microcracks and pores by mediating the cohesion of AuNPs via strong interaction between the thiol groups and the gold surface. The inkjet-printed AuNP electrode exhibits an electrical conductivity of 3.0×10^6 S/m and stable electrical properties under repeated cycles (>1000) of mechanical deformation even for a single printed layer and in a salt-rich phosphate-buffered saline solution, offering exciting potential for applications in flexible and 3D electronics as well as in bioelectronics and healthcare devices.

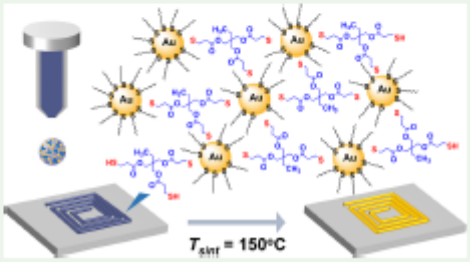

KEYWORDS: gold nanoparticles, conductive ink, cohesion, inkjet printing, flexible electronics, additive manufacturing

INTRODUCTION

There is a strong demand for conductive inks to enable the additive manufacturing of a new generation of functional electronics, including printed and flexible electronics, wearable and healthcare electronics, and consumer electronics.[1−3] Various types of conductive inks have been developed, including those containing metals (e.g., silver,[4,5] gold,[6−8] copper,[9,10] and so forth), carbon allotropes (e.g., graphene,[11,12] CNT,[13,14] and so forth), and conductive polymers (e.g., PEDOT:PSS).[15,16] Of particular interest are conductive inks based on metal nanoparticles (NPs), which can be sintered at a lower temperature compared to that of the corresponding bulk metal due to the high surface area to volume ratio,[17] and they exhibit relatively high electrical conductivities.[18]

To date, research efforts have mostly focused on silver NP inks. However, highly mobile Ag ions generated in the presence of heat and applied electric fields are capable of diffusion through pinholes in the SiO_2 layer, which has detrimental effect on the quality of the gate in Si/SiO_2-based electronic devices.[19,20] A gold NP (AuNP) conductive ink has the potential to overcome these limitations. Also, the chemical stability and biocompatibility of gold are particularly advantageous for bioelectronics that are operational in harsh environments, such as high humidity and salt-rich fluids (e.g., body sweat).[21]

Despite the body of work, the NP-based layer suffers from thermally induced microcracks and pores, causing device failure.[22,23] The attempts to resolve this issue focused on pressure- or ultrasonic-assisted sintering.[24,25] However, there is still a strong demand for new conductive inks, which will enable the deposition of stable and durable layers.

In this work, we develop a AuNP ink formulation with a cohesion enhancer, which prevents the formation of microcracks and pores and enables the deposition of stable layers with respect to their morphological and electrical properties. AuNP functionalization with a cohesion enhancer can be produced by a two-step method: (i) synthesis of octanethiol-functionalized AuNP (OT-AuNPs) and (ii) ligand exchange reaction. The Brust method is used for the synthesis of OT-AuNPs since it reliably produces large quantities of relatively monodisperse NPs.[26,27] The OT-AuNPs are further functionalized with a multifunctional thiol, trimethylolpropane tri(3-mercaptopropionate) (TrisSH), via ligand exchange. The

Received: February 17, 2022
Accepted: April 6, 2022
Published: April 25, 2022

b. Conference

● European Conference on Applications of Surface and Interface Analysis 2022 (ECASIA 22) with the theme “Surface Analyses for Advanced Manufacturing” hosted by the University of Limerick - Limerick, Ireland, 29.05-03.06.2022

Poster presentation 1: "Surface and interface study of the new gold conductive formulations in additive manufacturing"

Tien Thuy Quach[1,2], Gustavo F. Trindade[2,3], Jisun Im[2], Richard Hague[2], Clive J. Roberts[4]

● FORGE 2022 hosted by the Particle Characterisation Interest Group – Royal Society of Chemistry, Northern Ireland, the United Kingdom, 23-24.03.2022

Oral presentation: “Interface analysis of the new gold conductive ink formulation”

Tien Thuy Quach[1,2], Gustavo F. Trindade[2,3], Jisun Im[2], Richard JM Hague[2] and Clive J Roberts[1]

● Postgraduate Allied Health Research Conference (AHPGR) 2022 hosted by the University of Nottingham - Virtual session, the United Kingdom, 12-14.01.2022

Flash poster presentation: “Interface analysis of the new gold conductive ink formulation”

Tien Thuy Quach[1,2], Gustavo Trindade[2,3], Jisun Im[2], Richard JM Hague[2] and Clive J Roberts[1]

● 2021 Annual International Solid Freeform Fabrication Symposium (AISFFS), 02-04.08.2021. *Oral presentation: “Gold Conductive Ink Formulation with Enhanced Cohesion for Material Jetting”*

Jisun Im[2], Gustavo F. Trindade[2,3], Tien T. Quach[1,2], Ali Sohaib[2], Feiran Wang[2], Richard Hague[2] and Christopher Tuck[2]

● Formative Formulation 2 Conference, 12.03.2021

Poster presentation: “Micro/nanoscale analyses of the interfaces of the next-generation 3D-printed multi-materials”

Tien Thuy Quach[1,2], Gustavo F. Trindade[2,3], Richard JM Hague[2] and Clive J Roberts[1]

c. Internal seminar

● Oral presentation at the Advanced Materials and Healthcare Technologies Division, School of Pharmacy, University of Nottingham

CHAPTER 5: DEVELOPMENT OF PRACTICAL GUIDE TO INVESTIGATE THE PHYSIOCHEMICAL COMPATIBILITIES OF NEW INK FORMULATIONS IN ADDITIVE MANUFACTURING

5.1. INTRODUCTION

There are many new materials that could be synthesised and screened in the lab for the applications of biopharmaceuticals in additive manufacturing. For example, more photopolymers have been under investigation for high dielectric particles and the capacitors with complex geometries and capacitance [229]. Another example was new models of the drug-loaded systems with printable inks is recently developed to control release dosage forms and implants [236].

Recently, microstructure can be used to predict and monitor during the ink-jet printing process to design and manufacture personalized subdermal implants with targeted release [237]. However, it is challenging to offer effective manufacturing and characterising process to provide and confirm the homogenous mixtures of different combinations (such as organic-organic and organic-inorganic substances) especially at the desired locations [238,239]. Particularly, different ink formulations with separate physical and chemical properties will have dissimilar interfacial areas between ink formulations and substrates. This may limit the final functions of 3D-printed products, for example, the printability of several copolymers was diminished due to the instability under high temperature [238–243].

Therefore, Chapter 5 aims to develop a practical guide to investigate the physiochemical compatibilities of new ink formulations in additive manufacturing, particularly in pharmacy/healthcare applications (Figure 5.1). This would help to reveal the dynamic ink-substrate behaviour and offers the appropriate methodologies to investigate the ink-ink interactions.

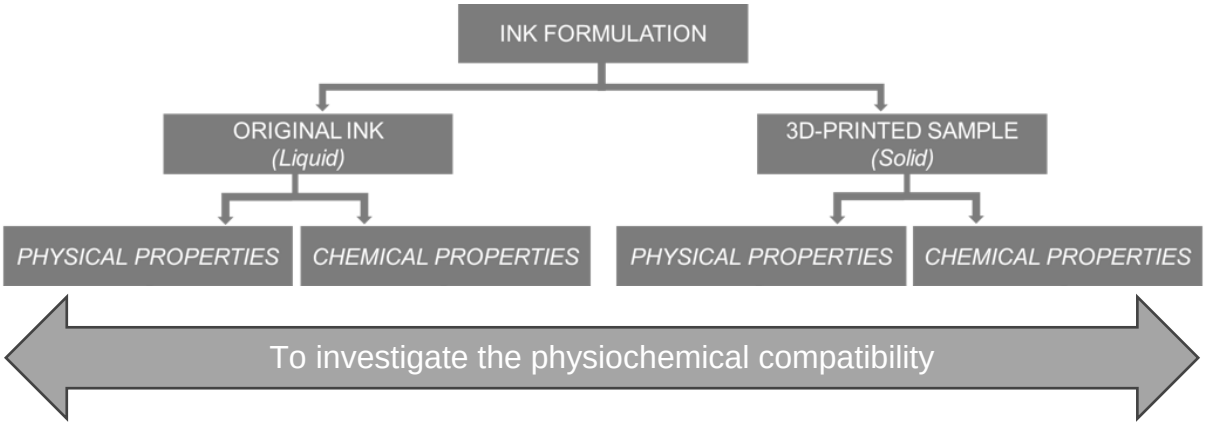

Figure 5.1. *New ink formulations in additive manufacturing have different physiochemical properties*

5.2. MATERIALS-METHODS

5.2.1. Formulation

a. Chemicals and substrates

Recently at Nottingham, several lab-based synthesized chemicals have proven to have novel properties such as bacteria-biofilm resistance [244–248]. These include a suitable combination of specific monomers and photoinitiators to be ready for ink-jet 3D-printing.

The interface study was constructed based on ink-jet printing of two inks:

i) The commercial substance SUP707^{TM} (Stratasys Company) was chosen as the water-soluble ink (WI) to help to formulate the more complex topography of ink-jet co-printed objects (due to their easy and fast dissolving in water during further post-processing)

**The components of commercial substance SUP707^{TM} were confidential according to the manufacturer.*

ii) Tricyclo decanedinmethanol diacrylate (TCDMDA), Ethylene glycol dicyclopentenyl ether acrylate (EGDPEA) and 2,2-Dimethoxy-2-phenylacetophenone (DMPA) (purchased from Sigma-Aldrich Ltd) were selected to formulate the structural ink (SI) having properties that are resistant to bacterial colonization and biofilm formation.

Three common substrates were investigated during the printing process: i) Glass slides with 1-2 mm thickness (Thermo Fisher Scientific Ltd), ii) Polyethylene naphthalate (PEN) films with 75 mm thickness (GTS Flexible Materials Ltd), and iii) Silicon wafers (SW) that had a low pressure chemical vapor deposition (LPCVD) coating on two sides with 500 nm Silicon

Nitride (Si_3N_4), p-type (boron-doped) (PI-KEM Ltd). The investigated substrates were treated with different solvents such as Water (Ctrl), Isopropanol (Iso), and Acetone (Ace) in the Ultrasonic Baths before being dried in a stream of Argon gas at room temperature in order to minimise the risk of residues and/or contaminants on the surface.
All remaining chemicals were purchased from Sigma-Aldrich Ltd.

b. Ink formulations

Two inks were used for the investigation: 1) Water-soluble ink (WI) included 100wt% SUP707™; and 2) Structural ink (SI) included 50wt% Tricyclo decanedinmethanol diacrylate (TCDMDA), 50wt% Ethylene glycol dicyclopentenyl ether acrylate (EGDPEA), and 1wt% 2,2-Dimethoxy-2-phenylacetophenone (DMPA). Table A2.1 in Appendix A2 shows the chemical structures of components forming SI.

The structural ink was prepared in 20mL vials each time by adding a corresponding amount of photoinitiators in the right combination of monomers before mixing on the Amicus hotplate with the 10mm-PTFE coated magnets at high speed (800-1000 rpm) and room temperature (20-25°C) in 15 minutes.

To reduce bubbles and particles, both inks were sonicated in a Bransonic Ultrasonic Cleaner for 15 minutes before being filtered through a 0.45µm Minisart filter, which were ready to fill up the printer chamber.

c. Inkjet 3D-printing

SUSS LP50 Inkjet Printer (from PiXDRO 50 Ltd.) with two printheads Spectra® SE-128 AA (from FUJIFILM Dimatix Inc.) was used; and each printhead had 128 nozzles (or maximum addressable jets) has the nozzle diameter of 35 µm (and nozzle spacing of 508 µm). The Advanced Drop Analysis (ADA) Model was used to check and calibrate the active nozzles. The dual head assembly was equipped with the LED UV curing unit Phoseon Firefly™ (from Intertronics Co.) that could produce up to 4W/cm^2 peak irradiance at 395nm with the emission window of 25 x 10 mm [57].

To generate stable film formation and reduce potential cross-contamination, each printhead was used for single ink with specific set-up. Printhead 1 with the setting nozzle temperature of 85°C was used for WI, and the printhead 2 with the setting nozzle temperature of 55°C was used for SI (while the setting temperature was set of 25°C for all investigated substrates). The whole system was installed inside a glovebox maintaining low oxygen level (< 3%) at room temperature (20-25°C), and it was equipped with the Oxygen Analyser EC933 (from Systech Illinois Co.) to keep track of the set-up environmental parameters. This approach was applied to help to reduce the inhibition effect caused by oxygen during the free radical photo-polymerization curing procedure.

5.2.2. Characterisation

a. Origin inks

i. Rheology Measurement including Surface Tension & Viscosity Measurement

A high-precision balance (WXS205SDUV/15, Mettler Toledo) which was integrated into the STARlet liquid handler and is used to facilitate surface tension measurement. 110 μl of a sample liquid was aspirated to a 300 μl pipette, which is then moved to the position above the balance. Once in position, it started to dispense the sample at 5 μl/s for 20 s.

The STARlet liquid handler was also used for measuring viscosity at room temperature (25°C), and 55°C, and 75°C to cover the range of processing temperatures for an inkjet printhead. This was achieved by heating the well-plate to each testing temperature using the integrated heating module. The temperature was checked using a thermometer before measurement.

Equation 5.1 shows Fromm's Z parameter could be used to evaluate the printability of an ink as a stable droplet ejection will occur when $Z>2$ [249]. Reiz and Derby later refine the range to be $1 < Z<10$ where it is determined that satellite droplets are likely to form if the ink has a Z parameter>10, and the ink is likely too viscous to be ejected from the nozzle if $Z < 1$ [250].

$$Z = (\rho\, r\, \gamma\,)/\mu \qquad \text{Equation 5.1}$$

where ρ is the density ($g \cdot cm^{-3}$), γ is the surface tension ($mN \cdot m^{-1}$), μ is dynamic viscosity of the ink (mPa·s), and r is the nozzle diameter (μm).

ii. Contact Angle Measurement

Droplet Shape Analysis (DSA100) from KRÜSS GmbH was used to acquire the contact angle data (in the pendant droplet model) of three liquids including distilled water (as the control), water-soluble ink (WI) and structural ink (SI) on a range of investigated substrates. Three substrates such as polyethylene naphthalate (PEN), glass, and silicon wafer (SW) were treated via following treatment: i) cleaning with water as control (Ctrl), ii) Isopropanol (Iso), and iii) Acetone (Ace). The dynamic contact angles were recorded via the DSA4 software after the drop was released from a stainless-steel needle from the initial contact to 120 seconds.

Generally, the contact angle lines started at high value and had a decrease tendency before maintaining its steady state at certain point of time, which was considered as its equilibrium point of specific liquid-substrate. For analysing the wettability of two inks on tested substrates by contact angle measurement, I proposed to use the new index to investigate the dynamic contact angles, which could reveal the physical compatibility of ink and substrate (Equation 5.2):

$$\Delta = \left| \frac{\theta}{t} \right| \qquad \text{Equation 5.2}$$

where Δ is the new index for micro-wetting of ink-substrate, θ is the average contact angle [º], and t is the equilibrium time [sec].

iii. Elemental Analysis

Carbon (C), Hydrogen (H) and Nitrogen (N) contents were identified by Microanalysis using a CE-440 Elemental Analyser. To extract the results of WI & SI, the internal standard S-Benzyl Thiuronium Chloride was used.

The samples to be analysed were weighed into disposable tin capsules. The sample was injected into a high temperature furnace and combusted in pure oxygen under static

conditions. The analyser furnace temperature was set at 975 °C. If tin capsules were used for the sample container, an initial exothermic reaction occurred raising the temperature of combustion to over 1800 °C. At the end of the combustion period, a dynamic burst of oxygen was added to ensure total combustion of all inorganic and organic substances.

The resulting combustion products passed through specialized reagents to produce from the elemental carbon (C), hydrogen (H), and nitrogen (N); carbon dioxide (CO_2), water (H_2O) and nitrogen (N_2) and N oxides.

These reagents also removed all other interferences including halogens (Hal), sulphur (S), and phosphorous (P). The gases were then passed over copper to scrub excess oxygen and reduce oxides of nitrogen to elemental nitrogen. After scrubbing, the gases entered a mixing volume chamber to ensure a homogeneous mixture at constant temperature and pressure.

The mixture then passed through a series of high-precision thermal conductivity detectors, each containing a pair of thermal conductivity cells. Between the first two cells were a water trap. The differential signal between the cells was proportional to the water concentration, which was a function of the amount of hydrogen in the original sample. Between the next two cells was a carbon dioxide trap for measuring carbon. Finally, nitrogen was measured against a helium reference.

iv. Nuclear Magnetic Resonance (NMR) Spectroscopy

^{1}H and ^{13}C NMR spectra were recorded on a Bruker AV3400 400 MHz spectrometer using Deuterated Dimethyl sulfoxide (DMSO-d6) as the solvent reference (2.5 ppm). Chemical shifts of WI, SI, and their components were acquired in parts per million (d) from the MestreNova software.

v. Inductively Coupled Plasma Optical Emission Spectroscopy (ICP-OES)

ICP-OES employed an inductively coupled argon plasma into which a sample aerosol in introduced, via a nebuliser, resulting in sample desolvation, followed by ionisation. ICP-OES utilised the distinct wavelengths of light emitted by specific elements, the intensity of which was proportional to the concentration of the metal in solution. The use of commercial

standards of known concentrations allowed the construction of calibration curves, to which the intensities of the emission spectra of samples of unknown concentration could be compared to determine the concentration of the element of interest.

To determine the concentration of the other elements such as Phosphorous (P) and Sulfur (S), the Perkin Elmer Optima 2000 ICP-OES instrument was used in radial mode, equipped with an autosampler. The element of interest of WI and SI were analysed at the characteristic wavelengths to quantify trace impurities.

Samples were prepared for analysis as aqueous solutions by adding concentrated nitric acid (5 mL, aristar grade) to a known quantity of sample. This was stirred overnight to ensure full digestion of organic material and subsequently volumetrically diluted to 25 mL for analysis. One sample was prepared and optimised for the analysis of phosphorous.
Each element of interest was analysed at characteristic wavelengths to quantify trace impurities, with two replicates of each measurement performed. Certified 1000 ppm (+/- 5 ppm) calibration standards in 2 % HNO_3 were independently volumetrically prepared to give a suitable range of standards for calibration (100 ppm, 60 ppm, 40 ppm, 20 ppm, 5 ppm, 1 ppm, 0 ppm) together with further known concentration standards to be used for quality control purposes (10 ppm).

Quality control samples analysed immediately before and after analysis gave results within 1 ppm of the expected value (10 ppm). WI was prepared for analysis by digesting 574.2 mg of WI in 50 mL – Analysed following calibration at wavelengths characteristic for Phosphorous.

vi. Inductively Coupled Plasma Mass Spectroscopy (ICP-MS)
Multi-element analysis of diluted solutions was undertaken by ICP-MS (Thermo-Fisher Scientific iCAP-Q, Thermo Fisher Scientific, Bremen, Germany). Samples were introduced (flow rate 1.2 mL min-1) from an autosampler (Cetac ASX-520) incorporating an ASXpress™ rapid uptake module through a perfluoroalkoxy (PFA) Microflow PFA-ST nebuliser (Thermo Fisher Scientific, Bremen, Germany). Sample processing was

undertaken using Qtegra™ software (Thermo-Fisher Scientific) utilizing external cross-calibration between pulse-counting and analogue detector modes when required.

ICP-MS analysis was carried out to determine the concentration of other elements. The sample was prepared for analysis by digesting in concentrated nitric acid (2 mL), stirring overnight and then diluting to a final volume (10 mL) with ultrapure water.

The iCAP-Q employed in-sample switching between two modes using a collision cell (i) charged with He gas with kinetic energy discrimination (KED) to remove polyatomic interferences and (ii) using H_2 gas as the cell gas. The latter was used only for Se determination. Typically, in-sample switching was used to measure Se in H_2-cell mode and all other elements in He-cell mode. Peak dwell times were 100 mS for most elements with 150 scans per sample.

Internal standards, used to correct for instrumental drift, were introduced to the sample stream on a separate line (equal flow rate) via the ASXpress unit. Internal standards typically included combinations of Sc (10 µg L^{-1}), Ge (10 µg L^{-1}), Rh (5 µg L^{-1}), Re (5 µg L^{-1}) and Ir (5 µg L^{-1}). The matrices used for internal standards, calibration standards and sample diluents were typically 2% Primar grade HNO_3 (Fisher Scientific, UK) with 4% methanol (to enhance ionization of some elements).

Calibration standards typically included (i) a multi-element solution with Ag, Al, As, Ba, Be, Cd, Ca, Co, Cr, Cs, Cu, Fe, K, Li, Mg, Mn, Mo, Na, Ni, P, Pb, Rb, S, Se, Sr, Ti, Tl, U, V and Zn, in the range 0 – 100 µg L^{-1} (0, 20, 40, 100 µg L^{-1}) (Claritas-PPT grade CLMS-2 from SPEX Certiprep Inc., Metuchen, NJ, USA); (ii) a bespoke external multi-element calibration solution (PlasmaCAL, SCP Science, France) with Ca, Mg, Na and K in the range 0-30 mg L^{-1} and (iii) a mixed phosphorus, boron and sulphur standard made in-house from salt solutions (KH_2PO_4, K_2SO_4 and H_3BO_3).
For Inductively Coupled Plasma Mass Spectroscopy (ICP-MS), WI was prepared for analysis by digesting 574.7 mg of WI in 10 mL.

b. 3D-printed samples

i. Optical Microscopy

The sizes of the 3D-printed samples were investigated by an optical microscope (Nikon Eclipse LV100ND with the NIS-Elements and ImageJ software.

ii. In-situ Photography

The morphology of 3D-printed samples was investigated by acquiring the photos (or screen-capturing) via a high-speed camera that was equipped with the ink-jet printer.

iii. Profilometry

Optical profilometry scans were acquired in a Z range of 5 µm in the Zeta-profilometer (Zeta-20, Zeta Instrument). The number of steps was set to 402 with the step size of 0.5 µm/step and the objective lenses of 5x, 10x, and 20x magnification. Thickness-roughness data were acquired and progressed in the SurfaceLab software.

Two features were evaluated when operating the 3D-profilometer for the interface study of 3D-printed multi-materials: 1) two magnification levels such as x5000 and x10000; and 2) two stitching modes such as AutoLevel Stitching and XY-Alignment Stitching.

iv. Interferometry

The Coherence Scanning Interferometer - Zygo NexView™ NX2 (Zygo Company) was used to study the layer thickness of the 3D-printed patterns. The scan range was 100 µm with the objective lenses of 5x and 20x. and data acquisition was done at the scan speed of 20 µm/s. The surface topography was acquired and progressed in the Mx™ software.

v. Fourier-Transform Infrared Spectroscopy (FT-IR)

FT-IR spectra were obtained by an Agilent Cary 630 FT-IR spectrometer using a diamond Attenuated Total Reflectance (ATR) accessory and MicroLab Expert software. A small amount of sample was placed on top of the ATR crystal before recording the spectra at room temperature (25^{o}C) in the region of 4000 – 650 cm^{-1} with a resolution of 4 cm^{-1} using 100 scans. An empty ATR cell without any samples was recorded for a background spectrum (at the same settings) to ensure no substances (from previous measurements) being remained on the ATR crystal.

vi. Time of Flight Secondary Ion Mass Spectrometry (ToF-SIMS) and OrbiSIMS

ToF-SIMS analyses of 3D-printed samples were carried out using 3D OrbiSIMS (Hybrid SIMS) instrument from IONTOF GmbH. ToF-SIMS images were acquired in positive ion polarity with delayed extraction mode using a 30 keV Bi_3^+ primary ion beam delivering 0.3 pA. The analysis was performed in the "non-interlaced" mode with a low-energy (20 eV) electron flood gun employed to neutralise charge build up. One sputter frame was performed per cycle and the pause time per level was set 0.5 s. ToF-SIMS images were performed by rastering the Liquid Metal Ion Gun (LMIG) over the sample surface, obtaining secondary ion spectra at each pixel for the area of 500 × 500 µm for ToF-SIMS small area images. ToF-SIMS large area images (such as 1x2 mm or 3.5x3.5 mm for studying x-y and x-z interfaces respectively) were constructed in SurfaceLab by measuring adjacent images which are combined into the large image. All ion assignments showed deviation ($\Delta M/M$) ≤ 150 ppm. The ToF analyser was set with 200 µs cycle time, resulting in a mass range between 0 and 3493 mass units. For dataset, Surface Lab 7.1 or 7.2 (IONTOF GmbH) software was used to perform an automated peak search on the total spectra restricted only to peaks with intensity higher than 100 counts and masses between 30 u and 300 u [251].

orbiSIMS analyses of a 3D-printed samples were carried out using 3D orbiSIMS (Hybrid SIMS) instrument [129]. A 20 keV Ar_{2000}^+ was used as primary ion beam with 0.73% duty cycle producing a primary ion current of 24 pA for the surface profiling (GCIB). For the surface spectra, the primary ion beam was raster scanned over different areas with the total dose kept under the static limit of 10^{13} ions/cm^2. The GCIB was operated with 20 keV and 2000 atoms in the cluster (Ar_{2000}^+ ion beam) delivering a pulsed 5 nA beam current. A dual-beam mode was used by raster scanning the primary ion beam over regions of 200 x 200 µm^2 at the centre of a 500 x 500 µm^2 crater formed using an Argon gas cluster ion beam (GCIB). The spectra were collected in positive polarity, in the mass range of 75-1125 *m/z* with mass resolution of 240000.

5.3. RESULTS AND DISCUSSION

5.3.1. Investigation of the physical properties of the original inks

a. Printability

Table 5.1 showed that Structural ink (SI) had surface tension of $\gamma = 39.73 \pm 0.50$ mN/m and viscosity of 27.20 mPa·s at room temperature (25°C). The viscosity of SI was 15.51 mPa·s

at 55°C and 70°C. Reis & Derby used numerical simulation of drop formation to propose 10 > Z > 1 as suitable for stable drop formation in ink-jet printing (Derby, 2010). Following this guideline, SI was confirmed as printable with Z values within the printable range (Z = 9.5 for both high temperatures and Z = 4.5 for room temperature).

Table 5.1 also shows that the water-soluble ink (WI) has a surface tension of $\gamma = 30.42 \pm 0.86$ mN/m, and this value was lower than 40 mN/m matching the commonly appropriate materials for the ink-jetting process (B. He et al., 2017). The viscosity of WI was measured at room temperature as 123.35 mPa·s while no viscosity data of WI were recorded at high temperatures as WI crosslinked quickly under the light compared to SI.

Table 5.1. Results of surface tension, viscosity, and Z parameter of WI and SI

Sample	**Surface tension γ (mN/m)**		
	Room Temperature (25°C)		
WI	30.42 ± 0.85		
SI	39.73 ± 0.55		
Sample	**Viscosity μ (mPa·s)**		
	70°C	***55°C***	***Room Temperature (25°C)***
WI	N/A*	N/A*	123.35
SI	15.51	15.51	27.20
Sample	**Z parameter**		
	70°C	***55°C***	***Room Temperature (25°C)***
WI	N/A*	N/A*	0.97
SI	9.5	9.5	5.42
**No viscosity data of WI were recorded (i.e. N/A for Z parameter of WI) at high temperatures as WI crosslinked quickly under the light*			

b. Wettability

The choice of substrates with suitable cleaning strategies (before 3D printing new ink formulations on those cleaned substrates) is usually underestimated due to its simple steps. Monitoring substrate treatment helps maintain process consistency, reducing variability and defects in printed parts. For example, if the substrate is not cleaned effectively, there may be dust, residues, or other contaminants on the surface [253,254]

In general, water is a relatively mild solvent and is generally safe to clean a range of substrates, but it may not be effective for several stubborn dust or for certain contaminants that do not mix well with water. Isopropanol can help to remove oils or greases on the surface, and acetone can help to remove some organic adhesives. Compared to water, both isopropanol and acetone evaporate relatively quickly, leaving a clean surface. Acetone is more hazardous than isopropanol, so it sometimes can weaken or damage the surface [255]. In this study, I investigated the compatibility between ink formulations and substrates after being cleaned with different solvents) to prepare for the lateral 3D-printing.

Three substrates (as PEN, Glass, and SW) with three cleaning solvents (as Water, Isopropanol, and Acetone) for cleaning substrates were used to investigate the wetting behaviour of WI and SI. Before measuring the contact angles, the tested substrates are washed with water (as a control), isopropanol (as a hydrogen-bond donating solvent or Lewis acid), and acetone (as a hydrogen-bond receiving solvent or Lewis base). Figure 5.2 shows the changes of the average contact angles of water, WI, and SI on a PEN substrate (Firgures 5.2a-b-c (in green)); on Glass (Firgures 5.2d-e-f (in blue)), and on SW (Figures 5.2g-h-i (in grey)).

In the data in Figures 5.2a-d-g, water show the largest contact angles (with all values above 70° for SW, above 58° for PEN, equal and above 20° for Glass). The contact angle lines of water would become stable as straight line in the shortest time (Figure 5.2a-d-g). Compared to WI (in Figures 5.2b-e-h) and SI (in Figures 5.2c-f-i), water (in Figures 5.2a-d-g) also had the medium equilibrium point as all measurement lines flattened approximately after 50 sec. A small contact angle of less than 90° corresponds to high wettability or hydrophilicity (whereas a large contact angle of more than 90° signifies low wettability or hydrophobicity).

Therefore, WI and SI have the tendency of hydrophilicity on tested substrates (regardless of cleaning solvents).

WI wets PEN substrate best (with relatively small contact angle of 25°), moderately wets glass (with a moderate contact angle of 32°), and has the least wetting on SW (with a higher contact angle of higher contact angle of 45°), which reveled the usge of PEN for 3D printing of WI. SI has the lowest contact angles observed on PEN (as 15°) compared to SW (as 20°) and glass (as 27°), which suggests wettability with these surfaces. SW substrate is not ideal for 3D printing of SI as it has the higher contact angle. It is essential to consider other factors such as surface roughness and the printing paramaters when determining the most suitable substrate for 3D-printing of new ink formulations.

Furthermore, compared to water on PEN (Figure 5.2a), Figure 5.2b and 5.2c showed that WI and SI with measurement lines decreased more at the beginning before reaching the equilibrium point and stablising until the end of 120 sec. For PEN substrate, Water with averaged angles of 70° at Eq. 60 sec, WI with averaged angles of 25° at Eq. 60 sec, and SI with averaged angles of 15^{o} at Eq. 60 sec. For glass substrate, Water with averaged angles of 35° at Eq. 50 sec, WI with averaged angles of 32° at Eq. 40 sec, and SI with averaged angles of 27° at Eq. 25 sec. For SW substrate, Water with the highest averaged angles of 86° at Eq. 20 sec, WI with lower averaged angles of 40° at Eq. 35 sec, and SI with averaged angles of 20° at Eq. 38 sec.

Table 5.2. shows each pair of tested liquid-substrate has dissimilar averaged angles at the equilibrium times, which results in the difference in new index values. The new index of WI and SI varies most for the SW substrate (Δ_{WI_SW} = 1.1 and Δ_{SI_SW} = 0.5) compared to Glass substrate (Δ_{WI_Glass} = 0.8 and Δ_{SI_Glass} = 1.1) and PEN substrate (Δ_{WI_PEN} = 0.4 and Δ_{SI_PEN} = 0.3) regardless of the substrates' treatment. Hence, PEN substrate was more compatible with both WI and SI (compared to Glass and SW substrate). When two materials are physically compatible, the liquid droplet will rapidly reach a stable contact angle (short equilibrium time) and exhibit a contact angle that indicates good wetting (small contact angle). In this case, the ratio of the average contact angle to the equilibrium time is low. Conversely, if two materials are not physically compatible, it may take a long time for the droplet to reach

equilibrium (long equilibrium time), and the contact angle may be large, suggesting poor wetting. In this case, the ratio of the average contact angle to the equilibrium time is high.

As can be seen, WI and SI were dissimilar in the values of surface tension γ, viscosity μ, and dynamic contact angle (or index value Δ). It might be due to the differences in chemical structures between two inks (with more details at the section 5.3.1c). Those variants of physical properties result in physical incompatibility at the interfacial areas between ink-substrate.

A hyphothesis is that the difference of index values between two inks could lead to different physical properties when co-printing two inks together as the changes of average angle through time of two materials would be dissimilar. SW has larger difference (with $|\Delta_{WI\_SW} - \Delta_{SI\_SW}| = |1.1 - 0.5| = 0.6$) compared to Glass (with $|\Delta_{WI\_Glass} - \Delta_{SI\_Glass}| = |0.8 - 1.1| = 0.3$) and PEN (with $|\Delta_{WI\_PEN} - \Delta_{SI\_PEN}| = |0.4 - 0.3| = 0.1$). This revealed the wetting dissimilarity of WI and SI on different substrates, particularly usge of SW (for co-printing of WI and SI) might have the largest physical incompatibility of ink-substrate compared to usage of Glass and PEN. A smaller difference of index values between two inks indicates that the two inks can wet the surface and reach equilibrium similarly, which is a sign of good wetting of both inks on specific substrate. Hence, PEN is the most potential substate for co-printing of WI and SI compared to Glass and SW.

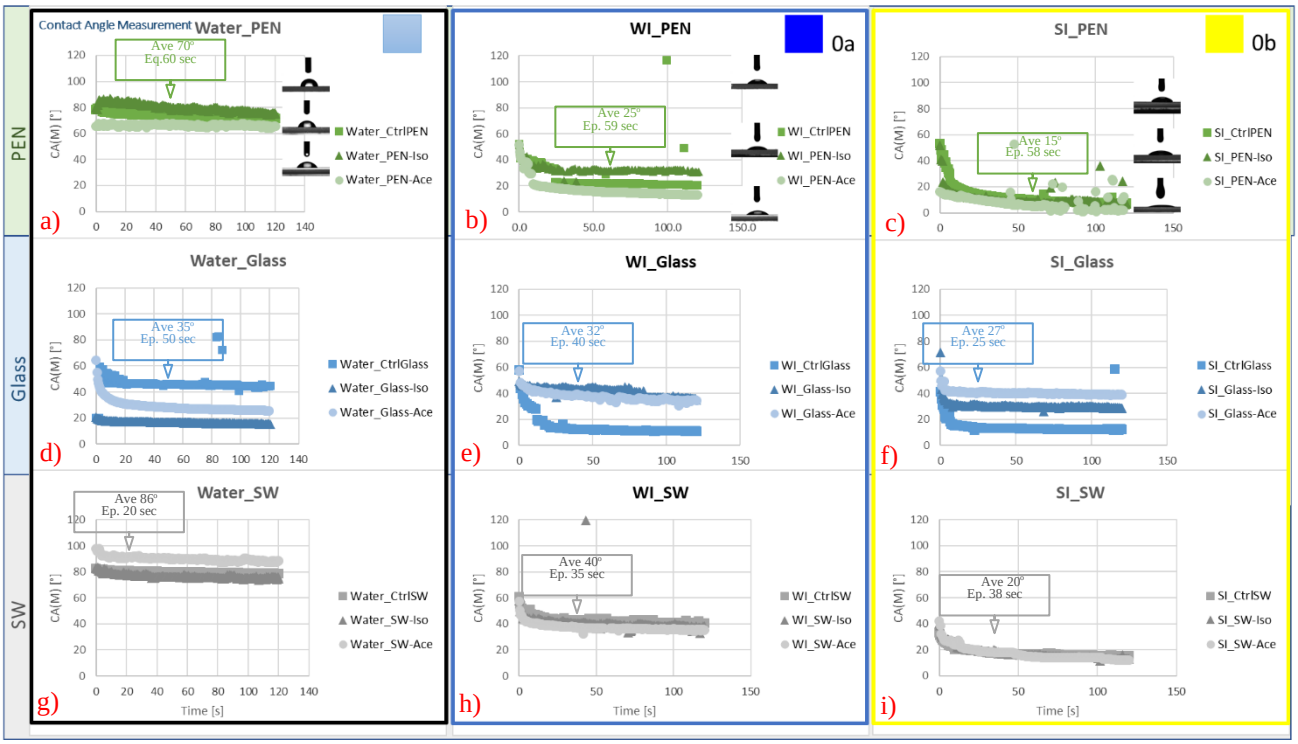

Figure 5.2. *Contact angle measurement of water, WI, and SI on three substrates such as PEN, Glass and SW after using three substrate-cleaning solvents water, Isopropanol (Iso), and Acetone (Ace)*

Table 5.2. Summary of average angle (°) and equilibrium point (sec) of water (as control), water-soluble ink - WI, structural ink - SI on PEN, Glass, and SW. The results was correlated to the results from the Figure 5.2.

Average angle (°) (at equilibrium state)	**Water (as control)**	**Water-soluble ink WI**	**Structural ink SI**
PEN	70	25	15
Glass	35	32	27
SW	86	40	20
Equilibrium time (sec)	**Water (as control)**	**Water-soluble ink WI**	**Structural ink SI**
PEN	60	59	58
Glass	50	40	25
SW	20	35	38

Average angle (°) **Equilibrium time (sec)**	**Water (as control)**	**Water-soluble ink WI**	**Structural ink SI**
PEN	1.2	0.4	0.3
Glass	0.7	0.8	1.1
SW	4.3	1.1	0.5

5.3.2. Investigation of the chemical properties of the original inks

a. Fundamental elements (C, H, N)

The data in Table 5.3 shows the theoretical and measured microelemental composition of WI and SI. Both internal standard and SI had the accurate concentration of Carbon (C), Hydrogen (H), Nitrogen (N). This method would be reliable for differentiation between WI and SI through the presence of Nitrogen in WI. Figure 5.3 shows the ^{1}H-NMR and ^{13}C-NMR shifts of original inks and their components helped to strengthen the elemental considerations. Data from Figure A3.1-A3.2 in Appendix A3 shows SI had similar dominant peaks of its components such as TCDMDA, EGDPEA, and DMPA.

Compared to SI, WI had unique different peaks including those at 7 ppm and 3.7 ppm in the ^{1}H-NMR and those at 75 ppm and 73 ppm in the ^{13}C-NMR shifts (as orange arrows). The peaks at 7 ppm in ^{1}H-NMR and 75 ppm in ^{13}C-NMR are typically correlated with protons on aromatic rings, and the peaks at 3.7 ppm ^{1}H-NMR and 73 ppm in the ^{13}C-NMR are often found in the region associated with aliphatic (saturated) protons. Certain oxygen-containing functional groups can influence the chemical shifts and coupling patterns of neighboring hydrogen atoms, resulting in characteristic proton NMR signals. Compounds with ester groups (COOR) or ether groups (R-O-R) may exhibit distinctive proton signals typically in the range of 2-4 ppm or 3-4 ppm. A compound containing nitrile group (-CN) has unique proton signals, which usually are in the range of 2-4 ppm in ^{1}H-NMR. Therefore, this difference between peaks of WI and SI in ^{1}H-NMR and ^{13}C-NMR could come from the existence of element oxygen and nitrogen, and further chemical analyses were conducted to confirm this result (in the following sections).

Table 5.3. Microelemental analysis of WI and SI

Sample	Elemental composition *(Theoretical)*				Measured element concentration		
	%C	**%H**	**%N**		**%C**	**%H**	**%N**
Internal standard	47.4	5.47	13.82		47.38	5.38	13.78
WI	N/A*	N/A*	N/A*		52.35	8.82	2.1
SI	71.85	7.96	0		71.68	8.01	0.17
**The ingredients of WI were confidential, so N/A for theoretical elemental composition of WI*							

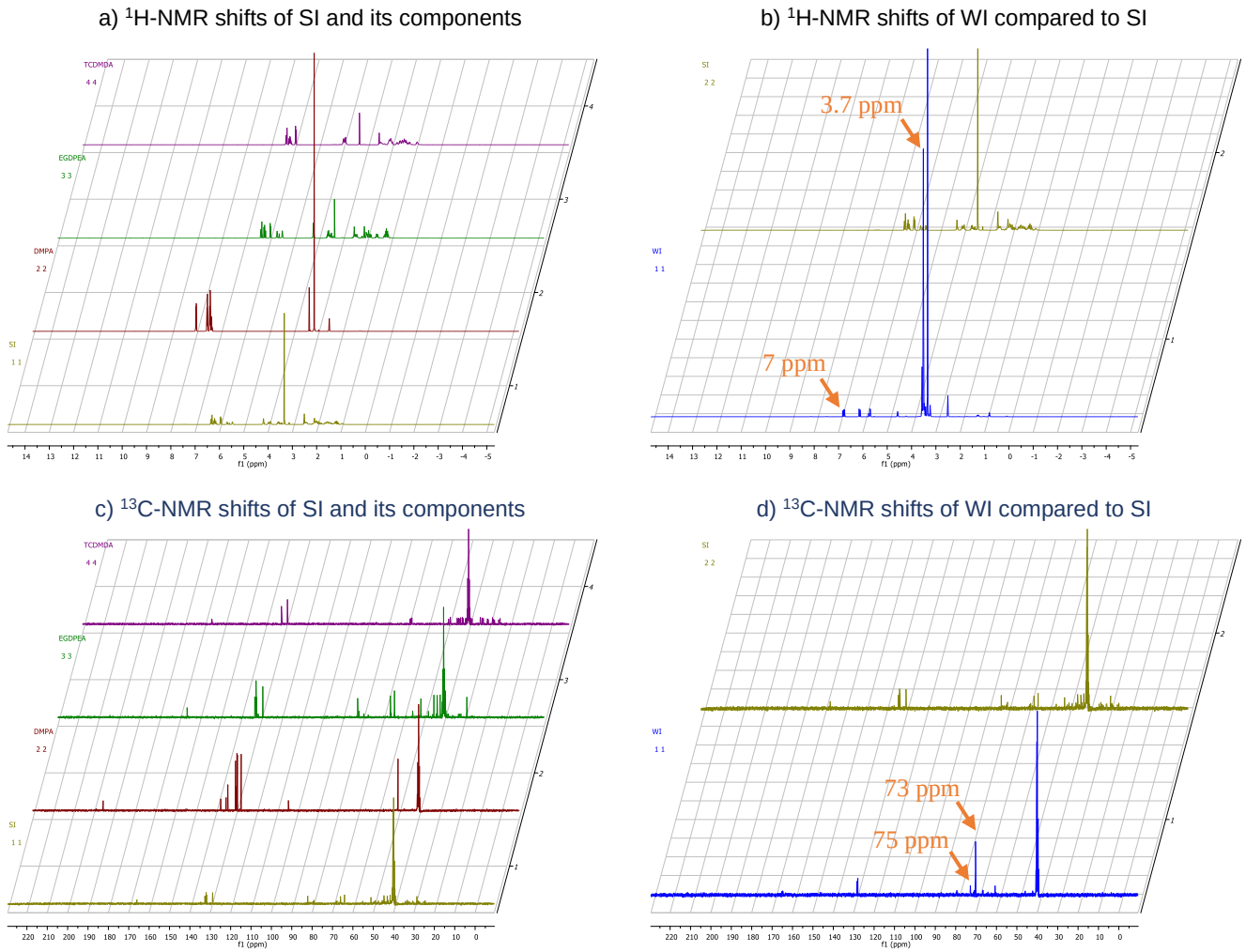

Figure 5.3. *^{1}H-NMR and ^{13}C-NMR shifts of original SI and its components (if known): a) ^{1}H-NMR shifts of SI and its components; b) ^{1}H-NMR of WI compared to SI; c) ^{13}C-NMR shifts of SI and its components; and d) ^{13}C-NMR shifts of WI compared to SI*

b. Additional elements (if exist)

ICP-OES and ICP-MS were used to identify other elements that could potentially be present in WI. After applying the calibration at wavelengths characteristic, ICP-OES analysis was used for the identification of potential Phosphorous (P) in WI (Table 5.4). The Phosphorous content was 0 ppm for both inks, which might be either Phosphorous (P) did not exist or the content was out of the limit of detection of the measurement. Based on the ICP-MS analysis, the phosphorous (P) concentration of the analyte solution is determined to be 10.01 ppm, and the sulfur (S) concentration of the analyte solution is determined to be 1.96 ppm. This was equivalent to the sample of WI consisting of 0.017 % P, and 0.0034 % S (by weight) (Table 5.5).

The elemental analyses via different analytical techniques revealed a better understanding of the commercial ink (WI). It was also important information to help to differentiate between two inks, through the existence of Nitrogen (as other elements like Phosphorous or Sulphur existed in a very limited amount in WI). After recognizing the special elements in WI, experimental time and cost could be reduced in future measurements such as looking for fingerprint functional groups in further ToF-SIMS and orbiSIMS analyses of 3D-printed samples.

Table 5.4. ICP-OES analysis results of WI

Sample	**Wavelength (nm)**	**Calibrated range (ppm)**	**R2**	**P (ppm)**
WI	214.91	0 – 100	0.997	0
WI	213.62	0 – 100	0.997	0

Table 5.5. ICP-MS analysis results of WI

Sample	**Analyte solution**	
	P (ppm)	**S (ppm)**
WI	10.01	1.96
	Sample as supplied	
	P (%)	**S (%)**
WI	0.017	0.0034 %

5.3.3. Investigation of the physical properties of 3D-printed samples

a. Morphology

Although optical microscope is an often used approaches to reveal the morphology of material after printing process [256], there are certain difficulties when capturing and interpreting the images: 1) image stitching towards X and Y directions, 2) subjective nature of image acquisition and interpretation (due to different reasons such as the presence of environmental contamination)t. Existing common solutions include: 1) usage of imaging software (such as ImageJ) to deal with the stitching issues from the optical microscope images, and 2) preserve the 3D-printed samples at the proper storage conditions such as vacuum or a lower-pressure (low humidity) environment.

Single square blocks of WI and SI at small sizes (of 0.5x0.5 and 1x1 mm) were ink jetted and recorded for ensuring the uniformity of the surface. Figure 5.4 shows both WI and SI achieved good film formation. This result confirmed the previous data of the printability of WI and SI (at section 5.3.1a). Moreover, it was quicker and more convenient to make decisions about the next printing based on the images captured by the printer camera (rather than optical microscope). It helped to save time to determine whether to continue the same printing condition or not. It also reduced the risk of post-contamination such as by fibres or dust (as thin black chains in Figure 5.4).

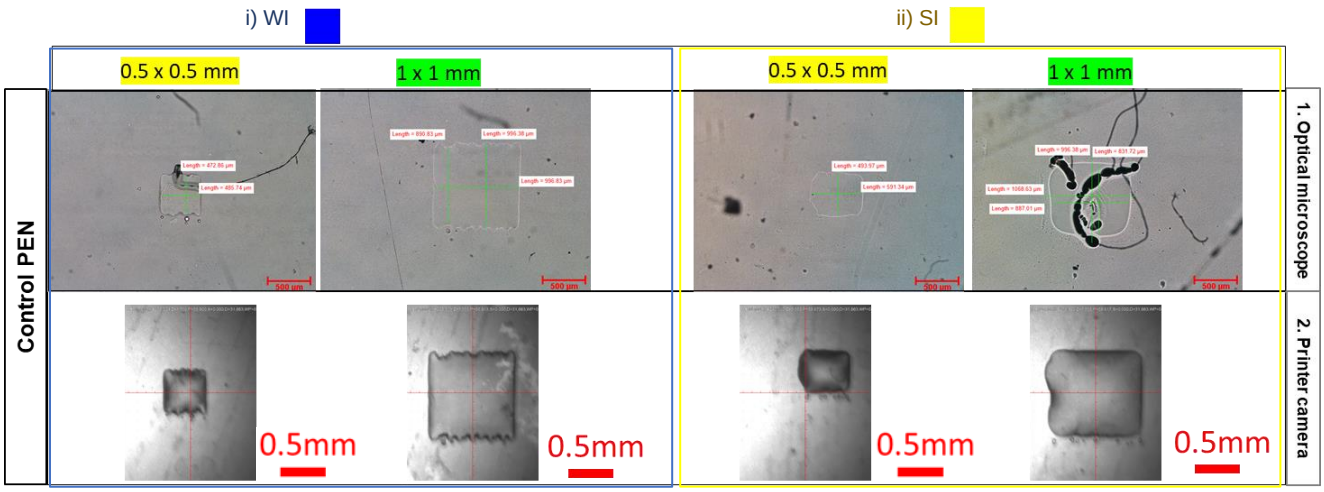

Figure 5.4. *3D-printing of WI with colour coding as blue (i) and SI with colour coding as yellow (ii) on PEN at the sizes of 0.5 x 0.5 mm and 1 x 1 mm): 1) In-situ photography from the printer camera and 2) Optical microscopy (after completing 3D-printing)*

Although there was similar topography observed by the optical microscope and printer camera, it was difficult to capture the images of interface patterns at larger scale due to the limitation of the camera. After investigating and discussing with the manufacturer, I successfully applied a new coding for auto-capturing function into the current manufacturing software to enable multiple screen-capturing. Table 5.6 shows how the new coding allowed monitoring of morphological changes between ink-substrate and material-material. Images of morphology could be saved synchronously and accurately for both X and Y directions. The appropriate values of X and Y as required inputs could be adjusted for recording the whole square block at the larger sizes. The uniformity of surface-interface of 3D-printed samples will be enhanced by quick observation or screening for good film formation (without any cracks or pores), clear borders (represented original square), and no contamination (existed on the surface). Hence, the in-situ morphology during the ink-jetting process was successfully designed and optimised.

Table 5.6. New coding "camera_capture.cs" for automatic photo-capturing function embedded into the printer's software

Camera_capture.xml

```
<?xml version="1.0" encoding="utf-8"?>
<RecipeFlow xmlns:xsi="http://www.w3.org/2001/XMLSchema-instance"
xmlns:xsd="http://www.w3.org/2001/XMLSchema">
  <RecipeScript>camera_capture.cs</RecipeScript>
  <Parameters>
  </Parameters>
</RecipeFlow>
```

The glass and silicon wafer (after being treated with different solvents) were used to investigate the micro-nano behaviours of ink-substrate. Larger square blocks of both inks (sizes of 4x4 mm or 16x16 mm) were 3D-printed and recorded (Figure 5.5 and 5.6). Figure 5.5a reveals a significant contrast between two inks as WI (not SI) provided the most stable film with a clear border. For glass cleaned with water and isopropanol, a medium and small number of pores were observed respectively. No pores were found for 3D printing of WI on glass and SW being cleaned with acetone (and continuous printed samples were marked as

green squares at Figure 5.5). This result was due to the wetting differences when using different solvents to clean substrate before 3D-printing WI and SI (which was well-explained in section 5.3.1).

Figure 5.5b shows the unsuitability of the silicon wafers for the inkjet-printing of SI due to its disrupted film formation. The printed pattern on SI yielded a visually rougher film with discontinuous edges. It happened due to differences of viscosity characteristics between two inks, which matched the printability data (in section 5.3.1).

Figure 5.6 highlights one significant advantage of ultilising this automatic photo-capturing function for confirming the good filming in a shorter time. The results proved that it was more convenient and quicker to use the printer camera compared to the conventional optical microscope in post-analyses (where the stitching of multiple image unit needed to be done by additional software) to study the in-line morphology during the ink-jetting process. Therefore, it supports a high-throughput screening methodology where the experimental time and cost for evaluating the real-time morphology are significantly reduced.

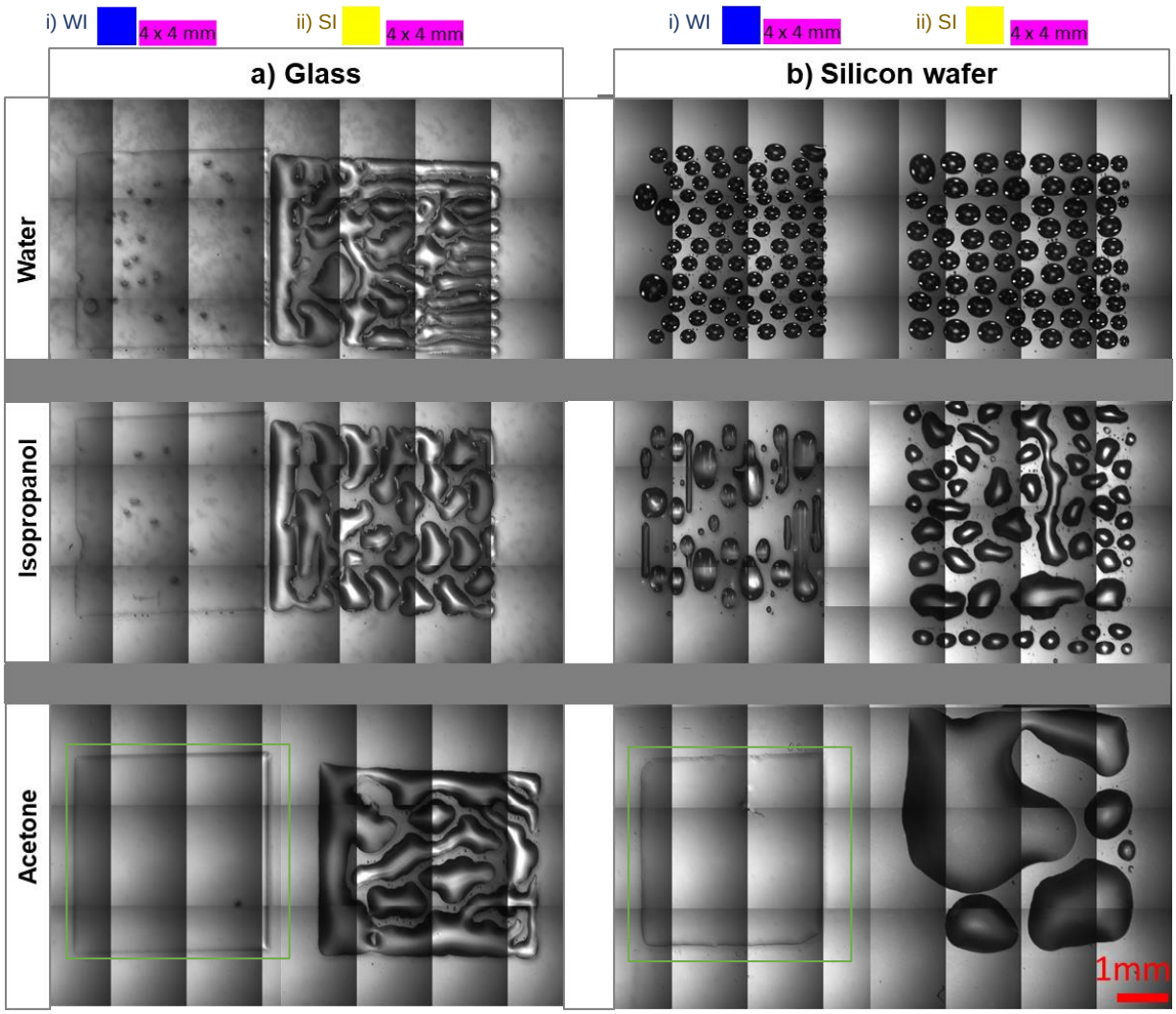

Figure 5.5. *Printer camera images of single square blocks of WI with colour coding as blue (1) and SI with colour coding as yellow (2) at the larger size (4x4 mm): a) glass and b) SW. Three cleaning solvents (as substrates' treatment) were tested including Water, Isopropanol, and Acetone. The result showed no pores were found for 3D printing of WI on glass and SW being cleaned with acetone (and continuous printed samples were marked in green squares)*

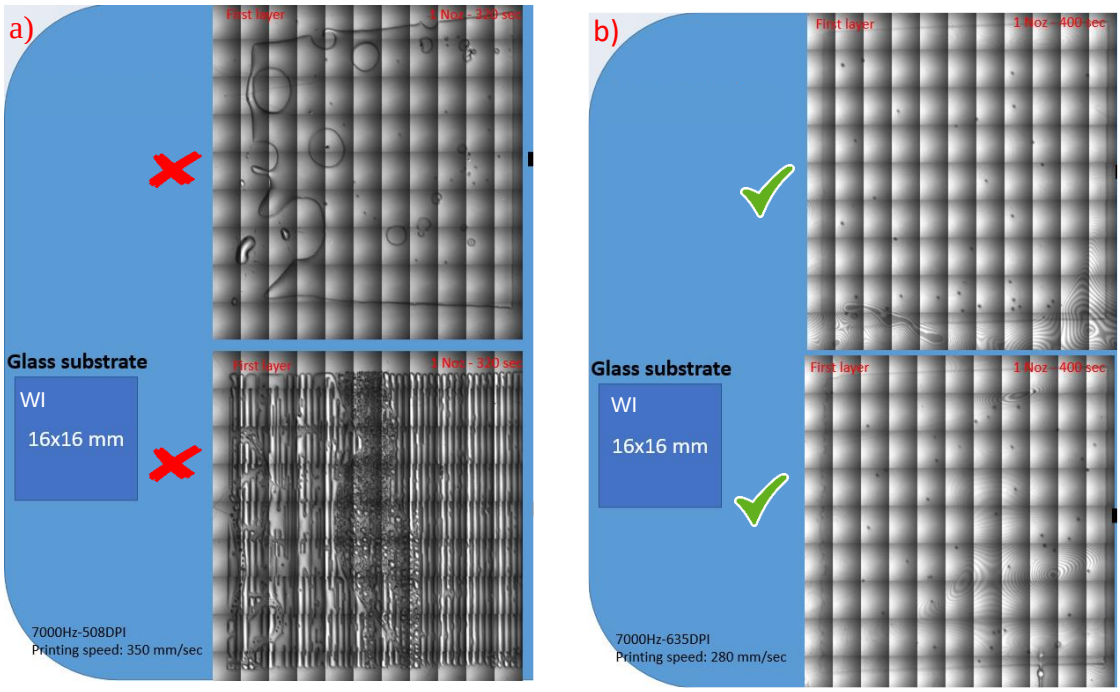

Figure 5.6. *Example of printer camera images of single square blocks of WI (with colour coding as blue) after being printed at the enormous sizes of 16x16 mm at different printing speeds: a) 350 mm/sec and b) 280 mm/sec. These in-situ morphology results showed that printing speed of 280 mm/sec offered continuous printed samples (marked as green checks) compared to discontinuous printed samples (marked as red checks) at the printing speed of 350 mm/sec*

b. Thickness-roughness

After ink-jetting, the thickness of a single layer of WI and SI on PEN and glass was evaluated by a Zeta-profilometer (in Figure 5.7-5.9) and Zygo-interferometer (Figure 5.10 and 5.11).

Compared to the printer camera and the optical microscope, the Zeta-profilometer gave similar topographical results (towards X and Y direction) (Figure 5.7). There were still certain limitations such as incorrect brightness/contrast and magnification that might hinder accurate assessment of the thickness of the printed lines. The “valley-peaks” or the areas with significant height variations were presented throughout the sample patterns (noticed as red circles in Figure 5.7a). Changing to higher magnification (from x5000 to x10000), which could reduce the incorrect interpretation of thickness values because at higher magnification,

the instrument can reduce the overshooting the edges of the peaks and giving better averaging over smaller areas, reducing the impact of localised variations in a smoother and more accurate representation. Hence, applying higher magnification (such as x20000 or x10000 rather than x5000) would be useful for measuring the layer thickness on PEN and other substrates. The profiler data of patterns proved this.

Figure 5.8 shows the Zeta-profilometer images of co-printed samples (size of 0.5x1 mm) at higher magnification (x 20000). The interfacial areas between WI and SI were recorded around 60 x 400 µm. WI kept the initial square design pattern. A liquid with a lower surface tension will wet the surface more easily, so WI (with lower surface tension) will have higher wettability compared to SI. This confirmed good wetting behaviour of WI (compared to SI) on PEN to promote strong adhesion at the printing process, which was correlated with the wettability results.

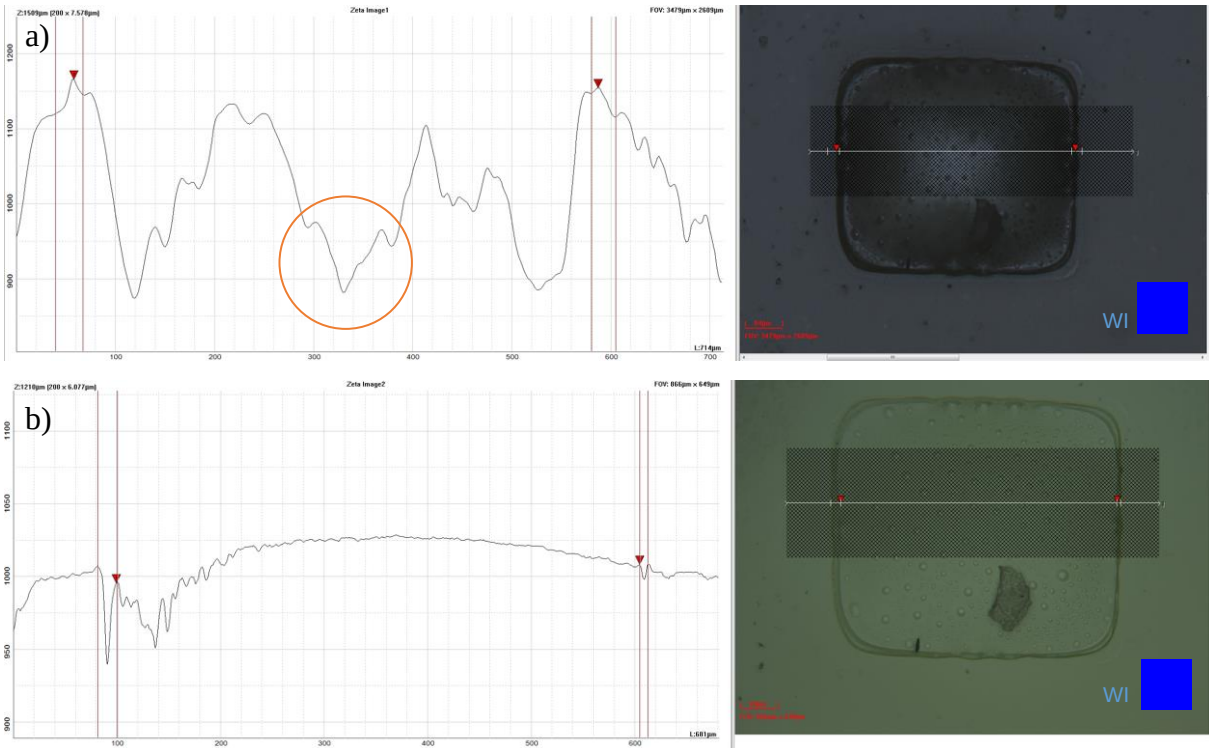

Figure 5.7. *Zeta-profilometer images of WI (with colour coding as blue) after being 3D-printed on PEN (size 0.5x0.5 mm) with thickness profile at different magnifications: a) x5000, and b) x10000.*

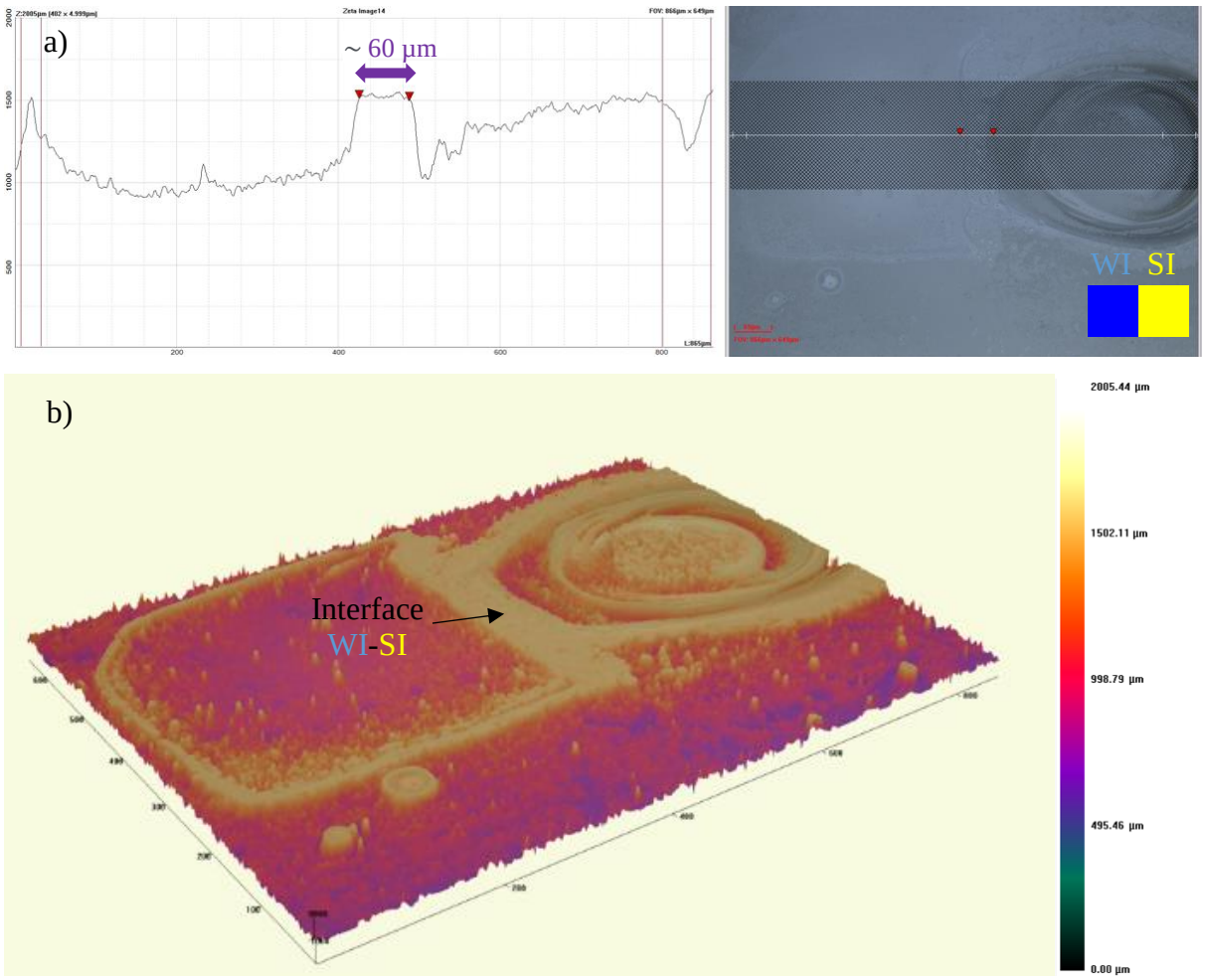

Figure 5.8. *Zeta-profilometer images of co-printed samples including WI (with colour coding as blue) and SI (with colour coding as yellow) at the size of 0.5x1 mm on PEN without stitching (at magnification x20000): a) 2D image with thickness profile and b) 3D image*

The stitching function was optimised to capture the whole image of 3D-printed patterns, so different set-up modes were investigated including a) AutoLevel Stitching and b) XY-Alignment Stitching. Figure 5.9 shows that the gap of height between componential images still existed in the final optical profiles from both stitching modes. This was due to the difficulty when detecting the correct borders between different sections of the colourless WI or SI inks on the transparent substrate like glass. Therefore, I suggested an extra step in the workflow of operating the profilometer is sticking the co-printed samples on the marked

opaque base (such as silicon wafer). This alternative base could fasten the stitching process because each single section could be recognised before putting them together into the final image.

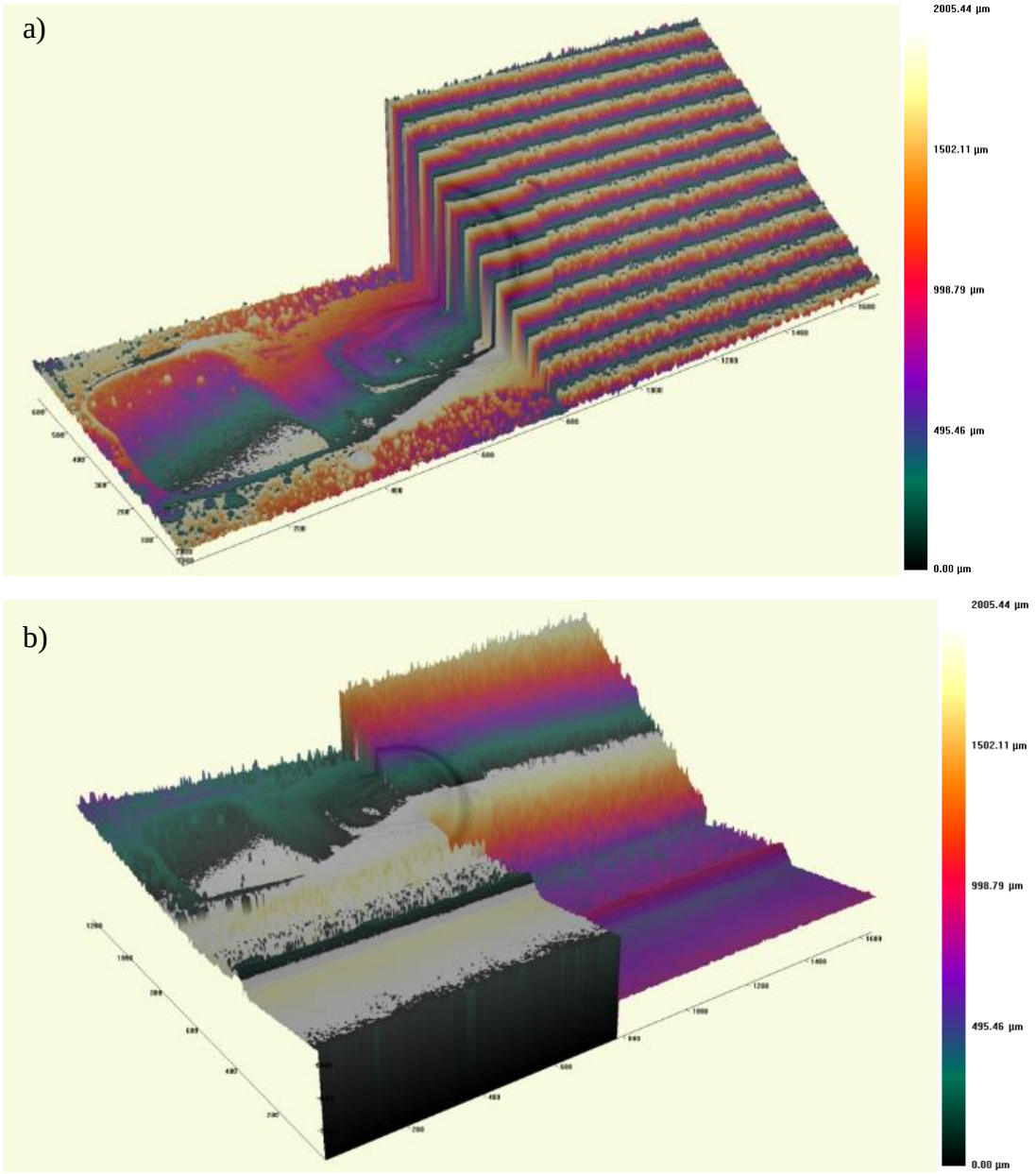

Figure 5.9. *Zeta-profilometer images of co-printing of WI and SI (size of 0.5x1 mm) on PEN at different stitching modes (at magnification x20000): a) AutoLevel Stitching and b) XY Alignment Stitching*

Compared to the manual stitching in Zeta-profilometer, the Zygo-interferometer had an automatic stitching function, which was more effective for measuring the layer thickness (Figure 5.10 and 5.11).

From a test of analysing the 3D-printed sample as WI and SI at small sizes (0.5 x 0.5 mm and 1 x 1 mm), a disruption in the thickness of the printed lines at lower magnification (x5000) compared to higher magnification (x20000) was observed at certain positions as red circles in Figure 5.10.

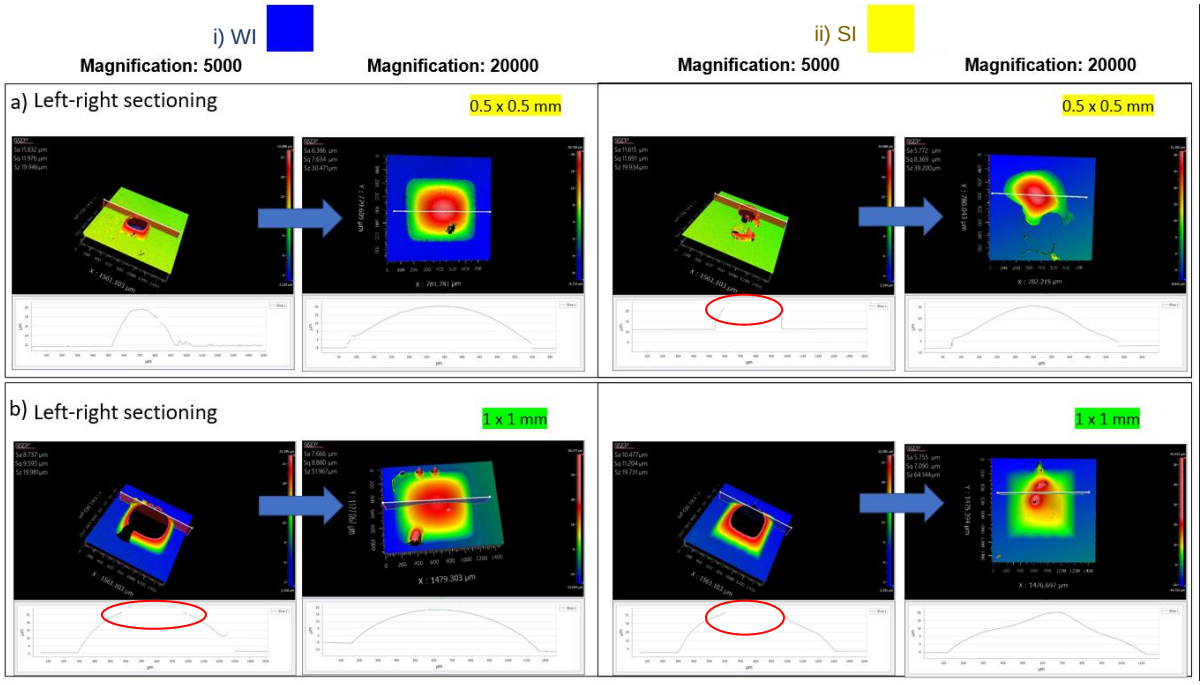

Figure 5.10. *Zygo-interferometer images (with left-right sectioning at the magnification of x5000 and x20000) of WI with colour coding as blue (i) and SI with colour coding as yellow (ii) on PEN at different sizes: a) 0.5x0.5 mm, and b) 1x1 mm. A disruption in the thickness of the printed lines at lower magnification (x5000) compared to higher magnification (x20000) was observed at certain positions as red circles*

The data in Figure 5.11 also represents the ability of the Zygo-interferometer (rather than Zeta-profilometer) to measure layer thickness of WI and SI at different sizes. Whereas WI has constant thickness lines revealing the homogeneous surface at most sizes, SI had one irregular thickness line with few sharp peaks due to tiny contamination of dust (marked as

purple circles in Figure 5.11). This strengthened the previous result that PEN substrate is the most suitable for good adhesion and compatibility for 3D printing with WI as it has the lowest contact angle and exhibits good wetting behaviour.

Additionally, the data in Table 5.7 summarises the thickness results of a single layer of WI and SI on PEN at different image sizes using Zygo-interferometer (with left-right and top-bottom sectioning and magnification x20000). The thickness values were consistent when comparing left-right and top-bottom image cross sectioning (as 25.0 ± 0.0 and 26.9 ± 0.6 µm for WI, and 24.3 ± 3.5 and 22.5 ± 3.8 µm for SI respectively). Therefore, WI had an average line thickness of 25.9 ± 0.5 µm and SI of 23.4 ± 2.3 µm for a single layer, from Zygo-interferometry. They are correlated to the thickness measured from the Zeta-profilometer, which meet the expectations of the results. This thickness results confirms more uniform surface of 3D-printing of WI compared to SI, which matches the previous morphological data.

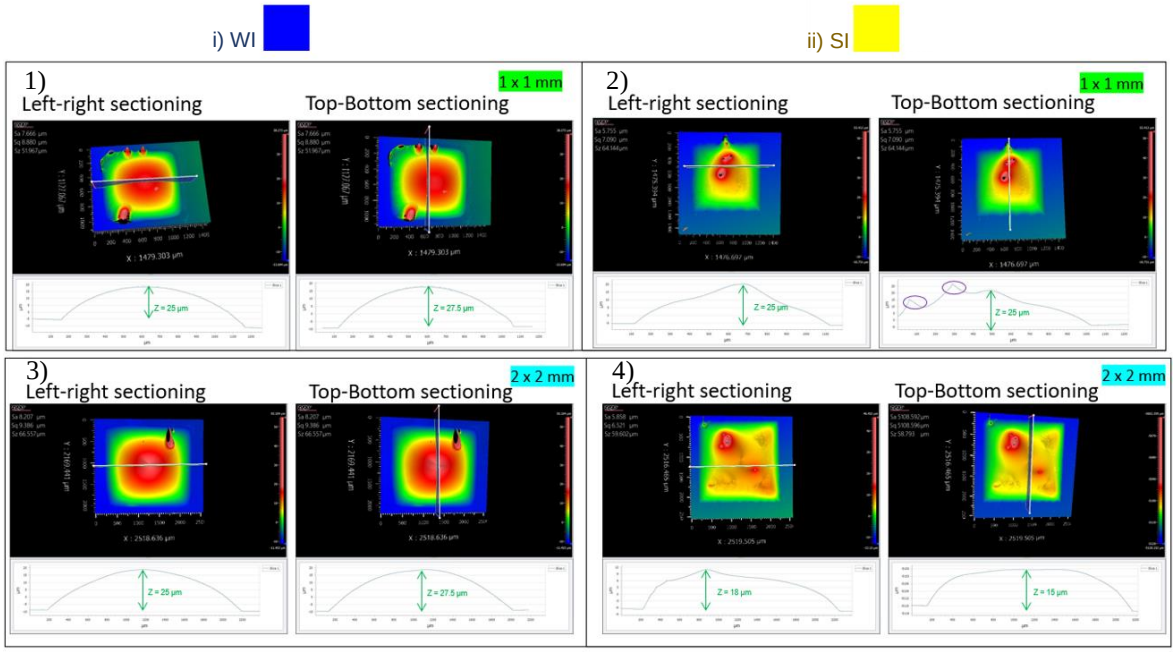

Figure 5.11. *Zygo-interferometer images with left-right sectioning and top-bottom sectioning of single ink including WI with colour coding as blue (i) and SI with colour coding as yellow (ii) after being 3D printed on PEN at different sizes (Magnification x20000): 1) WI of 1x1 mm, 2) SI of 1x1 mm, 3) WI of 2x2 mm, and 4) SI of 2x2 mm. The result showed that WI has constant thickness lines revealing the homogeneous surface at most sizes, while SI had one irregular thickness line (at size 1x1 mm) with few sharp peaks due to tiny contamination of dust (marked as purple circles).*

Table 5.7. Thickness results of a single layer when inkjet 3D printing of WI and SI

Square size	WI		SI	
0.5x0.5 mm	25.0	Left-right sectioning (XZ)	30.0	Left-right sectioning (XZ)
1x1 mm	25.0		25.0	
2x2 mm	25.0		18.0	
4x4 mm	25.0	*25.0 ± 0.0 (µm)*	N/A*	*24.3 ± 3.5 (µm)*
0.5x0.5 mm	25.0	Top-Bottom sectioning (YZ)	27.5	Top-Bottom sectioning (YZ)
1x1 mm	27.5		25.0	
2x2 mm	27.5		15.0	
4x4 mm	27.5	*26.9 ± 0.6 (µm)*	N/A*	*22.5 ± 3.8 (µm)*
Mean (µm)	*25.9*		*23.4*	
Standard deviation (µm)	*1.3*		*5.7*	
Standard error (µm)	*0.5*		*2.3*	
Thickness (µm)	**25.9 ± 0.5**		**23.4 ± 2.3**	
			**Excluding thickness value at the size 4x4 mm (due to no filming formation*	

Finally, the comparison of theoretical and measured line thickness (Figure 5.12) showed that the types and sizes of thickness line could be affected by the behaviour of ink formulation on substrate (such as over-shrinking or over-spreading). In other words, good filming and shaping formation of ink droplet could help to provide a well-defined line of expected height. In other words, Zygo-interferometry was proven to be helpful for measuring the thickness and exposing the behaviour of multi-materials (after ink-jetting and UV-sintering).

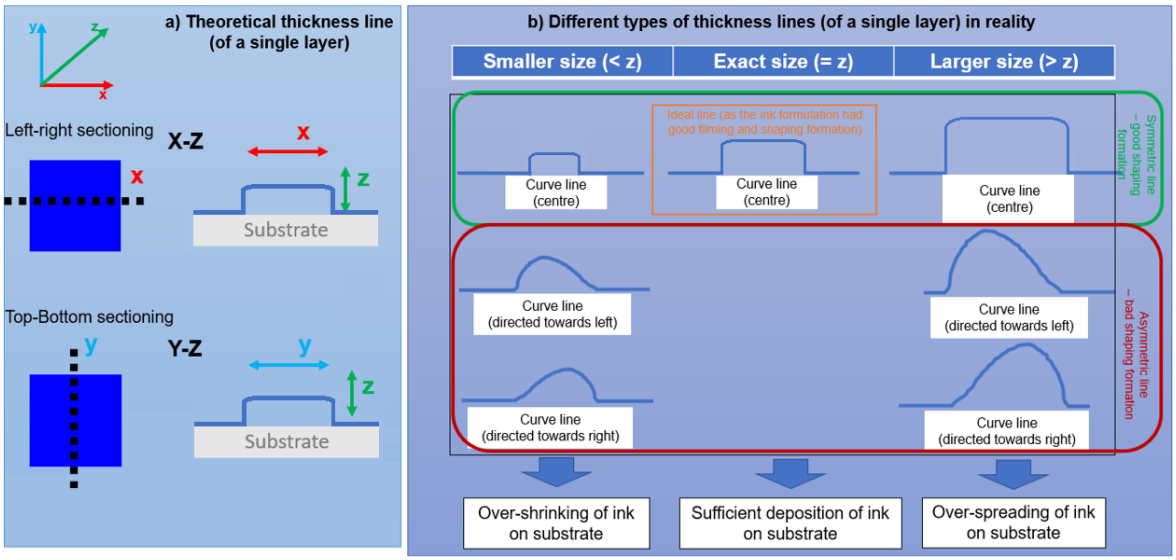

Figure 5.12. *Comparison of thickness lines in theory (a) and as measured (b)*

5.3.4. Investigation of the chemical properties of 3D-printed samples

a. Fundamental elements

Figures 5.13 - 5.14 and Table 5.8 show IR bands between 4000 – 650 cm^{-1} for the original inks and the raw materials of the known components of both inks. The 3D-printed sample of SI and original SI had similar dominant peaks as the components of SI including TCDMDA, EGDPEA, and DMPA. SI was expected to have functional groups of aliphatic esters (due to similar bands in TCDMDA), aliphatic ether and alkoxy (due to similar bands in EGDPEA), and aryl ketone (due to similar bands in EGDPEA) in Figure 5.13.

Figure 5.14 also shows exclusive peaks in both original and printed SI, for example at 1718-1740 cm^{-1} corresponding to C=O stretch. Compared to SI, WI had different peaks including those at 2975-2910 & 2865-2830 cm^{-1} corresponding to a C-H stretch (CH_2) in aryl, at 1813-1865 cm^{-1} corresponding to C-C stretch in aryl (ring), 1275-1140 cm^{-1} correspond to the C-N stretch in aliphatic amine functional group (e.g. morpholine).

Hence, functional groups of unknown material (WI) could also be identified after comparing FT-IR spectra of WI to SI and other chemicals in the library software. The FT-IR spectra of the ink (in both original or printed state) and their components reveals the consistency with the previous microelemental results (in Figure 5.5).

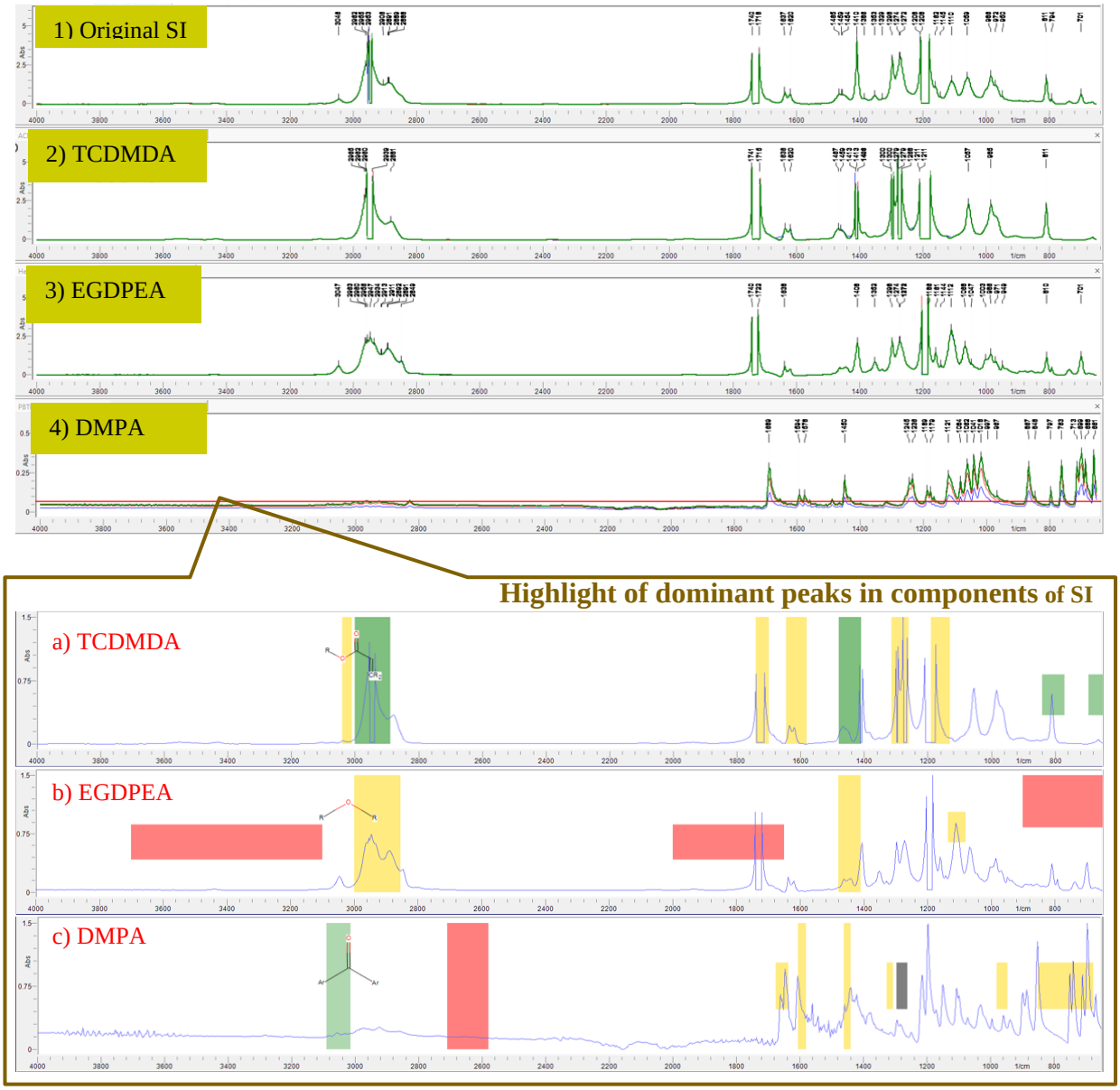

Figure 5.13. *FT-IR spectra of SI and its components including 3 replicates of each scanning samples: 1) original SI, 2) TCDMDA, 3) EGDPEA, and 4) DMPA. Highlight of dominant peaks of TCDMDA (a), EGDPEA (b), and DMPA (c).*

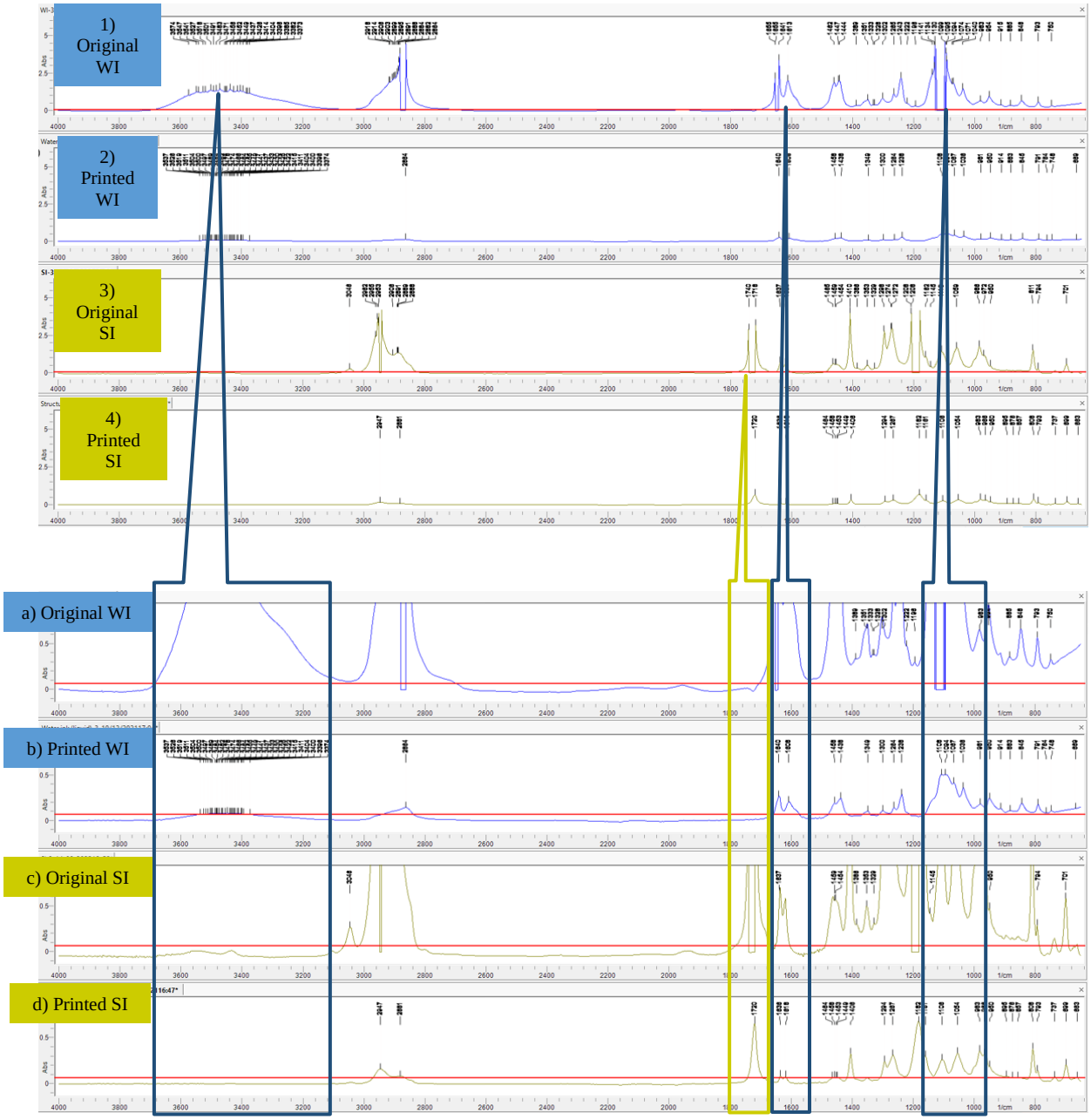

Figure 5.14. *FT-IR spectra results included: 1) original WI, 2) Printed WI, 3) original SI, and 4) Printed SI. Focused bands were zoom-in to show the peaks' difference among original WI (a), printed WI (b), original SI (c), and printed WI (d).*

Table 5.8. Data interpretation for FT-IR analyses of each component in SI including a) TCDMDA, b) EGDPEA, and c) DMPA

a) TCDMDA

Vibration	Start WN	End WN	Threshold	Priority
C-H Stretch, Alkyl	3000	2890	Variable	Very High
C=O Stretch	1740	1700	Variable	Mandatory
C=C Stretch	1645	1580	Variable	Mandatory
C-H Bend, CH2/CH3	1480	1410	Variable	Very High
COC Stretch, asym	1315	1260	Variable	Mandatory
COC Stretch, sym	1190	1130	Variable	Mandatory
COC def	840	770	Medium	High
COC def	695	650	Medium	High
C-H Stretch, olefinic	3040	3010	Variable	Mandatory

b) EGDPEA

Vibration	Start WN	End WN	Threshold	Priority
C-H Stretch, Alkyl	3000	2855	Variable	Mandatory
C-H Bend, CH2/CH3	1480	1410	Variable	Mandatory
C-O Stretch	1135	1080	Strong	Mandatory
No Band Region	3700	3100	Medium	Excluded
No Band Region	2000	1650	Medium	Excluded
No Band Region	900	650	Very Strong	Excluded

c) DMPA

Vibration	Start WN	End WN	Threshold	Priority
C-H Stretch, Aryl	3090	3015	Variable	Medium
No Band Region	2710	2580	Variable	Excluded
C=O Stretch	1675	1635	Strong	Mandatory
C-C Stretch, Ring	1605	1580	Variable	Mandatory
C-C Stretch, Ring	1460	1440	Variable	Mandatory
C-CO, Aryl Skeletal	1325	1305	Strong	Mandatory
C-CO, Aryl Skeletal	1295	1260	Strong	Mandatory
C-H Bend, OOP	850	675	Strong	Mandatory

I developed the protocol for data acquisition and interpretation in Orbi-SIMS analyses. Initially, both positive and negative polarities spectra were obtained to check the peak intensity of the control samples. Then, the positive spectra were fixed in this study because more intense and well-defined signals were recorded in this operation mode (Figure 5.15 and Table 5.9). The potential pair of chemical groups $C_8H_5NO_2^+$ [*m/z* 147.03] and $C_7H_7^+$ [*m/z* 91.04] for representing WI and SI correspondingly. These results are correlated to the previous results from FT-IR analyses, particularly the high possibility of nitrogen existence in WI exclusively.

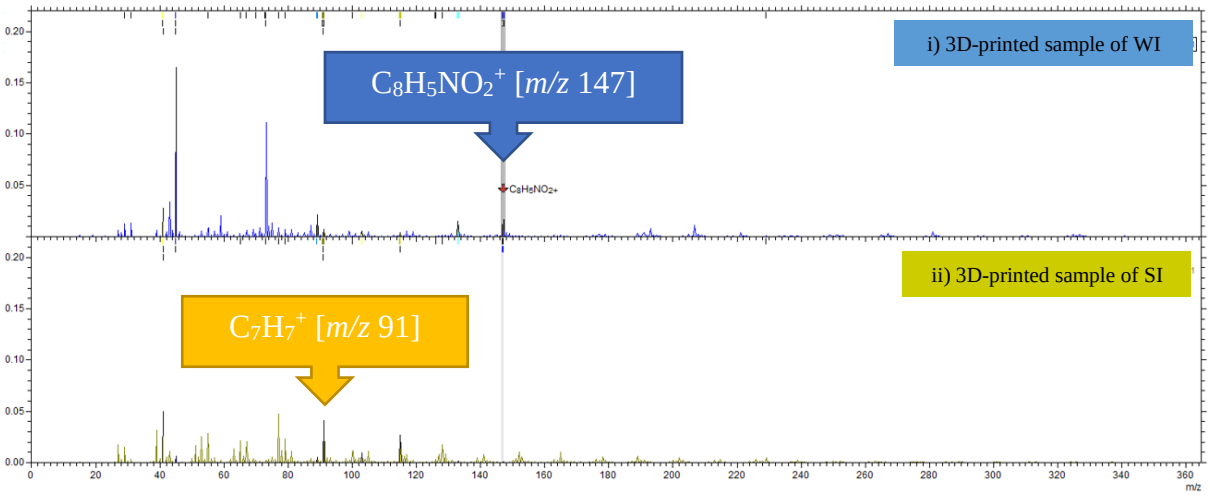

Figure 5.15. *Full spectra of the 3D-printed sample of WI with colour coding as blue (i) & SI with colour coding as yellow (ii). The results highlighted the potential pair of chemical groups $C_8H_5NO_2^+$ [m/z 147.03] and $C_7H_7^+$ [m/z 91.04] for representing WI and SI correspondingly*

Table 5.9. Peak lists for the controls WI & SI

m / z	Area / cts	Norm. by Total Ion Intensity	Color	Deviation / ppm	Desc...	Assignment	Explaine...	Peak Label
45.0360	6131665	1.66e-001		335.7		CH_3NO+	100.0%	CH_3NO+
41.0397	1072630	2.90e-002		26.7		C_3H_5+	100.0%	C_3H_5+
147.0253	892356	2.42e-002		-41.8		$C_8H_5NO_2+$	100.0%	$C_8H_5NO_2+$
89.0516	857156	2.32e-002		50.4		$C_3H_7NO_2+$	100.0%	$C_3H_7NO_2+$
133.0105	597031	1.62e-002		-313.4		C_8H_7NO+	100.0%	C_8H_7NO+
103.0074	278690	7.54e-003		-454.0		C_8H_7+	100.0%	C_8H_7+
91.0405	271616	7.35e-003		-151.0		C_7H_7+	100.0%	C_7H_7+
115.0320	154369	4.18e-003		-193.6		C_9H_7+	100.0%	C_9H_7+

b. Fingerprint functional groups

I developed the protocol for data acquisition and visualisation in ToF-SIMS analyses. The next two figures were used to establish a linescan analysis method and the baseline signals that come out of it. This is a cornerstone to progress the interface analyses of co-printed samples (see Chapter 6 for more details).

Development of step-by-step protocol for data processing

The step-by-step protocol for data processing in ToF-SIMS analyses of 3D-printed samples was firstly developed in this thesis. Figure 5.16 shows three main steps for examining the 3D-printed control: Step 1) Acquiring-calibrating signals with 3 spatial maps of ions(a), $C_8H_5NO_2^+$ [*m/z* 147.03] (b), $C_7H_7^+$ [*m/z* 91.04] (c); Step 2) Normalising-overlaying signals with 3 maps of normalised $C_8H_5NO_2^+$ [*m/z* 147.03] (a), normalised $C_7H_7^+$ [*m/z* 91.04] (b), and Overlay (c), and Step 3) Analysing with mapping and linescans from position 1 to 5 via x-axis (i.e. linescan left-right C1-C5) and y-axis (i.e. linescan top-bottom D1-D5).

Figure 5.17 illustrated clearer data acquisition and interpretation. Particularly, each sample was analysed at the same positions on these linescan pairs: i) Linescan left-right including five positions of C1-Top, C2-Second Top, C3-Middle, C4-Second Bottom, and C5-Bottom; and ii) Linescan top-bottom including five positions of D1-Left, D2-Second Left, D3-Centre, D4-Second Right, and D5-Right). The mapping and linescan data revealed the signal for $C_8H_5NO_2^+$ [*m/z* 147.03] (in navy blue) could be separated from the signal for $C_7H_7^+$ [*m/z* 91.04] (in yellow green), that were distributed homogeneously on sample's surface.

For all following analyses, all signals were compared against the baseline signal from these 3D-printed samples (as the control). The data acquisition and interpretation of ToF-SIMS analyses are presented at Figure A3.3 - A3.8 in Appendix A3. This technique was ultilised for monitoring the distribution and changes of ink formulation in additive manufacturing focusing on their interfaces.

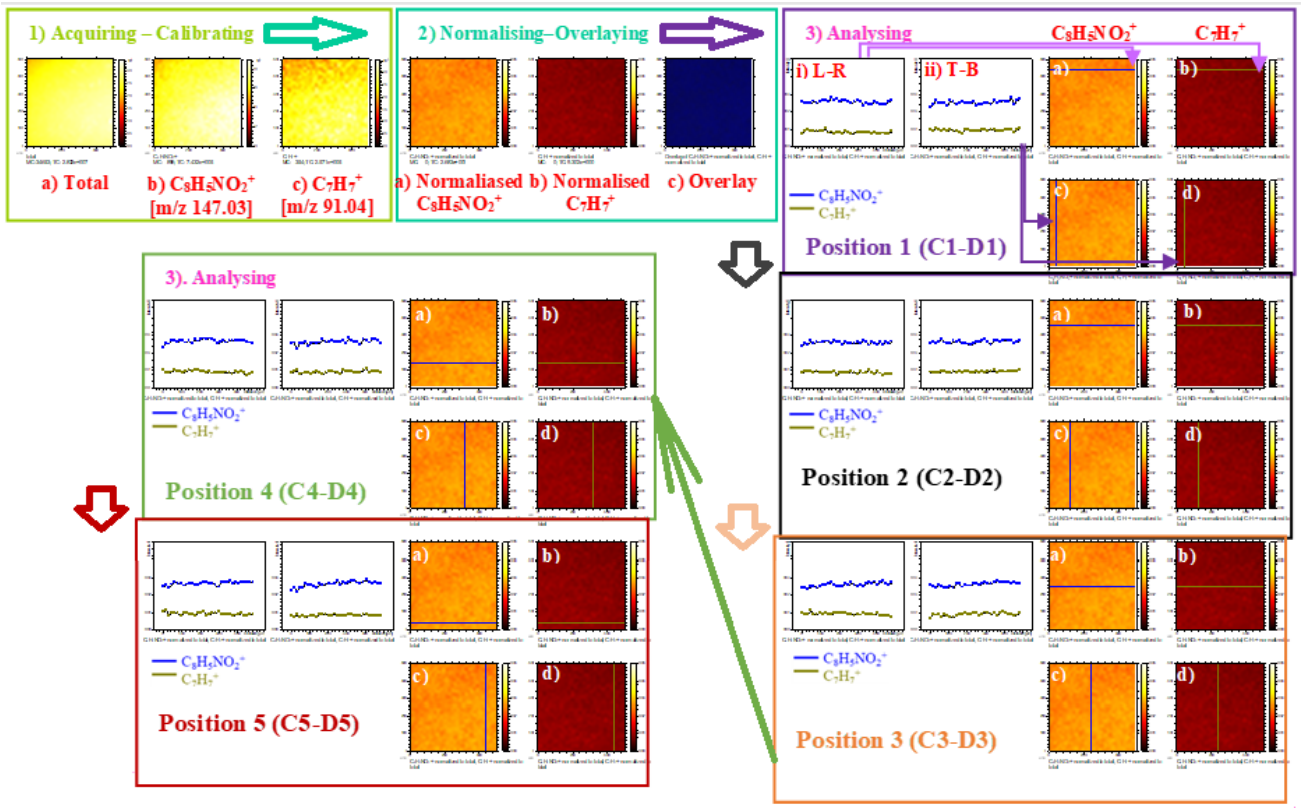

Figure 5.16. *Step-by-step protocol for data processing in ToF-SIMS analyses of 3D-printed sample of WI: Step 1) Acquiring-calibrating signals with 3 spatial maps of ions(a), C8H5NO2+ [m/z 147.03] (b), C7H7+ [m/z 91.04] (c); Step 2) Normalising-overlaying signals with 3 maps of normalised C8H5NO2+ [m/z 147.03] (a), normalised C7H7+ [m/z 91.04] (b), and Overlay (c), and Step 3) Analysing with mapping and linescans from position 1 to 5 via x-axis (i.e. linescan left-right C1-C5) and y-axis (i.e. linescan top-bottom D1-D5).*

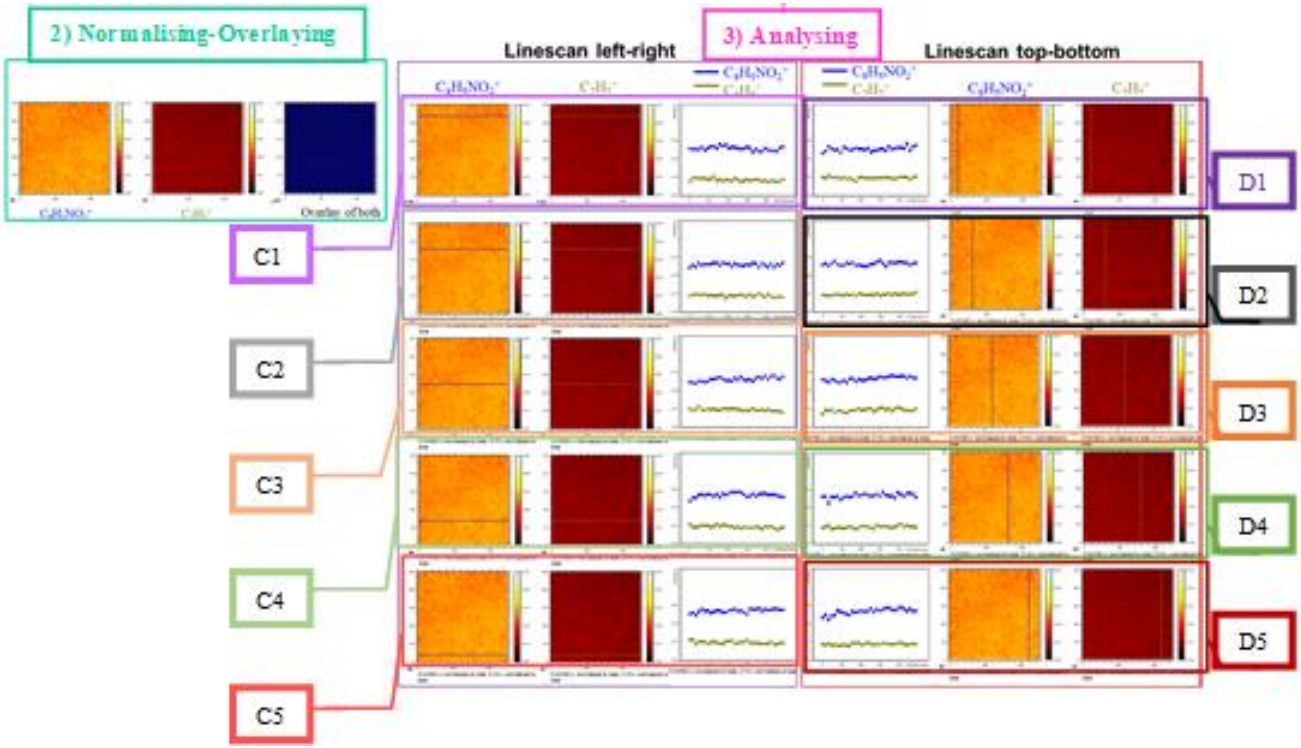

Figure 5.17. *Comparison of multiple mappings and linescans in Step 3: each sample was analysed at the same positions on these linescan pairs: i) Linescan left-right including five positions of C1-Top, C2-Second Top, C3-Middle, C4-Second Bottom, and C5-Bottom; and ii) Linescan top-bottom including five positions of D1-Left, D2-Second Left, D3-Centre, D4-Second Right, and D5-Right). The mapping and linescan data revealed the signal for C8H5NO2+ [m/z 147.03] (in navy blue) could be separated from the signal for C7H7+ [m/z 91.04] (in yellow green), that were distributed homogeneously on sample' s surface.*

Testing of 3D-printed samples of each ink

After developing the practical guide for data acquisition and interpretation, ToF-SIMS analyses were carried out on three samples of WI (as samples WI 1 - WI 3) and three samples of SI (as samples SI 1 - SI 3).

Table 5.10 revealed the peak assignments from ToF-SIMS (compared to OrbiSIMS analyses) to strengthen a range of fingerprint functional groups such as $C_8H_5NO_2^+$ [*m/z* 147.03] representing WI and $C_7H_7^+$ [*m/z* 91.04] representing SI. A pair of functional groups was confirmed to represent each ink, which matched the results from the previous spectra data. The trending of signals was revealed via mapping images (Figure 5.17a-c) and two types of linescan (Figure 5.17d-e). Thanks to the smoother linescan in sample WI 2 and WI 3 (Figure 5.17e), WI was proven to have more even distribution of signals at the surface (compared to SI). In other words, WI can distribute more homogeneously on the substrate, matching the previous data of physical properties of original inks and 3D-printed samples (in section 5.3.1 and 5.3.3).

Hence, the methodologies for studying interfaces are successfully developed and validated, which will be applied to investigate the co-printed samples later (in Chapter 6).

Table 5.10. Peak assignments from ToF-SIMS and OrbiSIMS analyses

ToF-SIMS (LMIG data)					**OrbiSIMS (GCIB data)**			
WI	***m/z***	**SI**	***m/z***		**WI**	***m/z***	**SI**	***m/z***
CH_3NO^+	45.04	$C_3H_5^+$	41.04		$C_8H_5NO_2^+$	147.0315	$C_7H_7^+$	91.0405
$C_3H_4NO^+$	70.03	$C_7H_7^+$	91.04		$C_9H_{15}NO_2^+$	169.0307	$C_7H_{11}^+$	95.0502
$C_3H_7NO^+$	89.02				$C_9H_{17}NO_2^+$	171.0130	$C_8H_9^+$	105.0701
$C_5H_{10}N_2O^+$	114.07				$C_{11}H_{11}NO_2^+$	189.0735	$C_9H_7^+$	115.0511
$C_6H_{10}N_2O^+$	128.01				$C_{13}H_{25}NO_2^+$	227.0214	$C_9H_9^+$	117.0726
$C_8H_5NO_2^+$	147.03				$C_{13}H_{27}NO_2^+$	229.0311	$C_{10}H_8^+$	128.0603
					$C_{14}H_{33}NO_2^+$	247.0103		

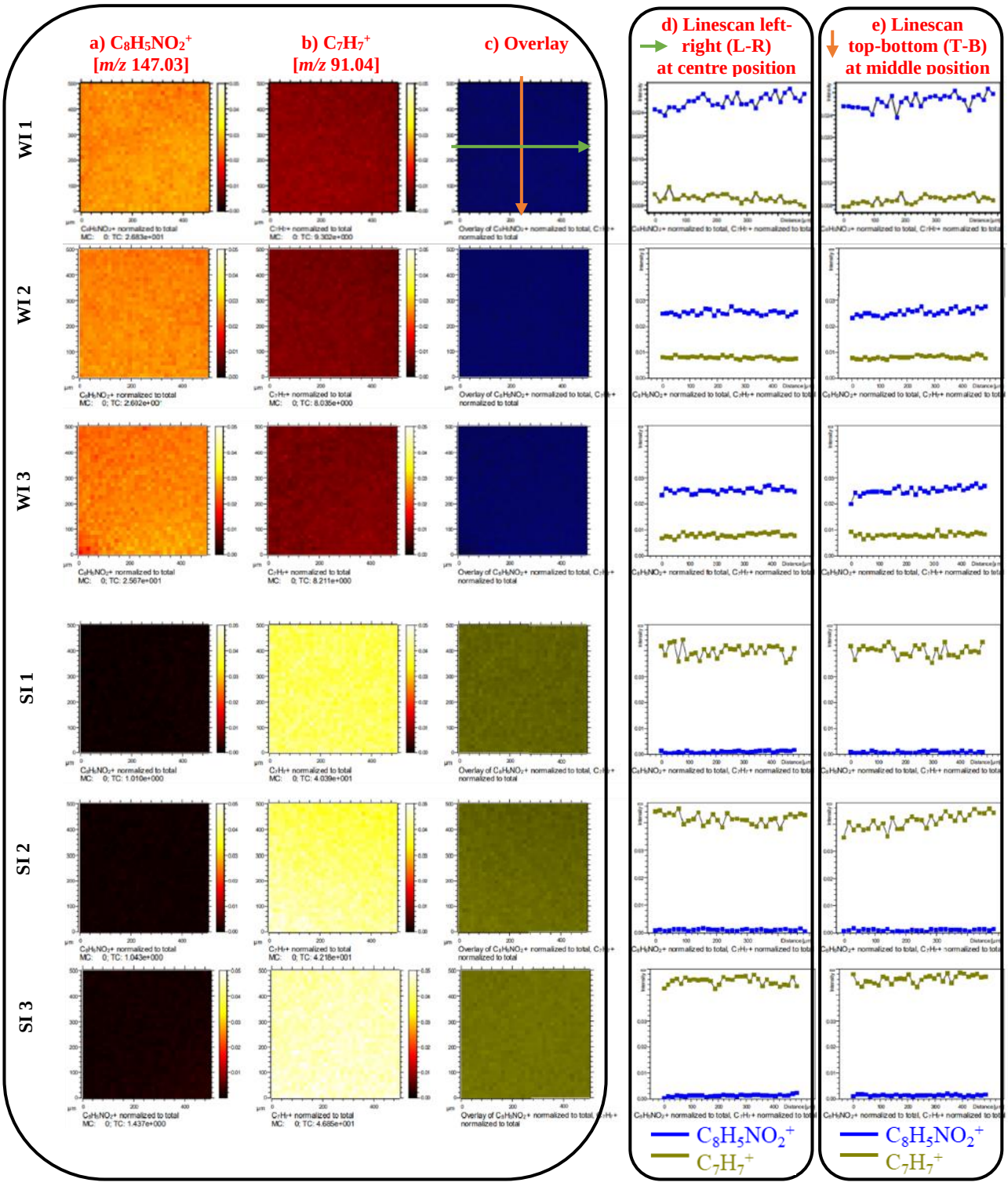

Figure 5.18. *Initial ToF-SIMS results of 3D-printed samples (3 samples for each ink printed): a) Normalised $C_8H_5NO_2^+$ [m/z 147.03], b) Normalised $C_7H_7^+$ [m/z 91.04], c) Overlay of both normalised signals (with colour coding for WI as blue, and colour coding for SI as yellow), d) Linescan left-right (L-R) at centre position, and e) Linescan top-bottom (T-B) at middle position.*

5.4. CONCLUSIONS

5.4.1. Summary

a. Physiochemical compatibility

WI could provide smooth surface and kept square block at all sizes, whereas SI only gave good performance at smaller sizes (0.5x0.5 and 1x1 mm), but not larger sizes (2x2 and 4x4 mm). For the ink-jetting of WI and SI, PEN (rather than glass or silicon wafer) was a good substrate and acetone (rather than water or isopropanol) was a good cleaning solvent. Additionally, WI had a thickness of 25.9 ± 0.5 µm and SI of 23.4 ± 2.3 µm for a single layer, which expanded the opportunity for future investigation of electrical, chemical, and physical properties. The following chemical results of original inks would help to reveal and understand different organic-inorganic structures between WI and SI that had major impacts on the faster solidification.

The investigation of the physiochemical properties of original inks and 3D-printed samples helps to expose the significant impact of substrate treatment on the quality of the final 3D printed object: 1) Ink spreading and resolution: substrate treatment can influence how ink or material droplets spread and interact with the substrate surface. Monitoring this treatment allows for precise control over the print resolution and quality; and 2) Substrate materials: different substrates, such as plastics, metals, or composites, may require different treatments to optimise adhesion and print quality. The right treatment of substrates applied for the specific ink formulation can improve their physical compatibility.

In summary, a practical guide was built and developed to help to understand and monitor the physiochemical compatibility at the interface of ink-substrate and ink-ink. I presented how enhancing the analyses with in-situ morphology and interferometry could help to optimise the ink-jetting and study the micro-behaviour of inks on different substrates. Compared to an optical microscope, the high-speed printer camera with a new embedded coding was shown to be able to acquire in-situ morphological data of the 3D-printed samples. The interferometer with auto-stitching function became more effective for measuring the layer thickness that could help to study the ink-jetted multi-materials. By comparing the optical images captured by optical microscope and the printer camera (with enhanced new coding), I can select the method to effectively study morphology. The in-situ

morphology during the ink-jet printing would be effectively investigated thanks to the high-speed printer camera (compared to the post-characterisation with optical microscope after the ink-jetting). Moreover, without auto-stitching function like Zygo-interferometer, Zeta-profiler required to be assessed for desirable analytical parameters before being used for measuring the layer thickness.

Furthermore, Figure 5.18 summarises two approaches for interface/surface study. As the first approach for interface/surface study, I started to design, 3D-print and evaluate patterns ink-jetted (on PEN) from the smaller sizes at the lower printing speeds to larger sizes at the higher printing speeds. On the second approach, I started to design, 3D-print and evaluate patterns (with the substrates of glass and silicon wafer) from the larger sizes at the higher printing speeds to the smaller sizes at lower printing speeds. Thanks to previous results, both approaches were appropriate for interface/surface study and the second approach showed more advantages when using analyses due to its offered fast reaction backwards to the ink-jetting in real time.

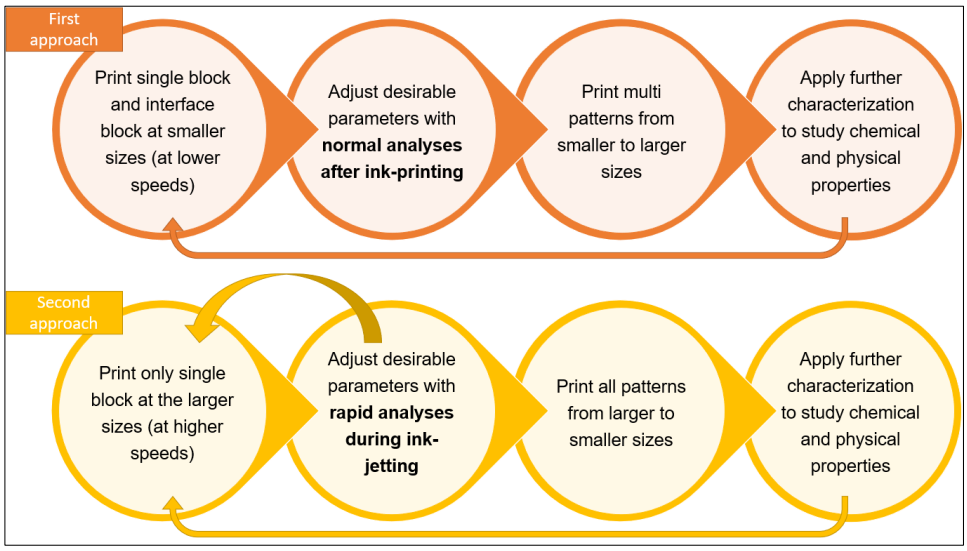

Figure 5.19. *Two strategic approaches for interface/surface study of 3D-printed multi-materials in biopharmaceutical fields*

b. Practical guide

Figure 5.19 shows the practical guides for the investigation of the physiochemical compatibility of ink formulation in additive manufacturing. It will be based on three main checks:

1) checking single ink (as the starting point to ensure the qualified control sample) by evaluating the results from Printability testing (via Rheology Measurement (RM) including Surface Tension and Viscosity Measurement), and Wettability testing (via Contact Angle Measurement (CAM)), Element contents (via Microelemental Analysis (MA), and Nuclear Magnetic Resonance Spectroscopy (NMR), Inductively Coupled Plasma Optical Emission Spectroscopy (ICP-OES), and Inductively Coupled Plasma Mass Spectroscopy (ICP-MS).

2) checking the behaviours of inks-substrates by evaluating the results from Contact Angle Measurement (CAM), Optical Microscopy (OM), In-situ Photography (IP), Profilometry, Interferometry.

3) checking the behaviours of inks-inks, particularly in the co-printed multi-functional multi-materials by evaluating the results from Fourier-Transform Infrared Spectroscopy (FT-IR), Time Of Flight Secondary Ion Mass Spectrometer (ToF-SIMS), and Hybrid Orbitrap Secondary Ion Mass Spectrometer (OrbiSIMS).

The practical guide also helps to explore some micro-nano behaviours at the surfaces-interfaces that affect the quality of final 3D-printed samples:

- Rheological behaviour: The viscosity of each ink influences their deposition on the interface during 3D-printing. The rheological properties should be monitored to ensure the correct deposition of ink formulation and prevent issues such as nozzle blockage.
- Wetting behaviour: The levels of inks' spreading on the substrate needs to be controlled to achieve a more uniform surface finish. Appropriate wetting is also essential for efficient interfaces between two inks and helps to decrease the artefacts in the following physiochemical analyses.
- Adhesive behaviour: The porosity or trapped air bubbles can weaken the structure and damage the uniformity of final surface. The interaction of ink-substrate is important to ensure that the printed material deposits properly on substrate and continues building on previous layers. Other micro-nano behaviours of ink-substrate

and ink-ink that can affect the jetting consistency will receive further investigation (more details in Chapter 6).

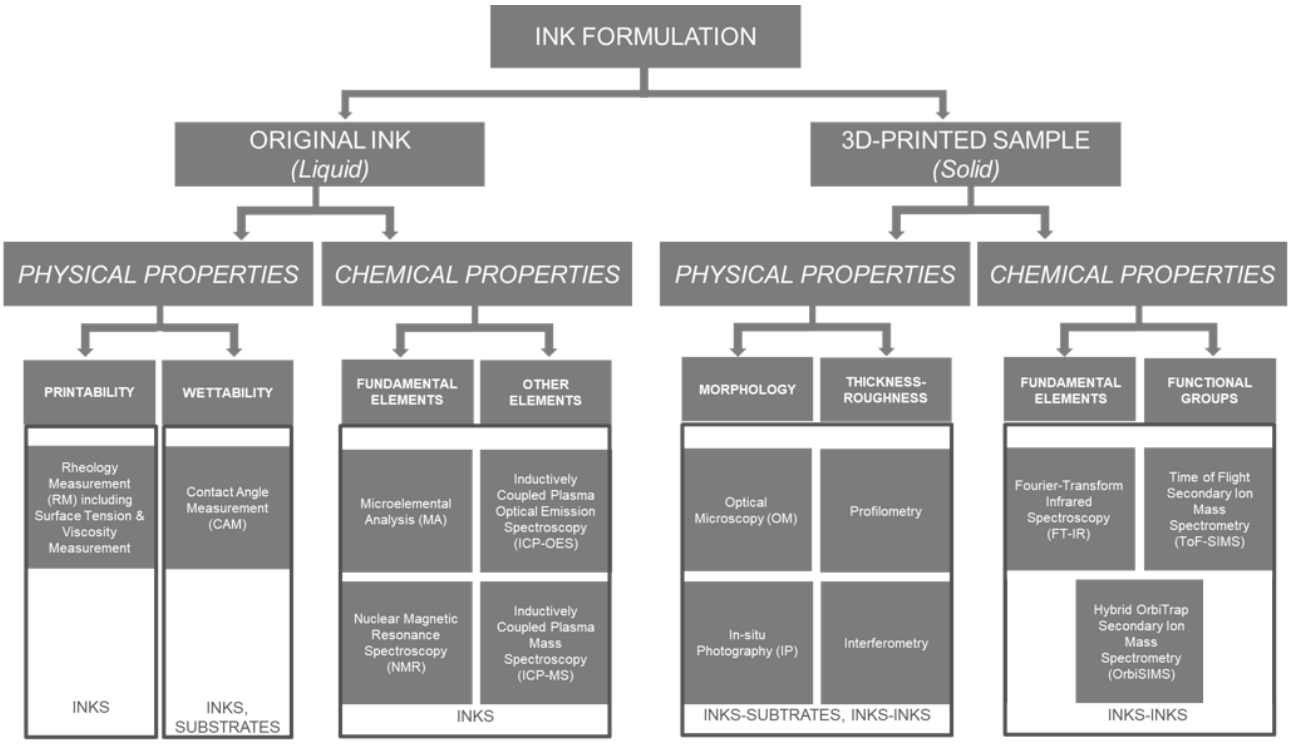

Figure 5.20. *Diagram of useful characterisation to examine the physiochemical compatibility of new ink formulations in additive manufacturing, focusing on testing the physical and chemical properties of original ink (liquid) and 3D-printed samples (solid). The results also revealed three main checks: 1) checking single ink (as the starting point to ensure the qualified control sample), 2) checking the behaviours of inks-substrates, and 3) checking the behaviours of inks-inks*

5.4.2. Outputs related to Chapter 5

a. Publication

Quach, T. T., Trindade, G. F., Hague, R., & Roberts C. J. Development of practical guide to investigate the physiochemical compatibilities of new ink formulations in additive manufacturing (in preparation).

b. Conference

● EPSRC Next Generation of Additive Manufacturing – Annual meeting 2022 hosted by the Centre for Additive Manufacturing - University of Nottingham, Nottingham, the United Kingdom, 28.04.2022

Poster presentation: "Micro/nano scale characterisation of interfaces in next generation multi-materials additive manufacturing (3D-printing)"

Tien Thuy Quach[1,2], Gustavo F. Trindade[2,3], Richard JM Hague[2] and Clive J Roberts[5]

● Microscience Microscopy Congress (mmC) incorporating Electron Microscopy & Analysis Group (EMAG) 2021, 07.07.2021

Poster presentation: "Interface analysis for the next-generation of multi-materials additive manufacturing"

Tien Thuy Quach[1,2], Gustavo F. Trindade[2,3], Richard JM Hague[2] and Clive J Roberts[1]

● The FORGE: Characterization of Pharmaceutical Formulations, 25.03.2021:

Poster presentation: "Micro/nanoscale characterisation for the next-generation 3D-printed multi-materials"

– Best Interactive Researcher on 25.03.2021

Tien Thuy Quach[1,2], Gustavo F. Trindade[2,3], Jisun Im[2], Richard JM Hague[2] and Clive J Roberts[1]

● European Advanced Materials Congress (EAMC 2021) (Stockholm, Sweden) **Onsite, Online & On-demand Hybrid Participation Setups*, 23-25.08.2021

Oral presentation: "Interface characterisation for the next generation of multi-materials additive manufacturing" – Best Oral Presentation Prize (25.08.2021)

Tien Thuy Quach[1,2], Gustavo F. Trindade[2,3], Richard JM Hague[2] and Clive J Roberts[1]

● East Midlands Doctoral Network Postgraduate (EMDOC PGR) Research Conference 2020 with the theme "Sustainability", hosted by the University of Leicester and De Montford University - Virtual session, the United Kingdom, 9-10th September 2020

Poster presentation: "Designing and optimising micro/nanoscale characterisation methodologies for next-generation multi-functional 3D-printed products"

Tien Thuy Quach[1,2], Gustavo F. Trindade[2,3], Laura Ruiz-Cantu[2], Richard JM Hague[2] and Clive J Roberts[1]

c. Internal seminar

● Oral presentation at the Advanced Materials and Healthcare Technologies Division, School of Pharmacy, University of Nottingham

● Oral presentation at the PGR Seminar of the Centre for Additive Manufacturing, University of Nottingham

CHAPTER 6: DESIGN OF ACTIVE PROCESS WORKFLOW TO INVESTIGATE THE INTERFACES OF CO-PRINTED PHARMACEUTICAL PRODUCTS

6.1. INTRODUCTION

This exclusive AM technology can offer multi-layered products with the precise positioning of materials. For example, hot melt extrusion could help to produce drug loaded filaments as the feedstock [257,258]. Multi-materials additive manufacturing involves combining dissimilar materials to enhance the performance of one component and/or whole product, which has several restrictions in the manufacturing process. For example, it is difficult to create strong, long-lasting bonds in the composite materials due to differences in design factors (such as material dimension and thickness) or process factors (such as thermal expansion and mismatch in cooling rates) [240,241]. Other examples are providing enough energy to build a multi-material system or manufacturing smart responsive materials at the same time under the same environment [242,243].

MAM can be monitored at precise sites, gradually enhanced, and tailored for different specific applications. Medical implants (such as stents or catheters), and drugs with multiple active ingredients could be printed [259,260]. However, it is still challenging to co-print (simultaneously different materials) and control the final products as different functional formulations may interact differently at interfaces, especially in context of dissimilar deposition and curing strategies [261–263].

Therefore, Chapter 6 aims to develop robust methodologies to investigate interface/interphase regions of the functional formulations in pharmaceutical field. As a case study, Figure 6.1 shows the theory of different interfaces resulted from co-printing a water-soluble ink (WI) (having a support function) and a structural ink (SI) (having a bacterial biofilm resistance function). I investigated the interface/interphase between formulations and substrates, formulations and formulations from functional multi-materials AM to investigate the optimal co-printing workflow.

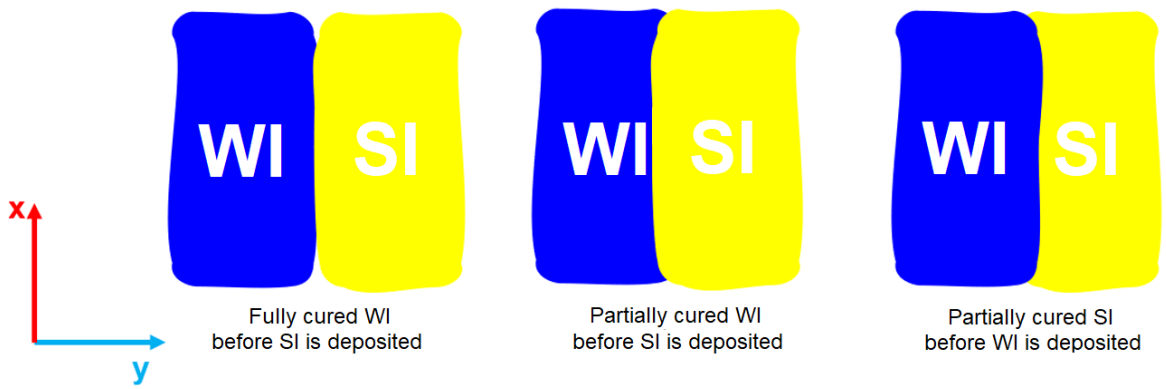

** WI and SI are different functional formulations (e.g. medicinal or supportive functions)*

Figure 6.1. *Dissimilar deposition and curing strategies could result in different interfaces and affect the functionalities of 3D-printed pharmaceutical products*

6.2. MATERIALS-METHODS

6.2.1. Formulation

Formulation has the same information as in section 5.2.1.

6.2.2. Characterisation

Characterisation has the same information as in section 5.2.2.

In Chapter 6, there are adjustments for the preparation and analyses of 3D-printed samples to enable the reliable workflow. There are five main stages of ink-jet 3D-printing including: 1) Selecting chemicals and substrates; 2) Preparing ink formulations; 3) Designing interface patterns; 4) Setting system features; and 5) Optimising process parameters (Figure 6.2). The modification of the system parameters can facilitate better adhesion, print quality, and material compatibility for a given application.

To investigate possible factors enabling the effective workflow, I proposed using five key questions to explore the details and look for consideration/suggestion for improvement (Figure 6.3).

+ Type and number of 3D-printer ➔ Question 1: “Which 3D-printer to use?”

+ Type and number of materials, substrates ➔ Question 2: “Which materials, substrates to use?”

+ Type and number of designed patterns ➔ Question 3: “What are the design interests?”

+ Type and number of machine factors ➔ Question 4: “What are the operation set-up?”

+ Type and number of process parameters ➔ Question 5: “How to improve the procedure?”

Figure 6.2. *Simple ink-jet 3D-printing process*

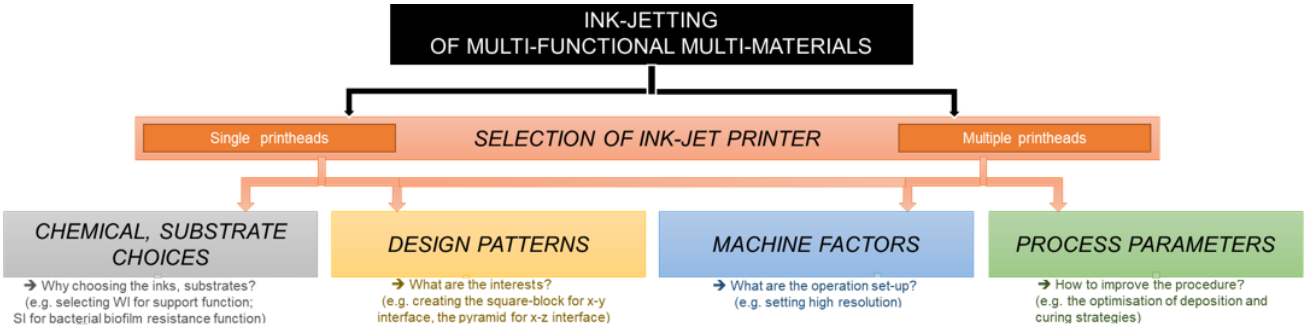

Figure 6.3. *My proposal of using five key questions to enable effective workflow for co-printed functional multi-materials in (bio)pharmaceutical field*

Following to five key questions in Figure 6.3, I can monitor high quality ink-jetting of functional multi-materials in pharmaceutical field.

i. Question 1: "Which 3D-printer to use?"

Different 3D-printers will have different build volumes, resolution, and accuracy which can affect the level of details that can be achieved in the final print. For example, larger build volumes can accommodate larger objects, while smaller printers are limited to smaller designs [264–266].

In this study, LP50 ink-jet printer with multiple printheads was chosen to reduce the time when co-printing multiple materials with dual printheads. Chapter 5 already revealed the results when printing individual inks using single printhead, so we continued optimising the workflow process according to the previous results and discussion.

ii. Question 2: "Which materials, substrates to use?"

3D-printing can use a range of materials, but not all of are compatible with each other in the creation of multi-materials additive manufacturing. Some materials require light-curing, typically ultraviolet (UV) light, to solidify or harden a liquid to create a 3D object [261–263]. Substrate treatment is an essential aspect to monitor in inkjet 3D printing for several reasons. For example, proper substrate treatment ensures that the printed material adheres well to the substrate surface. It can help reduce issues like warping, delamination, and curling, which can occur if the substrate isn't prepared correctly [254,267].

In this study, WI was chosen for support function and SI was chosen for bacterial biofilm resistance function because the commercialized ink WI was commonly used and SI has confirmed functionalities thanks to previous research [245,268,269]. The printability and wettability of WI and SI were tested on several substrates. The physiochemical compatibility of single ink was already evaluated and improved before moving to co-printing both inks.

iii. Question 3: "What are the design interests?"

Types and number of designed patterns are important in 3D printing due to several reasons [270–272]: 1) Accuracy: the geometry of printed object can affect the structural integrity, for example, larger sizes require more consideration of calibration for higher accuracy; 2) Printing time: sample with smaller sizes or layers generally require less time to produce (compared to large ones); and 3) Printing cost: more materials are usually required to produce larger prints, which in turn take higher cost to produce. Depending on targeted purposes, a series of sizes can be tested to ensure the desirable details within available time and budget.

In this study, the interface patterns were designed and tested to evaluate interface/interphase towards x-y and x-z direction. Table 6.1 summaries the whole pattern development of co-printing of WI and SI (with colour coding as blue and yellow respectively): 1) Testing x-y interfaces via patterns from 0a to 4b (as the number was correlated to the number of interfaces formed by two inks WI & SI; the followed word "a" or "b" was correlated to the different ink distribution); and 2) Testing x-z interfaces via patterns a-b-a and b-a-b (as the replicates of (WI printed on SI) or (SI printed on SI) respectively). The computer software

only processed black-white patterns (as black square representing with ink; and white square representing without ink). Bitmaps are created using Paint software and GNU Image Manipulation Program (from GIMP Team).

As there was a large number of screening printed samples, I kept the name coding following the formula as **[Pattern name]_[Sample size x-y]_[Layer z] (Printing_Curing Strategy)**. Figure 6.4 illustrates an example of co-printed sample of WI and SI with pattern 4b. Pattern 4b with 4 interfaces formed by 1 square block of SI and 4 square blocks of WI (observed from top view). For example, sample 4b_1.5x1.5_1lay (S0_UV 3sec to S1_UV 3sec) has single square block of 0.5x0.5 mm. For initial testing, single layer is recommended, so z = 1 if no further notice was given.

Printhead 1 contains WI and printhead 2 contains SI. Inks are deposited from left to right and bottom to top. For each printhead, the same single nozzle is examined and calibrated (prior to applying more nozzles for 3D-printing) in order to reduce the nozzles' variations.

Table 6.1. Pattern development when inkjet 3D-printing of WI (with colour coding as blue) and SI (with colour coding as yellow): i) pattern for testing x-y interfaces; ii) pattern for testing x-z interfaces

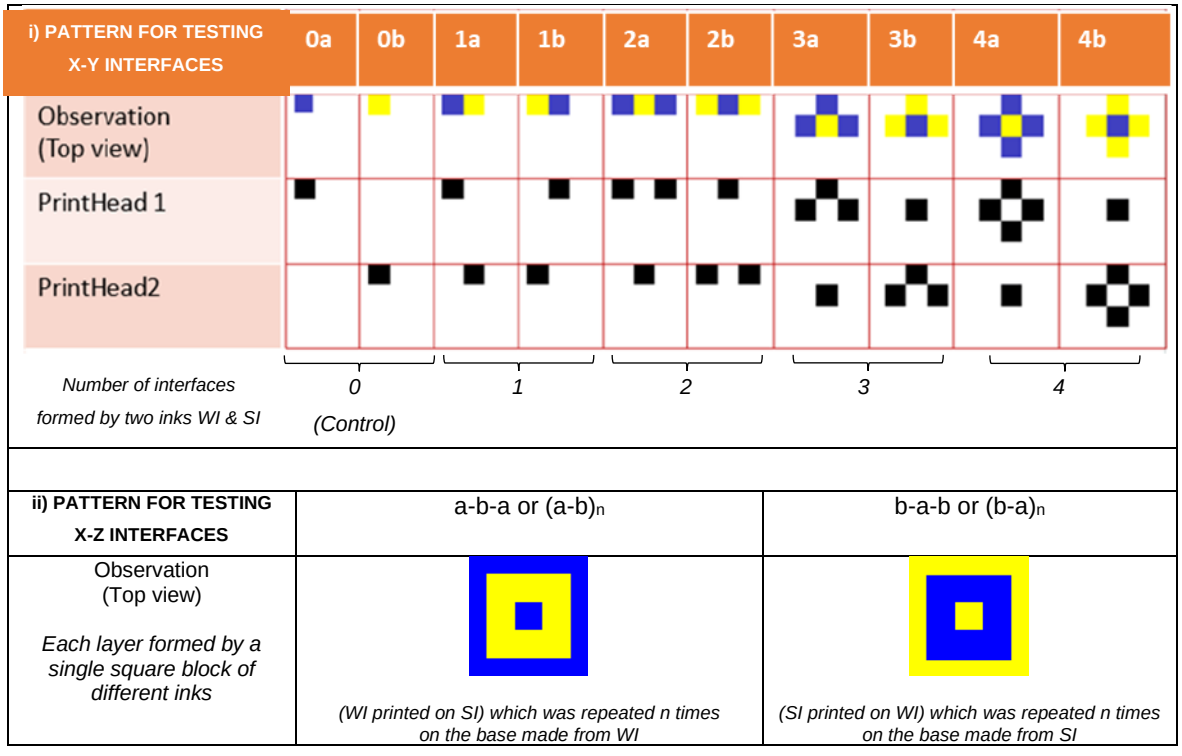

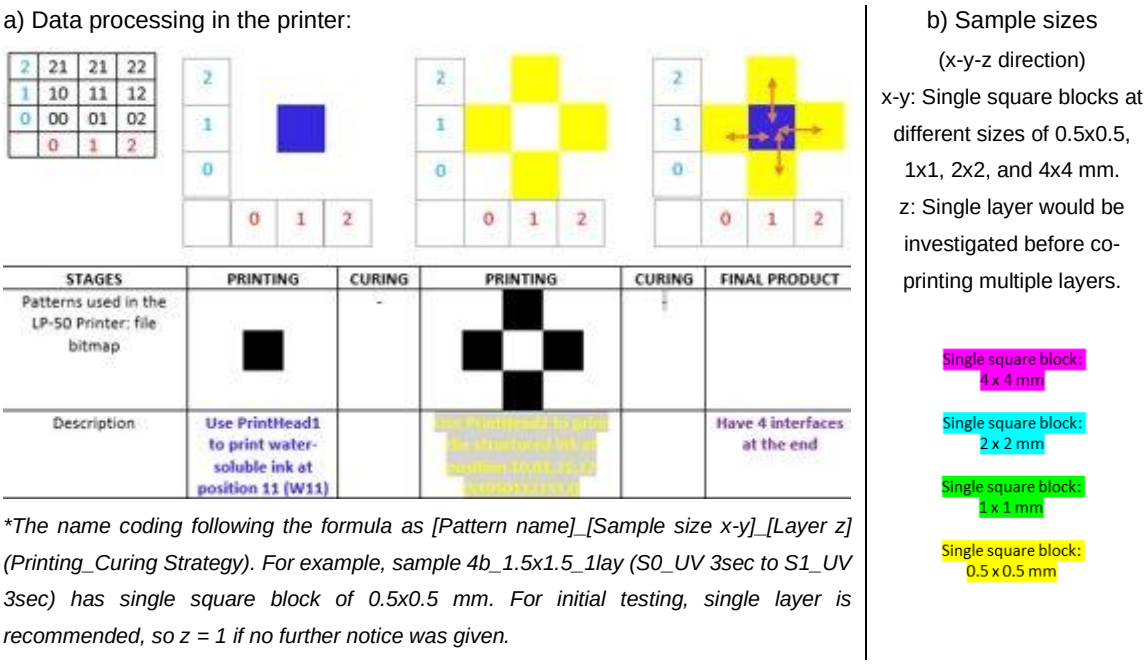

**The name coding following the formula as [Pattern name]_[Sample size x-y]_[Layer z] (Printing_Curing Strategy). For example, sample 4b_1.5x1.5_1lay (S0_UV 3sec to S1_UV 3sec) has single square block of 0.5x0.5 mm. For initial testing, single layer is recommended, so z = 1 if no further notice was given.*

Figure 6.4. *Example of co-printed sample of WI and SI with pattern 4b: a) Data processing in the printer (with the name coding as [Pattern name]_[Sample size x-y]_[Layer z] (Printing_Curing Strategy), and b) Sample sizes such as single square blocks at different sizes of 0.5x0.5, 1x1, 2x2, and 4x4 mm.*

iv. Question 4: "What are the operation set-up?"

A 3D-printer has different parameters that need to be considered to produce qualified products. Some factors include: 1) Nozzle Size: the diameter of the ink droplets is determined by the nozzle size, which then affects the size of final sample, for example, a larger nozzle can work faster but may give less detailed prints; 2) Printing speed: more 3D-printed products can be produced in shorter time at higher speed, which results in using less energy and money. For example, some materials may require curing time between intervals of printing or before handling, so faster printing speeds can reduce the overall time needed for those materials to be cured by light [273–275].

Therefore, the set-up operation will be investigated in terms of following parameters: the drop spacing of 40 and 50 µm (with the resolution of 635 and 508 dpi respectively), and the firing frequency of 5000 or 7000 kHz. This generates four printing speeds of 200, 250, 280, and 350 mm/sec (Table 6.2), which were the first testing variables in this thesis.

In-situ photography will be used to evaluate the morphology of 3D-printed samples to evaluate the testing variables (e.g. identify the optimal printing speed). There was a small notice that single smaller-sized figures will be automatically collected and stitching into the final larger-sized figure to observe the whole products. The sizes of single figures can be adjusted and will be fixed at the beginning of every printing experiments.

The expected results will be good film formation (without any cracks or pores), clear borders (represented initial design), and no contamination (existed on the surface). This can confirm the uniformity of the surfaces-interfaces of co-printed samples.

Table 6.2. System parameters were investigated

Printing parameters		**Drop spacing (μm) [with Resolution (dpi) respectively]**		
		40 [635]	**50 [508]**	
Firing frequency (Hz)	**5000**	200	250	**Printing speed* (mm/sec)**
	7000	280	350	
**The LP-50 inkjet printer with the specialised software had the function to convert the printing speed (mm/sec) based on the firing frequency (Hz) and resolution (dpi).*				

v. Question 5: "How to improve the procedure?"

Several approaches can be considered to improve the 3D-printing process. One of the common choices is ensuring proper ink deposition due to its essential impacts: 1) Dimensional accuracy: properly deposited ink can reduce the need for multiple passes or corrections during printing, improving overall efficiency; 2) Print quality: the quality of the 3D printed object depends on the accuracy of ink deposition; and 3) Process efficiency: suitable ink deposition ensures that the printing process is not only accurate but also faster, and reduce the time lag and material waste. To achieve proper ink deposition in inkjet 3D printing, various factors should be controlled, including ink viscosity, nozzle size, print speed, curing or drying methods, and calibration of the printer [276,277]

Another option to improve the manufacturing procedure is the optimization of the light-curing strategies because the wavelength of the light, the type of materials, and the curing energy can impact the mechanical properties, flexibility, and durability of the printed part. For example, overexposure to UV light, for example, can result in an overly brittle part that

requires additional post-curing steps to achieve the desired material properties. Also, UV light is potentially harmful to human skin and eyes, so it is important to ensure the user safety throughout the curing process (via proper shielding and the use of personal protective equipment) [261,275,278].

In this study, the ink deposition and light-curing strategies were prioritised. Table 6.3 reveals testing factors: 1) two light-curing strategies including UV-curing for each deposition and UV-curing at final deposition, and 2) two deposition strategies including deposition of WI before SI and deposition of SI before WI.

ToF-SIMS and OrbiSIMS are used to evaluate the chemical changes of 3D-printed samples in order to identify the optimal strategies for deposition and light-curing. The expected results will be representative functional groups (that is fingerprint for each ink), chemical shifts (following the micro/nanostructures), and no intermixing (at the interfacial areas). This can verify chemical compatibility of the surfaces-interfaces of co-printed samples.

Table 6.3. Process strategies investigated

2 DEPOSITION STRATEGY *Depositing WI before SI (i.e. S0 to S1) or reverse*	**2 CURING STRATEGY** *UV-curing for each deposition (i.e. UV 3 sec) or at final deposition*	**4 TESTING VARIABLES** ***Deposition-curing strategies (known as (i), (ii), (iii), (iv))***	***Accumulated UV-curing exposure time (sec)*** *WI | SI*
S0 to S1	UV 3 sec for each deposition	(S0_UV 3sec) to (S1_UV 3sec) (i)	6 sec | 3 sec
S1 to S0	UV 3 sec for each deposition	(S1_UV 3sec) to (S0_UV 3sec) (ii)	3 sec | 6 sec
S0 to S1	UV 3 sec at final deposition	(S0_UV 0sec) to (S1_UV 3sec) (iii)	3* sec | 3 sec
S1 to S0	UV 3 sec at final deposition	(S1_UV 0sec) to (S0_UV 3sec) (iv)	3 sec | 3* sec
*Notice: * Delayed time of T_i (sec) before UV-curing, which depends on the deposition time of previous part.*			

6.3. RESULTS AND DISCUSSION

6.3.1. Optimisation of printing speed

a. Inkjet 3D-printing on glass

Figure 6.5 and Figure 6.6 show printed samples of WI and SI (with patterns 0a and 0b respectively) at all sizes from 4x4 mm to 0.5x0.5 mm at different printing speeds (of 350, 280, 250, and 200 mm/sec). Excluded from very tiny pores at lower printing speeds, the similar results of good film formation and clear border for WI exist at all sizes at the printing

speed of 280 and 350 mm/sec. Contradicted to WI, SI does not provide any qualified film formation at larger sized blocks (of 4x4 and 2x2 mm), except from the most of smaller sized blocks (of 1x1 and 0.5x0.5 mm). They have rectangle shapes (rather than initial designed squares). This result matches the printability and wettability of each ink (in Chapter 5).

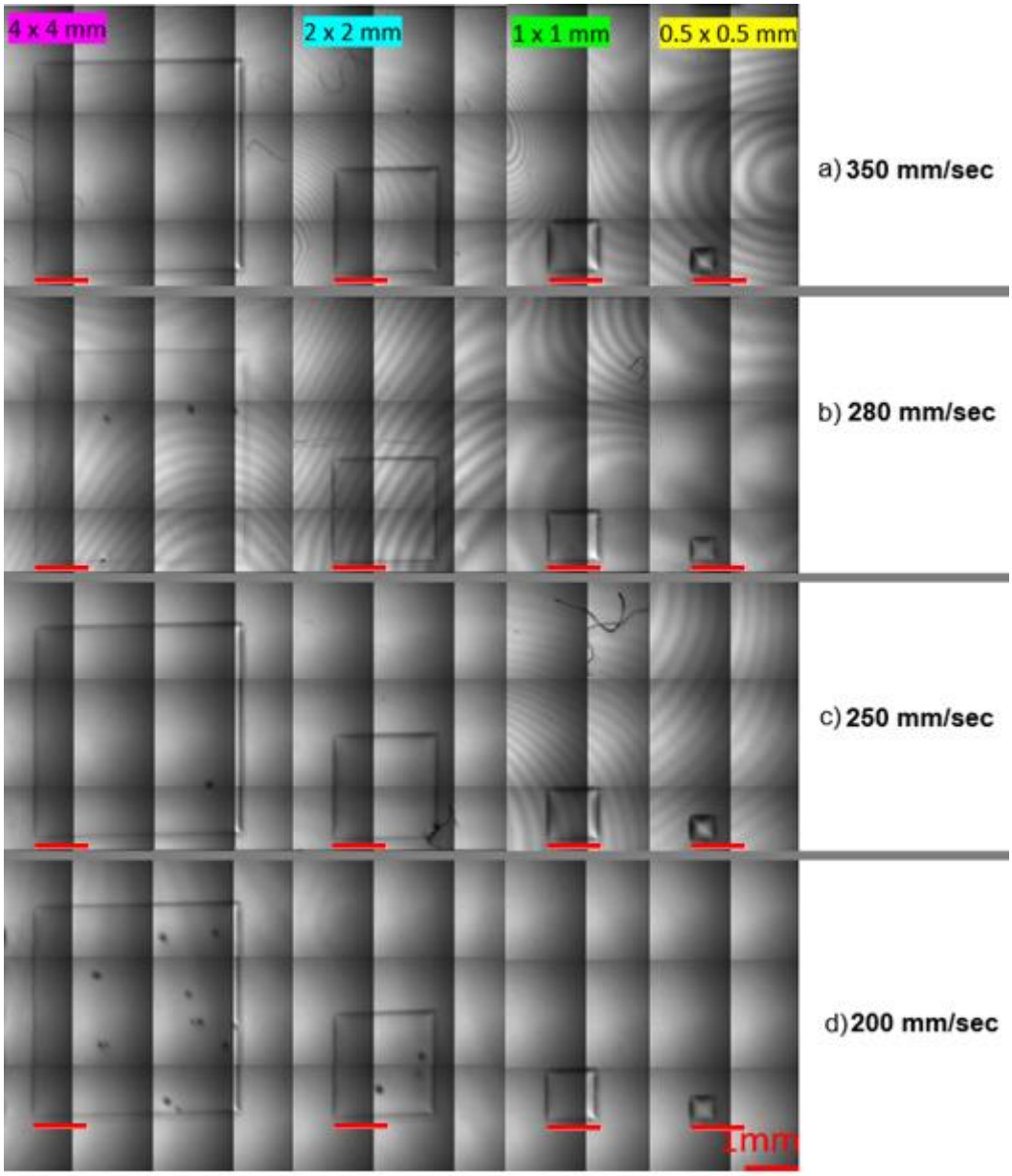

Figure 6.5. *Printer camera images of single square blocks of WI with pattern 0a from larger to smaller sizes (of 4x4 mm, 2x2 mm, 1x1 mm, and 0.5x0.5 mm) on glass cleaned with acetone at different printing speeds: a) 350 mm/sec, b) 280 mm/sec, c) 250 mm/sec, and d) 200 mm/sec. The sample differences were linked to the differences of four printing speeds, which correlated to the Table 6.2.*

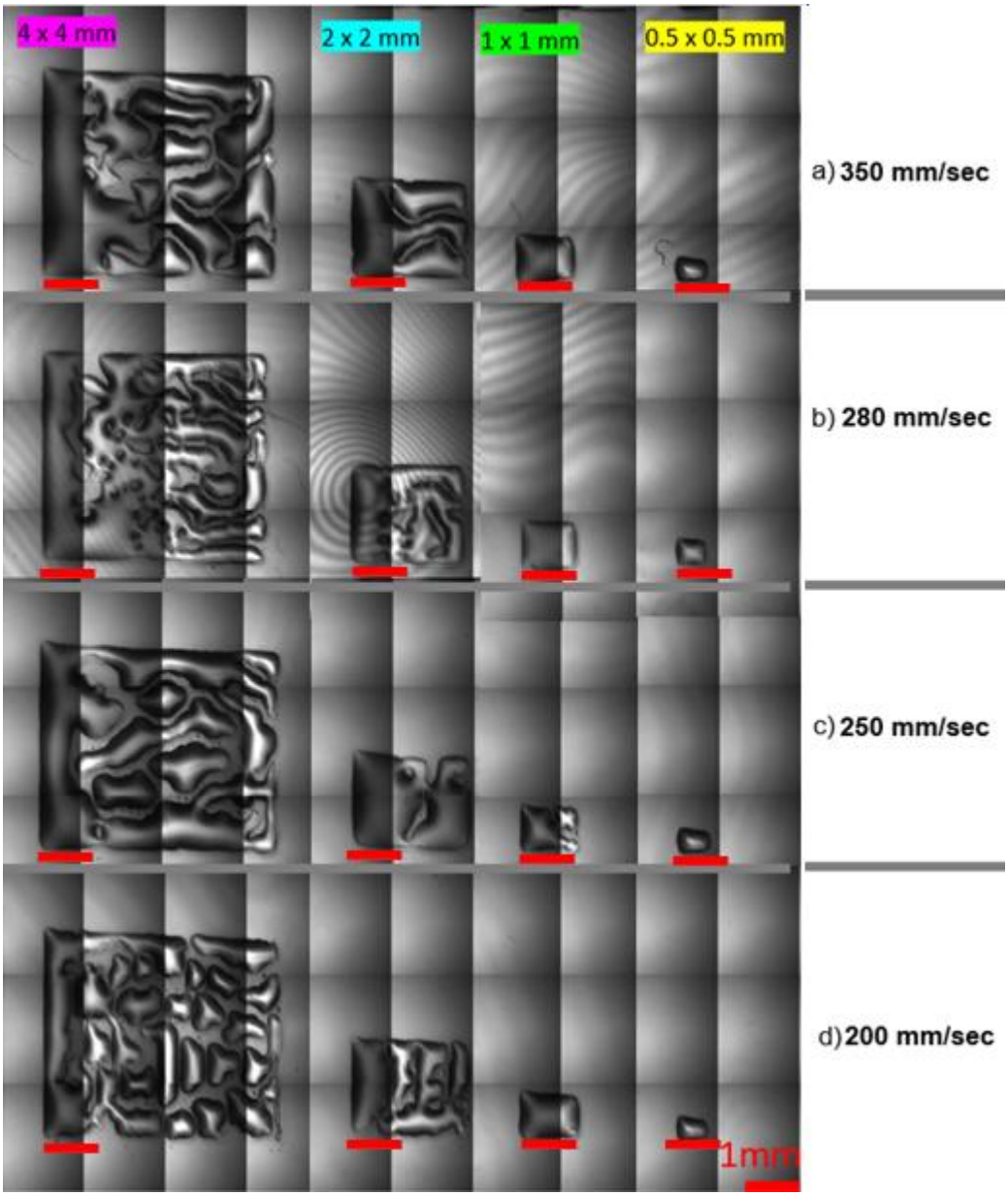

Figure 6.6. *Printer camera images of single square blocks of SI with pattern 0b from larger to smaller sizes (of 4x4 mm, 2x2 mm, 1x1 mm, and 0.5x0.5 mm) on glass cleaned with acetone at different printing speeds: a) 350 mm/sec, b) 280 mm/sec, c) 250 mm/sec, and d) 200 mm/sec. The sample differences were linked to the differences of four printing speeds, which correlated to the Table 6.2.*

Figure 6.7 shows initial results of co-printed samples on glass at the smallest size (with square block unit of 0.5 x 0.5 mm). The results show varied overlapping areas for all co-

printed samples due to the abnormal shapes of SI (compared to WI). This matches the previous results of difference of printability and wettability between WI and SI.

Particularly, to develop and estimate the analysis framework, I investigated the profile of different interfaces between WI and SI with patterns 1a, 1b, 2a, 2b, 3a, 3b, 4a, 4b that were made from square block units (in different sizes 2x2, 1x1, and 0.5x0.5 mm).

Figure 6.8 and 6.9 shows WI has even film formation with well-defined borders whereas SI tends to have uneven film formation without clear borders after 3D-printing on glass. This reveals that glass (even with optimised cleaning solvent) is still not a good option for co-printing samples at larger sizes (with square block units of 2x2 mm).

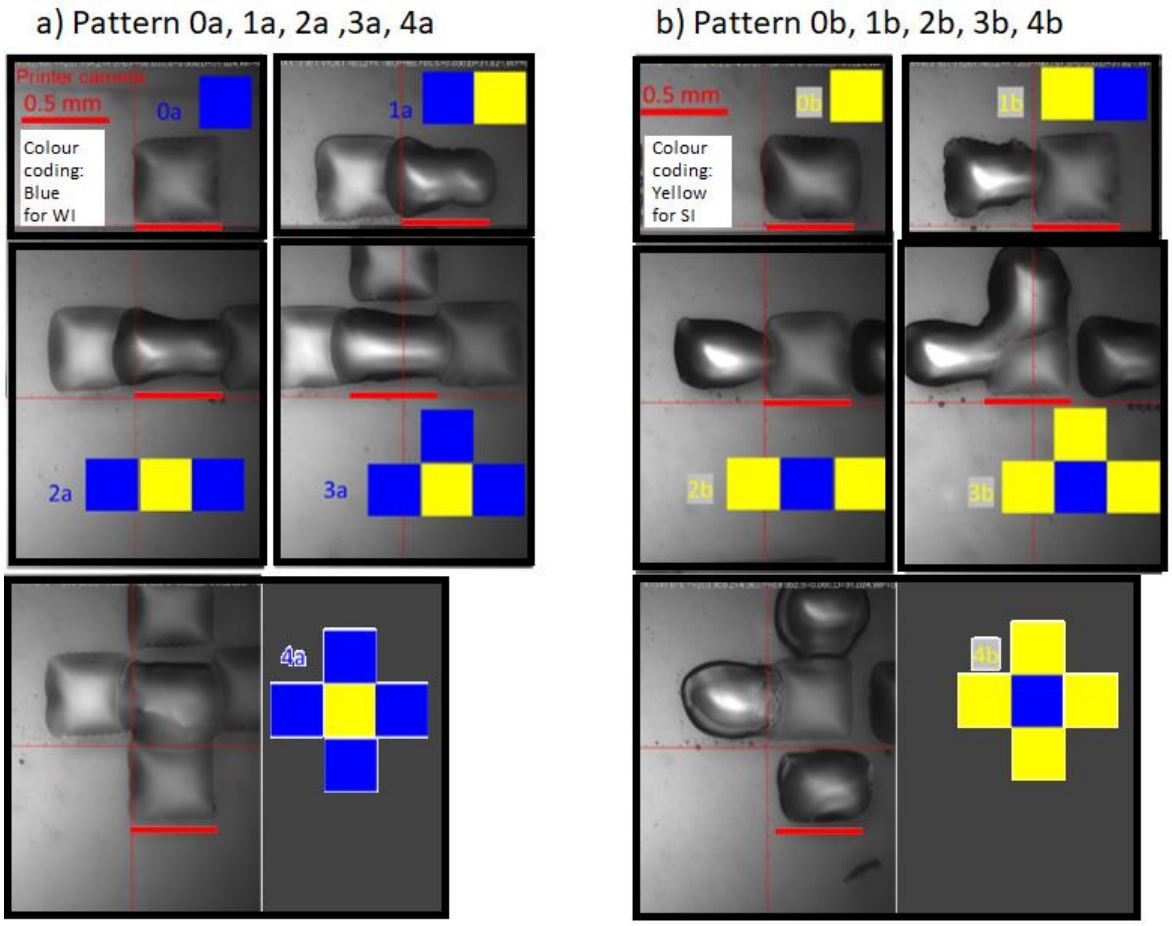

Figure 6.7. *Printer camera images of the co-printing of WI and SI (with the colour coding as blue for WI and as yellow for SI) on glass: a) pattern 0a, 1a, 2a, 3a, and 4a; and b) pattern 0b, 1b, 2b, 3b, and 4b. Single square block has the size of 0.5x0.5 mm. The sample differences were correlated to the table 6.1.*

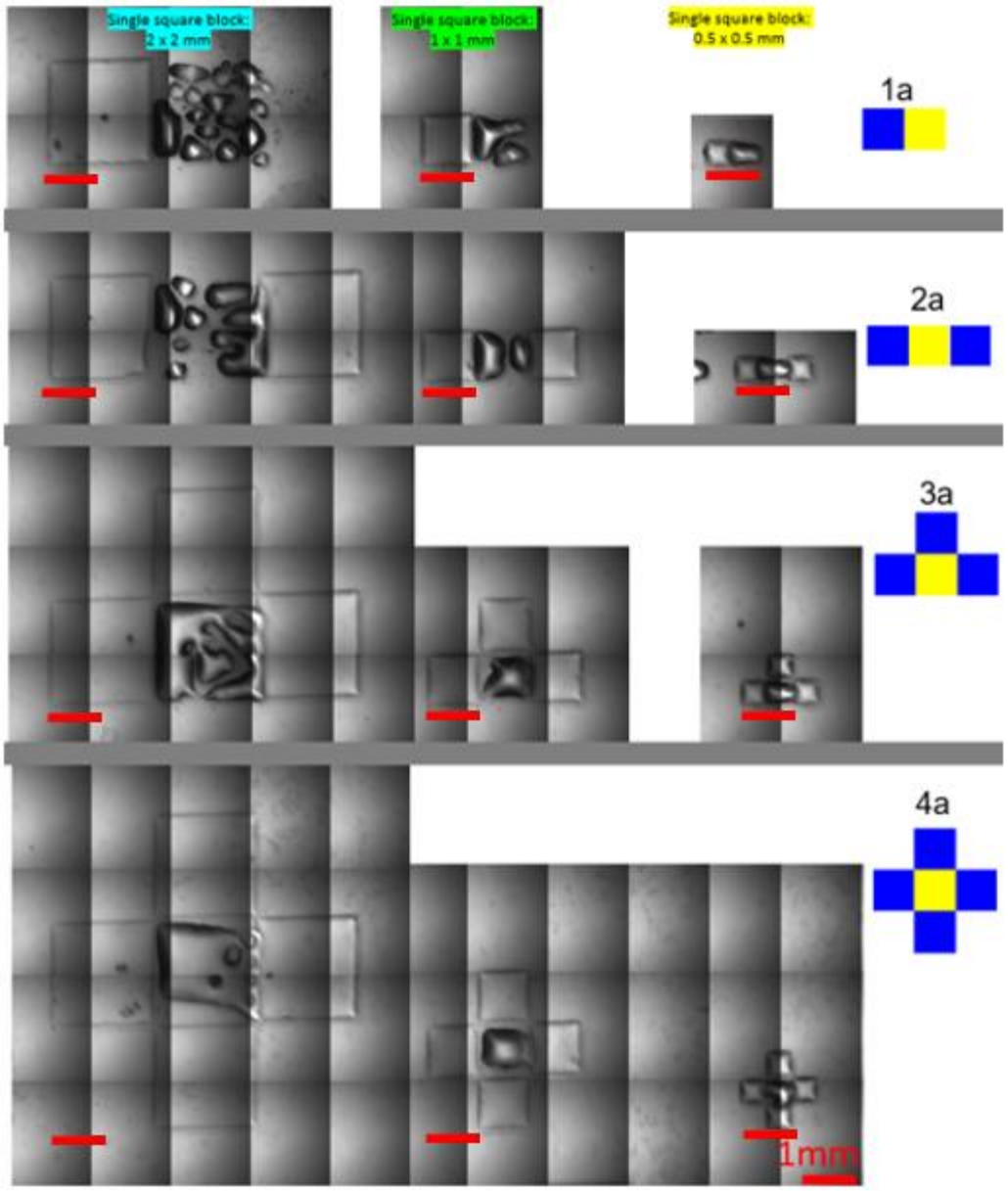

Figure 6.8. *Printer camera images of the co-printing of WI and SI SI (with the colour coding as blue for WI and as yellow for SI) on glass: a) pattern 1a, b) pattern 2a, c) pattern 3a, and d) patterns 4a. Single square block has the sizes of 2x2 mm, 1x1 mm, and 0.5x0.5 mm. The sample differences were correlated to the table 6.1.*

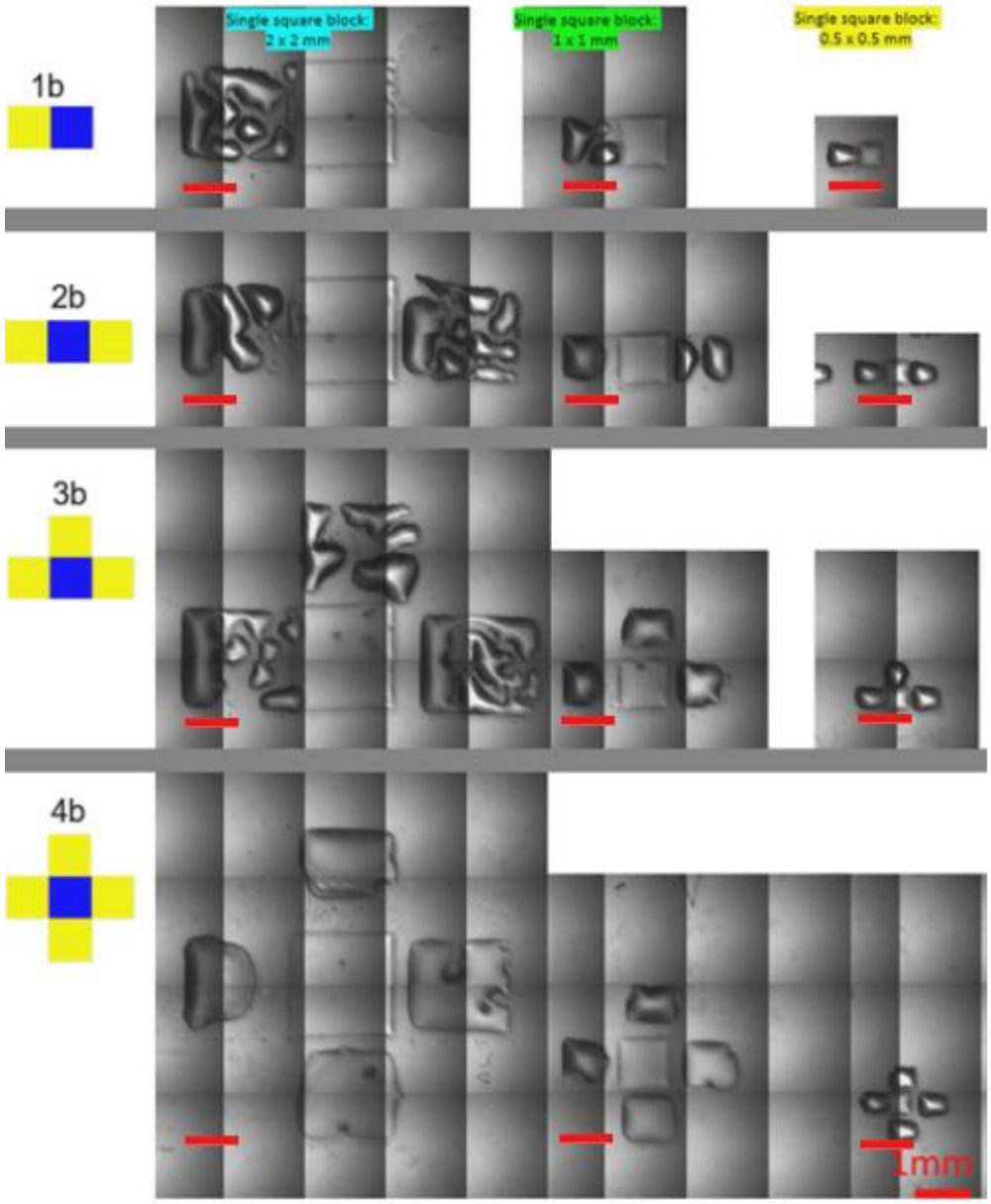

Figure 6.9. *Printer camera images of the co-printing of WI and SI (with the colour coding as blue for WI and as yellow for SI) on glass: a) pattern 1b, b) pattern 2b, c) pattern 3b, and d) patterns 4b. Single square block has the sizes of 2x2 mm, 1x1 mm, and 0.5x0.5 mm. The sample differences were correlated to the table 6.1.*

b. Inkjet 3D-printing on PEN

Figure 6.10 shows new prints with square block unit at larger size (2x2 mm) at different printing speeds on PEN. More spreading at the borderline of WI sample is clearly found at the larger size (2x2mm) after printing with lower speeds of 200 and 250 mm/sec (as blue circles in Figure 6.10a-b). This is improved when printing at higher speeds of 280 mm/sec or 350 mm/sec (as red circles in Figure 6.10c-d). Ink-jet 3D printing technology has evolved to provide a range of options in terms of resolution and precision. The results match the theory that smaller sizes and higher resolutions (with higher printing speeds in this case) allow for more consistent film formation and smoother surface in the final objects.

While speed is important, it should not compromise print quality. Advances in inkjet technology have allowed for high-speed printing without sacrificing print quality, ensuring that fast printers can produce sharp and detailed prints at larger sizes. The results also prove that testing suitable printing speeds via in-situ photography can significantly increase the efficiency of a printing operation.

After selecting optimal substrate (PEN cleaned with acetone) and printing speed (280 mm/sec), I continue investigating the impact of deposition and light-curing strategies on final prints. I will highlight the results of co-printing samples with pattern 1a at large size of 4x8mm to examine the chemical changes at the interfaces.

Table A2.2 – A2.12 in Appendix A2 shows all co-printed samples with pattern 1a from small to large sizes (of 0.5x1, 1x2, 2x4, and 4x8 mm).

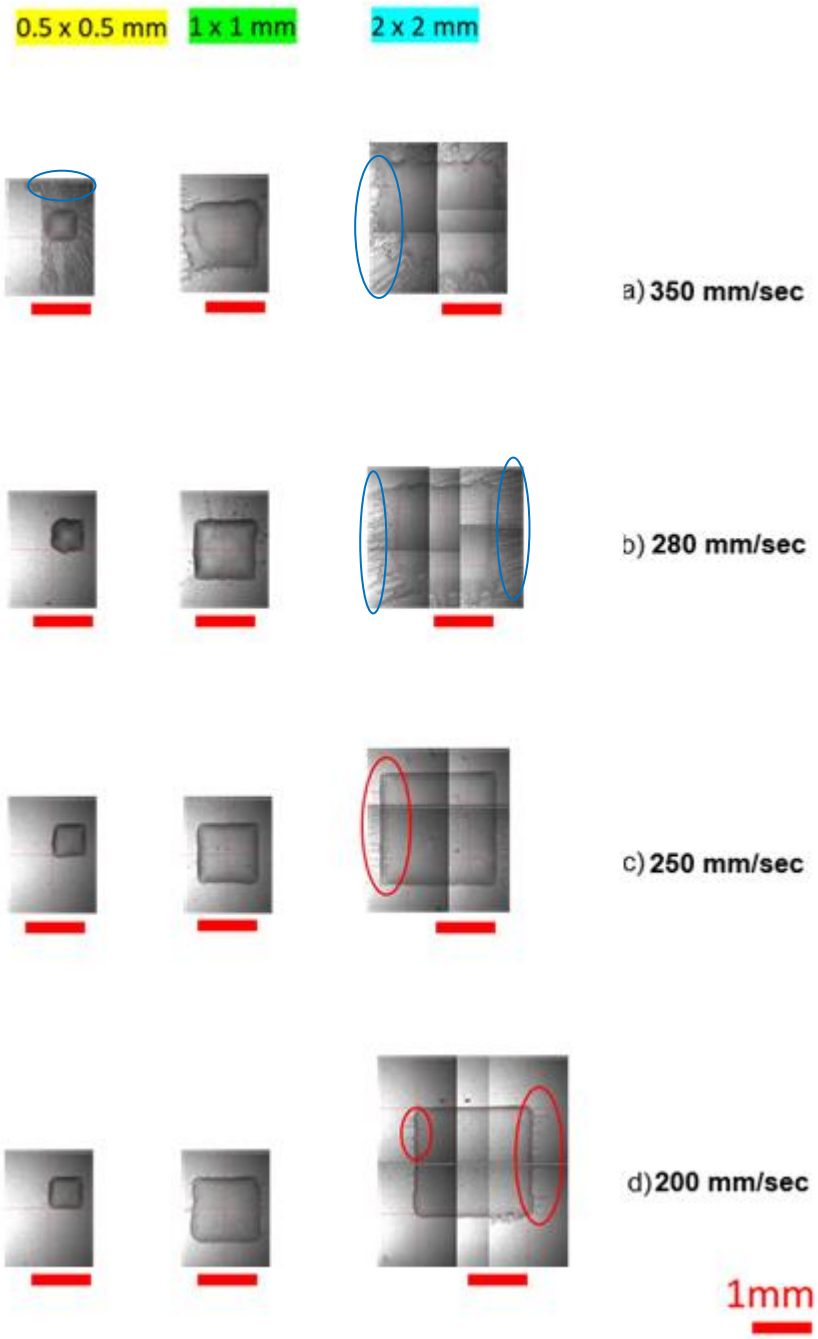

Figure 6.10. *Printer camera images of single square blocks of WI with pattern 0a from smaller to larger sizes (of 0.5x0.5 mm, 1x1mm, and 2x2 mm) on PEN cleaned with acetone at different printing speeds: a) 200 mm/sec, b) 250 mm/sec, c) 280 mm/sec, and d) 350 mm/sec. The borderline of printed samples improved from blue circles to red circles when increasing the printing speeds from 200 mm/sec to 350 mm/sec.*

6.3.2. Optimisation of light-curing strategy

a. Co-printing single-layered multi-materials

Table 6.4 shows co-printing of WI and SI with pattern 1a & 1b at chosen printing speed for investigation by ToF-SIMS & OrbiSIMS analyses. The printed samples were at large size of 4x8mm, which had differences due to the testing variables from the combination of two printing strategies (i.e. (S0 to S1) or (S1 to S0)) and two UV-curing strategies (i.e. (UV 3 sec for each deposition) or (UV 3 sec at final deposition)) in Table 6.3. Hence, the pattern 1a was printed with single layer as samples 17, 18, 21, 22. More layers require more time to print, so single layers were printed and tested to evaluate the duration of the UV-exposure of the interfaces these functional multi-materials. Only one nozzle was used for each printhead to ensure there was no nozzle' issues happening during the experiments.

ToF-SIMS analyses were carried out at large area (1x2 mm) as red rectangles and small area (500x500 µm) as brown squares in Table 6.4, which will be then discussed to investigate the chemical changes of the interfaces of the co-printed samples in Figure 6.11 and 6.12

From the result of method development and validation of ToF-SIMS & OrbiSIMS measurement (from Chapter 5), the signal of $C_8H_5NO_2^+$ [*m/z* 147.03] (in navy blue) represents WI and $C_7H_7^+$ [*m/z* 91.04] (in yellow green) represents SI. Co-printing WI & SI with pattern 1a with single layer towards x-y direction (with samples 17, 18, 21, 22) is considered as the first set (noticed as set 1a1) for investigation.

Figure 6.11 and 6.12 shows chemical changes at the interfacial areas when using ToF-SIMS to examine both large and small size images (in 1x2 mm and 500x500 µm respectively). Figure A3.9 - A3.16 in Appendix A3 shows data acquisition and interpretation of ToF-SIMS analyses for set 1a1.

From ToF-SIMS images in Figure 6.11, the changes in signals of two functional groups from left to right are clearer than from top to bottom. Although a transitional area exists in all samples, only sample 17 has the most straighten edging, and the remaining samples 18, 21, and 22 have angle, titled or wavery edging respectively. Incomplete curing or improper exposure can lead to poor layer adhesion, resulting in a weaker and less reliable final product. Significant changes happen when the inks are not fully cured by the UV light. Sample 21 has printing WI (without UV curing) before printing SI (with UV curing), which

is converse in sample 22 (that printing SI curing (without UV curing) before printing WI (with UV curing)). With the clear straightened line related to the signal shift, sample 17 and 18 are proven to have a higher level of UV-curing compared to sample 21 and 22. The result reveals that proper curing can enable good adhesion between WI and SI. Particularly, higher-intensity and shorter-duration exposures can lead to finer details and smoother surfaces, while lower-intensity and longer-duration exposures may result in coarser prints with less detail.

Generally, the interface of interest is exposed by the linescan left-right, but a similar trend for the linescans from top-bottom shows the homogeneity level of distribution of each ink in the co-printed samples: the linescan images from top to bottom shows sample 17 and 18 have similar tendency of higher or equal signal of $C_8H_5NO_2^+$ [*m/z* 147.03] (in navy blue) compared to $C_7H_7^+$ [*m/z* 91.04] (in yellow green). Otherwise, sample 21 and 22 have similar tendency of higher signal of $C_7H_7^+$ [*m/z* 91.04] (in yellow green) compared to $C_8H_5NO_2^+$ [*m/z* 147.03] (in navy blue). The reason for this tendency is due to the similar cumulative UV-exposure time as UV-6 sec for final sample 17 and 18 compared to cumulative UV-exposure time as UV-3 sec for sample 21 and 22. It received a shorter time of cumulative UV-exposure (UV 3 sec) which led to the partial curing of the materials. Hence, UV-exposure time should be considered and optimised to ensure the best possible prints.

Moreover, data in Figure 6.12 revealed the signal information at small size images (500x500 µm). With the linescan from left to right we could recognize each ink was fully cured after receiving longer time of cumulative UV-exposure (UV 3 sec & UV 3 sec) in sample 17 & 18 compared to sample 21 & 22. We could see the straighten line related to the sudden singal shift of $C_8H_5NO_2$+ [*m/z* 147.03] (in navy blue) in sample 17 and C_7H_7+ [*m/z* 91.04] (in yellow green) in sample 18. The reason why it happened was due to the better UV-curing of the WI in sample 18 compared to sample 22. The results confirm that the printed layers did not bond effectively due to insufficient time of UV-exposure, which lead to defects and poor print quality.

Table 6.4. Co-printing of WI and SI using pattern 1a (with colour coding of WI is blue and SI is yellow) at the size of 0.5x1 mm with single layer via four different deposition-curing strategies (as (i), (ii), (iii), (iv) in Table 6.3): samples 17, 18, 21, 22. Red rectangles and brown squares represented for the ToF-SIMS measurements at the large area (1x2 mm) and small area (500x500 µm) respectively.

17. 1a_4x8_1lay (S0_UV 3sec to S1_UV 3sec)

18. 1a_4x8_1lay (S1_UV 3sec to S0_UV 3sec)

21. 1a_4x8_1lay (S0_UV 0sec to S1_UV 3sec)

22. 1a_4x8_1lay (S1_UV 0sec to S0_UV 3sec)

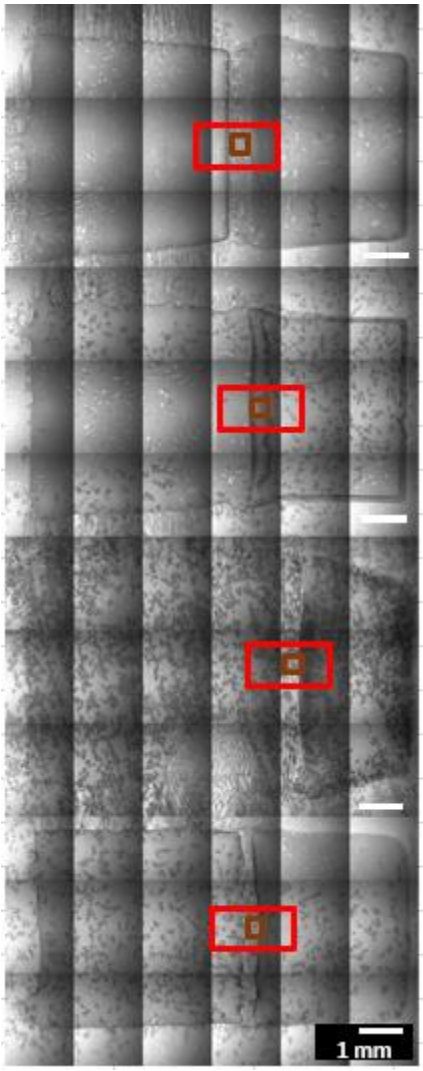

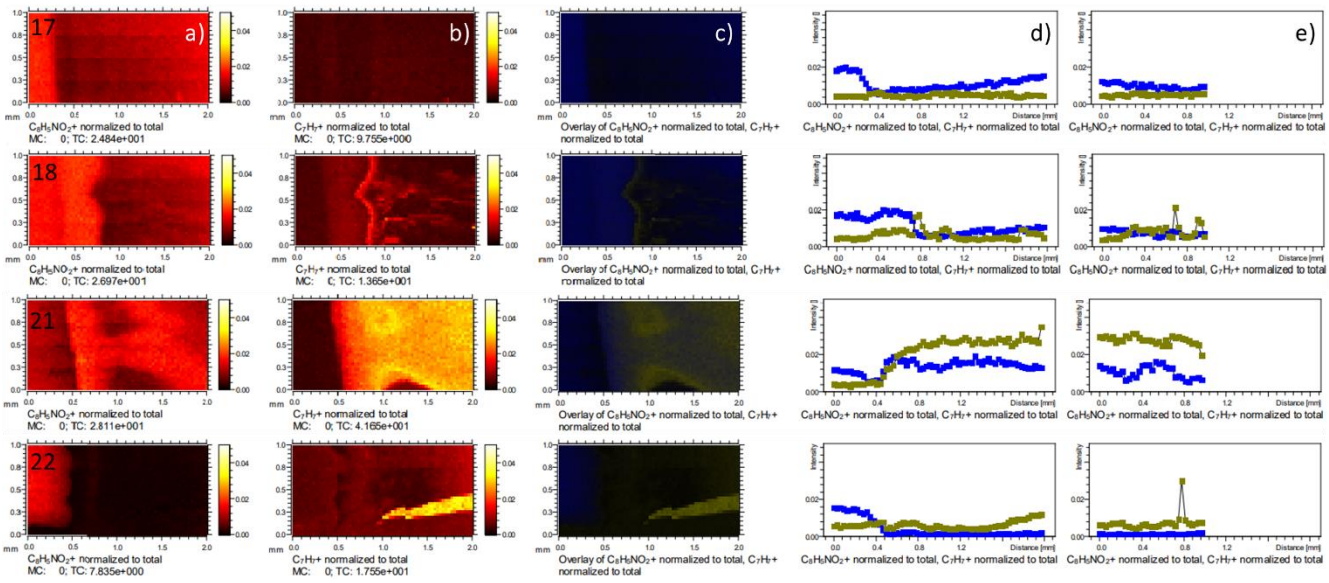

Figure 6.11. *ToF-SIMS results with large area (1x2 mm) of samples 17, 18, 21, 22 (which were correlated to red rectangles in Table 6.4): a) Normalised $C_8H_5NO_2^+$ [m/z 147.03], b) Normalised $C_7H_7^+$ [m/z 91.04], c) Overlay of both normalised signals, d) Linescan left-right (L-R) at centre position, and e) Linescan top-bottom (T-B) at middle position. The sample difference linked to the difference of testing variables (i), (ii), (iii), (iv) in Table 6.3.*

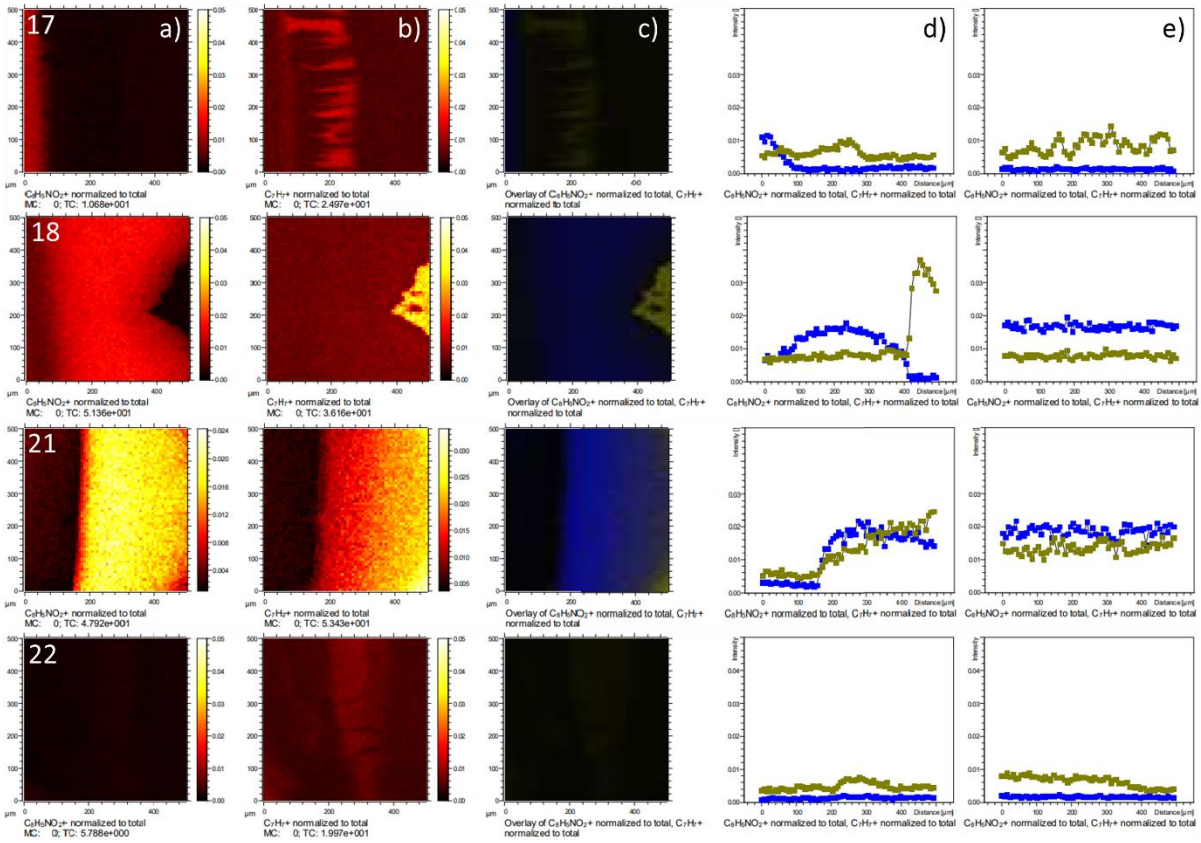

Figure 6.12. *ToF-SIMS results with small area (500x500 µm) of samples 17, 18, 21, 22 (which were correlated to brown squares in Table 6.4): a) Normalised $C_8H_5NO_2^+$ [m/z 147.03], b) Normalised $C_7H_7^+$ [m/z 91.04], c) Overlay of both normalised signals, d) Linescan left-right (L-R) at centre position, and e) Linescan top-bottom (T-B) at middle position. The sample difference linked to the difference of testing variables (i), (ii), (iii), (iv) in Table 6.3.*

b. Co-printing multi-layered multi-materials

Comparing to Table 6.4 which included 1-layer printed samples, the Table 6.5 represented all 2-layers printed samples. Table 6.5 shows the samples were 3D-printed using pattern 1a at large size of 4x8mm as samples 29, 33, 35, 34. The printed samples were different due to the testing variables from the combination of two printing strategies (i.e. (S0 to S1) or (S1 to S0)) and two UV-curing strategies (i.e. (UV 3 sec for each deposition) or (UV 3 sec at final deposition)), which has strong correlation with Table 6.3. ToF-SIMS analyses were then carried out at large area (1x2 mm) as red rectangle and small area (500x500 µm) as red

square in Table 6.5, which will be then discussed to investigate the chemical changes of the interfaces of the co-printed samples in Figure 6.13 and 6.14.

ToF-SIMS analyses were carried out to monitor the chemical changes of interfaces of co-printed samples in set 1a2 at large size image (1x2 mm) and small size image (500x500 µm) (in Figure 6.13 & 6.14). Figure A3.17 - A3.24 in Appendix A3 shows data acquisition and interpretation of ToF-SIMS analyses for set 1a2.

All samples had a higher level of signals of $C_8H_5NO_2^+$ [*m/z* 147.03] (in navy blue) compared to $C_7H_7^+$ [*m/z* 91.04] (in yellow green). The choice of layer numbers can influence production efficiency and throughput. A smoother and more polished surface can be achieved with more layers, whereas fewer layers might result in a rougher texture. However, UV-light needs to penetrate towards the material layers adequately to reduce uncured parts. The results reveal that WI receives better UV-curing compared to SI.

With the linescan from left to right, there are clearer signal changes particularly in the smaller size image. In larger size image (1x2 mm) in Figure 6.13, sample 29 has one signal shift: the line of $C_8H_5NO_2^+$ [*m/z* 147.03] (in navy blue) was fluctuated little to form the straight line; and the line of $C_7H_7^+$ [*m/z* 91.04] (in yellow green) was fluctuated little to form the straight line. Figure 6.13 shows results at smaller size (500x500 µm): sample 29 and 34 have signals of $C_8H_5NO_2^+$ [*m/z* 147.03] (in navy blue) increased gradually at the leap, whereas sample 33 and 35 have the signals of $C_8H_5NO_2^+$ [*m/z* 147.03] (in navy blue) decreased little at the leap. It confirms the timing and method of curing affecting the bond between ink layers and the final material properties. More layers can provide additional reinforcement and improve the object's overall strength, which is important for functional parts.

These results confirm the effect of the duration of the UV-exposure on the print resolution, which is correlated with the previous results, particularly from ToF-SIMS analyses at large areas (in section 6.3.2a). In other words, optimising the light-curing strategy is crucial for achieving the desired quality and properties in 3D printed objects, especially for those with complex geometries and overhanging structures.

Table 6.5. Co-printing of WI and SI using pattern 1a (with colour coding of WI is blue and SI is yellow) at the size of 0.5x1 mm with two layers via four different deposition-curing strategies (as (i), (ii), (iii), (iv) in Table 6.3): i) samples 29, 33, 35, 34. Red rectangles and brown squares represented for the ToF-SIMS measurements at the large area (1x2 mm) and small area (500x500 µm) respectively.

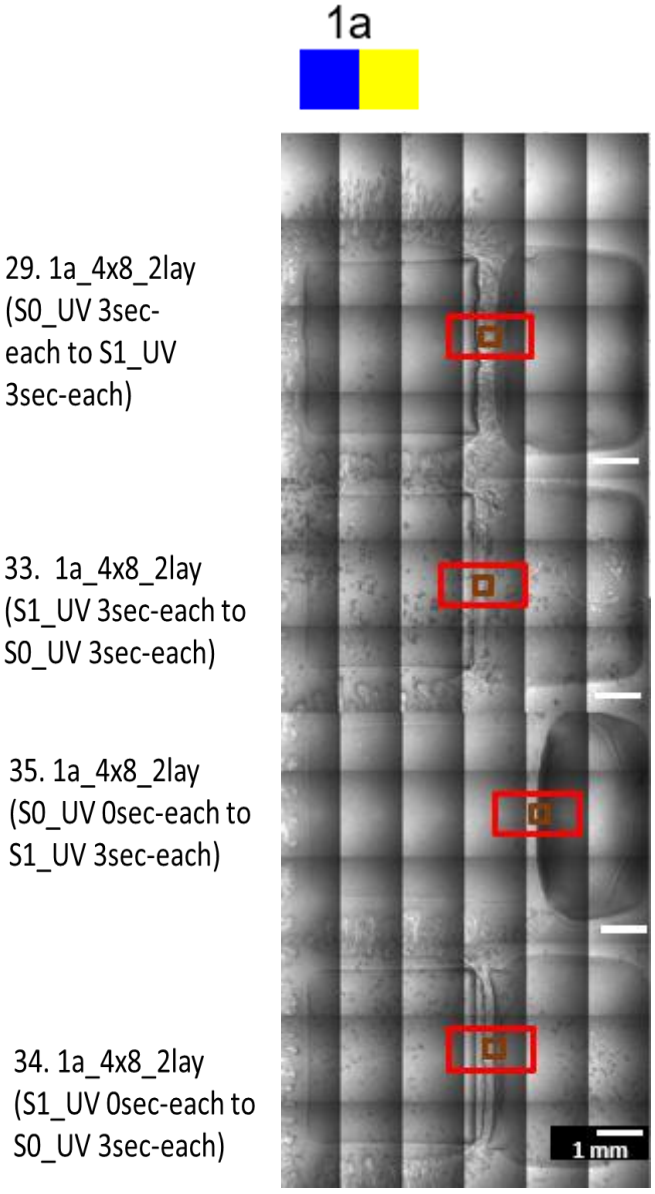

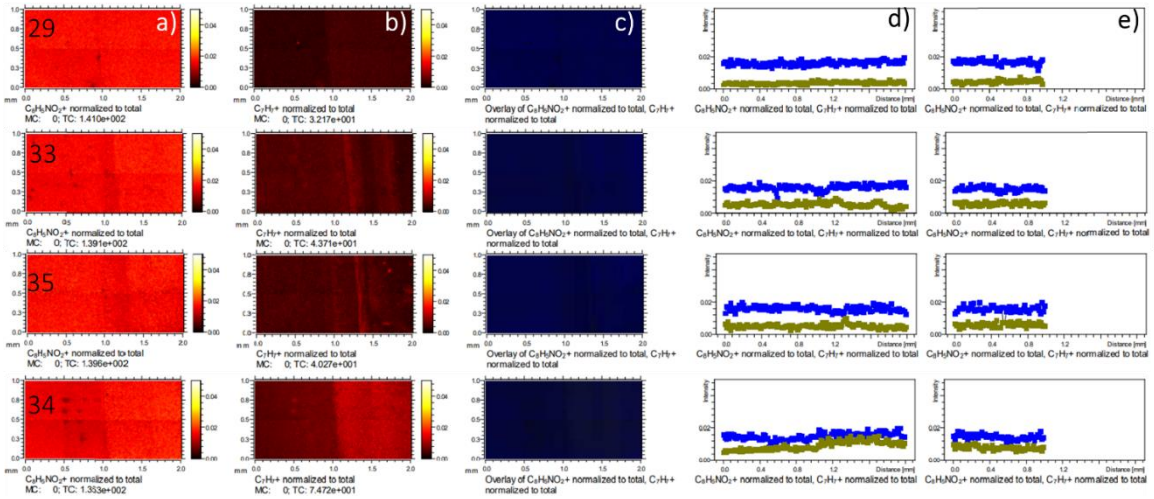

Figure 6.13. *ToF-SIMS results with large area (1x2 mm) of samples 29, 33, 35, 34 (which were correlated to red rectangles in Table 6.5): a) Normalised $C_8H_5NO_2^+$ [m/z 147.03], b) Normalised $C_7H_7^+$ [m/z 91.04], c) Overlay of both normalised signals, d) Linescan left-right (L-R) at centre position, and e) Linescan top-bottom (T-B) at middle position. The sample difference linked to the difference of testing variables (i), (ii), (iii), (iv) in Table 6.3.*

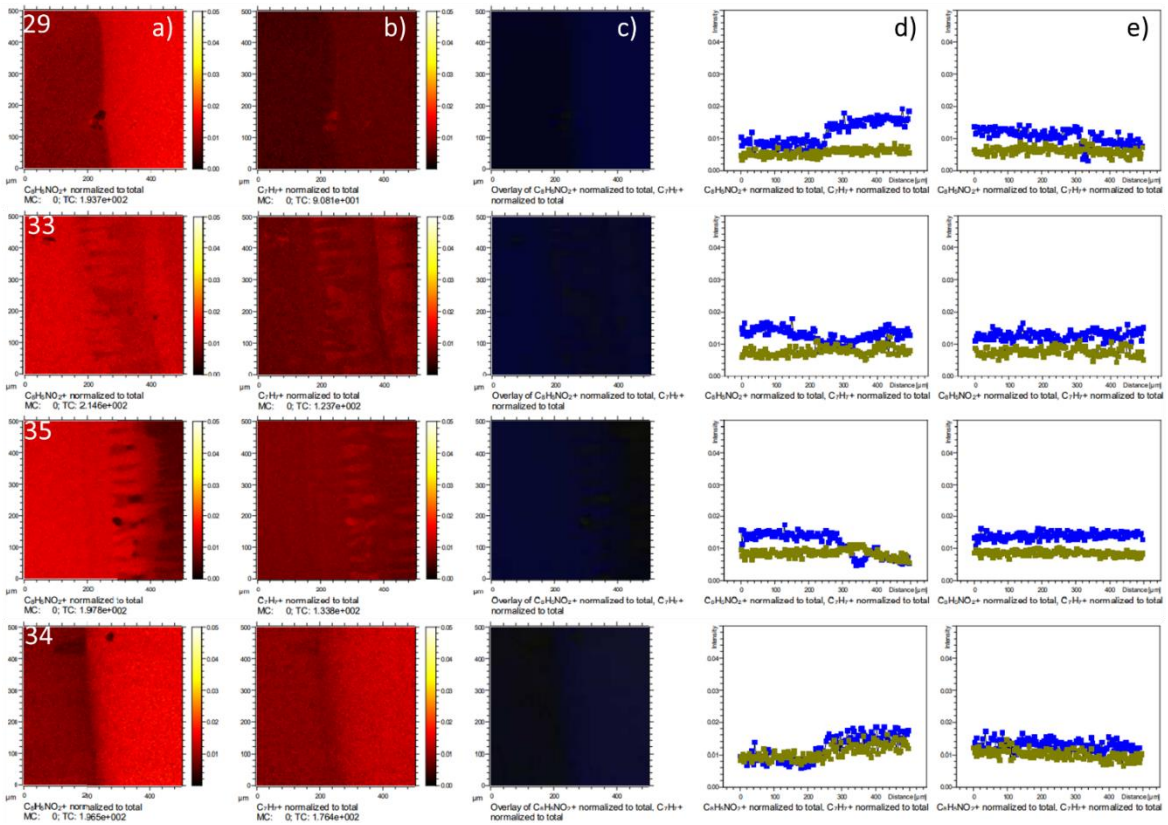

Figure 6.14. *ToF-SIMS results with small area (500x500 µm) of samples 29, 33, 35, 34 (which were correlated to brown rectangles in Table 6.5): a) Normalised $C_8H_5NO_2^+$ [m/z 147.03], b) Normalised $C_7H_7^+$ [m/z 91.04], c) Overlay of both normalised signals, d) Linescan left-right (L-R) at centre position, and e) Linescan top-bottom (T-B) at middle position. The sample difference linked to the difference of testing variables (i), (ii), (iii), (iv) in Table 6.3.*

6.3.3. Optimisation of deposition strategy

I tested two other set of samples to understand x-z interface of co-printed multi-materials:

1) Set 2a are pattern a-b-a with single layer on top of each other towards x-z direction (with samples 47-50), which was summarised in Table 6.6.

2) Set 2b are pattern b-a-b with single layer on top of each other towards x-z direction (with samples 43-46), which was summarised in Table 6.7.

The sample difference linked to patterns to study x-z interface in Table 6.1, and the samples' differences were correlated to four different deposition-curing strategies (as (i), (ii), (iii), (iv) in Table 6.3. Particularly, the printed samples were different due to the testing variables from the combination of two printing strategies (i.e. (S0 to S1) or (S1 to S0)) and two UV-curing strategies (i.e. (UV 3 sec for each deposition) or (UV 3 sec at final deposition)) in Table 6.3. ToF-SIMS analyses were then carried out at large area (3.5x3.5 mm) as red squares and small area (500x500 µm) as brown squares in Table 6.6, which will be then discussed to investigate the chemical changes of the interfaces of the co-printed samples in Figure 6.15 and 6.16.

Figure 6.15 and 6.16 shows ToF-SIMS results at large and small sizes (3.5x3.5 mm and 500x500 µm respectively). The signal of $C_8H_5NO_2^+$ [*m/z* 147.03] (in navy blue) representing WI and $C_7H_7^+$ [*m/z* 91.04] (in yellow green) representing for SI. Proper deposition is essential for achieving targeted purposes such as fine details and smooth surfaces, and the results confirm moderate adhesion among layers of WI and SI to lead to good print quality.

a. WI before SI: Deposit WI first (before SI) on the substrate

Set 2a include samples with pattern a-b-a with single layer, 1 layer on top of each other towards x-z direction (as samples 47-50). Figure A3.25 - A3.32 in Appendix A3 shows data acquisition and interpretation of ToF-SIMS analyses for set 2a.

In larger size images (3.5x3.5 mm) at Figure 6.15, the linescan from left to right, all samples have a higher level of $C_8H_5NO_2^+$ [*m/z* 147.03] (in navy blue) compared to $C_7H_7^+$ [*m/z* 91.04] (in yellow green). Sample 47 has earlier shift for signal $C_7H_7^+$ [*m/z* 91.04] (in yellow green) (towards left side) while sample 48 has later shift for signal $C_7H_7^+$ [*m/z* 91.04] (in yellow green) (towards right side). Only sample 49 reveals clear signal shifts for both $C_8H_5NO_2^+$

[*m/z* 147.03] (in navy blue) and $C_7H_7^+$ [*m/z* 91.04] (in yellow green) at the similar position of leap; and sample 50 does not have any signal shifts. For the linescan from top to bottom, there are not many differences of signals in all samples, except sample 49 still has obvious signal shifts. Inkjet 3D-printing typically involves the deposition of a liquid or semi-liquid material that solidifies to create the final object. The results reveal inaccurate or uneven ink deposition can cause rough or uneven surfaces, which require additional post-processing to achieve the desired finish.

Figure 6.16 shows signals from both inks at smaller size images (500x500 µm). Sample 47 does not show much signal in both ToF-SIMS image and linescan, which can be due to the measurement artifacts. In general, samples 48, 49, 50 have a higher level of signal $C_8H_5NO_2$+ [*m/z* 147.03] (in navy blue) compared to $C_7H_7^+$ [*m/z* 91.04] (in yellow green). Sample 48 and 49 have linescan left-right of $C_8H_5NO_2^+$ [*m/z* 147.03] (in navy blue) decreases little while linescan left-right of $C_7H_7^+$ [*m/z* 91.04] (in yellow green) increases little bit at the similar leap (in purple circle). It also has similar effect of the linescan top-bottom in sample 48, and sample 49 has overlapping signals of $C_8H_5NO_2^+$ [*m/z* 147.03] (in navy blue) and $C_7H_7^+$ [*m/z* 91.04] (in yellow green). The results reveal accurate ink deposition can be achieved to illustrate the correct dimensions of the co-printed object. Inkjet 3D printers allow for a degree of control over the layer thickness, and this can be adjusted based on the specific requirements.

Table 6.6. Co-printing of WI and SI (with colour coding WI for blue and SI for yellow) using pattern a-b-a via four different deposition-curing strategies (as (i), (ii), (iii), (iv) in Table 6.3): samples 47, 48, 49, 50. Red and brown squares represented for the ToF-SIMS measurements at the large area (3.5x3.5 mm) and small area (500x500 µm) respectively.

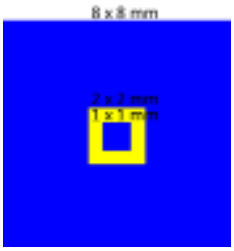

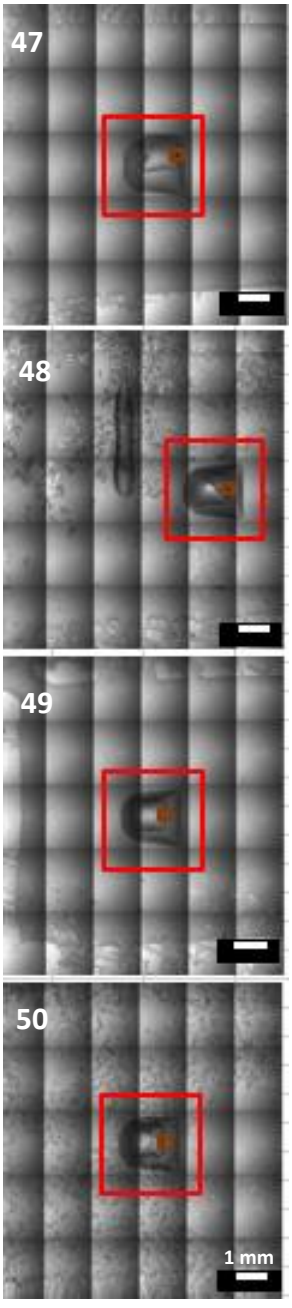

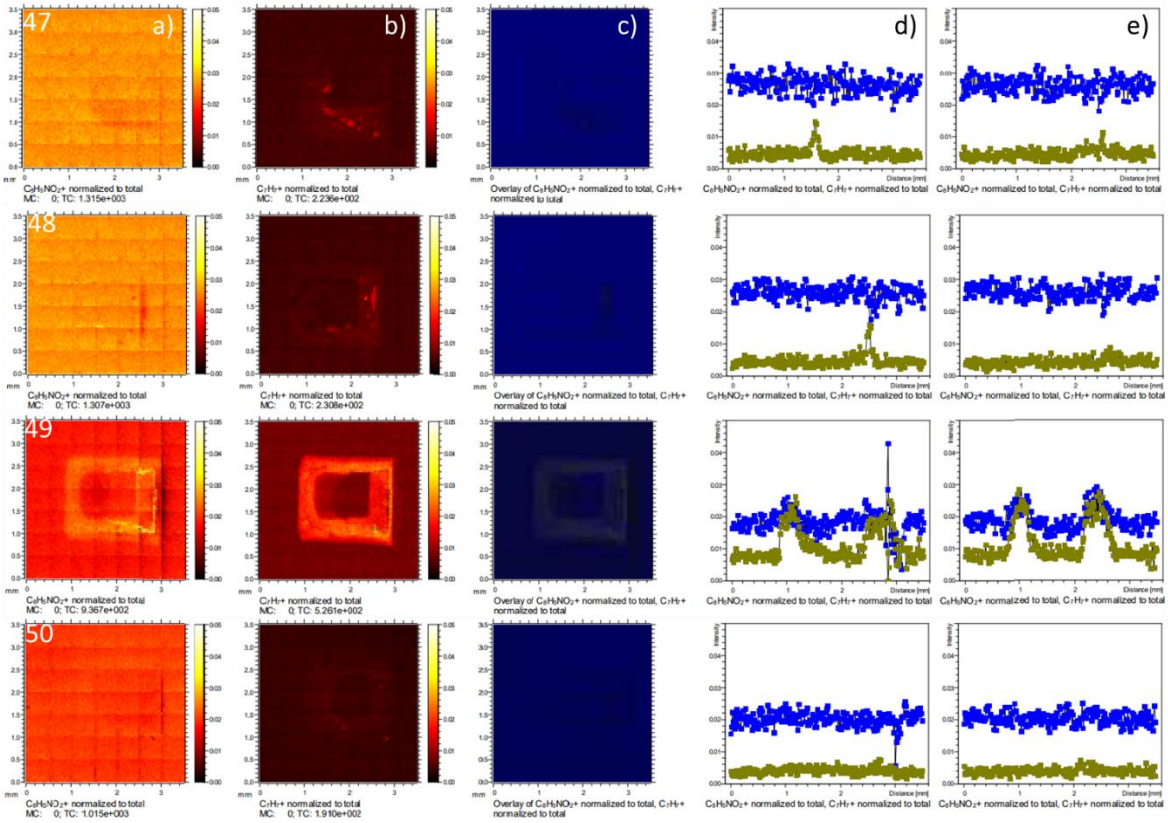

Figure 6.15. *ToF-SIMS results with large area (3.5x3.5 mm) of samples 47-50 (which were correlated to red squares in Table 6.6): a) Normalised $C_8H_5NO_2^+$ [m/z 147.03], b) Normalised $C_7H_7^+$ [m/z 91.04], c) Overlay of both normalised signals, d) Linescan left-right (L-R) at centre position, and e) Linescan top-bottom (T-B) at the middle. The sample difference linked to the difference of testing variables (i), (ii), (iii), (iv) in Table 6.3.*

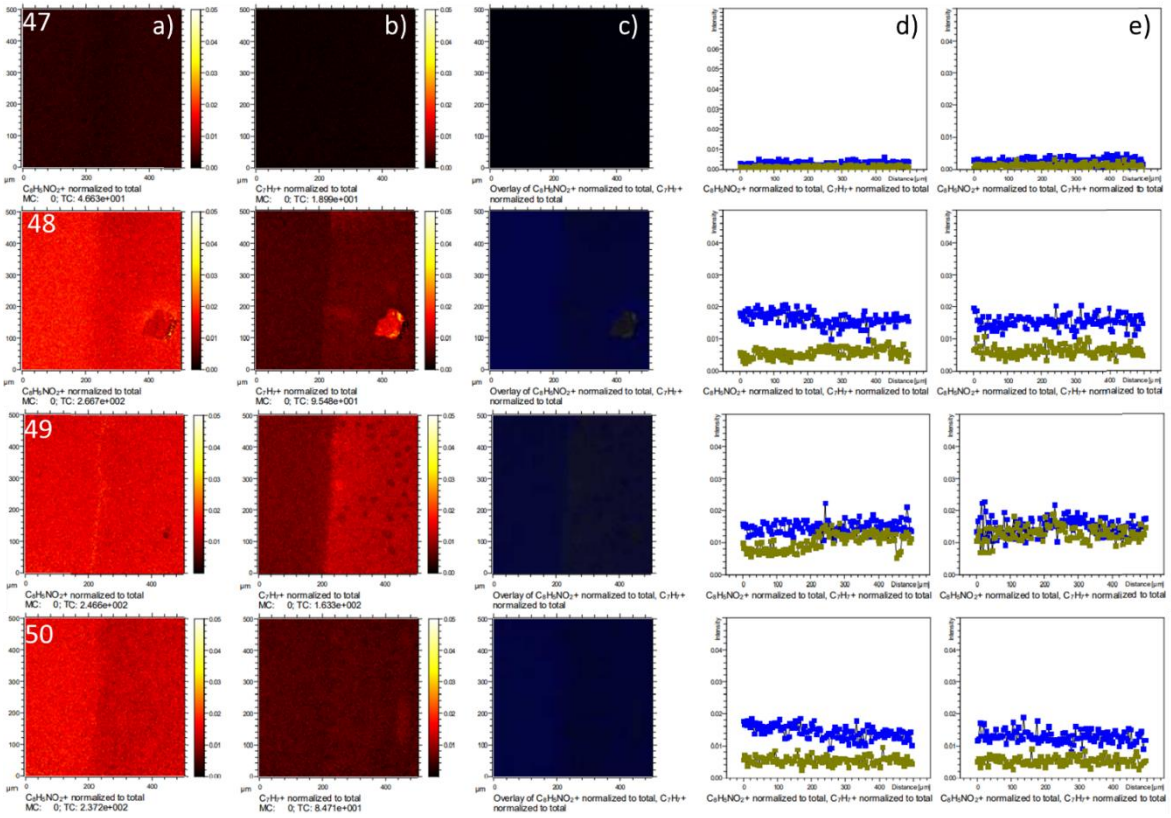

Figure 6.16. *ToF-SIMS results with small area (500x500 µm) of samples 47-50 (which were correlated to brown squares in Table 6.6): a) Normalised $C_8H_5NO_2^+$ [m/z 147.03], b) Normalised $C_7H_7^+$ [m/z 91.04], c) Overlay of both normalised signals, d) Linescan left-right (L-R) at centre position, and e) Linescan top-bottom (T-B) at middle position. The sample difference linked to the difference of testing variables (i), (ii), (iii), (iv) in Table 6.3.*

b. SI before WI: Deposit SI first (before WI) on the substrate

Table 6.7 shows samples being printed using pattern b-a-b with single layer to study x-z interfaces including samples 43-46. ToF-SIMS analyses were then carried out at large area (3.5x3.5 mm) as red squares and small area (500x500 µm) as purple squares in Table 6.7, which will be then discussed to investigate the chemical changes of the interfaces of the co-printed samples in Figure 6.17 and 6.18.

Figure A3.33 - A3.40 in Appendix A3 shows data acquisition and interpretation of ToF-SIMS analyses for set 2b.

In Figure 6.17 with larger size images (3.5x3.5 mm) for the left-right linescan, all samples have at least two signal shifts. Sample 43 has signal $C_8H_5NO_2^+$ [*m/z* 147.03] (in navy blue) increased and went to balance before decreasing again. Sample 44 has signal $C_8H_5NO_2^+$ [*m/z* 147.03] (in navy blue) increased to form steady straight line. Sample 45 and 46 has three signal shifts by two curve lines (next to each other) for signal $C_8H_5NO_2^+$ [*m/z* 147.03] (in navy blue) following increase-decrease-increase-decrease order, whereas signal $C_7H_7^+$ [*m/z* 91.04] (in yellow green) following decrease-fluctuate-decrease order. Signal $C_7H_7^+$ [*m/z* 91.04] (in yellow green) decreases, maintains straight and increases again in both sample 43 and 44. From the top-bottom linescan, sample 43 did not correctly represent the case of signal shifts, which might be due to spreading of ink outside the samples for $C_8H_5NO_2^+$ [*m/z* 147.03] (in navy blue). However, sample 45 and 46 shared a similar tendency of three signal shifts by two curve lines (next to each other) for $C_7H_7^+$ [*m/z* 91.04] (in yellow green). Achieving good adhesion between layers is essential to prevent delamination or other structural issues, for example, the number of layers and the quality of layer bonding are closely related here.

Figure 6.18 shows smaller size images (500x500 µm) for the left-right linescan, all samples have a higher level of $C_8H_5NO_2^+$ [*m/z* 147.03] (in navy blue) compared to $C_7H_7^+$ [*m/z* 91.04] (in yellow green). Sample 43 and 46 have one signal shift, but it is not too clear, and the sample 44 and 45 does not reveal any significant signal shifts. From the top-bottom linescan, all samples 43-46 are similar as no major tendency were identified. The results reveal incorrect ink deposition can lead to material incompatibilities. Inkjet 3D printing typically builds objects layer by layer, so if the ink is not deposited correctly, it can lead to poor adhesion between layers. This can cause weak and brittle parts that are prone to delamination or failure. In order words, the ink deposition significantly affects the surface finish of the printed object.

Table 6.7. Co-printing of WI and SI (with colour coding for WI as blue and SI as yellow) using pattern b-a-b via four different deposition-curing strategies (as (i), (ii), (iii), (iv) in Table 6.3): samples 43, 44, 45, 46. Red and brown squares represented for the ToF-SIMS measurements at the large area (3.5x3.5 mm) and small area (500x500 µm) respectively.

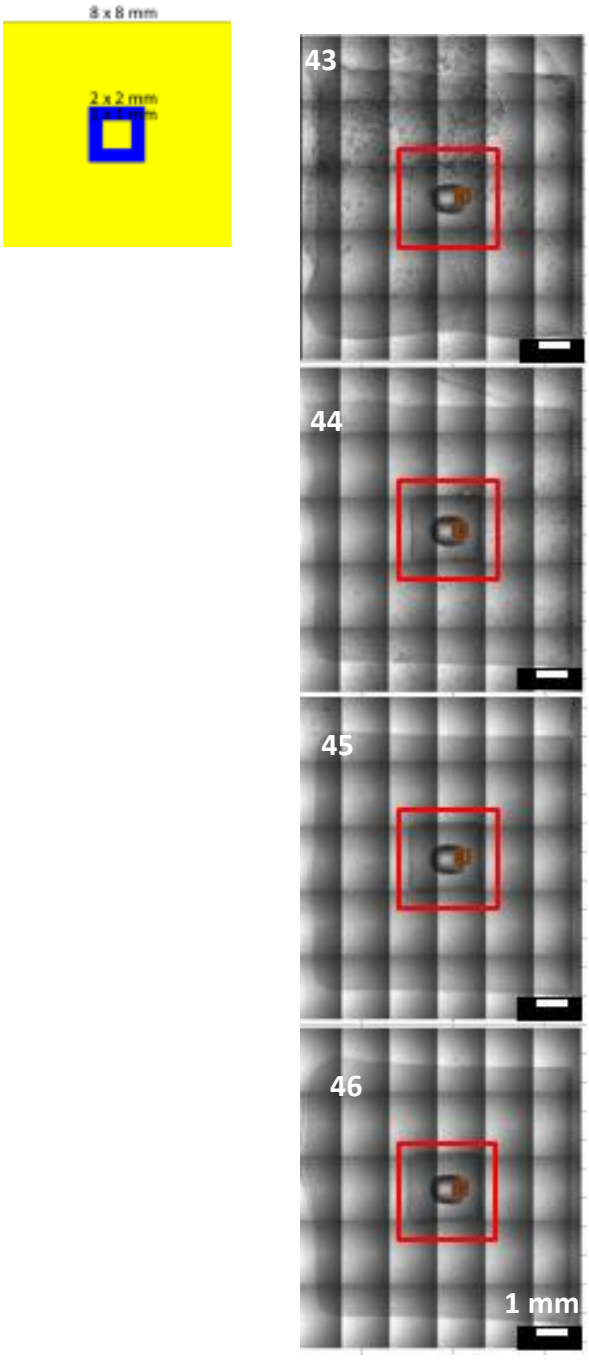

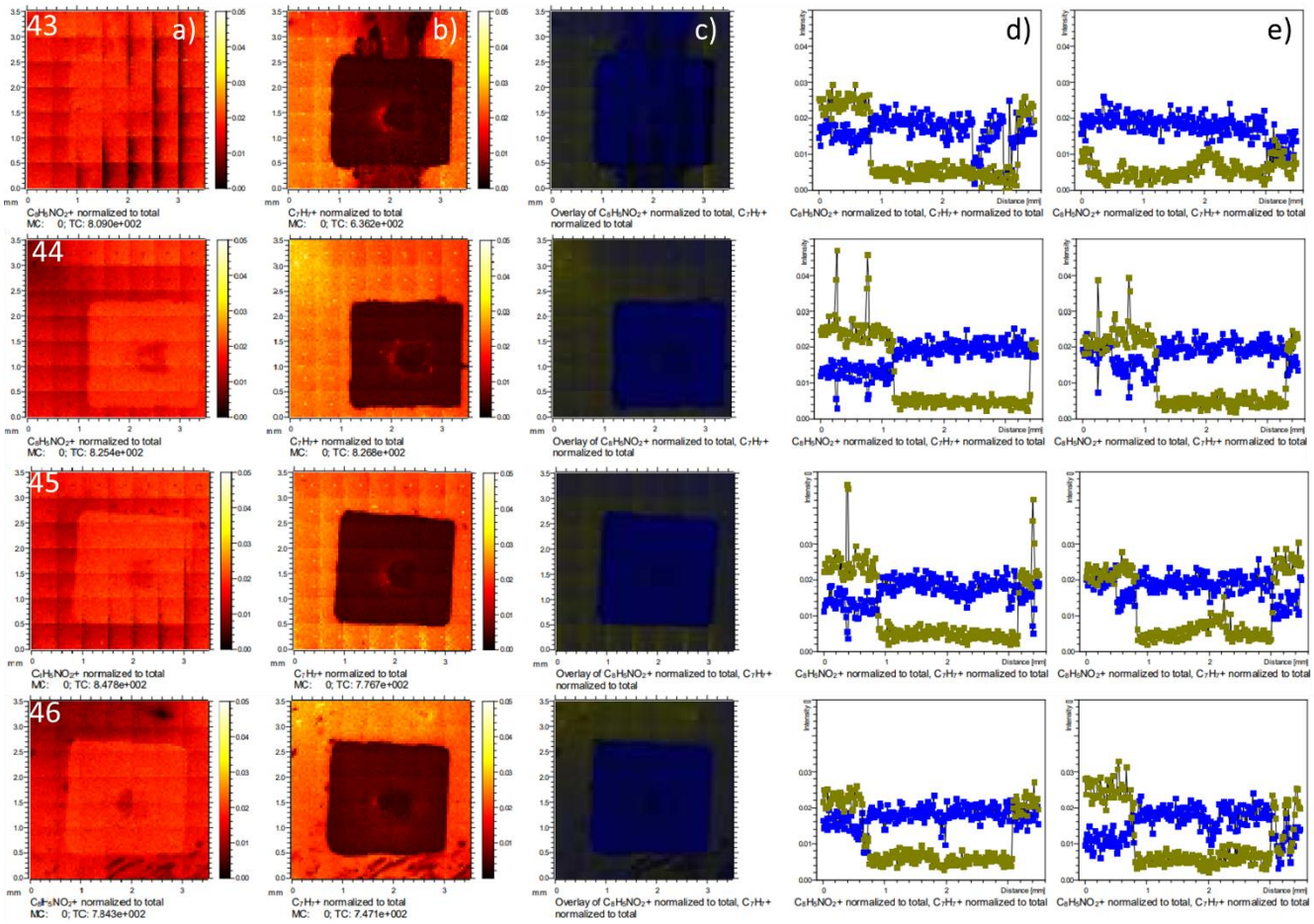

Figure 6.17. *ToF-SIMS results with large area (3.5x3.5 mm) of samples 43-46 (which were correlated to red squares in Table 6.7): a) Normalised $C_8H_5NO_2^+$ [m/z 147.03], b) Normalised $C_7H_7^+$ [m/z 91.04], c) Overlay of both normalised signals, d) Linescan left-right (L-R) at centre position, and e) Linescan top-bottom (T-B) at middle position. The sample difference linked to the difference of testing variables (i), (ii), (iii), (iv) in Table 6.3.*

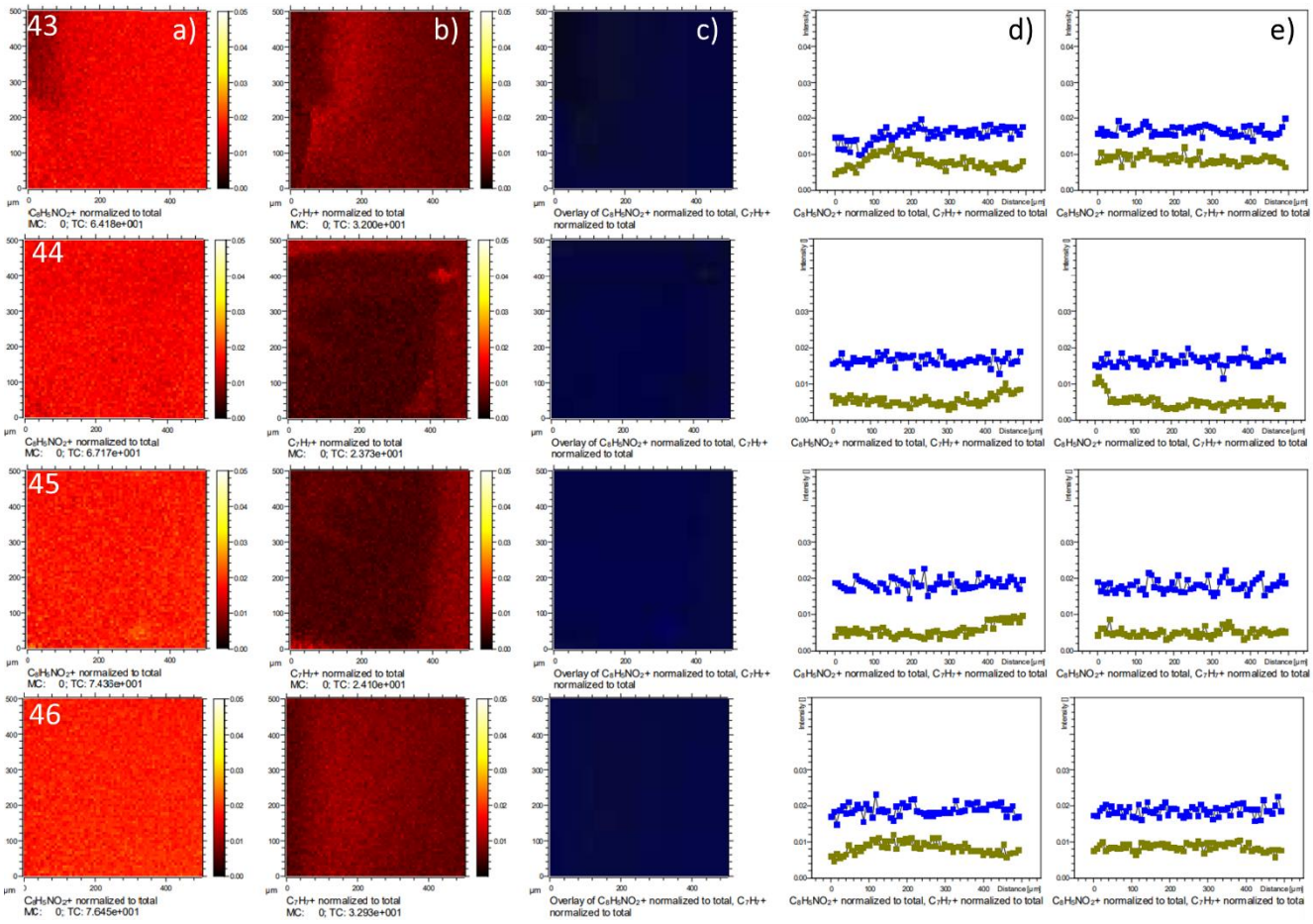

Figure 6.18. *ToF-SIMS results with small area (500x500 µm) of samples 43-46 (which were correlated to brown squares in Table 6.7): a) Normalised $C_8H_5NO_2^+$ [m/z 147.03], b) Normalised $C_7H_7^+$ [m/z 91.04], c) Overlay of both normalised signals, d) Linescan left-right (L-R) at centre position, and e) Linescan top-bottom (T-B) at middle position. The sample difference linked to the difference of testing variables (i), (ii), (iii), (iv) in Table 6.3.*

6.4. CONCLUSIONS

6.4.1. Summary

a. Key factors

Thanks to the surface-interface study, the key factors were identified and monitored to improve the efficiency of co-printing of multiple materials. For example, if the ink is deposited improperly, it can lead to material waste, increasing the cost of production.

Another example is faster curing methods may reduce the overall manufacturing time, but they may require more intense light sources consumption. The printing speed of the 3D print can also impact the amount of time for printing materials, which in turn affects the cost of the print.

The results help to strengthen the hypothesis that the micro/nano-scale interfaces can be optimised thanks to key factors such as: 1) Ink compatibility: In multi-material 3D-printing, the compatibility of different inks is essential to ensure that they can be deposited in layers without reacting adversely with each other or causing unwanted mixing; 2) Printing with suitable printing speed and deposition strategy: When printing in multiple layers, the ink-ink interaction is vital for the strength and integrity of the final part. Proper adhesion between successive layers from appropriate deposition strategy is essential to prevent delamination and ensure structural integrity; and 3) Curing: Different materials require specific light-curing strategies, for example, some may be sensitive to certain wavelengths of light, while others may require specific energy levels for proper curing.

b. Reliable workflow

Figure 6.22 summarises useful procedures for interface/interphase study of functional 3D-printed multi-materials in the biopharmaceutical field, including five main steps: 1) Check relevant background from existing data about materials, methods, etc; 2) Test ink formulations from selected compounds and substrates for potential wettability, printability, elemental contents); 3) Create appropriate design patterns to match targeted purposes with Bitmap or CAD files; 4) Evaluate the set-up features of the system and 3D-print the samples with desirable physiochemical properties; and 5) Optimise the process parameters to enhance the robust printing process with reliable analytical techniques. My study results also emphasize the fundamental point of confirming the physio-chemical compatibility at micro-nano scale before printing final product or scaling up the whole batch as this will save significant time and cost from only choosing the most compatible ink-substrate and ink-ink to move forward in order to achieve reliable manufacturing.

Inkjet 3D printing relies on the precise deposition of materials onto a substrate to create three-dimensional objects. Substrate treatment plays a critical role in ensuring that this

deposition process occurs correctly, leading to high-quality, functional, and consistent 3D printed parts. Monitoring micro-behaviour at the interfaces is necessary to achieve the desired results in inkjet 3D printing before moving to make larger scale of prints. To offer quick turnaround times and reduce costs, the active workflow is introduced for illustrating key factors for consideration in the successful ink-jetting of biopharmaceutical multi-functional multi-materials (Figure 6.23). This study confirms the optimal 3D-printed samples having a good film formation (without any cracks or pores) and good geometry definition (with a clear border and close to original designs) can be achieved by using double printhead LP50 inkjet printer at 280 mm/sec for co-printing of WI and SI directly on PEN substrate. In other words, the optimization of printing speeds, ink deposition and curing strategies can enable good quality of co-printed (bio-)pharmaceutical products.

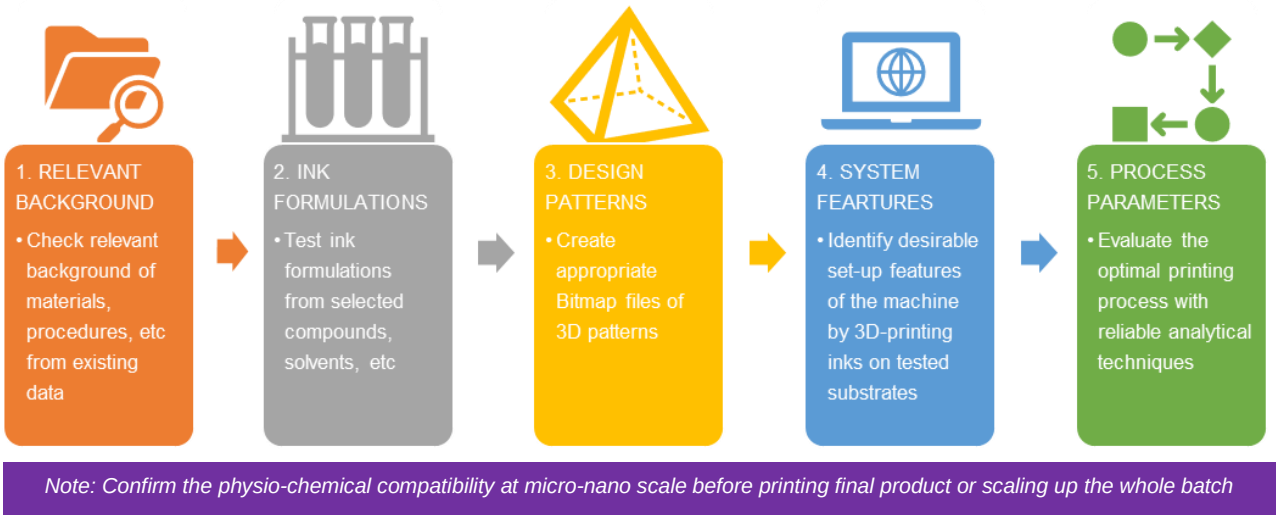

Figure 6.19. *Procedure for surface-interface study of the 3D-printed multi-functional multi-materials in biopharmaceutical fields*

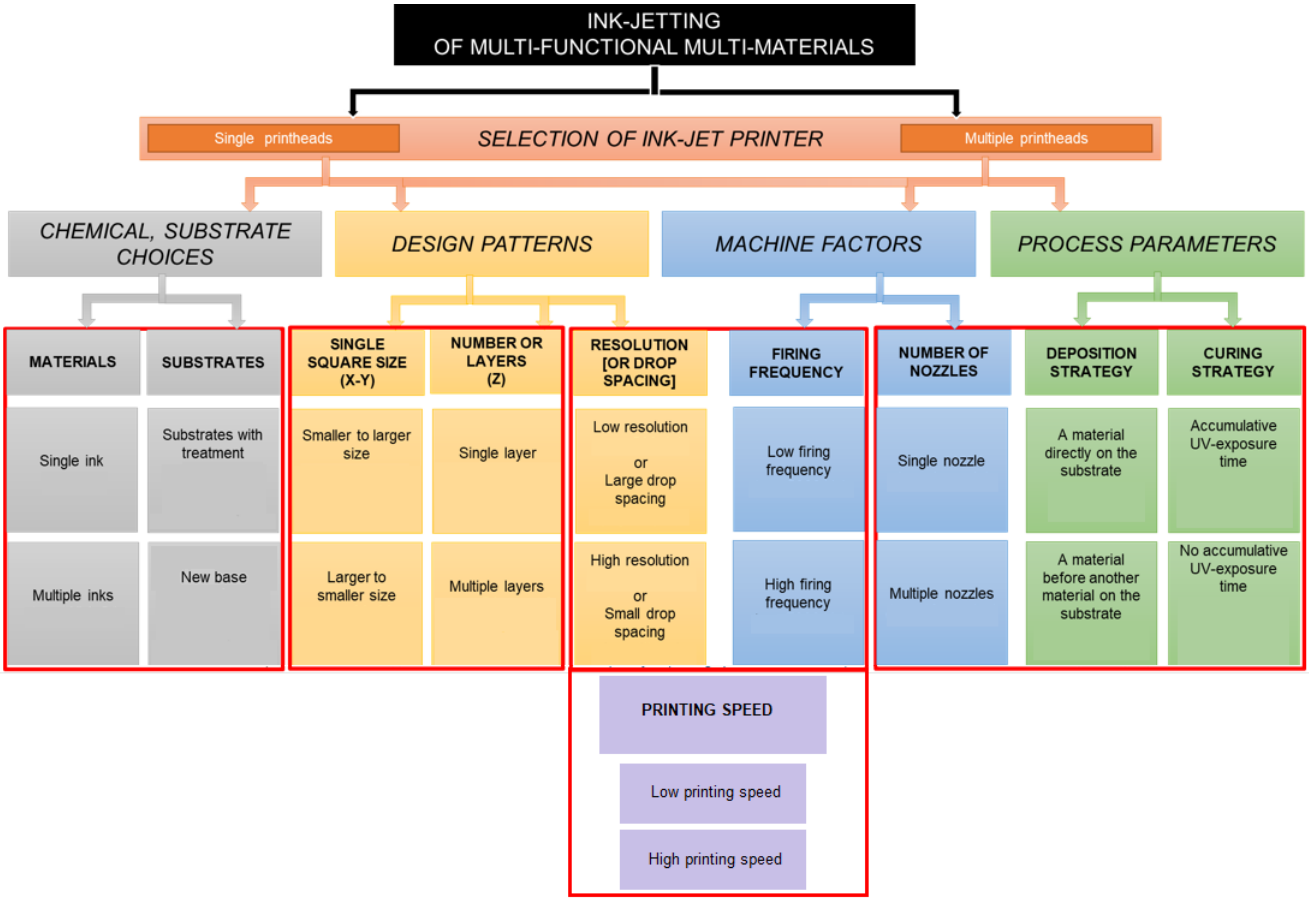

Figure 6.20. *Active workflow for the ink-jetting of biopharmaceutical multi-functional multi-materials. The red box representing for testing variables that can be flexibly adjusted when choosing another types of printers for co-printing*

6.4.2. Outputs related to Chapter 6

a. Publication

Quach, T. T., Trindade, G. F., He, Y., Zhao, P., Hague, R. & Roberts, C. J. Design of active process workflow to investigate the interfaces of co-printed (bio)pharmaceutical products (in preparation).

b. Conference

- The 52nd IUPAC General Assembly, 49th IUPAC World Chemistry Congress combined with the 11th edition of CHAINS, the largest chemistry congress from the Netherlands (20-25.08.2023) (IUPAC-CHAINS 2023) organized by the Royal Netherlands Chemical Society (KNCV) and the Dutch Research Council (NWO), Hague, Netherlands, 20-25.08.2023

Poster presentation: "Surface and interface study of 3D-printed biopharmaceutical products"

Tien Thuy Quach[1,2], Joseph Lamb[1], Gustavo F. Trindade[2,3], Yinfeng He[2], Peng Zhao[2], Richard Hague[2], Clive Roberts[4]

● EPSRC Next Generation of Additive Manufacturing – Annual meeting 2023 hosted by the Centre for Additive Manufacturing - University of Nottingham, the United Kingdom, 26.04.2023

Poster presentation: "Micro/nano scale characterisation of interfaces in next generation 3d-printed multi-functional multi-materials"

Tien Thuy Quach[1,2], Gustavo F. Trindade[2,3], Richard JM Hague[2] and Clive J Roberts[4]

● UK Surface Analysis Forum – Winter meeting 2022 hosted by the School of Physics - University of Bristol, Bristol, the United Kingdom, 13.04.2022

Poster presentation: "Developing the micro/nano scale characterisation of interfaces in multi-functional multi-materials additive manufacturing (3D-printing)"

Tien Thuy Quach[1,2], Gustavo F. Trindade[2,3], Laura Ruiz-Cantu[2,4], Richard JM Hague[2] and Clive J Roberts[5]

● Allied Health Professional Postgraduate Research Conference (AHPGR) 2021 hosted by the University of Nottingham - Virtual session, the United Kingdom, 13-15.01.2021

Flash poster presentation: "Developing micro/nanoscale analyses for the next-generation multi-functional 3D-printed products" – Best Flash Poster Prize on 15.01.2021

Tien Thuy Quach[1,2], Gustavo F. Trindade[2,3], Richard JM Hague[2] and Clive J Roberts[1]

c. Internal seminar

● Oral presentation at the Advanced Materials and Healthcare Technologies Division, School of Pharmacy, University of Nottingham

● Oral presentation at the PGR Seminar of the Centre for Additive Manufacturing, University of Nottingham

● Oral presentation at the PGR Seminar of the School of Pharmacy, University of Nottingham

CHAPTER 7: CONCLUSIONS AND SUGGESTED FUTURE WORK

7.1. CONCLUSIONS

This thesis includes the following key findings. Identifying the need and potential for enhanced analytics in future sustainable supply chains for Point-of-Care (POC) manufacture centred on consideration in the UK pharmaceutical sector (Chapter 3). A variety of data analytics along with relevant regulations-standards have been used to improve supply chains in different sectors such as the pharmaceutical manufacturing in the UK and worldwide. However, it is hard to monitor the efficiency of data and regulation management as well as their translation into good practices. Hence, I propose that the legal and regulatory frameworks with enhanced analytics should be clarified and reviewed to support supply chain innovation and new product development. I proposed a research methodology with three main steps, literature collection (via key words-documents), data analysis (of representative case studies), and policy consultancy (with focused strategic proposals). The legislation bodies that have great impact on the pharmaceutical supply chain were identified. One significant finding is an ongoing major shift into POC Manufacturing with(out) the support of enhanced data analytics. This was demonstrated via practical evidence examples, in terms of six key aspects i) POC Products, ii) POC Processes, iii) POC Premises, iv) POC Procedures, v) POC Personnel, and vi) POC Provision. The result provides the cornerstones for navigating future progression by assessing the most recent regulation-standards along with enhanced data analytics to control the quality of sustainable pharmaceutical supply chain in a post-pandemic world.

The second finding was the adaptive procedure for examining interfaces and nanostructures of additively manufactured electronic products (Chapter 4). The possibility of microcracks or pores in printed samples after ink-jet printing can limit the functionalities of the final products in the electronic materials field. It was challenging to use traditional techniques to reveal and analyse the morphology of specific interfacial areas of the 3D-printed electronics. With high-value applications in mind, commercialised and lab-based electronic printed products were chosen as test samples in this investigation. I investigated the ability of ultramicrotomy to expose buried interfaces for analysis. I created a protocol using Focused-Ion-Beam Electron Microscopy (FIB-SEM) as an alternative sample processing approach for examining interfaces in metal nanostructures in 3D-printed electronics. Scanning

Electron Microscopy (SEM), Transmission Electron Microscopy (TEM), and Atomic Force Microscopy (AFM) were used to confirm that the morphology of interfaces was maintained. In this example, the core structures with clusters of specific types of metal nanoparticles were proven to be beneficial in 3D-printing, which supported strengthening the main function of the 3D-printed products. Hence, a procedure was successfully developed to understand and improve the cohesion among metal-metal and metal-polymer materials.

Two other findings included the practical guide to investigate the physiochemical compatibilities of new ink formulations in additive manufacturing, and the active process workflow to investigate the interface - interphase of co-printed (bio)pharmaceutical products (Chapters 5 and 6). I carried out a novel interface study based on ink-jet printing of two inks; a commercial water-soluble ink (WI) to assist the complex-morphology function; and a novel structured ink (SI) developed at Nottingham which has a biofilm resistance function. Key micro-nano behaviours for AM interfaces were successfully monitored including rheological, wetting, and adhesive behaviour. Along with the physiochemical compatibility of the inks, the fundamental process parameters that impact on the final products also needs to be tested and optimised, which includes printing speed, light-curing strategy, and deposition strategy were studied.

An enhanced framework was built and developed to help to understand and monitor the pharmaceutical interface-interphase including five steps as follows: 1) identifying original inks via micro-elemental analysis, inductively coupled plasma optical emission spectroscopy (ICP-OES), and inductively coupled plasma mass spectroscopy (ICP-MS); 2) selecting suitable substrates via pre-testing with contact angel measurement, in-situ measurement with printer camera, and post-testing with optical microscopy; 3) confirming final roughness/thickness of single layer via profilometry and interferometry; 4) understanding the chemical changes of the printed patterns (compared to original inks) via Fourier-Transform Infrared Spectroscopy (FT-IR), and Nuclear Magnetic Resonance Spectroscopy (NMR); and 5) monitoring the effects of printing strategies and UV-exposure time on the interface-interphase via Scanning Electron Microscopy (SEM) With Energy Dispersive X-Ray Analysis (EDX), and Time of Flight Secondary Ion Mass Spectrometer (Tof-SIMS) With Hybrid Orbitrap (OrbiSIMS).

7.2. SUGGESTED FUTURE WORK

The need for enhanced analytics within legal frameworks was investigated in the context of their essential role for enabling pharmaceutical new product development and supply chain management, focusing on POC manufacture. As data analytics are enhancing quickly, the assessment of their applications and impacts should be evaluated and updated regularly. Some recommendations for actions include: 1) Qualitative interviews with delegates from legislation bodies (e.g. MHRA), public organisations (e.g. British Standard Institution), and private enterprises (e.g. international and national pharmaceutical companies); 2) Evidence-based risk assessments from representative case studies to identify the core cross-sector elements affecting not only pharmaceuticals but also other promising areas (e.g. environment, automotive, aerospace, etc); and 3) Proposals for changes in updating the current and developing regulation-standards where the regulators-managers can utilise new approaches in multi-disciplinaries including pharmaceutics and other fields (e.g. food, engineering, defence, etc).

The right choices for printers, materials-substrates, design patterns, machine factors, and process parameters can be made following the workflows presented. For example, more layers allow for finer and more intricate features to be printed, but they typically mean more material usage, which can impact the cost of printing and material waste. Although the number of layers directly affects the quality, resolution, and characteristics of the printed object, we can prioritize on investigating of the interfaces-interphases of single-layered co-printed prints before moving to co-printed prints with hundreds of layers to save the time and cost for manufacturing. Therefore, process consistency is key to improve upon to produce reliable and repeatable results in 3D printing, which can provide a competitive advantage.

Further research can be done to ensure the potential of transformation and application of my workflows to other multi-layered electronics devices or bio-pharmaceutical medicines. For example, along with engineering and healthcare, other research areas can have the time and cost-saving when applying the thesis results of effective workflows to investigate the behavioural interfaces at the micro/nanoscale before moving forward to co-printing the whole products. This needs to be monitored by further investigation, which is not limited to physiochemical analyses. For example, more research on quantitative biochemical analyses

can be carried out to validate the functionality of final products. It is beneficial for doing research to check the efficiency of this manufacturing-analyses because the cost, time, and energy consumption will play important roles for applying these guides-workflows in scaling up the operations. This will provide data evidence to support the productive design and growth of pharmaceutical Point-Of-Care Manufacturing in the future.

7.3. SUMMARY OF RESEARCH NOVELTY

My research delivers the first investigation into reliable interface framework for monitoring the physiochemical compatibilities of ink-substrate and ink-ink before co-printing multiple (bio)pharmaceutical materials. Particularly, this micro/nano scale interface study will help define a path to reduce the time and cost for manufacturing and analysis of new medicines when a series of functional substances can quickly be screened and tested for their compatibilities at the beginning of production. The thesis also offers the first tailored methodologies for using Ultramicrotomy/ FIB-SEM to expose interfaces of 3D-printed electronics as well as the great potential of ink-jet printing new metal nanoparticles. This can help investigate and construct the new inductors and electrodes in order to overcome the current global shortage of inductors after Covid-19 pandemic. Finally, the thesis presents the first prospects of data analytics and legislation framework that can help to achieve the optimal performance of sustainable supply chains with POC manufacture centered in the UK. This can enable the creation and analyses of original products via POC manufacturing that can be safely regulated and monitored, particularly for additive manufacturing.

REFERENCES

1. Nematollahi, M., Jahadakbar, A., Mahtabi, M. J. & Elahinia, M. Additive manufacturing (AM). in *Metals for Biomedical Devices* 331–353 (Elsevier, 2019). doi:10.1016/B978-0-08-102666-3.00012-2.
2. Plocher, J. & Panesar, A. Review on design and structural optimisation in additive manufacturing: Towards next-generation lightweight structures. *Materials and Design* vol. 183 Preprint at https://doi.org/10.1016/j.matdes.2019.108164 (2019).
3. Abdulhameed, O., Al-ahmari, A., Ameen, W. & Mian, S. H. Additive manufacturing : Challenges , trends , and applications. **11**, 1–27 (2019).
4. Lee, J. Y., An, J. & Chua, C. K. Fundamentals and applications of 3D printing for novel materials. *Applied Materials Today* vol. 7 120–133 Preprint at https://doi.org/10.1016/j.apmt.2017.02.004 (2017).
5. Gisario, A., Kazarian, M., Martina, F. & Mehrpouya, M. Metal additive manufacturing in the commercial aviation industry: A review. *Journal of Manufacturing Systems* vol. 53 124–149 Preprint at https://doi.org/10.1016/j.jmsy.2019.08.005 (2019).
6. Tack, P., Victor, J., Gemmel, P. & Annemans, L. 3D-printing techniques in a medical setting: A systematic literature review. *BioMedical Engineering Online* vol. 15 Preprint at https://doi.org/10.1186/s12938-016-0236-4 (2016).
7. Tofail, S. A. M. *et al.* Additive manufacturing: scientific and technological challenges, market uptake and opportunities. *Materials Today* vol. 21 22–37 Preprint at https://doi.org/10.1016/j.mattod.2017.07.001 (2018).
8. ASTM International. F2792-12 Standard Terminology for Additive Manufacturing Technologies. (2012) doi:https://doi.org/10.1520/F2792-12.
9. Overview over 3D printing technologies - Additively. https://www.additively.com/en/learn-about/3d-printing-technologies.
10. Toursangsaraki, M. A Review of Multi-material and Composite Parts Production by Modified Additive Manufacturing Methods. (2018).
11. Flynn, J. M., Shokrani, A., Newman, S. T. & Dhokia, V. Hybrid additive and subtractive machine tools - Research and industrial developments. *International*

Journal of Machine Tools and Manufacture vol. 101 79–101 Preprint at https://doi.org/10.1016/j.ijmachtools.2015.11.007 (2016).

12. Li, N. *et al.* Progress in additive manufacturing on new materials: A review. *Journal of Materials Science and Technology* vol. 35 242–269 Preprint at https://doi.org/10.1016/j.jmst.2018.09.002 (2019).
13. Bandyopadhyay, A. & Heer, B. Additive manufacturing of multi-material structures. *Materials Science and Engineering R: Reports* vol. 129 1–16 Preprint at https://doi.org/10.1016/j.mser.2018.04.001 (2018).
14. Loh, G. H., Pei, E., Harrison, D. & Monzón, M. D. An overview of functionally graded additive manufacturing. *Additive Manufacturing* vol. 23 34–44 Preprint at https://doi.org/10.1016/j.addma.2018.06.023 (2018).
15. MacDonald, E. & Wicker, R. Multiprocess 3D printing for increasing component functionality. *Science* vol. 353 Preprint at https://doi.org/10.1126/science.aaf2093 (2016).
16. Louzao, I. *et al.* Identification of Novel 'Inks' for 3D Printing Using High-Throughput Screening: Bioresorbable Photocurable Polymers for Controlled Drug Delivery. (2018) doi:10.1021/acsami.7b15677.
17. Chang, J. *et al.* Advanced material strategies for next-generation additive manufacturing. *Materials* vol. 11 Preprint at https://doi.org/10.3390/ma11010166 (2018).
18. Kamal, M. & Rizza, G. Design for metal additive manufacturing for aerospace applications. in *Additive Manufacturing for the Aerospace Industry* 67–86 (Elsevier, 2019). doi:10.1016/b978-0-12-814062-8.00005-4.
19. Fenollosa, F. *et al.* Foreseeing new multi-material FFF-Additive Manufacturing concepts meeting mimicking requirements with living tissues. in *Procedia Manufacturing* vol. 41 1063–1070 (Elsevier B.V., 2019).
20. Gao, W. *et al.* The status, challenges, and future of additive manufacturing in engineering. *CAD Computer Aided Design* **69**, 65–89 (2015).
21. Goole, J. & Amighi, K. 3D printing in pharmaceutics: A new tool for designing customized drug delivery systems. *International Journal of Pharmaceutics* vol. 499 376–394 Preprint at https://doi.org/10.1016/j.ijpharm.2015.12.071 (2016).
22. Norman, J., Madurawe, R. D., Moore, C. M. V., Khan, M. A. & Khairuzzaman, A. A new chapter in pharmaceutical manufacturing: 3D-printed drug products. *Advanced*

Drug Delivery Reviews vol. 108 39–50 Preprint at https://doi.org/10.1016/j.addr.2016.03.001 (2017).

23. Parandoush, P. & Lin, D. A review on additive manufacturing of polymer-fiber composites. *Composite Structures* vol. 182 36–53 Preprint at https://doi.org/10.1016/j.compstruct.2017.08.088 (2017).
24. Singh, R. *et al.* Multi-Material Additive Manufacturing of Sustainable Innovative Materials and Structures. *Polymers (Basel)* **11**, 62 (2019).
25. Murr, L. E. & Johnson, W. L. 3D metal droplet printing development and advanced materials additive manufacturing. *Journal of Materials Research and Technology* vol. 6 77–89 Preprint at https://doi.org/10.1016/j.jmrt.2016.11.002 (2017).
26. Morrin, A. Inkjet printed electrochemical sensors. in *Inkjet-based Micromanufacturing* 295–311 (Wiley-VCH Verlag, 2012). doi:10.1002/9783527647101.ch18.
27. Goyanes, A. *et al.* 3D Printing of Medicines: Engineering Novel Oral Devices with Unique Design and Drug Release Characteristics. *Mol Pharm* **12**, 4077–4084 (2015).
28. Lim, S. H., Chia, S. M. Y., Kang, L. & Yap, K. Y. L. Three-Dimensional Printing of Carbamazepine Sustained-Release Scaffold. *J Pharm Sci* **105**, 2155–2163 (2016).
29. Melocchi, A. *et al.* Hot-melt extruded filaments based on pharmaceutical grade polymers for 3D printing by fused deposition modeling. *Int J Pharm* **509**, (2016).
30. Prasad, L. K. & Smyth, H. 3D Printing technologies for drug delivery: a review. *Drug Dev Ind Pharm* **42**, 1019–31 (2016).
31. Trenfield, S. J. *et al.* Track-and-trace: Novel anti-counterfeit measures for 3D printed personalized drug products using smart material inks. *Int J Pharm* **567**, (2019).
32. Gupta, M. K. *et al.* 3D Printed Programmable Release Capsules. *Nano Lett* **15**, 5321–5329 (2015).
33. Kumar, A. *et al.* Low temperature additive manufacturing of three dimensional scaffolds for bone-tissue engineering applications: Processing related challenges and property assessment. *Materials Science and Engineering R: Reports* vol. 103 1–39 Preprint at https://doi.org/10.1016/j.mser.2016.01.001 (2016).
34. Swensen, J. P., Odhner, L. U., Araki, B. & Dollar, A. M. Printing three-dimensional electrical traces in additive manufactured parts for injection of low melting temperature metals. *J Mech Robot* **7**, (2015).

35. Wu, S. Y., Yang, C., Hsu, W. & Lin, L. 3D-printed microelectronics for integrated circuitry and passive wireless sensors. *Microsyst Nanoeng* **1**, (2015).
36. Zhang, W., Bi, E., Li, M. & Gao, L. Synthesis of Ag/RGO composite as effective conductive ink filler for flexible inkjet printing electronics. *Colloids Surf A Physicochem Eng Asp* **490**, 232–240 (2016).
37. Chang, Y. H. *et al.* A facile method for integrating direct-write devices into three-dimensional printed parts. *Smart Mater Struct* **24**, (2015).
38. University of Nottingham. Programme Grant - Next Gen AM - The University of Nottingham. https://www.nottingham.ac.uk/research/groups/cfam/major-epsrc-funding/programme-grant-next-gen-am/programme-grant-next-gen-am.aspx.
39. Determination of the interface/interphase evolution at the microscale - The University of Nottingham. https://www.nottingham.ac.uk/research/groups/cfam/major-epsrc-funding/programme-grant-next-gen-am/rc-1.aspx.
40. Bismarck, A. *et al.* Development of novel composites through fibre and interface/interphase modification. in *IOP Conference Series: Materials Science and Engineering* vol. 139 (Institute of Physics Publishing, 2016).
41. *Compendium of Surface and Interface Analysis*. *Compendium of Surface and Interface Analysis* (Springer Singapore, 2018). doi:10.1007/978-981-10-6156-1.
42. Brown, P. D., Edwards, H. K. & Fay, M. W. Microscopy at the life sciences / physical sciences interface Microscopy at the life sciences / physical sciences interface. (2010) doi:10.1088/1742-6596/241/1/012019.
43. Sun, Z., Zeng, X., Deng, X., Zhang, X. & Zhang, Y. Droplet interface in additive manufacturing: From process to application. *Droplet* **2**, (2023).
44. Dudley, J. J. & Kristensson, P. O. A review of user interface design for interactive machine learning. *ACM Trans Interact Intell Syst* **8**, 1–37 (2018).
45. Holm, R. & Storp, S. Surf ace and Interface Analysis in Polymer Technology : A Review. **2**, (1980).
46. Tian, X., Liu, T., Yang, C., Wang, Q. & Li, D. Interface and performance of 3D printed continuous carbon fiber reinforced PLA composites. *Compos Part A Appl Sci Manuf* **88**, 198–205 (2016).
47. Amancio-Filho, S. T. & Dos Santos, J. F. Joining of polymers and polymer-metal hybrid structures: Recent developments and trends. *Polym Eng Sci* **49**, 1461–1476 (2009).

48. Zema, L., Melocchi, A., Maroni, A. & Gazzaniga, A. Three-Dimensional Printing of Medicinal Products and the Challenge of Personalized Therapy. *Journal of Pharmaceutical Sciences* vol. 106 1697–1705 Preprint at https://doi.org/10.1016/j.xphs.2017.03.021 (2017).
49. Stansbury, J. W. & Idacavage, M. J. 3D printing with polymers: Challenges among expanding options and opportunities. in *Dental Materials* vol. 32 54–64 (Elsevier Inc., 2016).
50. Joo, Y. *et al.* The advent of a novel manufacturing technology in pharmaceutics: superiority of fused deposition modeling 3D printer. *Journal of Pharmaceutical Investigation* vol. 50 131–145 Preprint at https://doi.org/10.1007/s40005-019-00451-1 (2020).
51. Kabir, S. M. F., Mathur, K. & Seyam, A. F. M. A critical review on 3D printed continuous fiber-reinforced composites: History, mechanism, materials and properties. *Composite Structures* vol. 232 111476 Preprint at https://doi.org/10.1016/j.compstruct.2019.111476 (2020).
52. Singh, S., Ramakrishna, S. & Singh, R. Material issues in additive manufacturing: A review. *J Manuf Process* **25**, 185–200 (2017).
53. Dimatix Materials Printer DMP-2850.
54. Printer, I. INKJET PRINTER ADVANCED DESKTOP R & D INKJET PRINTER PiXDRO LP50.
55. Features, O., Refining, F. O. R. & Development, P. Enhancements for Lp50 Inkjet Printer Optional Features for Refining Process Development Inkjet Printing.
56. ENHANCEMENTS FOR LP50 INKJET PRINTER OPTIONAL FEATURES FOR REFINING PROCESS DEVELOPMENT INKJET PRINTING.
57. Firefly, T. P., Led, U. V, Firefly, T., Firefly, T. P. & Led, T. F. Phoseon Firefly high performance UV LED curing lamp available now.
58. Michler, G. H. & Electron. *Electron Microscopy of Polymers*. (2008).
59. Centre, N. An appraisal of ultramicrotomy , FIBSEM and cryogenic FIBSEM techniques for the sectioning of biological cells on titanium substrates for TEM investigation.
60. Bobik, K., Dunlap, J. R. & Burch-Smith, T. M. Tandem high-pressure freezing and quick freeze substitution of plant tissues for transmission electron microscopy. *Journal of Visualized Experiments* (2014) doi:10.3791/51844.

61. Gao, M. Cryo-Ultramicrotomy of Complex Molecular Fluids. *Micros Today* **26**, 32–41 (2018).
62. Carter, D. B. W. C. B. *Transmission Electron Microscopy Companion Text*. *Kobunshi* vol. 43 (2016).
63. Hagler, H. K. Ultramicrotomy for Biological Electron Microscopy. in 67–96 (2007). doi:10.1007/978-1-59745-294-6_5.
64. Clevenger, M. R. Ultramicrotome: A simple, easily constructed instrument. *Science (1979)* **142**, 241–242 (1963).
65. Rigort, A. & Plitzko, J. M. Cryo-focused-ion-beam applications in structural biology. *Arch Biochem Biophys* **581**, 122–130 (2015).
66. House, K. L., Pan, L., O'Carroll, D. M. & Xu, S. Applications of scanning electron microscopy and focused ion beam milling in dental research. *Eur J Oral Sci* **130**, 1–24 (2022).
67. Taillon, J. A., Pellegrinelli, C., Huang, Y. L., Wachsman, E. D. & Salamanca-Riba, L. G. Improving microstructural quantification in FIB/SEM nanotomography. *Ultramicroscopy* **184**, 24–38 (2018).
68. Zhao, L. *et al.* The 3D Controllable Fabrication of Nanomaterials with FIB-SEM Synchronization Technology. *Nanomaterials* **13**, (2023).
69. Preparation, S. Technical document for ZEISS Crossbeam Family.
70. Ersen, O., Florea, I. & Hirlimann, C. Exploring nanomaterials with 3D electron microscopy. *Biochem Pharmacol* **18**, 395–408 (2015).
71. Huszka, G. & Gijs, M. A. M. Super-resolution optical imaging: A comparison. *Micro and Nano Engineering* vol. 2 7–28 Preprint at https://doi.org/10.1016/j.mne.2018.11.005 (2019).
72. Mihara, I., Havelund, R. & Gilmore, I. S. Embedding-Free Method for Preparation of Cross-Sections of Organic Materials for Micro Chemical Analysis Using Gas Cluster Ion Beam Sputtering. *Anal Chem* **89**, 4781–4785 (2017).
73. Reed, S. J. B. *Electron Microprobe Analysis and Scanning Electron Microscopy in Geology*. (2005). doi:10.2136/sssabookser5.1.2ed.c10.
74. Zhang, P. *et al.* Industrial Applications of Electron Microscopy: A Shared Laboratory Perspective. *Microsc. Microanal* **25**, 2019 (2019).
75. Saitoh, S. Correlative Light-Electron Microscopy (CLEM) and 3D Volume Imaging of Serial Block-Face Scanning Electron Microscopy (SBF-SEM) of Langerhans

Islets. in *Electron Microscopy - Novel Microscopy Trends* (IntechOpen, 2019). doi:10.5772/intechopen.81716.

76. Kabayama, K. & Tero, R. Optical Microscopy. in 413–417 (2018). doi:10.1007/978-981-10-6156-1_68.
77. Fujita, K. Follow-up review: recent progress in the development of super-resolution optical microscopy. 275–281 (2016) doi:10.1093/jmicro/dfw022.
78. Lee, J. Y. *et al.* Near-field focusing and magnification through self-assembled nanoscale spherical lenses. *Nature* **460**, 498–501 (2009).
79. *Compendium of Surface and Interface Analysis*. *Compendium of Surface and Interface Analysis* (Springer Singapore, 2018). doi:10.1007/978-981-10-6156-1.
80. Donald, A. M. The use of environmental scanning electron microscopy for imaging wet and insulating materials. *Nat Mater* **2**, 511–516 (2003).
81. Wuhrer, R. Low voltage imaging and X-ray microanalysis in the SEM : challenges and opportunities Low voltage imaging and X-ray microanalysis in the SEM : challenges and opportunities. (2016) doi:10.1088/1757-899X/109/1/012019.
82. Nelson, B., Dong, L. & Arai, F. Micro/Nanorobots. in 411–450 (2008). doi:10.1007/978-3-540-30301-5_19.
83. Garini, Y., Vermolen, B. J. & Young, I. T. From micro to nano: Recent advances in high-resolution microscopy. *Current Opinion in Biotechnology* vol. 16 3–12 Preprint at https://doi.org/10.1016/j.copbio.2005.01.003 (2005).
84. Ul-Hamid, A. *A Beginners' Guide to Scanning Electron Microscopy*. *A Beginners' Guide to Scanning Electron Microscopy* (Springer International Publishing, 2018). doi:10.1007/978-3-319-98482-7.
85. Nelson, B. *Micro / Nanoro*. (2008). doi:10.1007/978-3-540-30301-5.
86. Yang, J. C., Small, M. W., Grieshaber, R. V. & Nuzzo, R. G. Recent developments and applications of electron microscopy to heterogeneous catalysis. *Chemical Society Reviews* vol. 41 8179–8194 Preprint at https://doi.org/10.1039/c2cs35371g (2012).
87. Jinschek, J. R. Advances in the environmental transmission electron microscope (ETEM) for nanoscale in situ studies of gas – solid interactions. 2696–2706 (2014) doi:10.1039/c3cc49092k.
88. Bandyopadhyay, A. & Heer, B. Additive manufacturing of multi-material structures. *Materials Science and Engineering R: Reports* vol. 129 1–16 Preprint at https://doi.org/10.1016/j.mser.2018.04.001 (2018).

89. Taheri, M. L. *et al.* Current status and future directions for in situ transmission electron microscopy. **134**, 86–95 (2016).
90. Carenco, S. *et al.* The core contribution of transmission electron microscopy to functional nanomaterials engineering †. 1260–1279 (2016) doi:10.1039/c5nr05460e.
91. Tang, C. Y. & Yang, Z. Transmission Electron Microscopy (TEM). in *Membrane Characterization* 145–159 (Elsevier Inc., 2017). doi:10.1016/B978-0-444-63776-5.00008-5.
92. Page, P. & Kurlov, V. N. Scanning Electron Microscopy. 499–504 (1999).
93. Okano, Y. Scanning Electron Microscopy. in *Compendium of Surface and Interface Analysis* 563–569 (Springer Singapore, Singapore, 2018). doi:10.1007/978-981-10-6156-1_91.
94. Rajesh Kumar, B. & Subba Rao, T. AFM studies on surface morphology, topography and texture of nanostructured zinc aluminum oxide thin films. *Dig J Nanomater Biostruct* **7**, 1881–1889 (2012).
95. de Groot, P. Coherence Scanning Interferometry. *Optical Measurement of Surface Topography* 187–208 (2011) doi:10.1007/978-3-642-12012-1_9.
96. Kohser, R. A. *Materials and Processes in Manufacturing*. *Journal of Manufacturing Systems* vol. 17 (1998).
97. ISO 21920-2:2021(en), Geometrical product specifications (GPS) — Surface texture: Profile — Part 2: Terms, definitions and surface texture parameters. https://www.iso.org/obp/ui/#iso:std:iso:21920:-2:ed-1:v2:en.
98. Blateyron, F. & Leroy, B. Optimal characterisation of profile features. *Surf Topogr* **9**, (2021).
99. Tokumasu, F. & Takeyasu, K. Atomic force microscopy for biochemist. *Seikagaku* **69**, 429–433 (1997).
100. Alunda, B. O. & Lee, Y. J. Review: Cantilever-Based Sensors for High Speed Atomic Force Microscopy. *Sensors (Basel)* **20**, 1–39 (2020).
101. (PDF) Materials Characterization and Problem Solving. https://www.researchgate.net/publication/283371116_Materials_Characterization_and_Problem_Solving.
102. Das, S. K. *et al.* Improvement of Alternative Non-Raster Scanning Methods for High Speed Atomic Force Microscopy: A Review. *IEEE Access* **7**, 115603–115624 (2019).

103. Bramowicz, M., Kulesza, S. & Rychlik, K. A Comparison Between Contact and Tapping AFM Mode in Surface Morphology Studies. *Technical Sciences* **15**, 307–318 (2012).
104. Bruker. PeakForce Tapping PeakForce Tapping How AFM Should Be — for 10 Years and Counting. (2019).
105. Hook, A. L. *et al.* Polymers with hydro-responsive topography identified using high throughput AFM of an acrylate microarray. *Soft Matter* **7**, 7194–7197 (2011).
106. Dokukin, M. E. & Sokolov, I. Quantitative mapping of the elastic modulus of soft materials with HarmoniX and PeakForce QNM AFM modes. *Langmuir* **28**, 16060–16071 (2012).
107. Clifford, C. A. & Seah, M. P. Quantification issues in the identification of nanoscale regions of homopolymers using modulus measurement via AFM nanoindentation. *Appl Surf Sci* **252**, 1915–1933 (2005).
108. Holton, I. Recent Major Advances IN 3D OPTICAL PROFILING OF MICRO SURFACES. **6**, 32–34.
109. Manual, O. Zeta-20 Optical Profiler.
110. Profilers, Z. O. ZDot ™ Technology. 1–3.
111. Zygo, P. N. Nexview NX2 OEM Optical Profiler Head. **44**, 764334 (2022).
112. Nexview™ NX2. https://www.zygo.com/en/products/metrology-systems/3d-optical-profilers/nexview-nx2.
113. Dist, W. Nexview NX2 / NewView 9000 / ZeGage Pro Objective Chart. **44**, 346–347 (2018).
114. Watson, G. D. *Pharmaceutical Analysis: A Textbook for Pharmacy Students and Pharmaceutical Chemists*. *Pharmaceutical Analysis: A textbook for pharmacy students and pharmaceutical chemists* (2005).
115. Sharma, A., Verma, R., Kumar, R., Chauhan, R. & Sharma, V. Chemometric analysis of ATR-FTIR spectra of fingernail clippings for classification and prediction of sex in forensic context. *Microchemical Journal* **159**, 105504 (2020).
116. Tyagi, P., Kumar, K., Rani, M. & Bhankar, V. Volumetric and FT-IR Studies of the Binary Liquid Mixtures of Tributylamine and Alkyl Ester (C1-C5). *J Chem Eng Data* **64**, 3213–3223 (2019).

117. Molecular spectrocopies at different wavelength. *https://www.hellma.com/en/process-probes-and-flow-cells/measurement-principles/* (2023).
118. Overview, T. Agilent Cary 630 FTIR sample interfaces. 6 (2011).
119. Agilent Technologies. Agilent cary 630 FTIR spectrometer user ' s guide. 1–58 (2011).
120. Agilent Technologies. Agilent Cary 600 Series FTIR Spectrometers and Microscopes: Users Guide. 1–50 (2013).
121. Note, A. Improved Measurement of Liquid Samples Using FTIR Cary 630 FTIR spectrometer with DialPath module. (1980).
122. Ausili, A., Sánchez, M. & Gómez-Fernández, J. C. Attenuated total reflectance infrared spectroscopy: A powerful method for the simultaneous study of structure and spatial orientation of lipids and membrane proteins. *Biomed Spectrosc Imaging* **4**, 159–170 (2015).
123. Bonnin, E. A., Rizzoli, S. O., Baird, E. & Kimball, B. A. Novel Secondary Ion Mass Spectrometry Methods for the Examination of Metabolic Effects at the Cellular and Subcellular Levels. **14**, 1–13 (2020).
124. Trindade, G. F., Bañuls-Ciscar, J., Ezeh, C. K., Abel, M. L. & Watts, J. F. Characterisation of wood growth regions by multivariate analysis of ToF-SIMS data. *Surface and Interface Analysis* **48**, 584–588 (2016).
125. Tiddia, M. *et al.* Chemical imaging of buried interfaces in organic-inorganic devices using FIB-ToF-SIMS. *ACS Appl Mater Interfaces* acsami.8b15091 (2019).
126. Noun, M. Cell and Tissue Imaging by TOF-SIMS and MALDI-TOF : An Overview for Biological and Pharmaceutical Analysis. 1–26 (2022) doi:10.1017/S1431927621013593.
127. Im, J. *et al.* Functionalized Gold Nanoparticles with a Cohesion Enhancer for Robust Flexible Electrodes. *ACS Appl Nano Mater* **5**, 6708–6716 (2022).
128. Li, K., Liu, J., Grovenor, C. R. M. & Moore, K. L. NanoSIMS Imaging and Analysis in Materials Science. *Annual Review of Analytical Chemistry* **13**, 273–292 (2020).
129. Passarelli, M. K. *et al.* The 3D OrbiSIMS—label-free metabolic imaging with subcellular lateral resolution and high mass-resolving power. *Nature Methods 2017 14:12* **14**, 1175–1183 (2017).

130. Zhang, C., Liu, Z. & Deng, P. Contact angle of soil minerals: A molecular dynamics study. *Comput Geotech* **75**, 48–56 (2016).
131. Grüßer, M., Waugh, D. G., Lawrence, J., Langer, N. & Scholz, D. On the Droplet Size and Application of Wettability Analysis for the Development of Ink and Printing Substrates. *Langmuir* **35**, 12356–12365 (2019).
132. Zhou, Z. *et al.* High-throughput characterization of fluid properties to predict droplet ejection for three-dimensional inkjet printing formulations. *Addit Manuf* **29**, 100792 (2019).
133. Yakhshi-Tafti, E., Kumar, R. & Cho, H. J. Measurement of Surface Interfacial Tension as a Function of Temperature Using Pendant Drop Images. *Int J Optomechatronics* **5**, 393–403 (2011).
134. Cinquino, M. *et al.* Effect of surface tension and drying time on inkjet-printed PEDOT:PSS for ITO-free OLED devices. *Journal of Science: Advanced Materials and Devices* **7**, (2022).
135. Illumina. Hamilton Microlab STAR Reference Guide. (2015).
136. De Gennes, P. G. Wetting: Statics and dynamics. *Rev Mod Phys* **57**, 827–863 (1985).
137. ZISMAN, W. A. Relation of the Equilibrium Contact Angle to Liquid and Solid Constitution. 1–51 (1964) doi:10.1021/ba-1964-0043.ch001.
138. Kern, K., David, R., Palmer, R. L. & Comsa, G. PhysRevLett.56.2823. **56**, 2823–2827 (1986).
139. Kruss. Drop Shape Analysis System DSA100 Installation and Operation. (2010).
140. Hoorfar, M. & W. Neumann, A. Recent progress in Axisymmetric Drop Shape Analysis (ADSA). *Adv Colloid Interface Sci* **121**, 25–49 (2006).
141. Bagalkot, N., Hamouda, A. A. & Isdahl, O. M. Dynamic interfacial tension measurement method using axisymmetric drop shape analysis. *MethodsX* **5**, 676–683 (2018).
142. D'Elia, C.F., Connor, E.E., Kaumeyer, N.L., Keefe, C.W., Wood, K.V., and Zimmermann, C. F. Nutrient Analytical Services Laboratory Standard Operating Procedures. *Chesapeake Biological Laboratory* **0038**, 77 (1995).
143. Krotz, L. *et al.* Fully automated analysis for CHNS and trace sulfur through an Elemental Analyzer. 92008 (2018).

144. Edney, M. K. *et al.* Spatially Resolved Molecular Compositions of Insoluble Multilayer Deposits Responsible for Increased Pollution from Internal Combustion Engines. *ACS Appl Mater Interfaces* **12**, 51026–51035 (2020).
145. Exeter Analytical Incorporated. CE-440 Elemental Analyzer. 1–10 (2014).
146. PJ, H. Hore PJ. Nuclear magnetic resonance. USA: Oxford U. 23.
147. Prof. Dr. Friebolin, H. Chemical shifts of 1H and 13C nuclei in organic compound. *Basic one- and two-Dimensional NMR Spectroscopy* 44–45 (2011).
148. Héctor Zamora Carreras, P. NMR Spectroscopy Principles, Interpreting an NMR Spectrum and Common Problems. *https://www.technologynetworks.com/analysis/articles/nmr-spectroscopy-principles-interpreting-an-nmr-spectrum-and-common-problems-355891*.
149. Christensen, B. Nuclear magnetic resonance line shape of Si in single-crystal silicon. (2017).
150. Bible, R. H. Interpretation of NMR Spectra : an Empirical Approach. 150 (2013).
151. Derome, A. E. Modern NMR techniques for chemistry research. 299 (2013).
152. Jacobsen, N. E. NMR data interpretation explained : understanding 1D and 2D NMR spectra of organic compounds and natural products. (2016).
153. Hatzakis, E. Nuclear Magnetic Resonance (NMR) Spectroscopy in Food Science: A Comprehensive Review. *Compr Rev Food Sci Food Saf* **18**, 189–220 (2019).
154. Aceto, M. *et al.* Determination of metals in wine with atomic spectroscopy (flame-AAS, GF-AAS and ICP-AES); a review. *Food Addit Contam* **19**, 126–133 (2002).
155. Ohls, K. & Bogdain, B. History of inductively coupled plasma atomic emission spectral analysis: from the beginning up to its coupling with mass spectrometry. *J Anal At Spectrom* **31**, 22–31 (2015).
156. ICP-OES Systems and Technologies. *https://www.thermofisher.com/uk/en/home/industrial/spectroscopy-elemental-isotope-analysis/spectroscopy-elemental-isotope-analysis-learning-center/trace-elemental-analysis-tea-information/icp-oes-information/icp-oes-system-technologies.html*.
157. Comparison of Atomic Spectroscopy Techniques and the Advantages of AA, ICP-OES, and ICP-MS. *https://csanalytical.com/comparison-atomic-spectroscopy-techniques-advantages-icp-ms-vs-aa-icp-oes/*.

158. Elmer, P. World Leader in Aa , Icp-Oes. *PerkinElmer, I. (2011). World Leader in Aa , Icp-Oes and Icp-Ms. PerkinElmer, 1–16. Retrieved from www.perkinelmer.com* (2011).
159. Ohls, K. & Bogdain, B. History of inductively coupled plasma atomic emission spectral analysis: from the beginning up to its coupling with mass spectrometry.
160. Fridman. TUTORIAL A Beginner ' s Guide to ICP-MS. *Spectroscopy* **16**, 38–55 (2001).
161. Thermo Scientific. Thermo Scientific iCAP Q ICP-MS, ICP-MS Dramatically Different ICP-Ms. 1–12 (2012).
162. Kasian, O., Geiger, S., Mayrhofer, K. J. J. & Cherevko, S. Electrochemical On-line ICP-MS in Electrocatalysis Research. *Chemical Record* **19**, 2130–2142 (2019).
163. Clases, D. & Gonzalez de Vega, R. Facets of ICP-MS and their potential in the medical sciences—Part 1: fundamentals, stand-alone and hyphenated techniques. *Anal Bioanal Chem* 7337–7361 (2022) doi:10.1007/s00216-022-04259-1.
164. Khaled, S. A., Burley, J. C., Alexander, M. R., Yang, J. & Roberts, C. J. 3D printing of tablets containing multiple drugs with defined release profiles. *Int J Pharm* **494**, 643–650 (2015).
165. Medicines and Healthcare products Regulatory Agency. *Horizon Scanning Case Study: Point of Care Manufacture - Case Study*. (2022).
166. European Medicines Agency, Substance and product data management services. https://www.ema.europa.eu/en/human-regulatory/research-development/data-medicines-iso-idmp-standards/spor-master-data/substance-product-data-management-services.
167. Mofid, S. *et al.* The Utility of Remote Inspections During the COVID-19 Health Emergency and in the Postpandemic Setting. *Clin Ther* **43**, 2046–2063 (2021).
168. Grassano, N. *et al.* The 2021 EU Industrial R&D Investment Scoreboard. (2021) doi:10.2760/559391.
169. Notice concerning regulation 251 - GOV.UK. https://www.gov.uk/government/publications/regulation-251-of-the-human-medicines-regulations-2020/notice-concerning-regulation-251.
170. European Union R&D Scoreboard 2021. (2021) doi:10.2760/559391.
171. 2021 EU Industrial R&D Investment Scoreboard. https://ec.europa.eu/commission/presscorner/detail/en/IP_21_6599.

172. United Nations. Statistical Division. *International Standard Industrial Classification of All Economic Activities (ISIC)*. (United Nations, 2008).
173. OECD Science, Technology and Innovation Outlook 2020. (2021) doi:10.1787/75F79015-EN.
174. Ho, W. R., Tsolakis, N., Dawes, T., Dora, M. & Kumar, M. A Digital Strategy Development Framework for Supply Chains. *IEEE Trans Eng Manag* (2022) doi:10.1109/TEM.2021.3131605.
175. MHRA. Putting patients first: A new era for our agency. Delivery Plan 2021 - 2023. 30 (2021).
176. MHRA. Management and use of IVD point of care test devices. *Crown. last accessed: 17/03/2014* 28 (2010).
177. Medicines Agency, E. EMA Final programming Document 2022-2024.
178. Cilurzo, F., Musazzi, U. M., Franzé, S., Fedele, G. & Minghetti, P. Design of in vitro skin permeation studies according to the EMA guideline on quality of transdermal patches. *European Journal of Pharmaceutical Sciences* **125**, 86–92 (2018).
179. Cilurzo, F. *et al.* On the characterization of medicated plasters containing NSAIDs according to novel indications of USP and EMA: Adhesive property and in vitro skin permeation studies. *Drug Dev Ind Pharm* **41**, 183–189 (2015).
180. EMA. Final programming document 2021-2023. *Ema/53919/2021* **31**, 153 (2021).
181. Oliver, P., Fernandez-Calle, P. & Buno, A. POCT Accreditation ISO 15189 and ISO 22870: Making the Point. *EJIFCC* **32**, 131 (2021).
182. ISO/IEC 17025:2017(en), General requirements for the competence of testing and calibration laboratories. https://www.iso.org/obp/ui/#iso:std:iso-iec:17025:ed-3:v1:en.
183. ISO - ISO 14971:2007 - Medical devices — Application of risk management to medical devices. https://www.iso.org/standard/38193.html.
184. ISO - ISO 13485:2016 - Medical devices — Quality management systems — Requirements for regulatory purposes. https://www.iso.org/standard/59752.html.
185. ISO 15190:2003(en), Medical laboratories — Requirements for safety. https://www.iso.org/obp/ui/#iso:std:iso:15190:ed-1:v1:en.
186. European Medicines Agency, Implementing ISO IDMP: introduction to SPOR data services. https://www.ema.europa.eu/en/events/implementing-iso-idmp-introduction-spor-data-services.

187. British Pharmacopoeia. https://www.pharmacopoeia.com/Subscriptions/ProductDetails?productId=100002301x (2022).
188. Consultation on Point of Care manufacturing. https://www.gov.uk/government/consultations/point-of-care-consultation/consultation-on-point-of-care-manufacturing (2021).
189. Medicines and Healthcare products Regulatory Agency. *Putting Patients First: A New Era for Our Agency*. (2022).
190. Europe's Digital Decade: digital targets for 2030 | European Commission. https://ec.europa.eu/info/strategy/priorities-2019-2024/europe-fit-digital-age/europes-digital-decade-digital-targets-2030_en.
191. European Commission. European industrial technology roadmap for the next generation cloud-edge offering. (2021).
192. European Medicines Agency. *Final Programming Document 2022-2024*. (2022).
193. European Medicines Agency. *Annual Report of the Good Manufacturing and Distribution Practice Inspectors Working Group 2021*. www.ema.europa.eu/contact (2022).
194. European Pharmacopoeia (Ph. Eur.) 11th Edition. https://www.edqm.eu/en/european-pharmacopoeia-ph.-eur.-11th-edition (2022).
195. eCFR :: 21 CFR Part 26 -- Mutual Recognition of Pharmaceutical Good Manufacturing Practice Reports, Medical Device Quality System Audit Reports, and Certain Medical Device Product Evaluation Reports: United States and the European Community. https://www.ecfr.gov/current/title-21/chapter-I/subchapter-A/part-26.
196. FDA Releases Update of 2022 Priority Guidance Topics for Foods Program | FDA. https://www.fda.gov/food/cfsan-constituent-updates/fda-releases-update-2022-priority-guidance-topics-foods-program.
197. Good Review Practices | GRPs | FDA. https://www.fda.gov/drugs/guidance-compliance-regulatory-information/good-review-practices-grps.
198. Mutual Recognition Agreement (MRA) | FDA. https://www.fda.gov/international-programs/international-arrangements/mutual-recognition-agreement-mra.
199. Regulations: Good Clinical Practice and Clinical Trials | FDA. https://www.fda.gov/science-research/clinical-trials-and-human-subject-protection/regulations-good-clinical-practice-and-clinical-trials.

200. Training for Pharmaceutical Companies in Leadership & Soft Skills - Good Behavioural Practice (GBP) Pharma. http://www.gbppharma.com/Good_Behavioural_Practices.php.
201. IDMP Standards - IDMP1 free information brochure download. https://www.idmp1.com/idmp-standards/.
202. ISO 14971:2019(en), Medical devices — Application of risk management to medical devices. https://www.iso.org/obp/ui/#iso:std:iso:14971:ed-3:v1:en.
203. ISO 22870:2016, Point-of-care testing (POCT) — Requirements for quality and competence. https://www.iso.org/obp/ui/#iso:std:iso:22870:ed-2:v1:en.
204. ISO 13485:2016(en), Medical devices — Quality management systems — Requirements for regulatory purposes. https://www.iso.org/obp/ui/#iso:std:iso:13485:ed-3:v1:en.
205. WHO Collaborative centres. https://www.who.int/teams/regulation-prequalification/regulation-and-safety/pharmacovigilance/health-professionals-info/collaborative-centers.
206. Icmra. International Coalition of Medicines Regulatory Authorities (ICMRA) Recommendations on common technical denominators for traceability systems for medicines to allow for interoperability.
207. International Council for Commonality in Blood Banking Automation (ICCBBA). ISBT 128 - ICCBBA. https://www.iccbba.org/.
208. *Overview of ICH International Council for Harmonisation of Technical Requirements for Pharmaceuticals for Human Use*. (2022).
209. Medicines and Healthcare products Regulatory Agency (MHRA). Unpublished documents: Point of Care Manufacture Workshops (13 & 21.07.2020). Preprint at (2020).
210. HL7, FHIR v4.3.0. https://www.hl7.org/fhir/modules.html.
211. GS1, Cooperating standards in healthcare. (2018).
212. Organisation, G. Cooperating standards in healthcare Cooperating standards in healthcare. (2018).
213. European industrial technology roadmap for the next generation cloud-edge offering. (2021).
214. Management and use of IVD point of care test devices. (2021).

215. Bicudo, E., Brass, I., Carmichael, P. & Farid, S. Regulatory Insights The UK's emerging regulatory framework for point-of-care manufacture: insights from a workshop on advanced therapies. *Cell Gene Ther Insights* **7**, 1005–1015 (2021).
216. Bicudo, E., Brass, I. & Carmichael, P. *Point-of-Care Manufacture of Advanced Therapies: Readiness Measures for Hospitals, Companies, and Regulatory Agencies.* https://www.researchgate.net/publication/362171382_Point-of-care_manufacture_of_advanced_therapies_readiness_measures_for_hospitals_companies_and_regulatory_agencies (2022).
217. The Advanced Therapy Treatment Centres network's Industry Advisory Group. *National Cell and Gene Therapy Vision for the UK*. (2022).
218. Catapult. *2021 GMP Manufacturing Report*. (2021).
219. Jang, S. H., Oh, S. T., Lee, I. H., Kim, H. C. & Cho, H. Y. 3-dimensional circuit device fabrication process using stereolithography and direct writing. *International Journal of Precision Engineering and Manufacturing* **16**, 1361–1367 (2015).
220. Seifert, T., Baum, M., Roscher, F., Wiemer, M. & Gessner, T. Aerosol Jet Printing of Nano Particle Based Electrical Chip Interconnects. in *Materials Today: Proceedings* vol. 2 4262–4271 (Elsevier Ltd, 2015).
221. Hoey, J. M., Lutfurakhmanov, A., Schulz, D. L. & Akhatov, I. S. A review on aerosol-based direct-write and its applications for microelectronics. *J Nanotechnol* (2012) doi:10.1155/2012/324380.
222. Rahman, T., Renaud, L., Heo, D., Renn, M. & Panat, R. Aerosol based direct-write micro-additive fabrication method for sub-mm 3D metal-dielectric structures. *Journal of Micromechanics and Microengineering* **25**, (2015).
223. Wu, S. Y., Yang, C., Hsu, W. & Lin, L. 3D-printed microelectronics for integrated circuitry and passive wireless sensors. *Microsyst Nanoeng* **1**, (2015).
224. Flowers, P. F., Reyes, C., Ye, S., Kim, M. J. & Wiley, B. J. 3D printing electronic components and circuits with conductive thermoplastic filament. *Addit Manuf* **18**, 156–163 (2017).
225. Zhang, F. *et al.* Reactive material jetting of polyimide insulators for complex circuit board design. *Addit Manuf* **25**, 477–484 (2019).
226. Kwok, S. W. *et al.* Electrically conductive filament for 3D-printed circuits and sensors. *Appl Mater Today* **9**, 167–175 (2017).

227. Https://www.nano-di.com/3d-printing-applications-for-electromagnets. DragonFly product. *Nano Dimension*.
228. Https://www.nano-di.com/3d-printing-applications-for-electromagnetsCompany, N. D. DragonFly product.
229. Yang, Y. *et al.* Three dimensional printing of high dielectric capacitor using projection based stereolithography method. *Nano Energy* **22**, 414–421 (2016).
230. Im, J. *et al.* Functionalized Gold Nanoparticles with a Cohesion Enhancer for Robust Flexible Electrodes. *ACS Appl Nano Mater* **0**, (2022).
231. Matzelle, T. R., Gnaegi, H., Ricker, A. & Reichelt, R. Characterization of the cutting edge of glass and diamond knives for ultramicrotomy by scanning force microscopy using cantilevers with a defined tip geometry. Part II. *J Microsc* **209**, 113–117 (2003).
232. Acetarin, J. -D, Carlemalm, E., Kellenberger, E. & Villiger, W. Correlation of some mechanical properties of embedding resins with their behaviour in microtomy. *J Electron Microsc Tech* **6**, 63–79 (1987).
233. Niittynen, J. *et al.* Alternative sintering methods compared to conventional thermal sintering for inkjet printed silver nanoparticle ink. *Thin Solid Films* **556**, 452–459 (2014).
234. Beedasy, V. & Smith, P. J. Printed electronics as prepared by inkjet printing. *Materials* vol. 13 Preprint at https://doi.org/10.3390/ma13030704 (2020).
235. ISO 21920-2:2021 - Geometrical product specifications (GPS) — Surface texture: Profile — Part 2: Terms, definitions and surface texture parameters. https://www.iso.org/standard/72226.html.
236. He, Y. *et al.* A Reactive Prodrug Ink Formulation Strategy for Inkjet 3D Printing of Controlled Release Dosage Forms and Implants. *Adv Ther (Weinh)* **3**, 1900187 (2020).
237. Ruiz-Cantu, L. *et al.* Microstructural control of polymers achieved using controlled phase separation during 3D printing with oligomer libraries: dictating drug release for personalized subdermal implants. *ChemRxiv.* (2020) doi:10.26434/CHEMRXIV.12440015.V1.
238. Shi, R. *et al.* Microstructural control in metal laser powder bed fusion additive manufacturing using laser beam shaping strategy. *Acta Mater* **184**, 284–305 (2020).

239. Zenou, M. & Grainger, L. Additive manufacturing of metallic materials. in *Additive Manufacturing: Materials, Processes, Quantifications and Applications* 53–103 (Elsevier, 2018). doi:10.1016/B978-0-12-812155-9.00003-7.
240. EWI. Dissimilar Materials Joining - EWI. https://ewi.org/dissimilar-materials-joining/.
241. van de Werken, N. *et al.* Additively manufactured carbon fiber-reinforced composites: State of the art and perspective. *Additive Manufacturing* vol. 31 100962 Preprint at https://doi.org/10.1016/j.addma.2019.100962 (2020).
242. Prakash, K. S., Nancharaih, T. & Rao, V. V. S. Additive Manufacturing Techniques in Manufacturing -An Overview. in *Materials Today: Proceedings* vol. 5 3873–3882 (Elsevier Ltd, 2018).
243. Tibbits, S. 4D printing: Multi-material shape change. *Architectural Design* **84**, 116–121 (2014).
244. Zhou, Z. *et al.* High-throughput characterization of fluid properties to predict droplet ejection for three-dimensional inkjet printing formulations. *Addit Manuf* **29**, 100792 (2019).
245. Louzao, I. *et al.* Identification of Novel 'inks' for 3D Printing Using High-Throughput Screening: Bioresorbable Photocurable Polymers for Controlled Drug Delivery. *ACS Appl Mater Interfaces* **10**, 6841–6848 (2018).
246. Ruiz-Cantu, L. *et al.* Microstructural Control of Polymers Achieved Using Controlled Phase Separation During 3D Printing with Oligomer Libraries: Dictating Drug Release for Personalized Subdermal Implants. (2020) doi:10.26434/CHEMRXIV.12440015.V1.
247. Ruiz-Cantu, L. *et al.* Bespoke 3D-Printed Polydrug Implants Created via Microstructural Control of Oligomers. *ACS Appl Mater Interfaces* **13**, 38969–38978 (2021).
248. He, Y. *et al.* A Reactive Prodrug Ink Formulation Strategy for Inkjet 3D Printing of Controlled Release Dosage Forms and Implants. *Adv Ther (Weinh)* **3**, 1900187 (2020).
249. Zhou, J., Zhang, Y. & Chen, J. K. Numerical simulation of laser irradiation to a randomly packed bimodal powder bed. *Int J Heat Mass Transf* **52**, 3137–3146 (2009).

250. Derby, B. Inkjet Printing of Functional and Structural Materials: Fluid Property Requirements, Feature Stability, and Resolution. *Annu Rev Mater Res* **40**, 395–414 (2010).
251. Trindade, G. F., Abel, M. L. & Watts, J. F. simsMVA: A tool for multivariate analysis of ToF-SIMS datasets. *Chemometrics and Intelligent Laboratory Systems* **182**, 180–187 (2018).
252. He, B., Yang, S., Qin, Z., Wen, B. & Zhang, C. The roles of wettability and surface tension in droplet formation during inkjet printing. *Scientific Reports 2017 7:1* **7**, 1–7 (2017).
253. Sun, Y. & Guo, Z. Recent advances of bioinspired functional materials with specific wettability: from nature and beyond nature. *Nanoscale Horizons* vol. 4 52–76 Preprint at https://doi.org/10.1039/c8nh00223a (2019).
254. Sandler, N. *et al.* Inkjet printing of drug substances and use of porous substrates-towards individualized dosing. *J Pharm Sci* **100**, 3386–3395 (2011).
255. SZ Guo, F. G. N. G. A. L. M. H. D. T. Solvent cast three-dimensional printing of multifunctional microsystems. *Small* **9**, 4118–4122 (2013).
256. Kabayama, K. & Tero, R. Optical Microscopy. in 413–417 (2018). doi:10.1007/978-981-10-6156-1_68.
257. Sadia, M. *et al.* Adaptation of pharmaceutical excipients to FDM 3D printing for the fabrication of patient-tailored immediate release tablets. *Int J Pharm* **513**, 659–668 (2016).
258. Pietrzak, K., Isreb, A. & Alhnan, M. A. A flexible-dose dispenser for immediate and extended release 3D printed tablets. *European Journal of Pharmaceutics and Biopharmaceutics* **96**, 380–387 (2015).
259. Daly, R., Harrington, T. S., Martin, G. D. & Hutchings, I. M. Inkjet printing for pharmaceutics - A review of research and manufacturing. *Int J Pharm* **494**, 554–567 (2015).
260. Alomari, M., Mohamed, F. H., Basit, A. W. & Gaisford, S. Personalised dosing: Printing a dose of one's own medicine. *Int J Pharm* **494**, 568–577 (2015).
261. Ni, P., Wei, X., Huang, B. & Wei, W. Study on the Curing Kinetics of UV-Curable Inkjet Ink. *Adv Mat Res* **174**, 397–400 (2011).

262. Simon, J. & Langenscheidt, A. Curing behavior of a UV-curable inkjet ink: Distinction between surface-cure and deep-cure performance. *J Appl Polym Sci* **137**, 49218 (2020).
263. Saleh, E. *et al.* 3D inkjet-printed UV-curable inks for multi-functional electromagnetic applications. *Addit Manuf* **13**, 143–148 (2017).
264. Tack, P., Victor, J., Gemmel, P. & Annemans, L. 3D-printing techniques in a medical setting: A systematic literature review. *BioMedical Engineering Online* vol. 15 Preprint at https://doi.org/10.1186/s12938-016-0236-4 (2016).
265. Shields, B. L. & Valencia, V. V. 3D-printing design using systems engineering. in *Additive Manufacturing Handbook* 57–74 (CRC Press, 2018). doi:10.1201/9781315119106-5.
266. Deters, J. 3D-printing impacts on systems engineering in defense industry. in *Additive Manufacturing Handbook* 49–56 (CRC Press, 2018). doi:10.1201/9781315119106-4.
267. Perelaer, J., Klokkenburg, M., Hendriks, C. E. & Schubert, U. S. Microwave flash sintering of inkjet-printed silver tracks on polymer substrates. *Advanced Materials* **21**, 4830–4834 (2009).
268. He, Y. *et al.* Exploiting Generative Design for Multi-Material Inkjet 3D Printed Cell Instructive, Bacterial Biofilm Resistant Composites. (2020) doi:10.26434/CHEMRXIV.12596999.V1.
269. Ruiz-cantu, L., Trindade, G. F., Taresco, V., Zhou, Z. & He, Y. Bespoke 3D printed polydrug implants created via microstructural control of oligomers. 1–12.
270. Blaesi, A. H. & Saka, N. Fibrous dosage forms by wet 3D-micro-patterning: Process design, manufacture, and drug release rate. *European Journal of Pharmaceutics and Biopharmaceutics* **130**, 345–358 (2018).
271. Johnson, A. R. & Procopio, A. T. Low cost additive manufacturing of microneedle masters. *3D Print Med* **5**, 2 (2019).
272. Krieger, K. J. *et al.* Simple and customizable method for fabrication of high-aspect ratio microneedle molds using low-cost 3D printing. *Microsyst Nanoeng* **5**, (2019).
273. Matsuzaki, R. *et al.* Three-dimensional printing of continuous-fiber composites by in-nozzle impregnation. *Sci Rep* **6**, (2016).

274. Geng, P. *et al.* Effects of extrusion speed and printing speed on the 3D printing stability of extruded PEEK filament. *J Manuf Process* (2019) doi:10.1016/j.jmapro.2018.11.023.
275. Kadry, H., Ahsan, F., Wadnap, S. & Xu, C. Digital light processing (DLP)3D-printing technology and photoreactive polymers in fabrication of modified-release tablets. *European Journal of Pharmaceutical Sciences* **135**, (2019).
276. Cuesta, E. *et al.* Dimensional accuracy analysis of Direct Metal Printing machine focusing on roller positioning errors. in *Procedia Manufacturing* vol. 41 2–9 (Elsevier B.V., 2019).
277. Farzadi, A., Solati-Hashjin, M., Asadi-Eydivand, M. & Osman, N. A. A. Effect of layer thickness and printing orientation on mechanical properties and dimensional accuracy of 3D printed porous samples for bone tissue engineering. *PLoS One* **9**, (2014).
278. Stowe, R. W. UV Curing of Ink Jet Printing. (2003).
279. Accessible Chemical Library. *https://pubchem.ncbi.nlm.nih.gov/*.

APPENDICES

A1. SCIENTIFIC BACKGROUND

TIEN THUY QUACH (QUÁCH THỦY TIÊN)

Nottingham, NG7 2RD | Tien.Quach@nottingham.ac.uk | https://orcid.org/0000-0002-4849-3364

PERSONAL STATEMENT

I have great passion, fundamental knowledge, and core skills in pharmaceutical formulation and characterisation. I can lead multi-disciplinary projects, provide technical consultancy, maintain robust collaboration, and progress effective teaching. It is not limited by but relies strongly on my high performance in experimental works - data collection, output implementation - network expansion, and knowledge exchange - public engagement. A range of outputs and activities such as conference presenting, paper writing, and grant securing have proven my great capability and impact to transform practical development and create new opportunities in building stronger and better communities. Hence, working in the new role will play an essential part in my pursuit of becoming a great researcher-mentor in pharmaceutical - chemical sciences.

QUALIFICATIONS

Doctor of Philosophy in Pharmacy **December 2019 – Present**

School of Pharmacy, University of Nottingham, UK

Project "Novel micro/nano scale characterization of interfaces in multi-material additive manufacturing (3D printing)"

Master of Science in Advanced Pharmaceutical Manufacturing **September 2018 – September 2019**

Strathclyde Institute of Pharmacy and Biomedical Sciences, University of Strathclyde, UK

Final project "Developing a machine learning database for amorphous solid dispersions" *(Distinction Degree)*

Bachelor of Pharmacy **September 2011 – September 2016**

Faculty of Pharmacy, University of Medicine and Pharmacy at Ho Chi Minh City, Vietnam

Final project "Formulation of pantoprazole delayed-release pellets" *(Upper Second-Class Honours Degree)*

WORK EXPERIENCE

Healthcare Assistant (part-time) **July 2020 – Present**

Mercia Social Care, United Kingdom

● I provided various types of care to support the individuals with physical disabilities and/or mental health at the nursing houses during and after Covid-19.

Personal Assistant (part-time) **August 2020 – Present**

Associate Professor Dr. Sonali Shah, United Kingdom

● I provided practical support to a disabled professional woman (who is a university senior researcher and disability rights activist) to live a full active independent life.

Postgraduate Support for Curriculum Transformation (part-time) March 2023 – September 2023

Faculty of Engineering, University of Nottingham, Nottingham, the United Kingdom

● I improved the student learning and experience and encouraged a culture of continuous improvement. I worked together with other 2 staff and students to support the redesigning of their programmes and co-creation of new learning.

Pharmacy Teaching Assistant (part-time) September 2021 – August 2023

School of Pharmacy, University of Nottingham, United Kingdom

● I taught/demonstrated and gave assessments to 40-60 MPharm students per class/lab in different modules such as Fundamentals of Pharmacy - Medicine Manufacturing; Gastrointestinal-Liver Diseases; and Bacterial-Fungal Infections.

Researcher Academy Demonstrator (part-time) September 2021 – August 2023

Researcher Academy, University of Nottingham, United Kingdom

● I facilitated 15-20 postgraduates and early-career researchers per course for good presenting and writing skills via a large number of sessions "Presenting Online", "Presentation Skills for Researchers (Face to Face)", and "Time to Write".

Lecturer and Dean-Assistant (full-time) March 2017 – August 2018

Faculty of Pharmacy, Ho Chi Minh City University of Technology (HUTECH), Vietnam

● I taught Pharmaceutical Sciences, Pharmacy Practice, and Microbiology-Biochemistry. As a Dean-Assistant, I supported the Dean to organize student activities and support their professional development (from 2017 to 2018). I offered online consultancy to support the Faculty's activities for advising and improving the students' performance (2018-present).

Technical-Assistant (internship programme) September 2016 – February 2017

Asia Shine Trading and Services Company Ltd., Vietnam

● I reviewed and updated the protocols of many active ingredients and excipients from different overseas companies. I transferred the practical knowledge and skills from some foreign experts to Vietnamese pharmaceutical staff at the factories.

ACADEMIC ACHIEVEMENTS

I published 2 articles with 3 further manuscripts in preparation. I delivered 8 talks/oral presentations and 16 poster presentations at internal and external symposia. I also represented different groups from over 12 distinguished organisations.

Selected publications

● Quach, T. T., Sheridan, B., Glass, E., & Roberts, C. (2022). Enhanced data analytics for the pharmaceutical supply chain in the United Kingdom. *https://doi.org/10.6084/m9.figshare.19802251.v1*

● Im, J., Trindade, G. F., Quach, T. T., Sohaib, A., Wang, F., Austin, J., Turyanska, L., Roberts, C. J., Wildman, R., Hague, R., & Tuck, C. (2022). Functionalized Gold Nanoparticles with a Cohesion Enhancer for Robust Flexible Electrodes. ACS Applied Nano Materials, 5(5), 6708–6716. *https://doi.org/10.1021/acsanm.2c00742*

● Quach, T. T., Nguyen, D. T., Kim, N. N., Le, T. T. V., and Le, H. (2017). Formulation of pantoprazole delayed-release pellets. Ho Chi Minh City Medical Journal, 21(1), 150-156.

Selected talks and posters

● Young Scientist Lecture Award: "Investigate the potential intermixing in the functional multi-materials additive manufacturing". *Advanced Functional Materials Congress 2023 at Orlando, USA (Hybrid), 27-30.04.2023.*

● Best Oral Presentation Prize: "Interface characterisation for the next generation of multi-materials additive manufacturing". *European Advanced Materials Congress 2021 at Stockholm, Sweden (Hybrid), 23-25.08.2021.*

● Best Poster Prize: "Developing micro/nanoscale analyses for the next-generation multi-functional 3D-printed products". *Allied Health Professional Postgraduate Research Conference 2021, UK, 13-15.01.2021.*

Selected national organisations

● Postgraduate Representative and then Communication Chair at the Emerging Technologies Focus Group of the Academy of Pharmaceutical Sciences (APS) (2021-Present).

● Committee Member at the East Midlands Branch and I&D Advocate at the Equality, Inclusion, and Diversity (EDI) Focus Group of the Institute of Physics (IOP) (2021-Present).

● Committee Member at the East Midlands Local Section and Lead of the Edition Team of the Particle Characterisation Interest Group of the Royal Society Chemistry (RSC) (2022-Present). I was shortlisted for the Broadening Horizons in the Chemical Sciences 2022.

● President of the Student Association at the Faculty of Pharmacy (2014 – 2016), Executive Member of the University Youth Union and Student Association (2012-2016)

Selected international organisations

● Vice-President (and next term President) of the International Younger Chemists Network (IYCN) (2023-Present).

● Fellow at the International Association of Advanced Materials (IAAM) (2023-Present)

● Learning Opportunities Manager at the Process Analytical Technology Community Board of the American Association of Pharmaceutical Scientists (AAPS) (2022-Present).

● Committee Member of the Early-Career Scientists Subcommittee at the Analytical Chemistry Division of the International Union Of Pure And Applied Chemistry (IUPAC) (2021-Present).

● Co-founder of the ASEAN Pharmacy students' network to transfer and apply new knowledge and skills at the ASEAN PharmNET (2015-2017).

RESEARCH HIGHLIGHTS

I was awarded 7 project grants (over £45000), 21 development-travel grants (over £9000), and 14 prestigious honours from different national and international organisations. *More details: https://www.linkedin.com/in/tien-thuy-quach/details/honors/*

Selected projects

● I applied and secured the Early Career Researcher Placement Award 2022 (£4000) to work with Dr. Ben Sheridan and Emma Glass from the British Standard Institution and Prof. Clive Roberts from the University of Nottingham. The project "Frameworks for enhanced analytics in the pharmaceutical industry in the United Kingdom" reviewed the regulatory documents and provided good practice in data management and analyses of pharmaceutics within the next 5 years.

● In collaboration with Dr. Gustavo F. Trindade, Dr. Yinfeng He, and Prof. Clive Roberts, I wrote the proposal to become a Winner of the Faculty Knowledge Exchange (KE) Enhancement Fund Award 2021 (£5000). The project (A126SF) "On-site training to exploit a novel hyphenated system Thermogravimetric - Infrared - Gas Chromatography/Mass Spectrometry to support KE activity" successfully progressed two on-site trainings and follow-on supports from the experts.

● I was a Principal Investigator (PI) to win a grant from the University of Nottingham Interdisciplinary Centre for Analytical Science 2022 (£7351.25). The project (A7I241) "Investigation of the potential cross-contamination in multi-functional additive manufacturing" based on the combination of state-of-art facilities and ingenious co-PIs across the Faculty of Engineering (Dr. Yinfeng He, Dr. Jisun Im, Dr. Geoffrey Rivers, Dr. Feiran Wang, and Dr. Peng Zhao), National Physical Laboratory (Dr. Gustavo F. Trindade), and the Faculty of Medicines and Health Sciences (Prof. Clive Roberts).

● I worked with other staff to prepare the proposal and secure the grant from the Strategic Innovation Fund 2022 (£28237.52). Our project (SIF-22-07) "Are All Women Thriving and Flourishing at Nottingham?" included multiple Equality Diversity and Inclusion activities, events, and group coaching that empower women from all job families and levels. The project managers were Dr. Elizabeth Hufton and Dr. Katy McKenzie, and other collaborators included Assistant Prof. Chantal Cappelletti, Dr. Amanda Tatler, Dr. Karl Booker, Dr. Isobel O'Neil, Ella Batchelor, and Hasidah A. Hamid.

Selected development-travel grants

● University grant examples included Engineering Travel Fund (£800) – April 2023; Faculty Of Science Grant (£322.4) – May 2022; and Researcher Academy Grant (£800) – March 2021, 2022

● External grant examples included Researcher Development Grant 2022, 2023 (£1000) from the Royal Society of Chemistry – February 2022, 2023; Travel Grant (£600) from the United Kingdom Surface Analysis Forum – September 2022; and Grant from the Connected Everything Network (£500) – May 2022.

Selected prestigious honours

University awards

● Highly Commended - Team Award for Commitment to Enhancing the Research Culture and Environment – May 2023, *https://uniofnottm.sharepoint.com/sites/ResearchCultureUoN/SitePages/Working-group-findings.aspx#agency*

● Winner of the Andrew Hendry Scholarship Endowed Award – May 2023

● Winner of the Vice-Chancellor's Medal Award – December 2022

● Winner of the Covid-19 Impact Award – May 2021

National and global awards

● Winner of the RSC Inspirational Member Award 2023 – July 2023, *https://www.rsc.org/prizes-funding/prizes/2023-winners/tien-thuy-quach/*

● Finalist of the international competition RISE 2022/23 – May 2023, *https://universitas21.com/RISE-2223*

● Winner of the IAAM Young Scientist Award – April 2023

● Finalist of the Individual Achievement of the Year Award of the UK GO National Award – May 2022

● Winner of the UK Young Observer 2021, 2023 at the World Chemistry Congress – August 2021, 2023

● Regional Finalist of the Build Community and Improve Health at the Ingenuity Impact – May 2021

EXTRA CURRICULA

Academia and research

● Speaker at the "Faculty Grant Writing" Training (July 2023); Speaker at the Pharmacy Careers and Placement Exhibition (November 2022): Along with my learning and research experience, I highlighted several practical tips when applying for grants, awards, and placements to empower a range of students and researchers from different backgrounds.

● Co-mentor at the Open-source Assistive Devices Scheme (September 2021 – September 2023): I instructed and supervised 10 undergraduates and postgraduates from different backgrounds in the "Accessible lab equipment (ALE)" project aiming to make more accessible and cheaper lab equipment for disabled students.

● Writer at the PLOS Early Career Researcher Community (PLOS ECR) (May 2021 – Present): I wrote several blog examples to motivate more researchers, and some examples include *https://ecrcommunity.plos.org/2022/08/22/a-good-use-of-time-during-the-covid-19-pandemic/, and https://ecrcommunity.plos.org/2021/05/10/a-new-scientific-journey-in-a-foreign-country/.*

● Postgraduate Newsletter Editor-Writer and PhD Representative (September 2020 – September 2022); Postgraduate and Class Representative at the MSc Program (September 2018 – September 2019)

Other volunteers

● Leader-Demonstrator at the "Science In The Park 2023 (SITP23)" (March 2022 – March 2023); Leader-Speaker at the "Festival Of Science & Curiosity (FOSAC)" (February 2021 – February 2023); Inspirer at the "Inspiring Women in STEM Outreach Programme" (January 2021 – January 2023)

● Co-creator at the IOP Girlguiding "I am a physicist" to motivate over 30000 young girls to the fascinating world of physics (July 2021-Present),*https://www.iop.org/sites/default/files/2023-05/girlguiding-i-am-a-physicist-challenge-syllabus-2023.pdf*

● Skydiver to raise funding for Alzheimer's Research UK (£2350) (July 2021 – November 2021) *Donation link: https://www.justgiving.com/team/UoN-PhD-Skydivers; Skydive link: https://www.youtube.com/watch?v=tLYywoKBqXw*

● Summary of my volunteers: https://www.linkedin.com/in/tien-thuy-quach/details/volunteering-experiences/

REFERENCES

● Available on request

A2. FORMULATION

a. Resin formulation (in Ultramicrotomy)

The original formulation, ERL 4206 (VCD) – DER® 736 embedding medium devised by Spurr (1969) combined very low viscosity components for rapid specimen penetration. This embedding medium has been especially suitable for a variety of mineral and biological specimens. Since ERL 4206 is no longer available, ERL 4221 has been substituted as a replacement*. It will work well for most users but it does have somewhat higher viscosity (180cp vs. 60cp) than the ERL 4206, which can impact some protocols employing vacuum embedding.

*Reference: Ellis, E. Ann Microscopy Today, July, 33 (2006)

A block of MEDIUM hardness can be obtained by using the following formula based on a batch of 10 grams without the flexibilizer, DER 736:

Part no.	Description	Hardness Medium	Harder	Softer	Rapid
AGR1047R	ERL 4221	4.10 g			
AGR1072/73/74	DER 736 Diglycidylether of Polypropyleneglycol	1.43 g	0.95 g	1.90 g	
AGR1054/55/56	NSA (Nonenyl Succinic Anhydride) redistilled	5.90 g			
AGR1066/67	S-1 (Dimethylaminoethanol)	0.10 g			0.20 g

A harder block can be produced by decreasing the DER® 736 component to 0.95g in the above formula; a softer block by increasing the DER 736 to 1.90g.

ALL STEPS MUST BE PERFORMED UNDER A HOOD AND GLOVES MUST BE WORN FOR PROTECTION.

Preparation:
Care should be taken to weigh the ingredients accurately into a beaker. The quantities given in the first column are for firm blocks. For harder blocks, decrease the DER 736 to 0.95g; for softer blocks, increase the DER 736 to 1.90g. For rapid cure, increase the DMAE. It is recommended to add the catalyst (dimethylaminoethanol) last, after having carefully mixed the other components. If bubbles are a problem, they may be eliminated by placing the beaker into a desiccator under a gentle vacuum.

Figure A2.1. *Traditional type of resin for the sample embedment in Ultramicrotomy*

AGAR 100 Resin AGR1031

Agar 100 resin is an exact equivalent of Epon 812, except that it has a rather tighter specification which results in more reproducible epoxide equivalents.

The specification of our resin is as follows:

Resin content	99% minimum
Epoxide equivalent	145 - 160
Viscosity at 25°C	150 - 170 cps
Density at 20°C	1.22 g/ml

Embedding media based on Agar 100 resin contain the anhydride hardeners dodecenylsuccinic anhydride (DDSA) and methyl nadic anhydride (MNA), and the accelerator benzyldimethylamine (BDMA).

The following formulations will give soft, medium or hard blocks:

	Soft	Medium	Hard
Agar 100 epoxy resin	20ml (24g)	20ml (24g)	20ml (24g)
Hardener, DDSA (EM grade)	22ml (22g)	16ml (16g)	9ml (9g)
Hardener, MNA (EM grade)	5ml (6g)	8ml (10g)	12ml (15g)
Accelerator, BDMA (c. 3%)	1.4ml (1.5g)	1.3ml (1.5g)	1.2ml (1.4g)

The anhydride/epoxide ratio of all these three mixes varies between 0.7 and 0.8 as the epoxide equivalent of the Agar 100 resin varies from 145 to 160. This variation has little effect on the cutting properties of the final blocks and so the same formulations can be used with all batches of Agar 100 resin.

Figure A2.2. *New type of resin for the sample embedment*

b. Ink formulation (in ink-jet 3D-printing)

Table A2.1. The chemical structure of components forming the structural ink (SI) [279]

Tricyclo decanedinmethanol diacrylate (TCDMDA)	Ethylene glycol dicyclopentenyl ether acrylate (EGDPEA)	2,2-Dimethoxy-2-phenylacetophenone (DMPA)
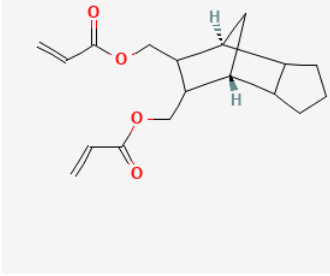	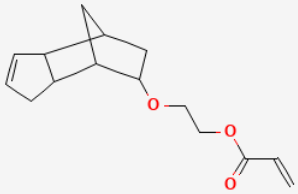	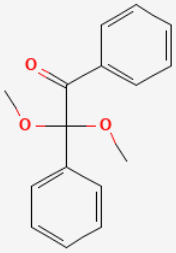

c. Final prints of interfaces of MAM

Table A2.2. Name list of single- and multiple- layered samples with pattern 1a from small to large sizes (via different deposition-curing strategies)

Single- & multiple- layered samples with square block unit of 0.5x1, 1x2, 2x4, 4x8 mm (via different deposition-curing strategies)	
23. 1a_0.5x1_1lay (S0_UV 3sec to S1_UV 3sec) 1&2 25. 1a_0.5x1_1lay (S1_UV 3sec to S0_UV 3sec) 1&2 27. 1a_0.5x1_1lay (S0_UV 0sec to S1_UV 3sec) 28. 1a_0.5x1_1lay (S1_UV 0sec to S0_UV 3sec)	68. 1a_0.5x1_2lay (S0_UV 3sec-each to S1_UV 3sec-each) 69. 1a_0.5x1_2lay (S1_UV 3sec-each to S0_UV 3sec-each) 70. 1a_0.5x1_2lay (S0_UV 0sec-each to S1_UV 3sec-each) 71. 1a_0.5x1_2ay (S1_UV 0sec to S0_UV 3sec)
2. 1a_1x2_1lay (S0_UV 3sec to S1_UV 3sec) 56. 1a_1x2_1lay (S1_UV 3sec to S0_UV 3sec) 1. 1a_1x2_1lay (S0_UV 0sec to S1_UV 3sec) 57. 1a_1x2_1lay (S1_UV 0sec to S0_UV 3sec)	65. 1a_1x2_2lay (S0_UV 3sec-each to S1_UV 3sec-each) 7. 1a_1x2_2lay (S1_UV 3sec-each to S0_UV 3sec-each) 66. 1a_1x2_2lay (S0_UV 0sec-each to S1_UV 3sec-each) 6. 1a_1x2_2lay (S1_UV 3sec-each to S0_UV 0sec-each)
13. 1a_2x4_1lay (S0_UV 3sec to S1_UV 3sec) 14. 1a_2x4_1lay (S1_UV 3sec to S0_UV 3sec) 15. 1a_2x4_1lay (S0_UV 0sec to S1_UV 3sec) 16. 1a_2x4_1lay (S1_UV 0sec to S0_UV 3sec)	61. 1a_2x4_2lay (S0_UV 3sec-each to S1_UV 3sec-each) 62. 1a_2x4_2lay (S1_UV 3sec-each to S0_UV 3sec-each) 63. 1a_2x4_2lay (S0_UV 0sec-each to S1_UV 3sec-each) 64. 1a_2x4_2lay (S1_UV 0sec-each to S0_UV 3sec-each)
17. 1a_4x8_1lay (S0_UV 3sec to S1_UV 3sec) 18. 1a_4x8_1lay (S1_UV 3sec to S0_UV 3sec) 21. 1a_4x8_1lay (S0_UV 0sec to S1_UV 3sec) 22. 1a_4x8_1lay (S1_UV 0sec to S0_UV 3sec)	29. 1a_4x8_2lay (S0_UV 3sec-each to S1_UV 3sec-each) 33. 1a_4x8_2lay (S1_UV 3sec-each to S0_UV 3sec-each) 35. 1a_4x8_2lay (S0_UV 0sec-each to S1_UV 3sec-each) 34. 1a_4x8_2lay (S1_UV 0sec-each to S0_UV 3sec-each)
Repeat 58. 1a_4x8_1lay (S0_UV 3sec to S1_UV 3sec)_5Noz 59. 1a_4x8_1lay (S1_UV 3sec to S0_UV 3sec)_5Noz 36. 1a_4x8_1lay (S0_UV 0sec to S1_UV 3sec-each) 37. 1a_4x8_1lay (S1_UV 0sec to S0_UV 3sec-each)	Repeat: 32i. 1a_4x8_2lay (S0_UV 3sec-each to S1_UV 3sec-each) 30. 1a_4x8_2lay (S1_UV 3sec-each to S0_UV 3sec-each) 31. 1a_4x8_2lay (S0_UV 0sec-each to S1_UV 3sec-each) 60. 1a_4x8_1lay (S1_UV 0sec-each to S0_UV 3sec-each)

Table A2.3. Co-printing of WI and SI with pattern 1a_size 0.5x1 mm_single layer (via different deposition-curing strategies) as samples 23, 25, 27, 28

Sample	Screen-capturing	Screen-capturing (with a new embeded coding)
23. 1a_0.5x1_1lay (S0_UV 3sec to S1_UV 3sec) 1&2		
25. 1a_0.5x1_1lay (S1_UV 3sec to S0_UV 3sec) 1&2		
27. 1a_0.5x1_1lay (S0_UV 0sec to S1_UV 3sec)		
28. 1a_0.5x1_1lay (S1_UV 0sec to S0_UV 3sec)		

Table A2.4. Co-printing of WI and SI with pattern 1a_size 0.5x1 mm_multiple layers (via different deposition-curing strategies) as samples 68, 69, 70, 71

Sample	Screen-capturing	Screen-capturing (with a new embeded coding)
68. 1a_0.5x1_2lay (S0_UV 3sec to S1_UV 3sec)	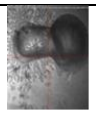	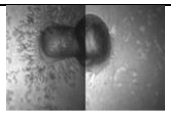
69. 1a_0.5x1_2lay (S1_UV 3sec to S0_UV 3sec)	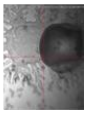	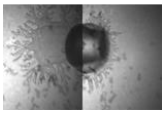
70. 1a_0.5x1_2lay (S0_UV 0sec to S1_UV 3sec)		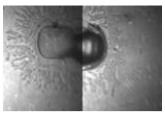
71. 1a_0.5x1_2ay (S1_UV 0sec to S0_UV 3sec)	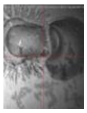	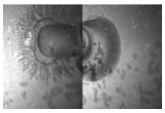

Table A2.5. Co-printing of WI and SI with pattern 1a_size 1x2 mm_single layer (via different deposition-curing strategies) as samples 2, 56, 1, 57

2. 1a_1x2_1lay (S0_UV 3sec to S1_UV 3sec) 56. 1a_1x2_1lay (S1_UV 3sec to S0_UV 3sec) 1. 1a_1x2_1lay (S0_UV 0sec to S1_UV 3sec) 57. 1a_1x2_1lay (S1_UV 0sec to S0_UV 3sec)	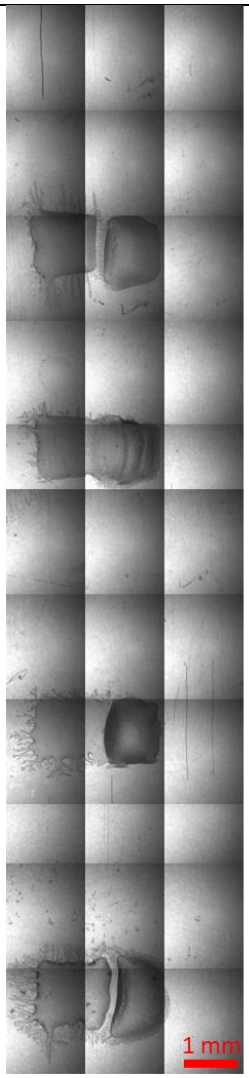

Table A2.6. Co-printing of WI and SI with pattern 1a_size 1x2 mm_multiple layers (via different deposition-curing strategies) as samples 65, 7, 66, 6

65. 1a_1x2_2lay (S0_UV 3sec to S1_UV 3sec) 7. 1a_1x2_2lay (S1_UV 3sec to S0_UV 3sec) 66. 1a_1x2_2lay (S0_UV 0sec to S1_UV 3sec) 6. 1a_1x2_2lay (S1_UV 3sec to S0_UV 0sec)	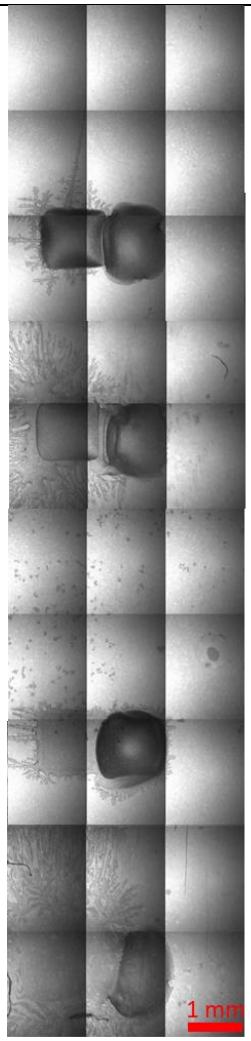

Table A2.7. Co-printing of WI and SI with pattern 1a_size 2x4 mm_single layer (via different deposition-curing strategies) as samples 13, 14, 15, 16

13. 1a_2x4_1lay (S0_UV 3sec to S1_UV 3sec) 14. 1a_2x4_1lay (S1_UV 3sec to S0_UV 3sec) 15. 1a_2x4_1lay (S0_UV 0sec to S1_UV 3sec) 16. 1a_2x4_1lay (S1_UV 0sec to S0_UV 3sec)	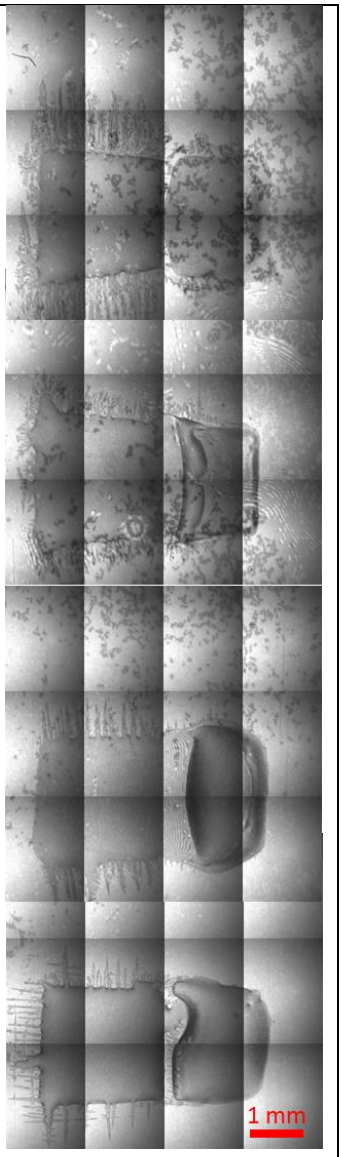

Table A2.8. Co-printing of WI and SI with pattern 1a_size 2x4 mm_multiple layers (via different deposition-curing strategies) as samples 61, 62, 63, 64

61. 1a_2x4_2lay (S0_UV 3sec to S1_UV 3sec) 62. 1a_2x4_2lay (S1_UV 3sec to S0_UV 3sec) 63. 1a_2x4_2lay (S0_UV 0sec to S1_UV 3sec) 64. 1a_2x4_2lay (S1_UV 0sec to S0_UV 3sec)	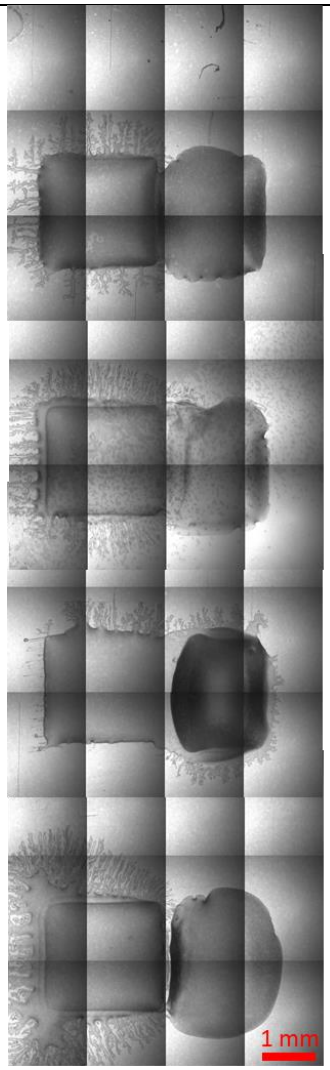

Table A2.9. Co-printing of WI and SI with pattern 1a_size 4x8 mm_single layer (via different deposition-curing strategies) as samples 17, 18, 21, 22

17. 1a_4x8_1lay (S0_UV 3sec to S1_UV 3sec) 18. 1a_4x8_1lay (S1_UV 3sec to S0_UV 3sec) 21. 1a_4x8_1lay (S0_UV 0sec to S1_UV 3sec) 22. 1a_4x8_1lay (S1_UV 0sec to S0_UV 3sec)	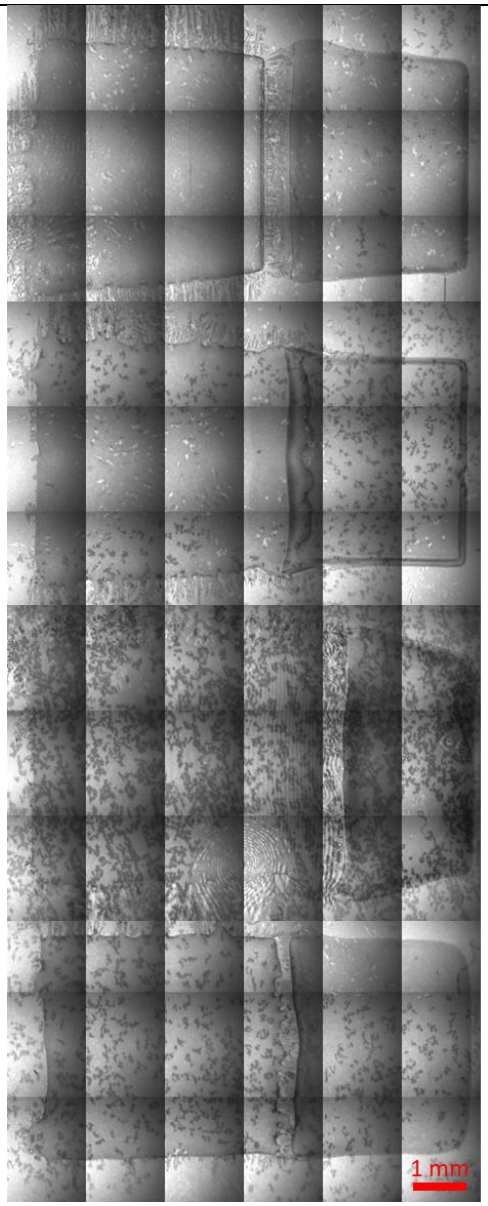

Table A2.10. Co-printing of WI and SI with pattern 1a_size 4x8 mm_single layer (via different deposition-curing strategies) as samples 29, 33, 35, 34

29. 1a_4x8_2lay (S0_UV 3sec-each to S1_UV 3sec-each) 33. 1a_4x8_2lay (S1_UV 3sec-each to S0_UV 3sec-each) 35. 1a_4x8_2lay (S0_UV 0sec-each to S1_UV 3sec-each) 34. 1a_4x8_2lay (S1_UV 0sec-each to S0_UV 3sec-each)	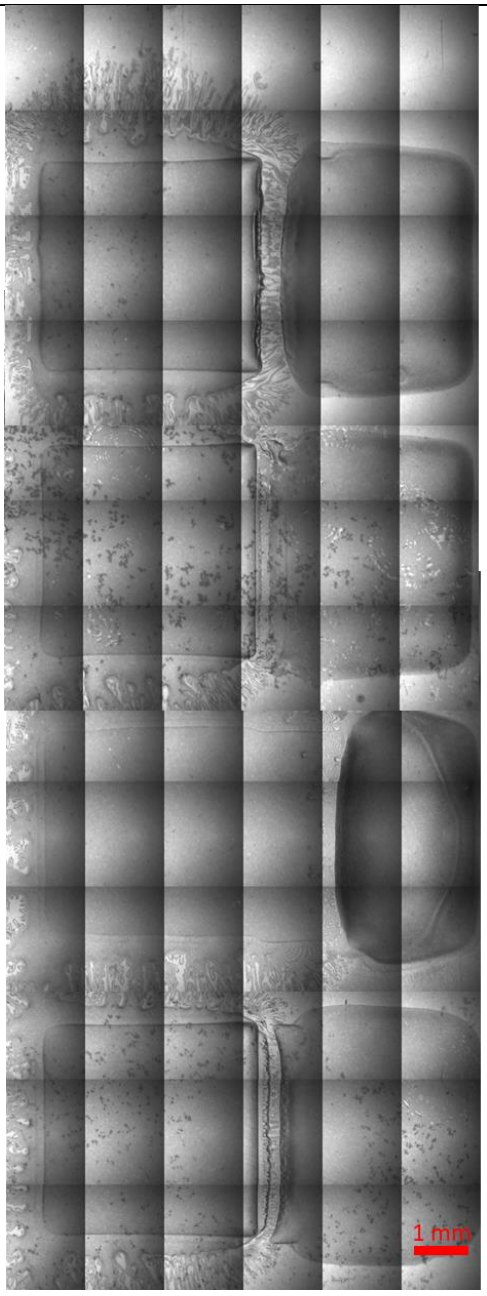

Table A2.11. Co-printing of WI and SI with pattern 1a_size 4x8 mm_single layer (via different deposition-curing strategies) as samples 58, 59, 36, 37 to evaluate the repeatability

Repeatability	
58. 1a_4x8_1lay (S0_UV 3sec to S1_UV 3sec)_5Noz 59. 1a_4x8_1lay (S1_UV 3sec to S0_UV 3sec)_5Noz 36. 1a_4x8_1lay (S0_UV 0sec-each to S1_UV 3sec-each) 37. 1a_4x8_1lay (S1_UV 0sec-each to S0_UV 3sec-each)	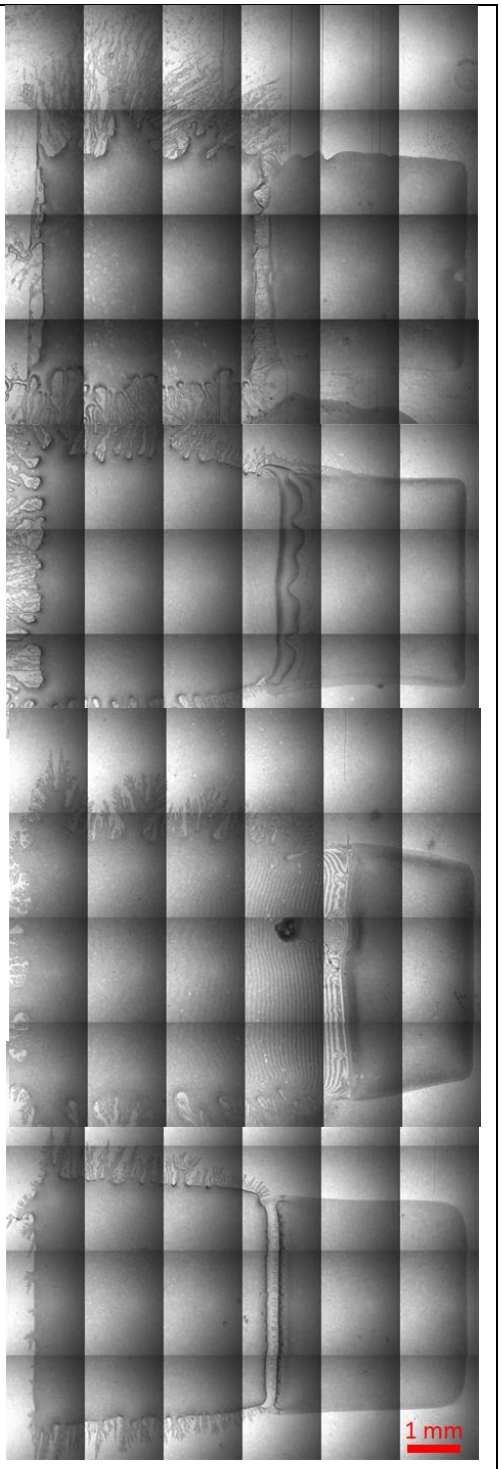

Table A2.12. Co-printing of WI and SI with pattern 1a_size 4x8 mm_single layer (via different deposition-curing strategies) as samples 32i, 30, 31, 60 to evaluate the repeatability

Repeatability	
32i. 1a_4x8_2lay (S0_UV 3sec-each to S1_UV 3sec-each) 30. 1a_4x8_2lay (S1_UV 3sec-each to S0_UV 3sec-each) 31. 1a_4x8_2lay (S0_UV 0sec-each to S1_UV 3sec-each) 60. 1a_4x8_1lay (S1_UV 0sec to S0_UV 3sec)_5Noz	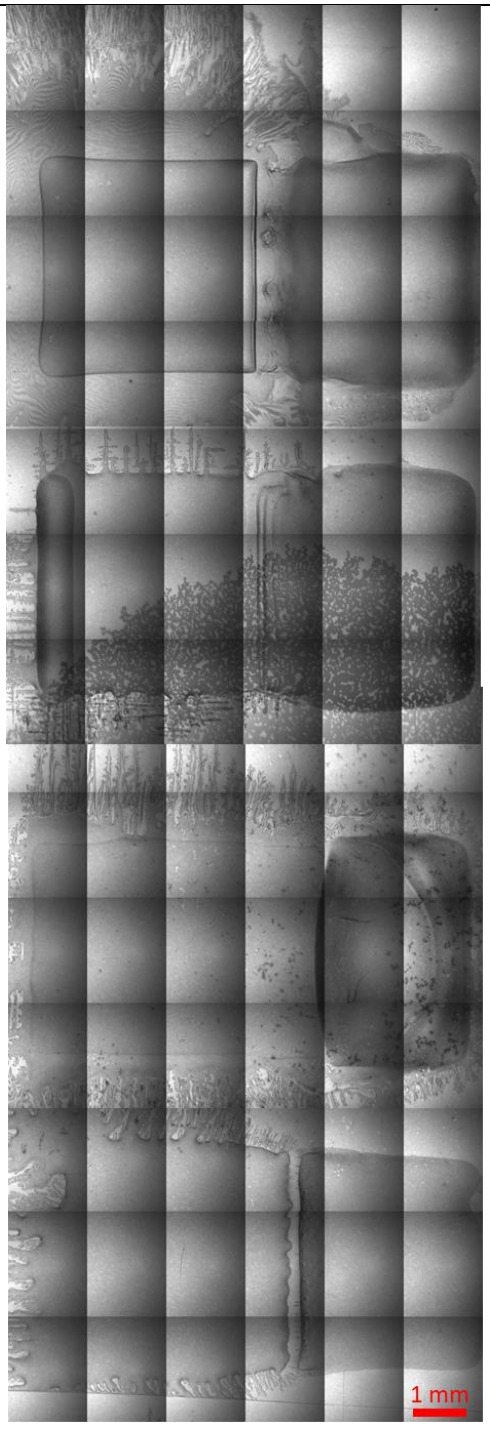

Table A2.13. Co-printing of WI and SI with pattern 1b_size 4x8 mm (via different deposition-curing strategies which correlated to Table 6.3): i) single layer (samples 75, 76, 78, 79); and ii) two layer (samples 80, 81, 82, 84)

75. 1b_4x8_1lay (S0_UV 3sec to S1_UV 3sec) 76. 1b_4x8_1lay (S1_UV 3sec to S0_UV 3sec) 78. 1b_4x8_1lay (S0_UV 0sec to S1_UV 3sec) 79. 1b_4x8_1lay (S1_UV 0sec to S0_UV 3sec)	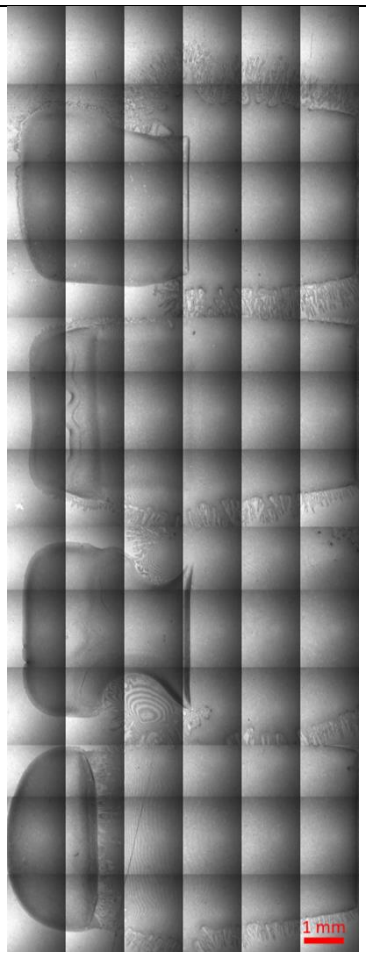
80. 1b_4x8_2lay (S0_UV 3sec-each to S1_UV 3sec-each) 81. 1b_4x8_2lay (S1_UV 3sec-each to S0_UV 3sec-each) 82. 1b_4x8_2lay (S0_UV 0sec-each to S1_UV 3sec-each) 84. 1b_4x8_2lay (S1_UV 0sec-each to S0_UV 3sec-each)	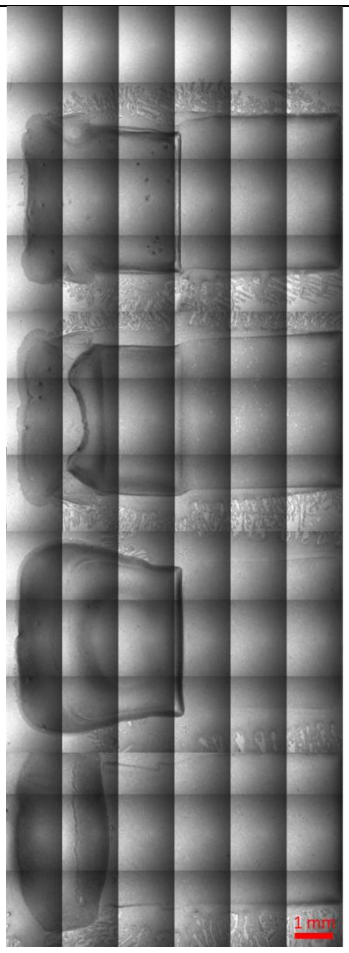

A3. CHARACTERISATION

a. NMR spectra

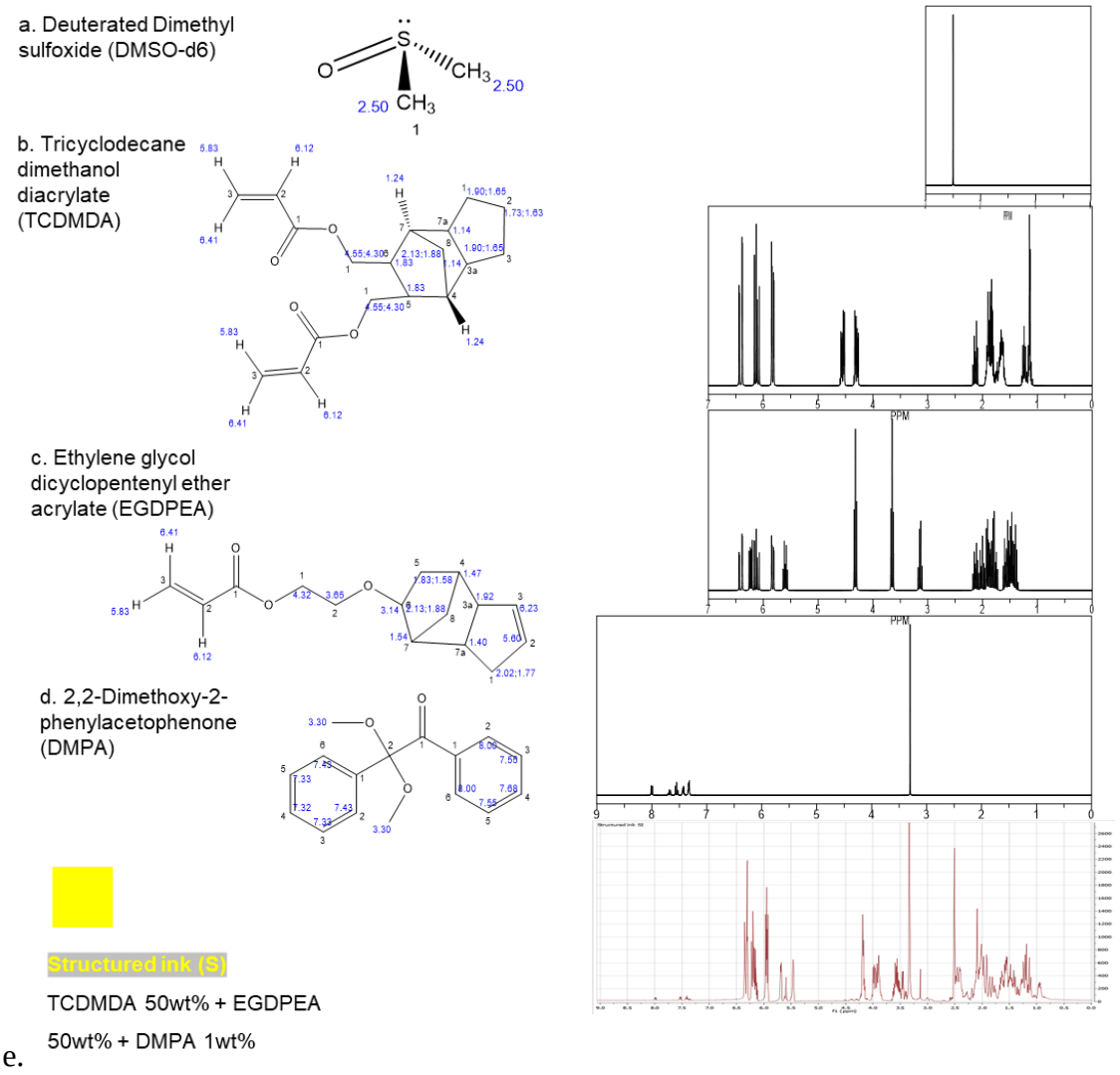

Figure A3.1. *^{1}H-NMR shifts of SI and its components*

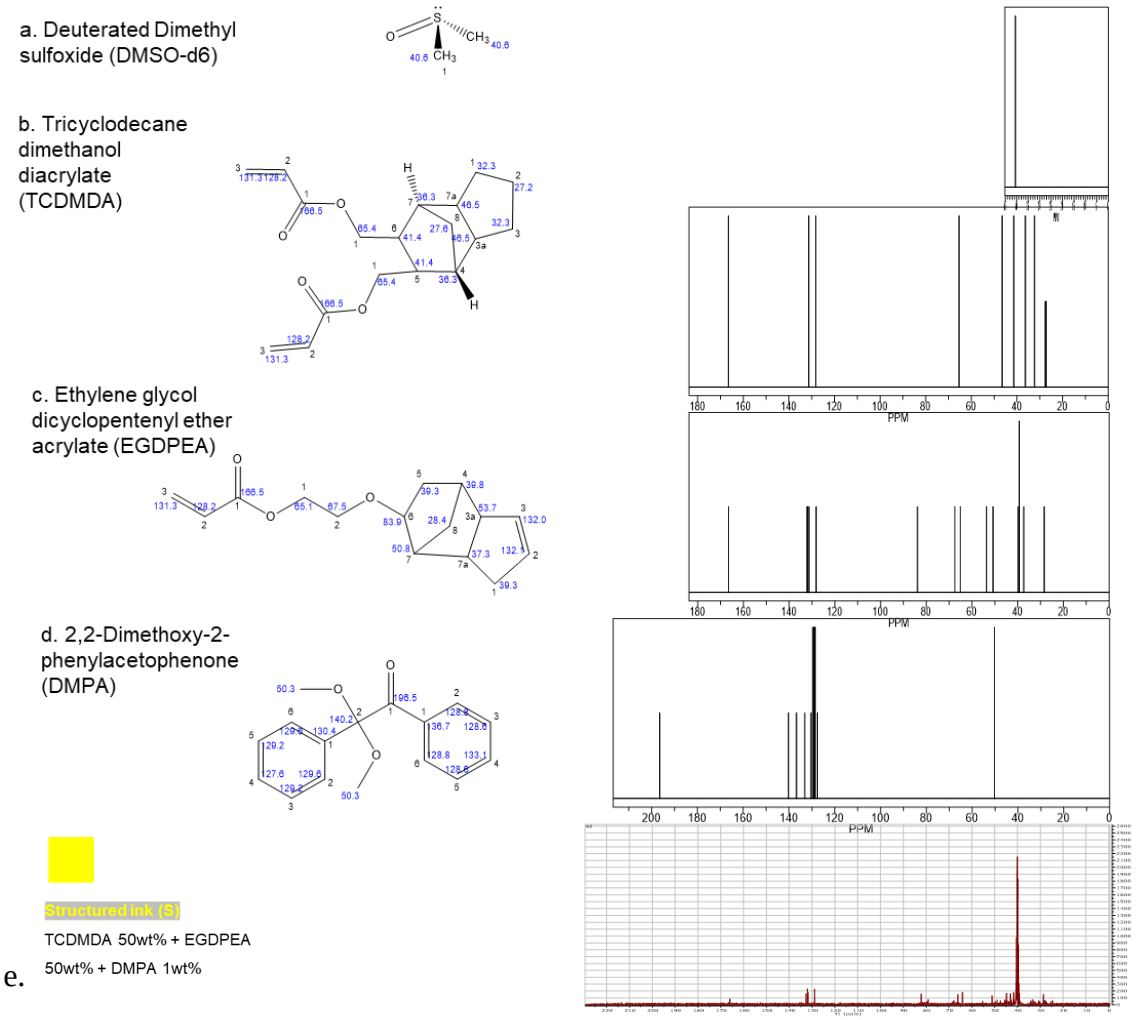

Figure A3.2. *^{13}C-NMR shifts of SI and its components*

b. ToF-SIMS images and linescans

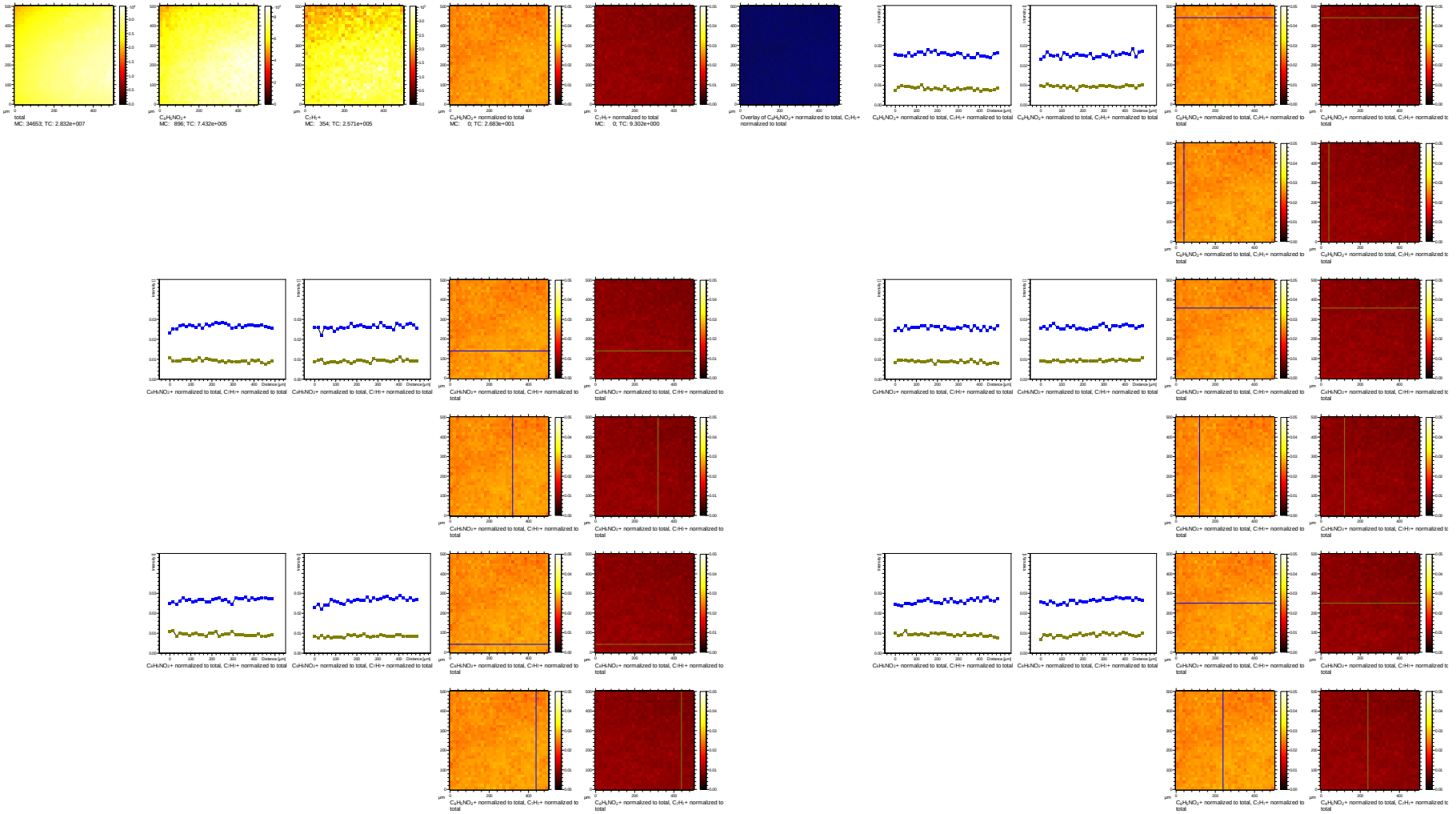

Figure A3.3. *ToF-SIMS results with small area 500x500 µm of sample WI 1*

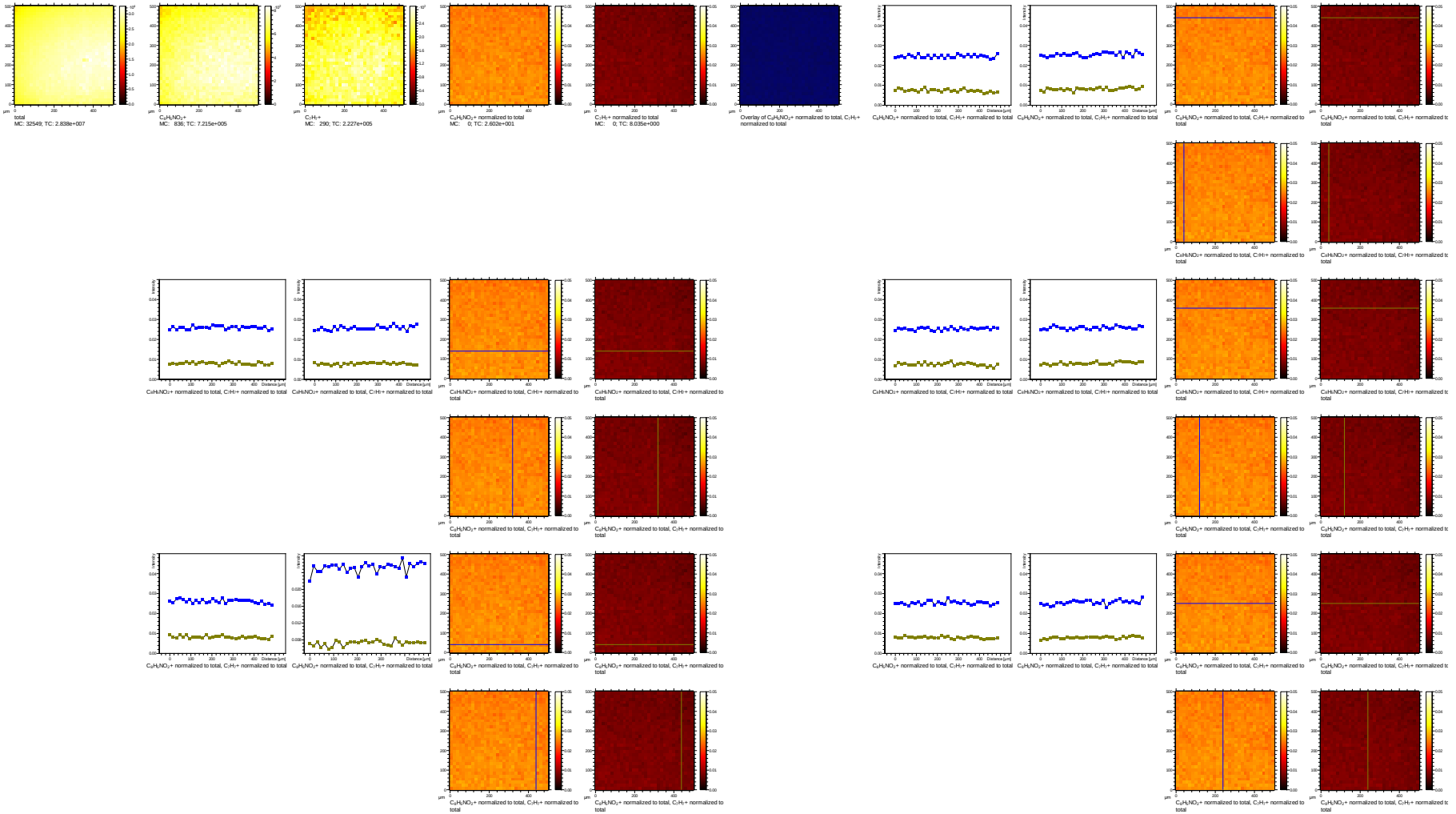

Figure A3.4. *ToF-SIMS results with small area 500x500 µm of sample WI 2*

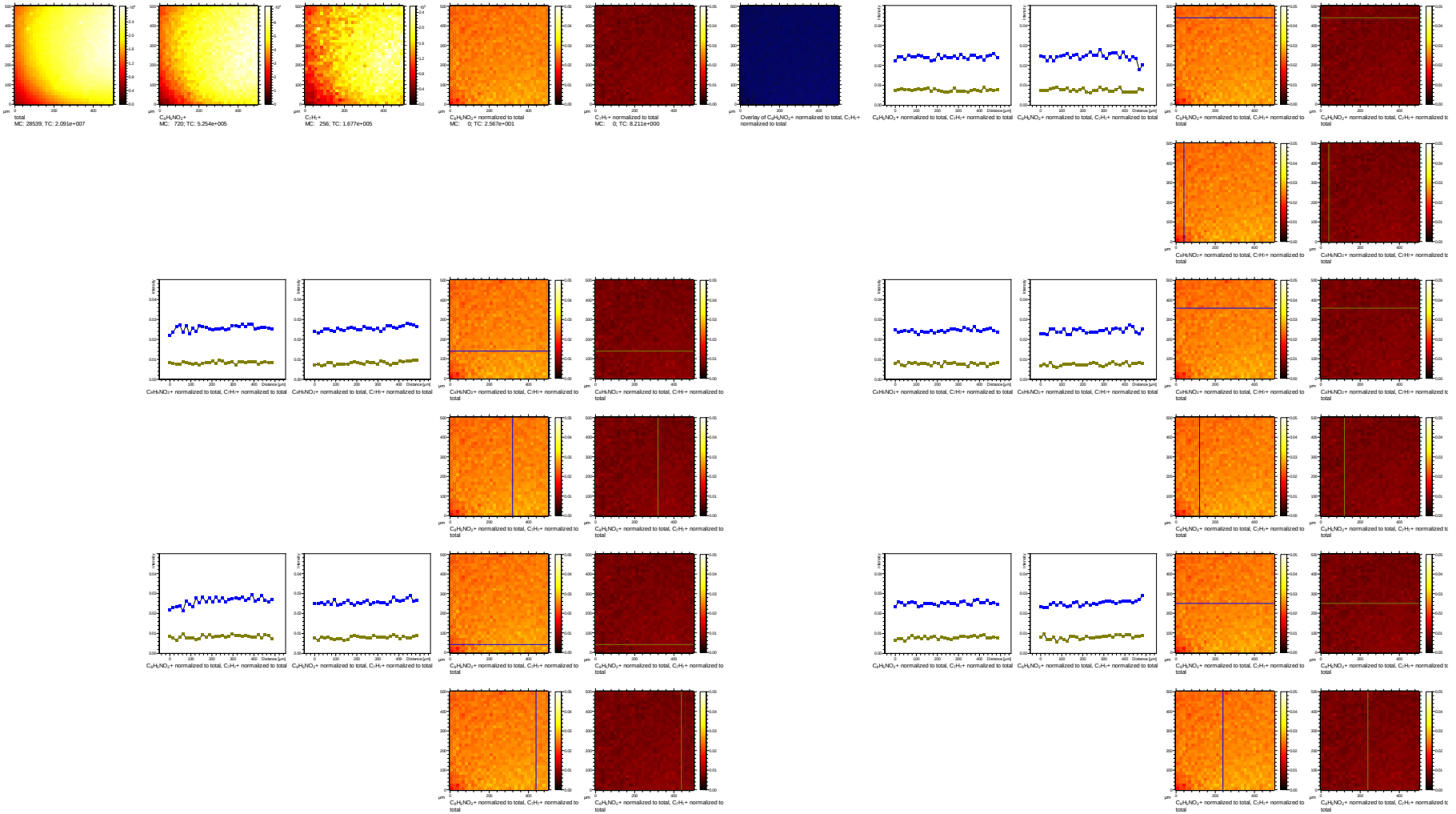

Figure A3.5. *ToF-SIMS results with small area 500x500 µm of sample WI 3*

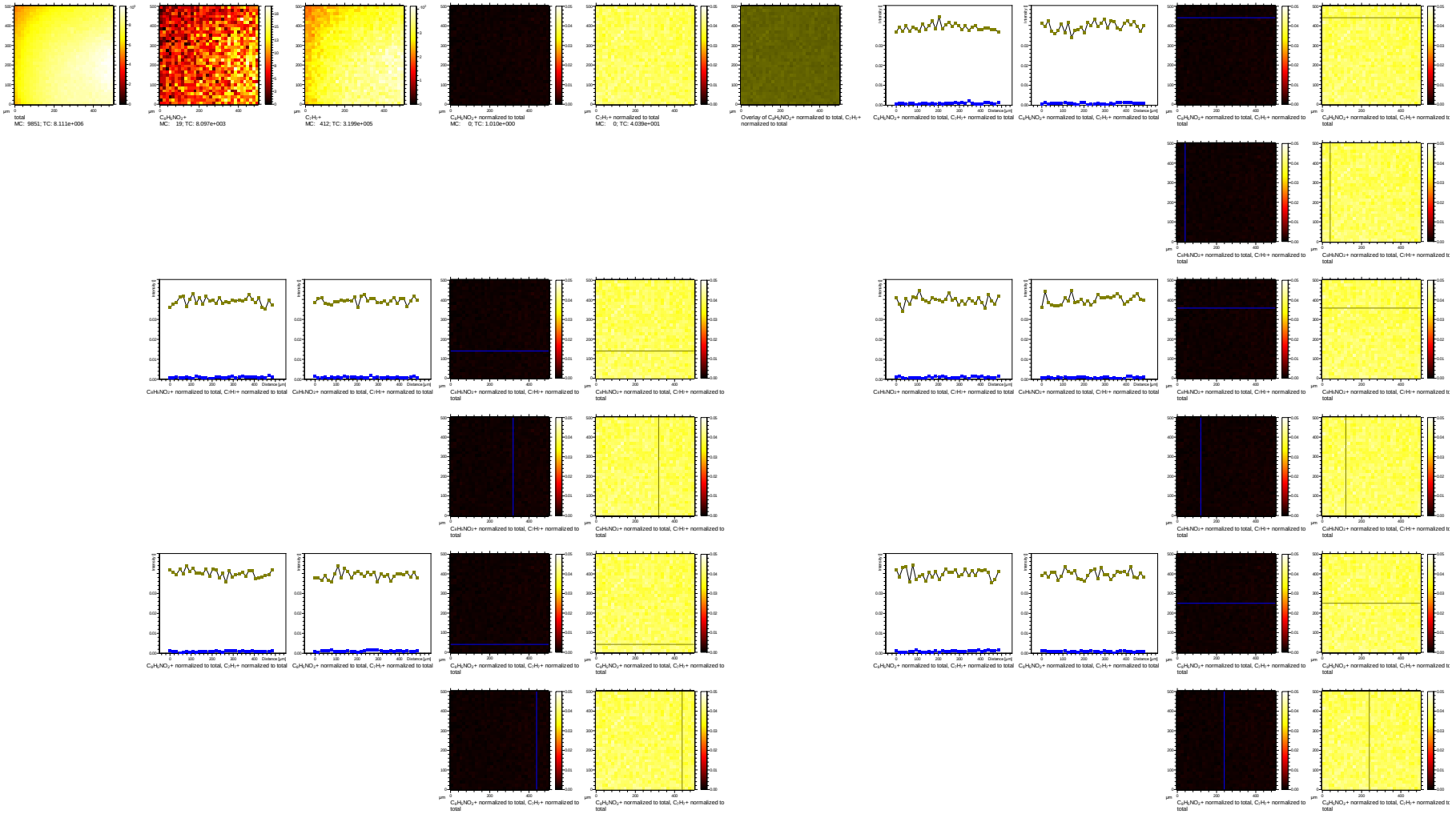

Figure A3.6. *ToF-SIMS results with small area 500x500 µm of sample SI 1*

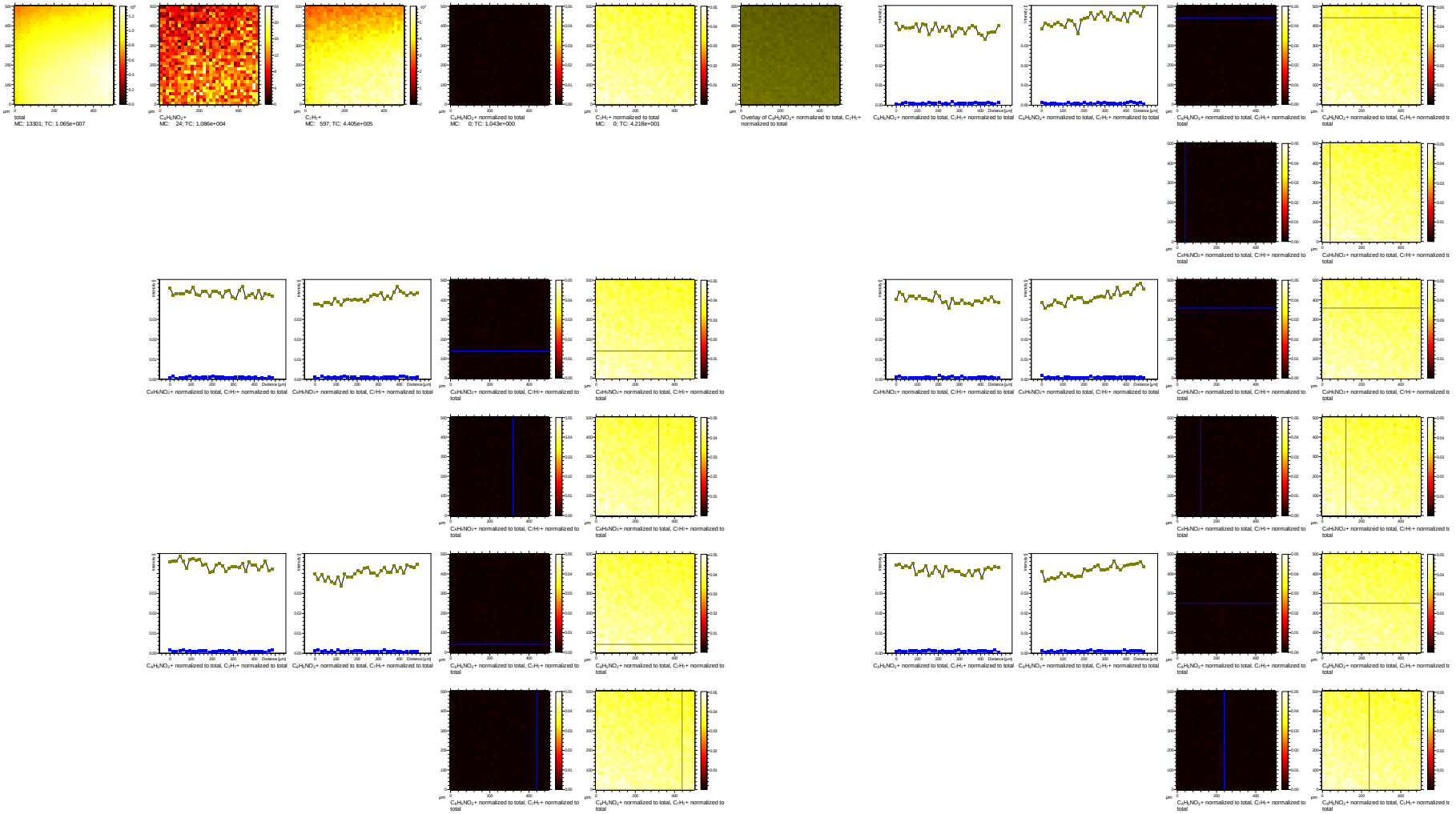

Figure A3.7. *ToF-SIMS results with small area 500x500 µm of sample SI 2*

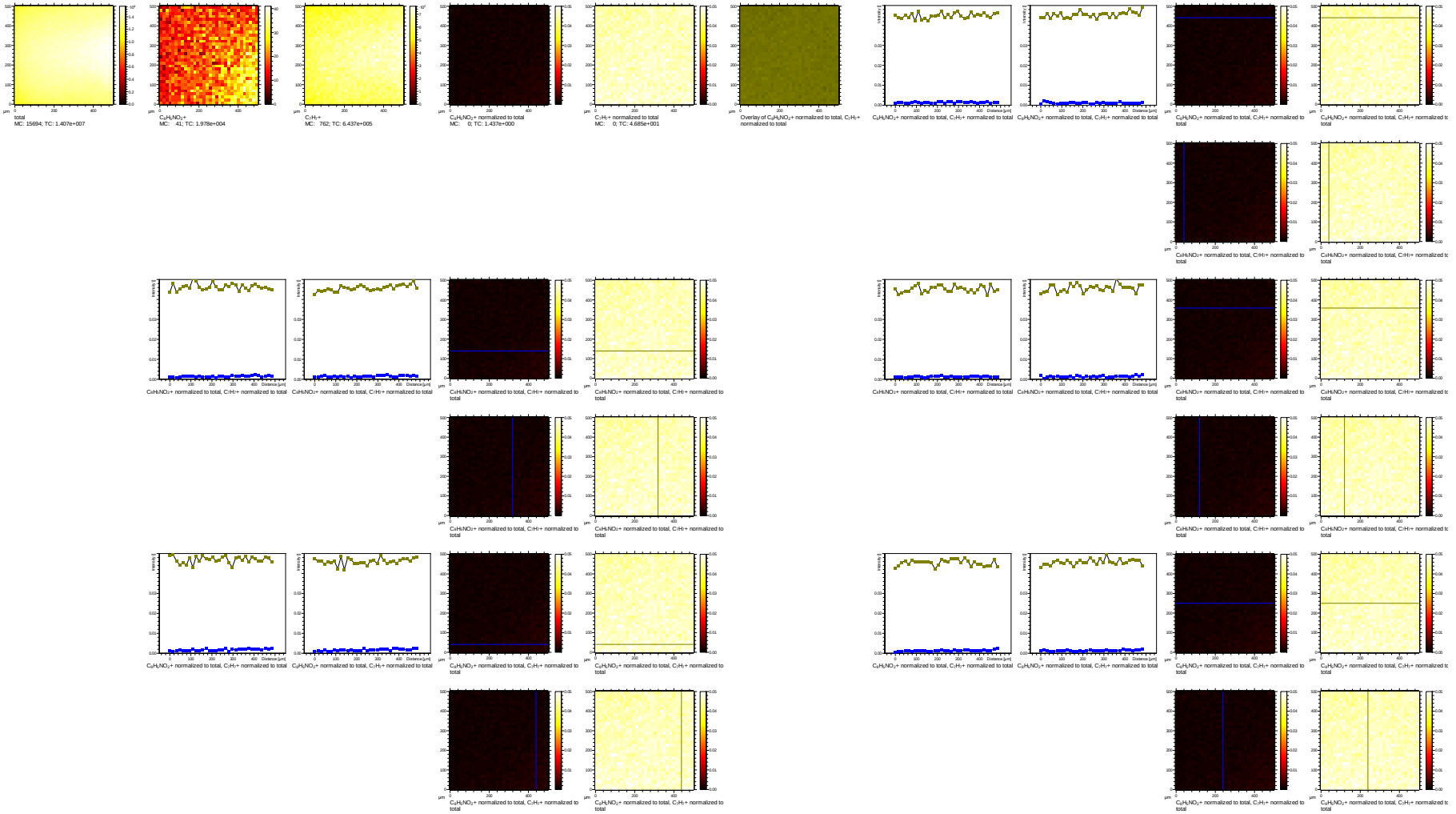

Figure A3.8. *ToF-SIMS results with small area 500x500 µm of sample SI 3*

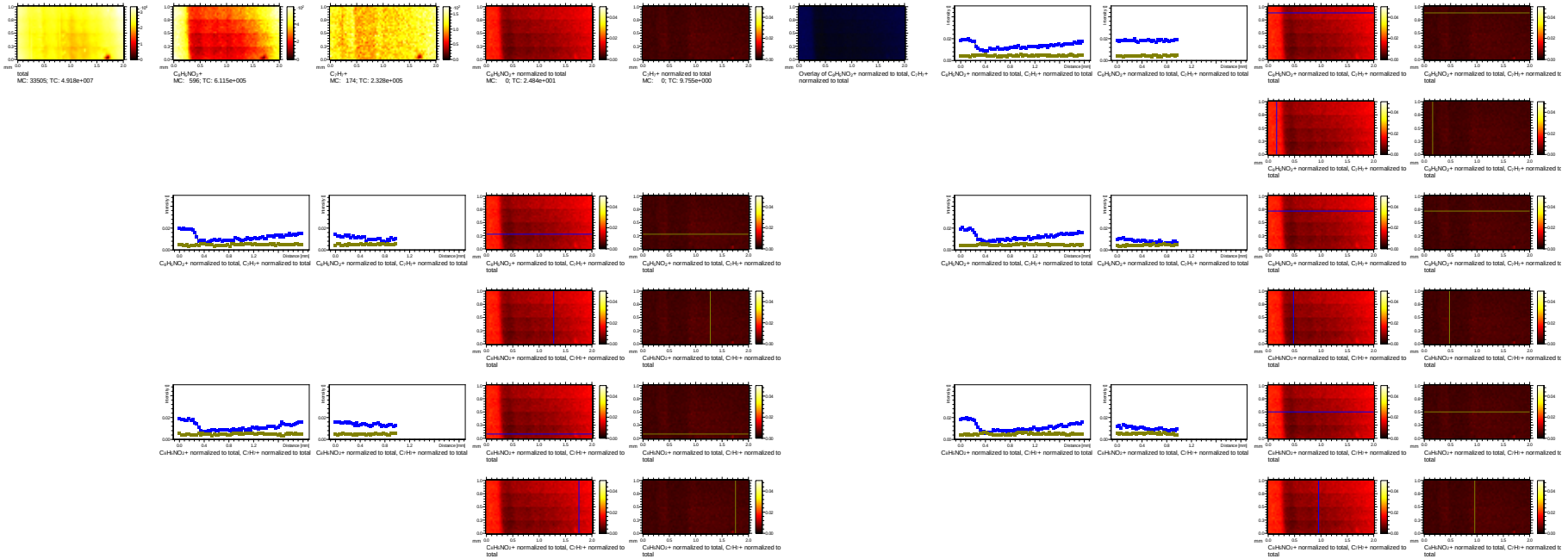

Figure A3.9. *ToF-SIMS results with large area 1x2mm of sample 17*

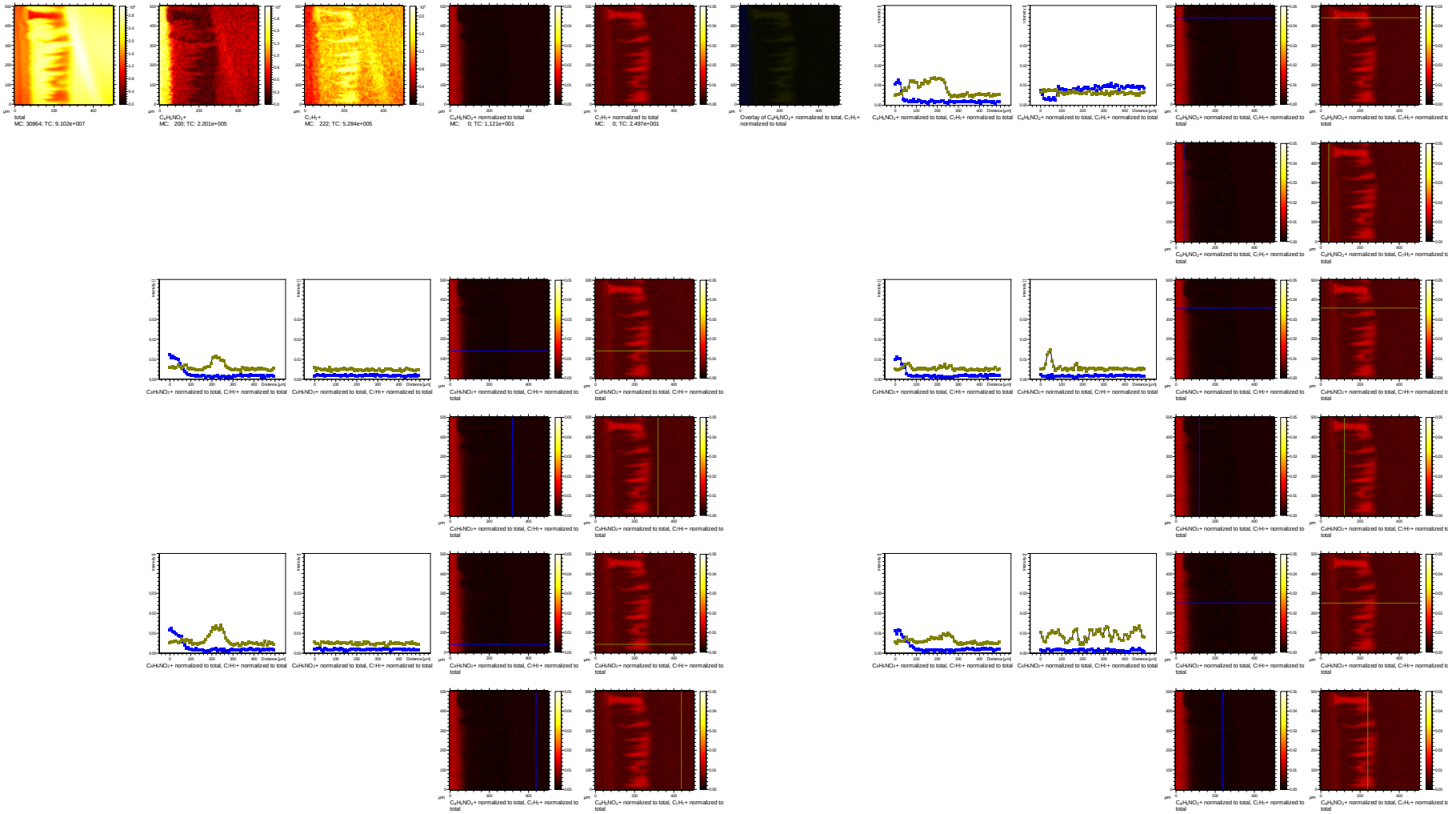

Figure A3.10. *ToF-SIMS results with small area 500x500 µm of sample 17*

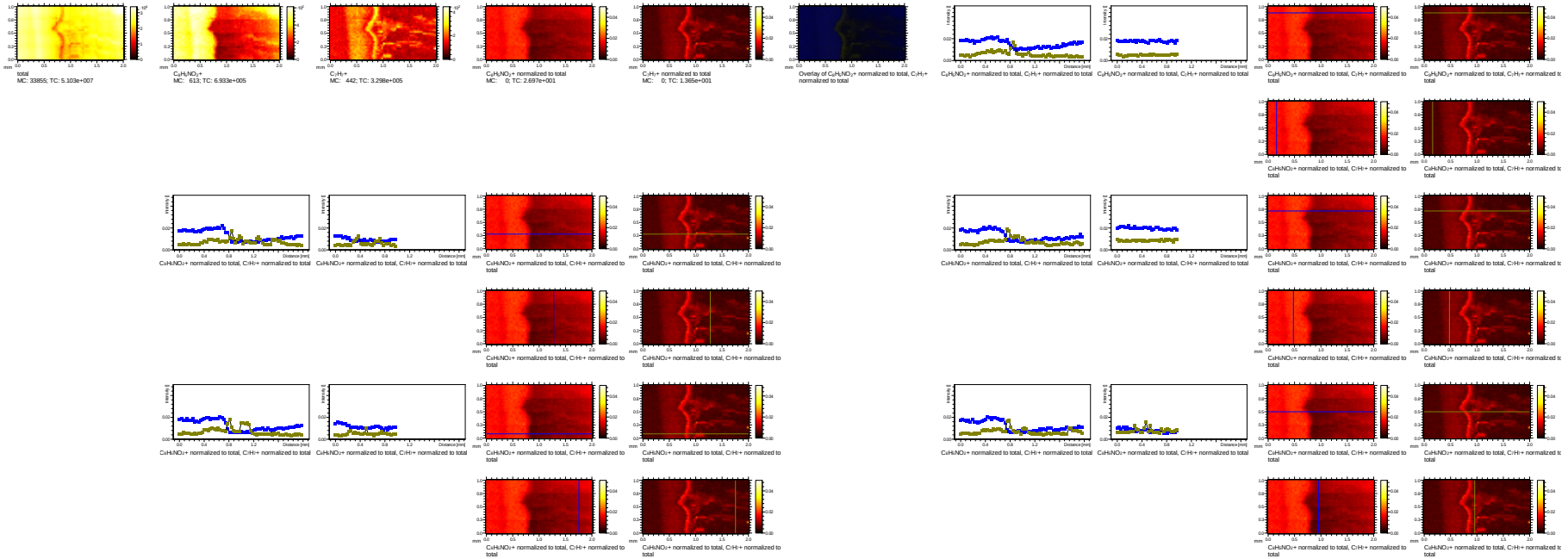

Figure A3.11. *ToF-SIMS results with large area 1x2mm of sample 18*

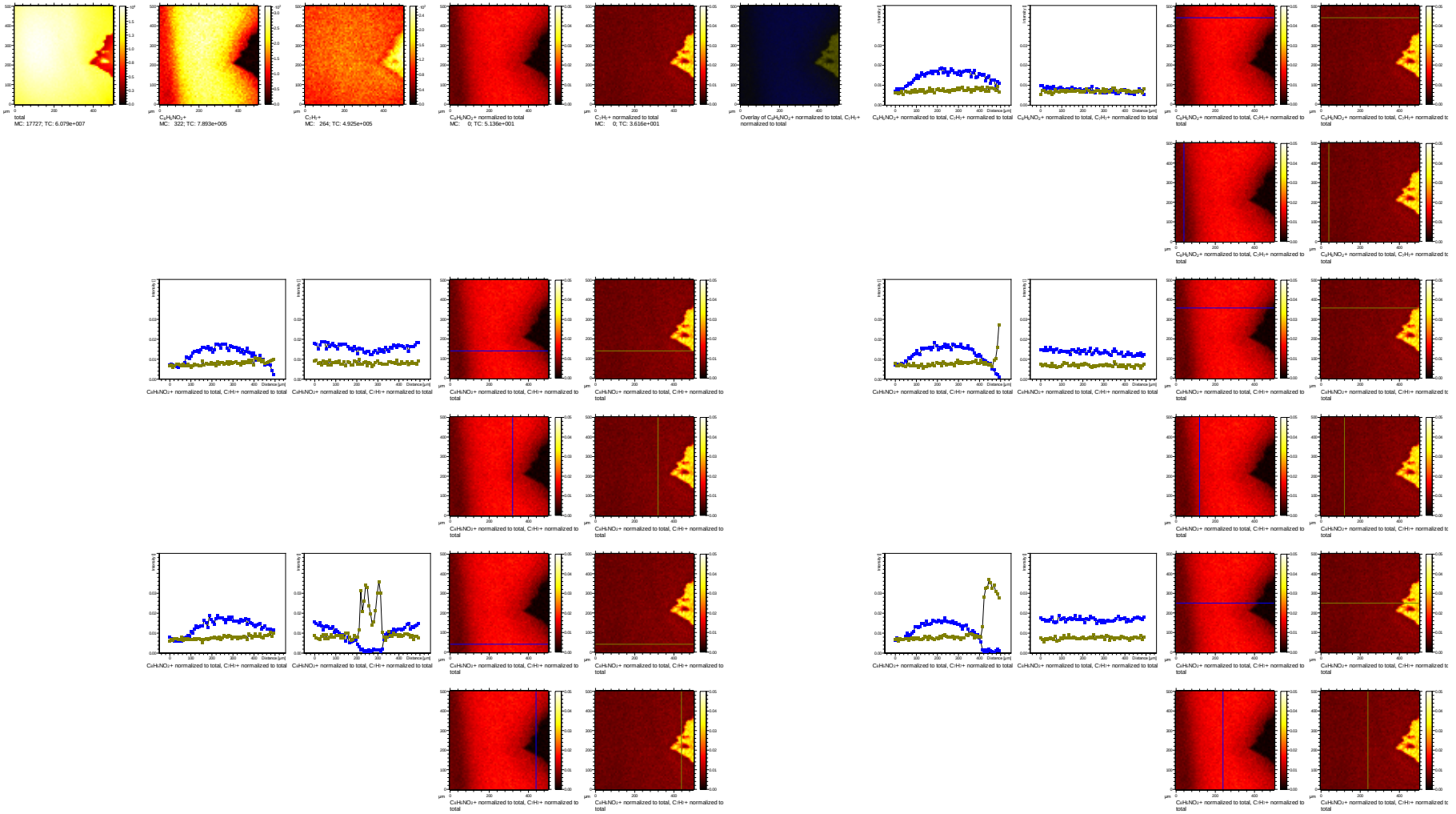

Figure A3.12. *ToF-SIMS results with small area 500x500 µm of sample 18*

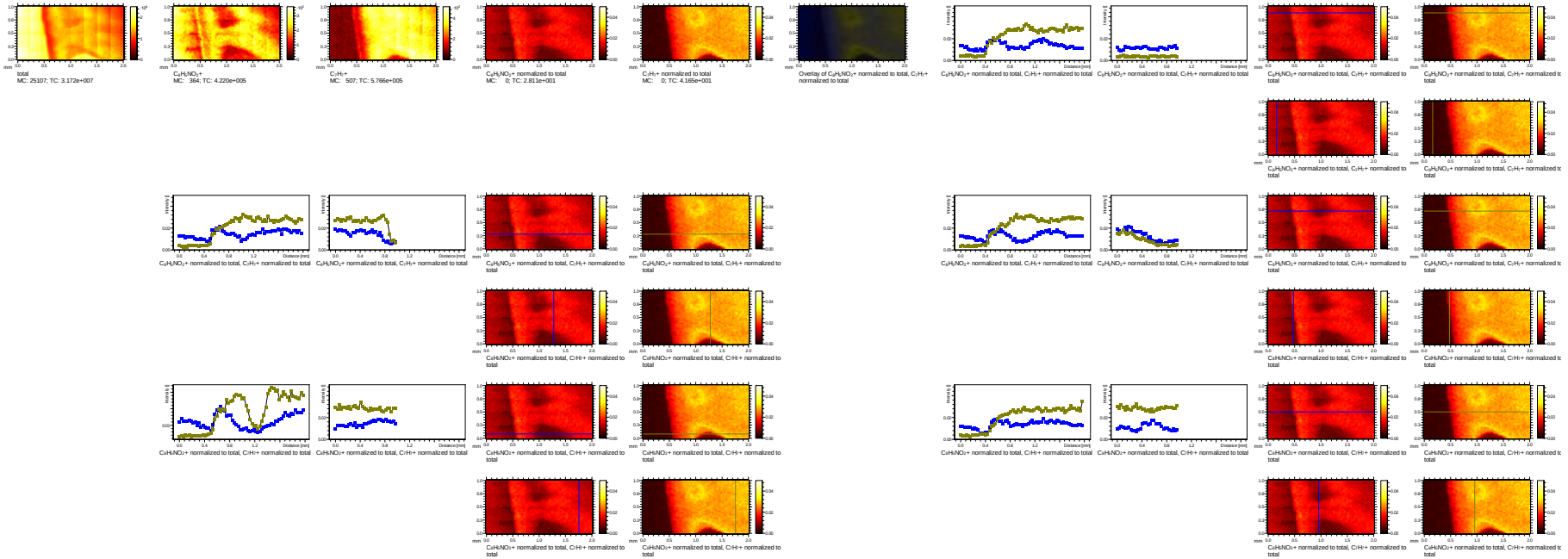

Figure A3.13. *ToF-SIMS results with large area 1x2 mm of sample 21*

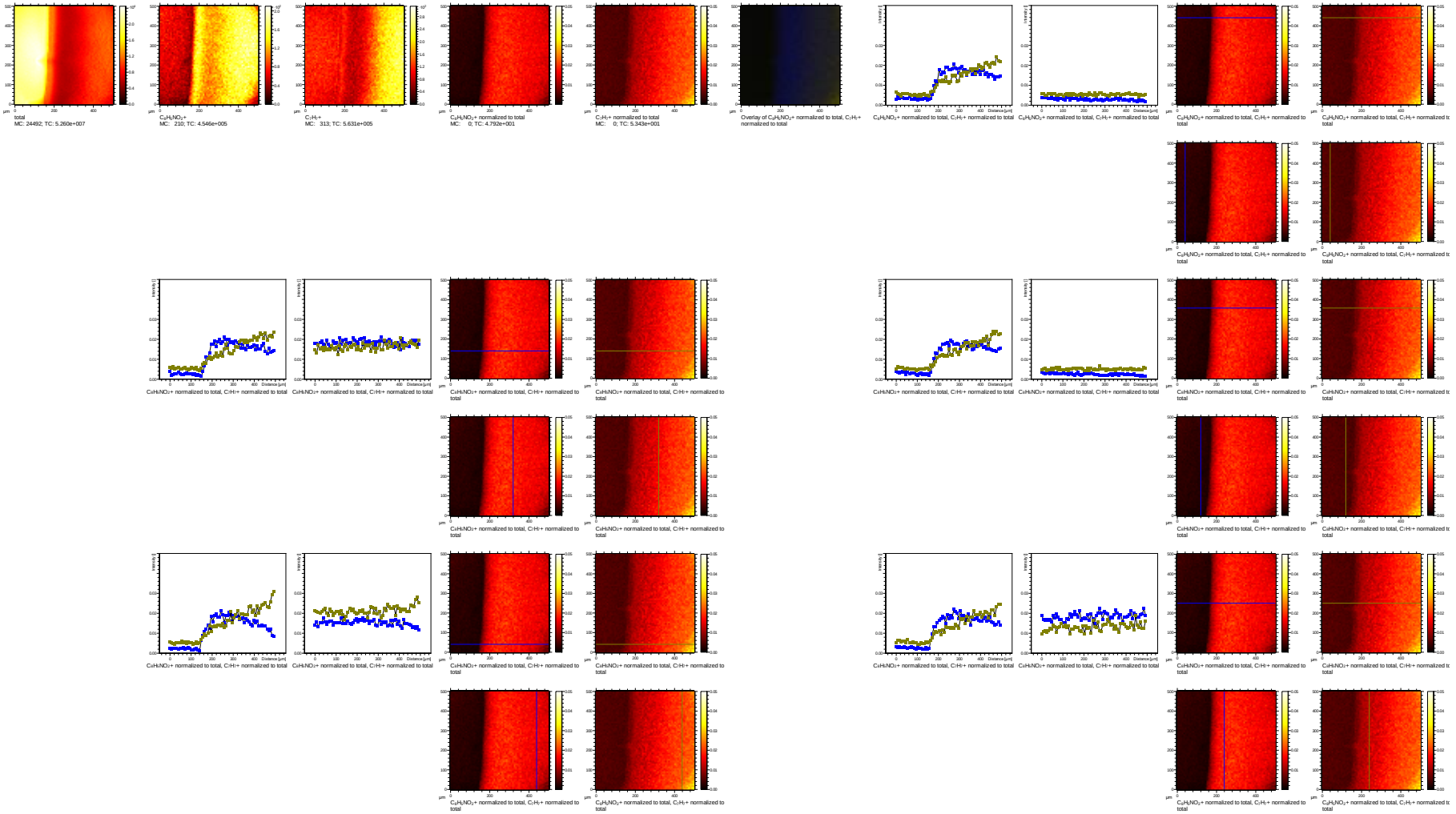

Figure A3.14. *ToF-SIMS results with small area 500x500 µm of sample 21*

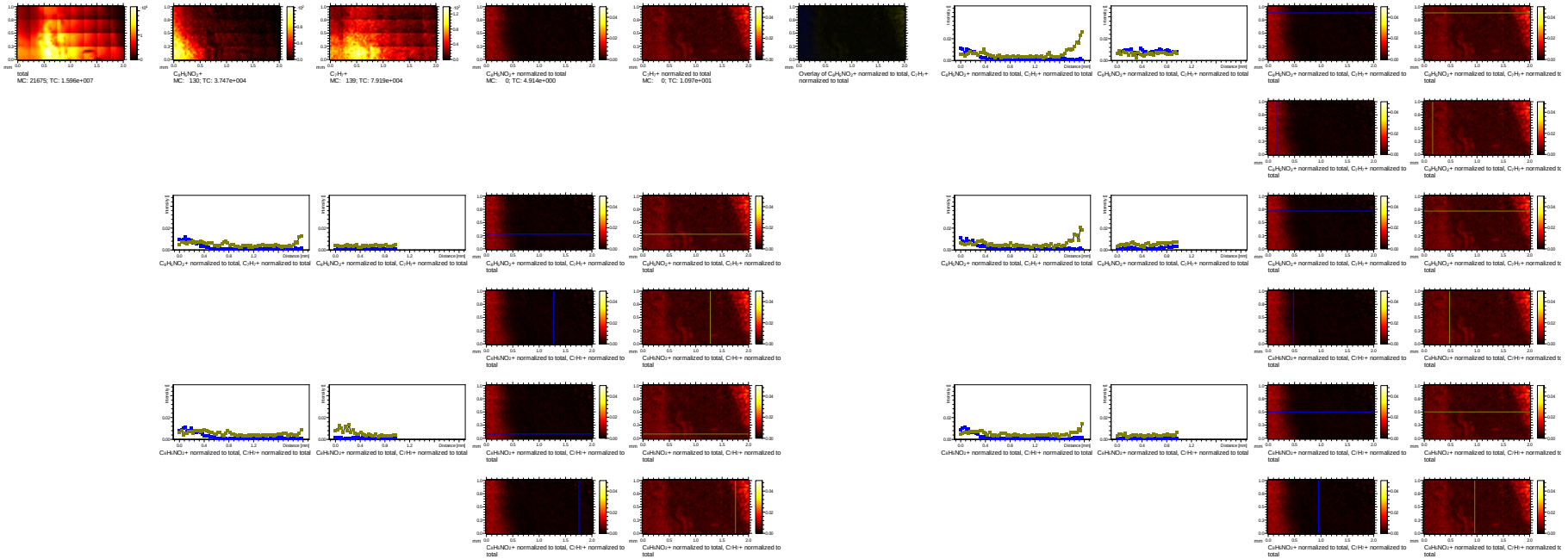

Figure A3.15. *ToF-SIMS results with large area 1x2 mm of sample 22*

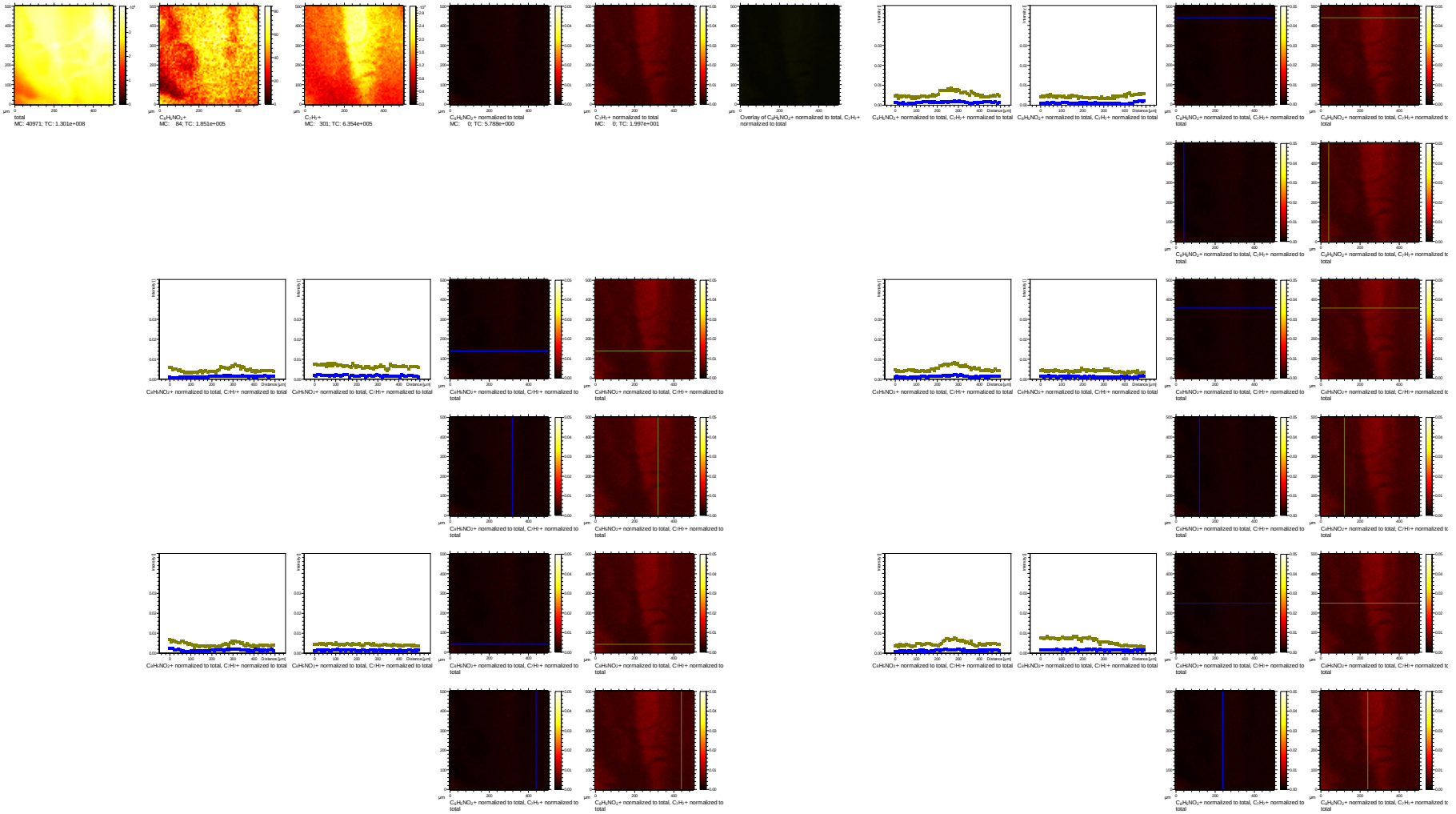

Figure A3.16. *ToF-SIMS results with small area 500x500 µm of sample 22*

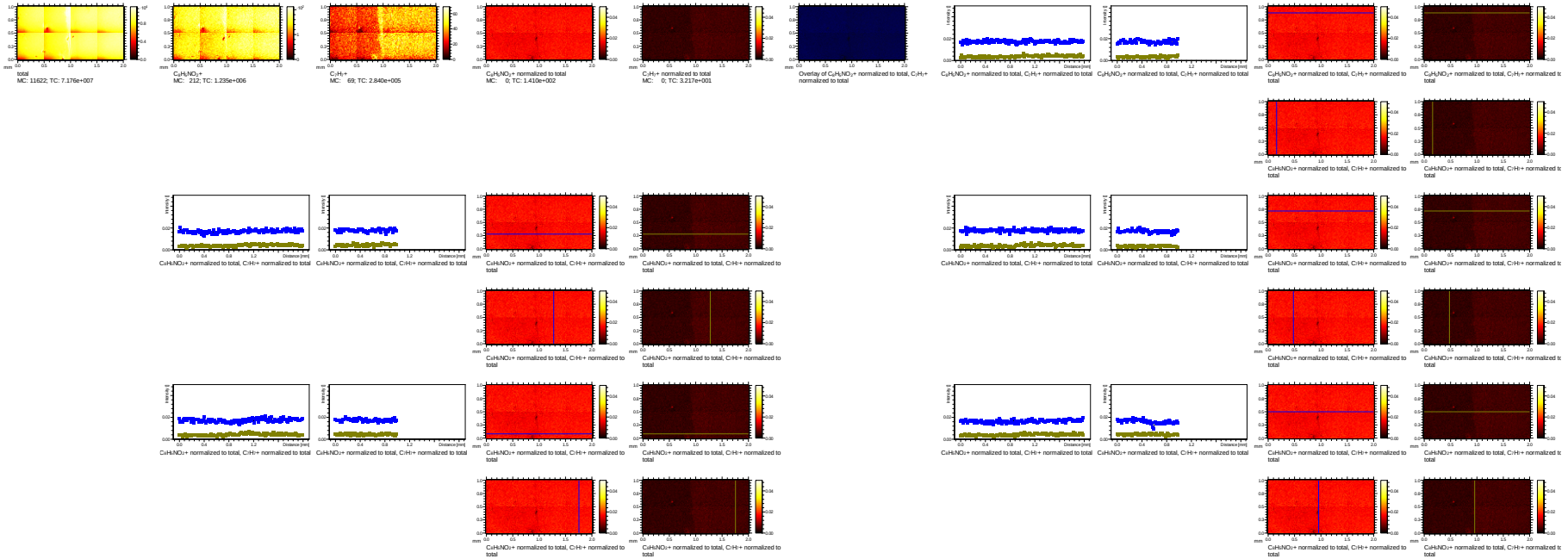

Figure A3.17. *ToF-SIMS results with large area 1x2 mm of sample 29*

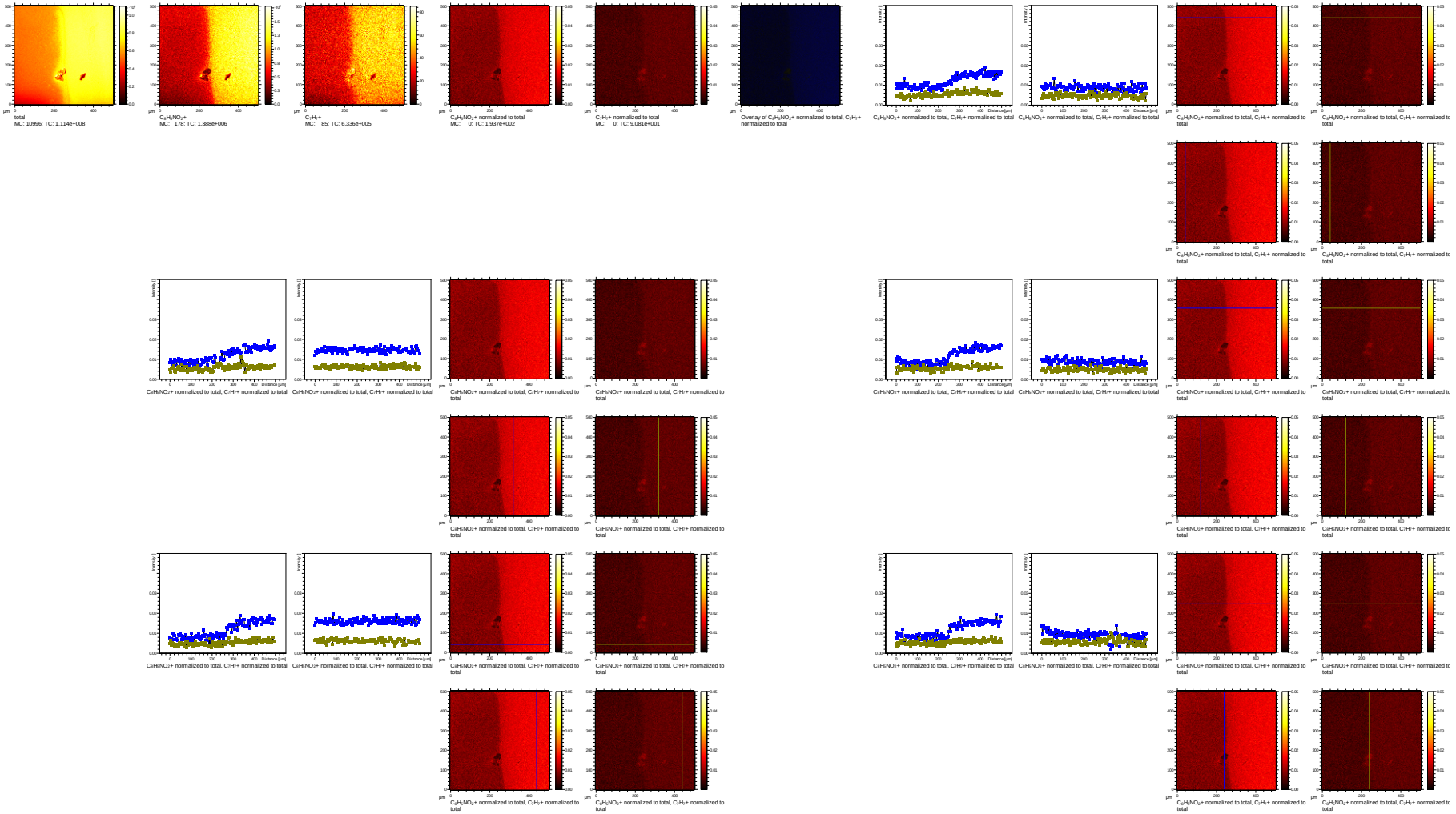

Figure A3.18. *ToF-SIMS results with small area 500x500 µm of sample 29*

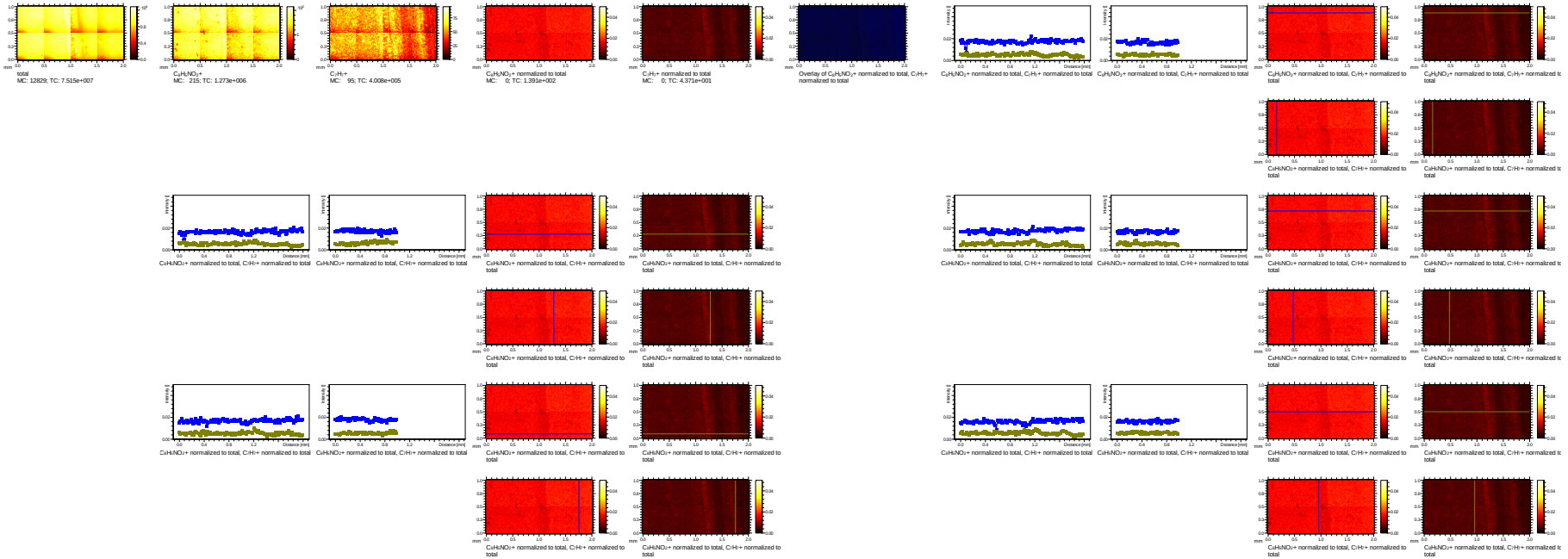

Figure A3.19. *ToF-SIMS results with large image 1x2 mm of sample 33*

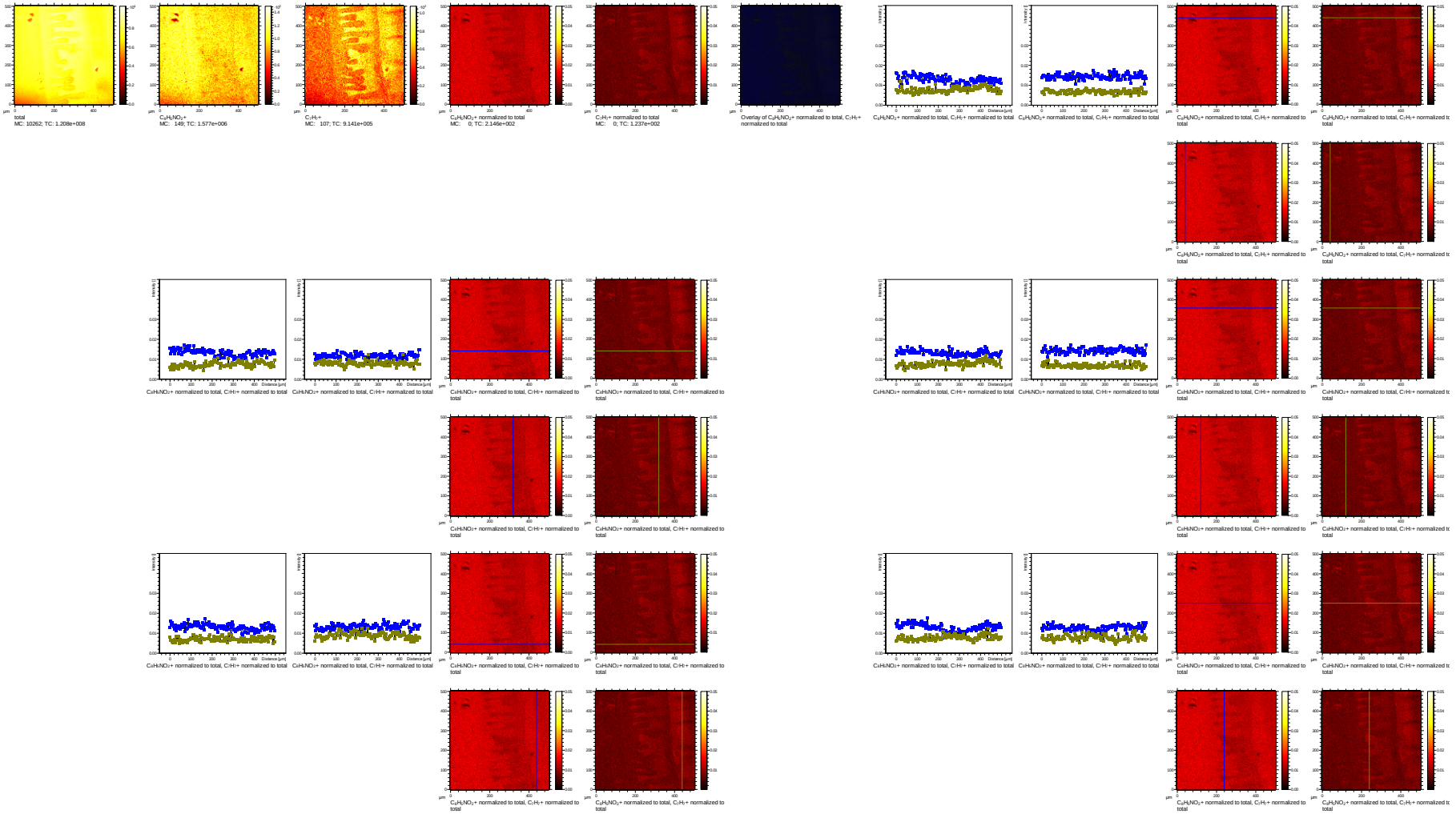

Figure A3.20. *ToF-SIMS results with small area 500x500 µm of sample 33*

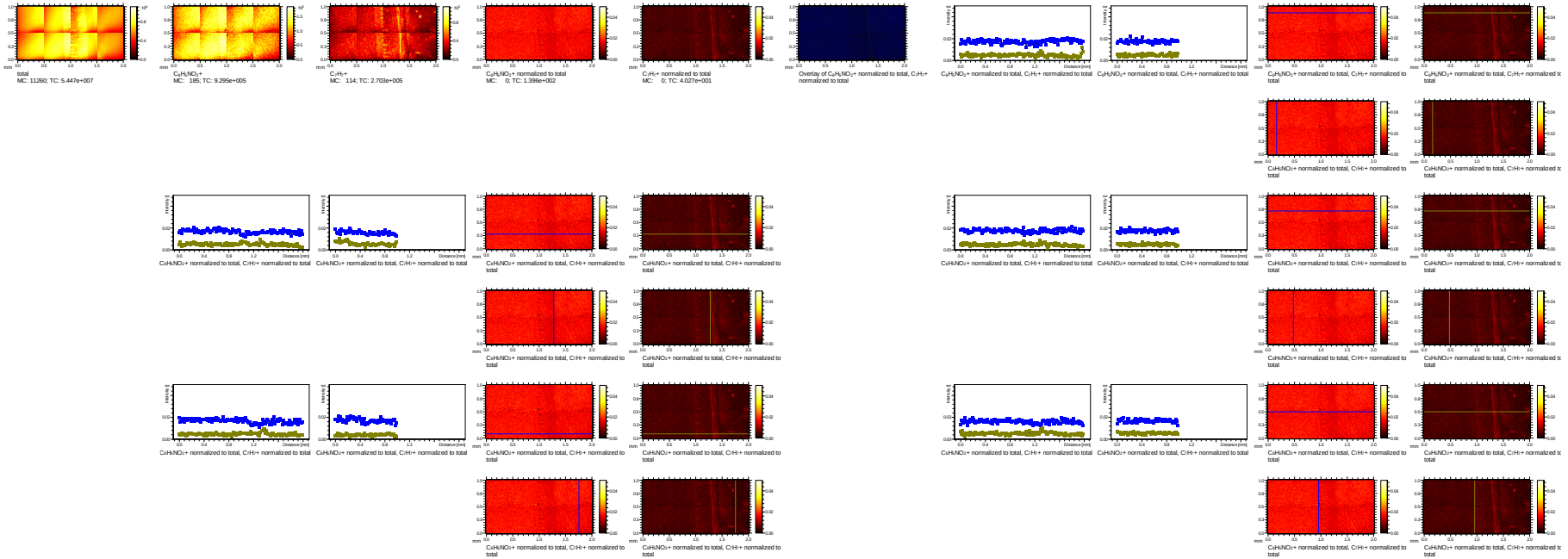

Figure A3.21. *ToF-SIMS results with large area 1x2 mm of sample 35*

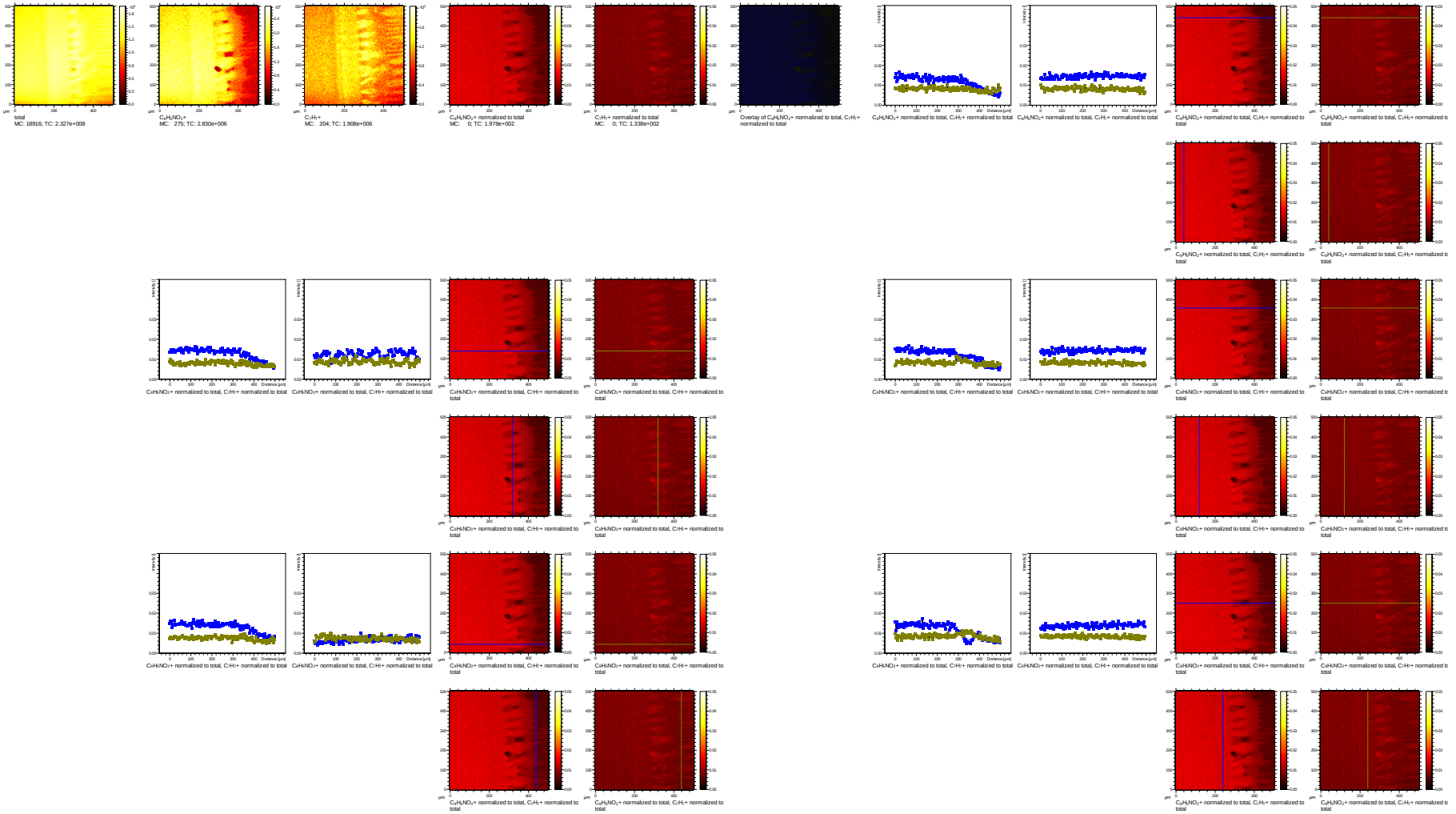

Figure A3.22. *ToF-SIMS results with small area 500x500 µm of sample 35*

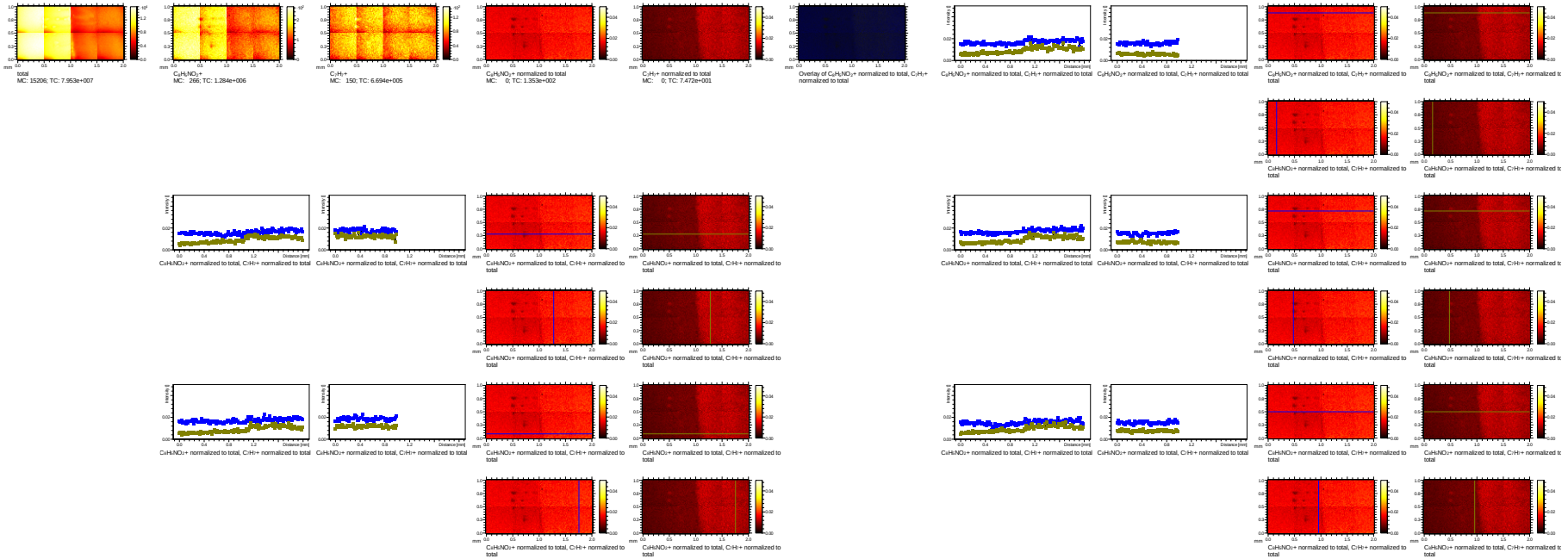

Figure A3.23. *ToF-SIMS results with large area 1x2 mm of sample 34*

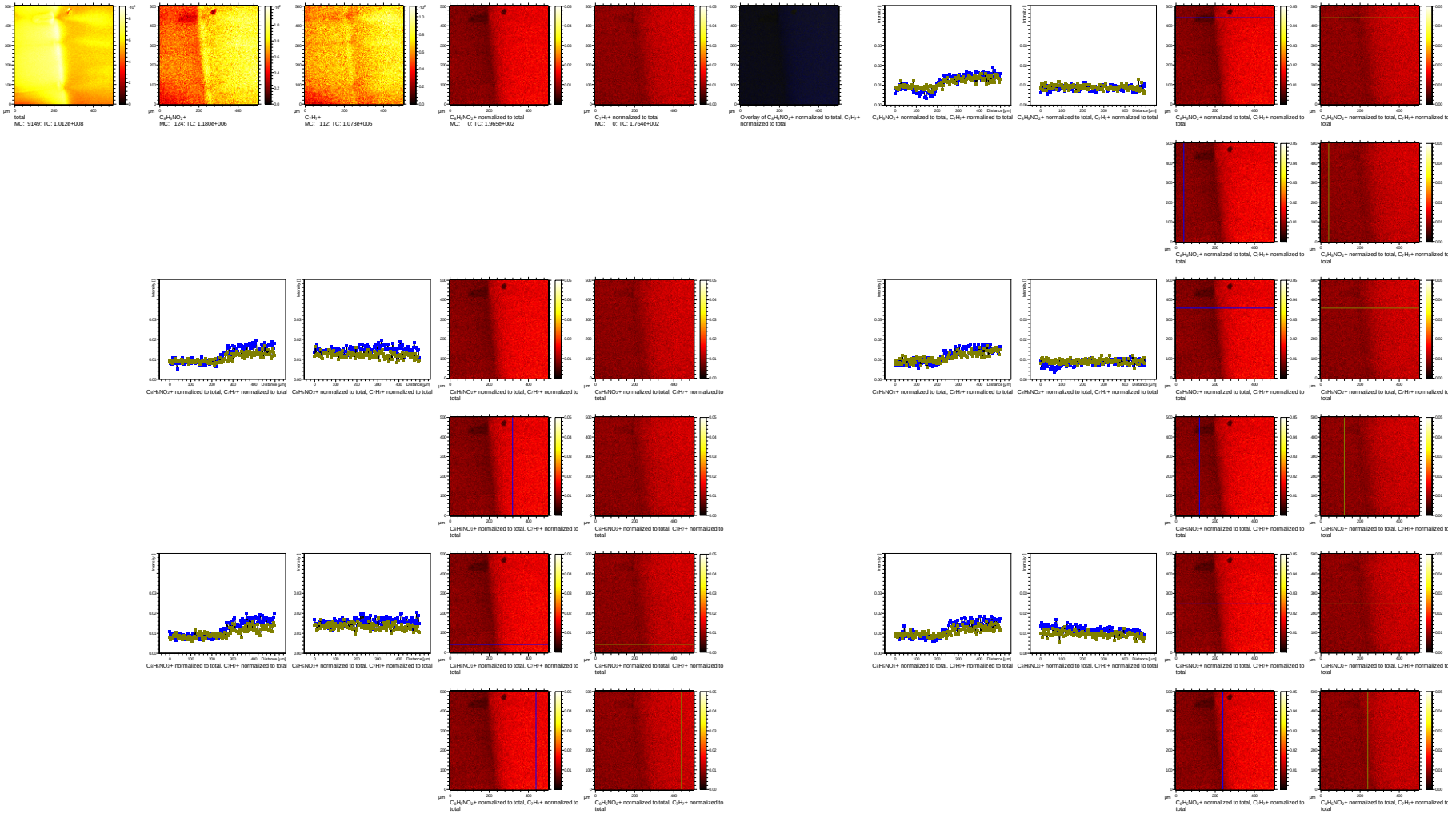

Figure A3.24. *ToF-SIMS results with small area 500x500 µm of sample 34*

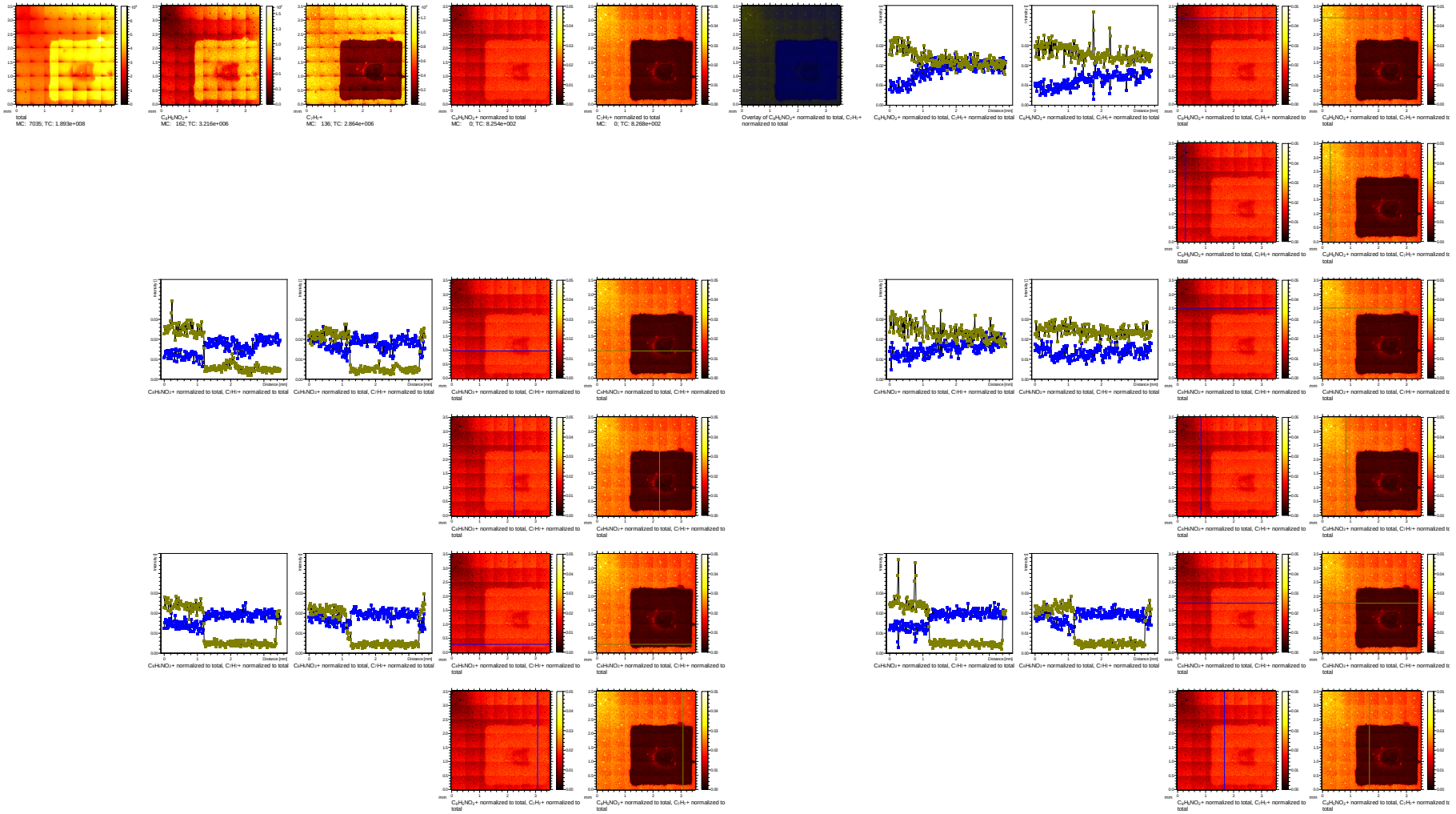

Figure A3.25. *ToF-SIMS results with large area 3.5x3.5 mm of sample 44*

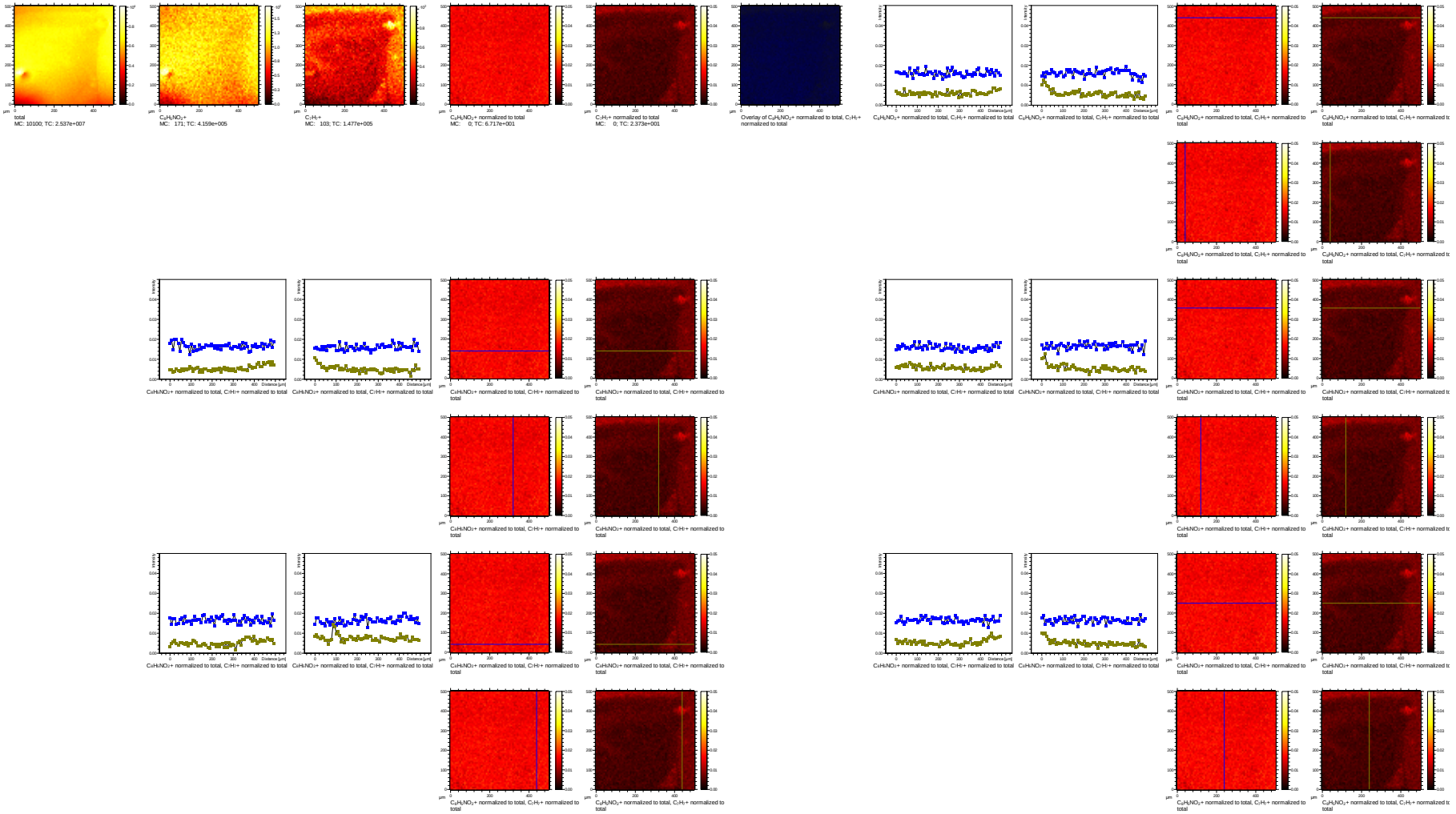

Figure A3.26. *ToF-SIMS results with small area 500x500 µm of sample 44*

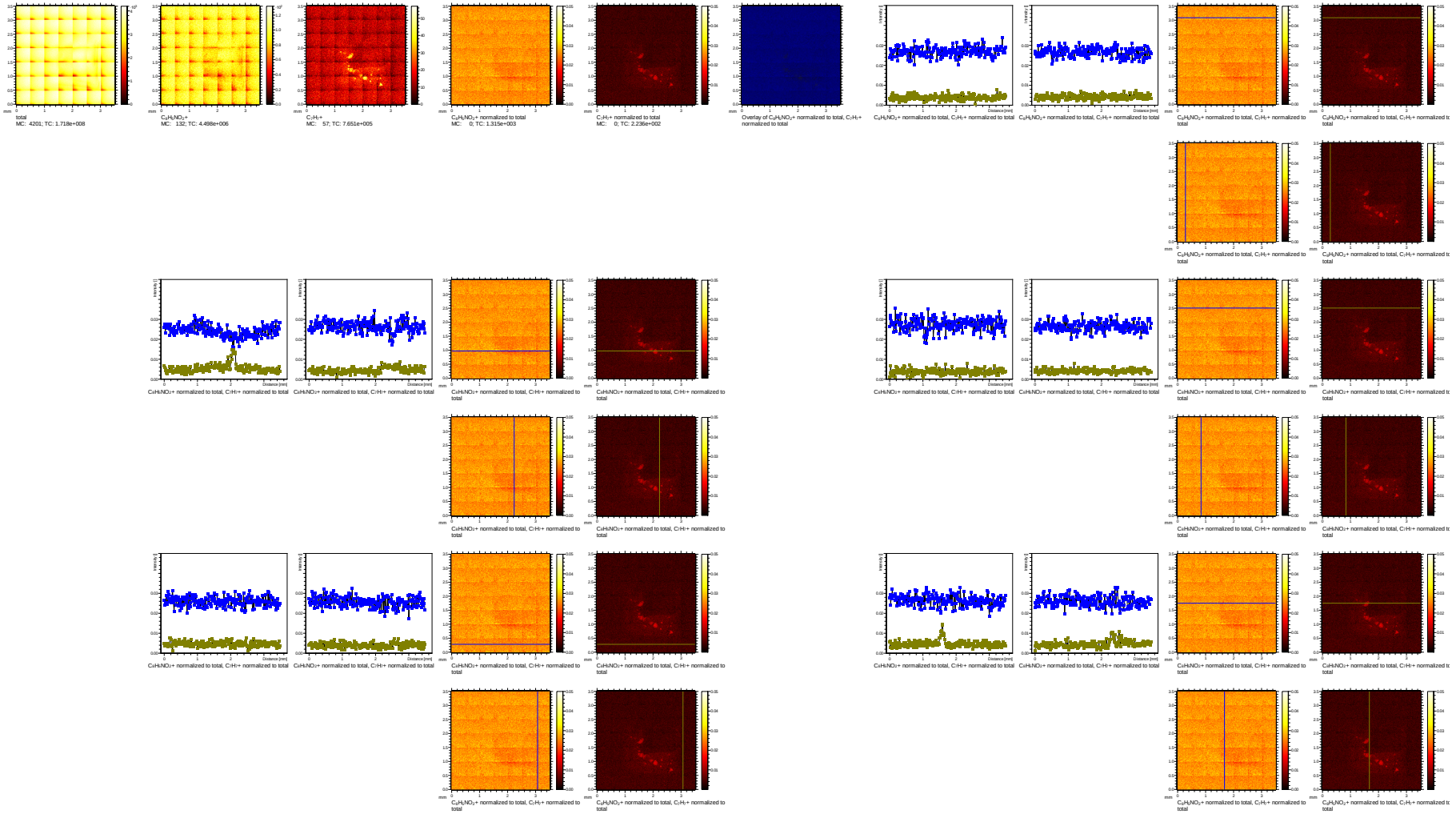

Figure A3.27. *ToF-SIMS results with large area 3.5x3.5 mm of sample 47*

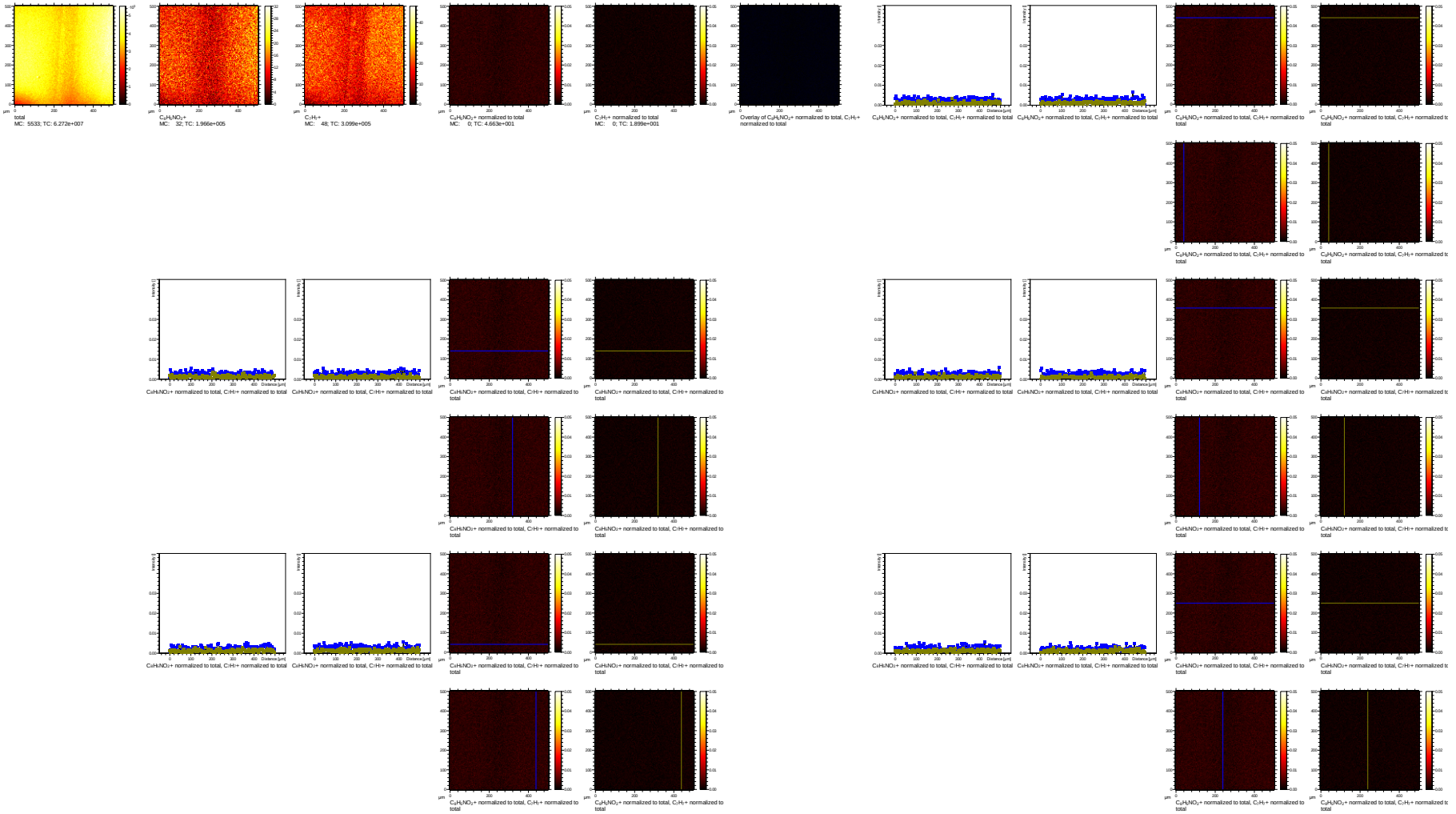

Figure A3.28. *ToF-SIMS results with small area 500x500 µm of sample 47*

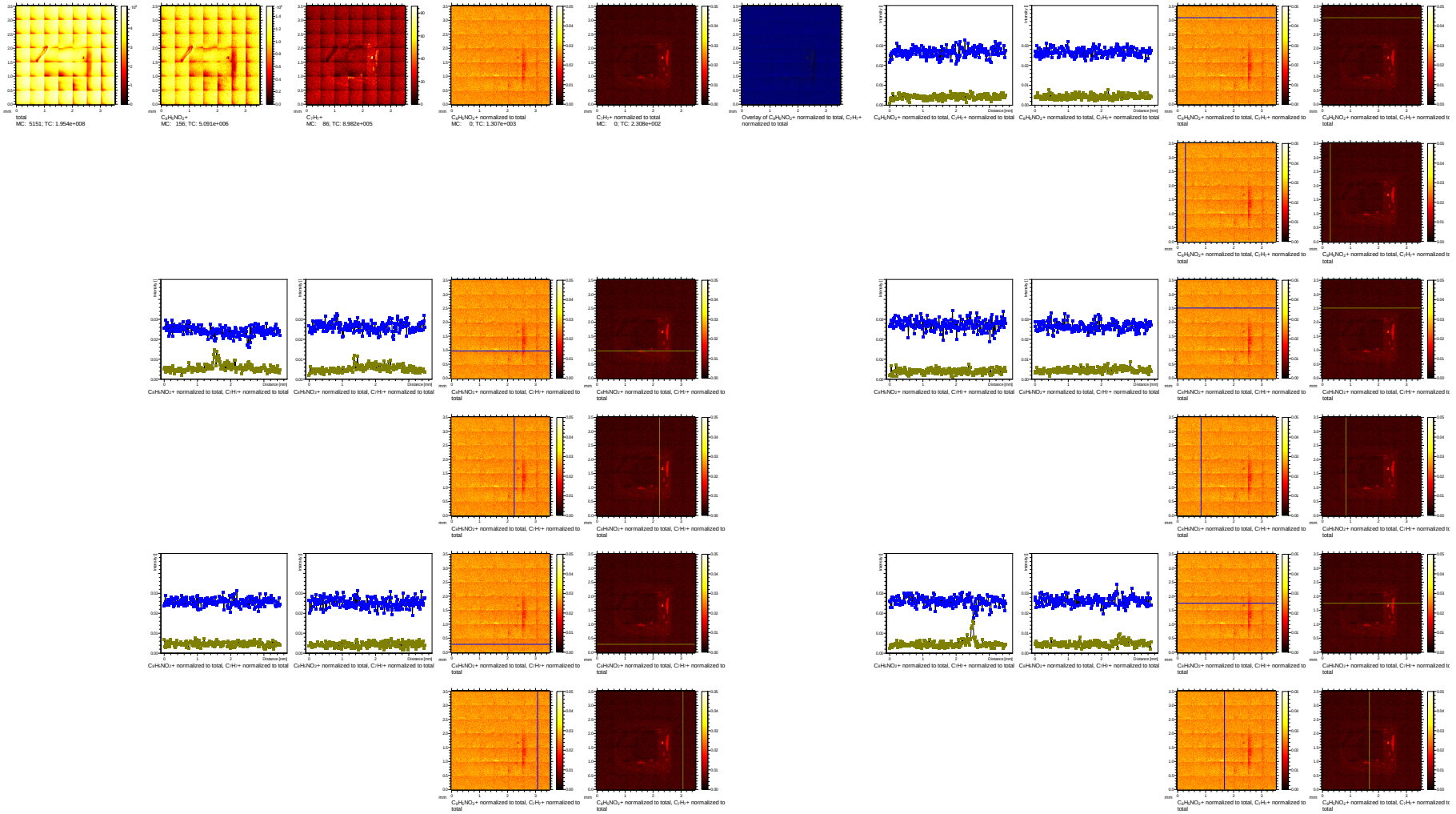

Figure A3.29. *ToF-SIMS results with large area 3.5x3.5 mm of sample 48*

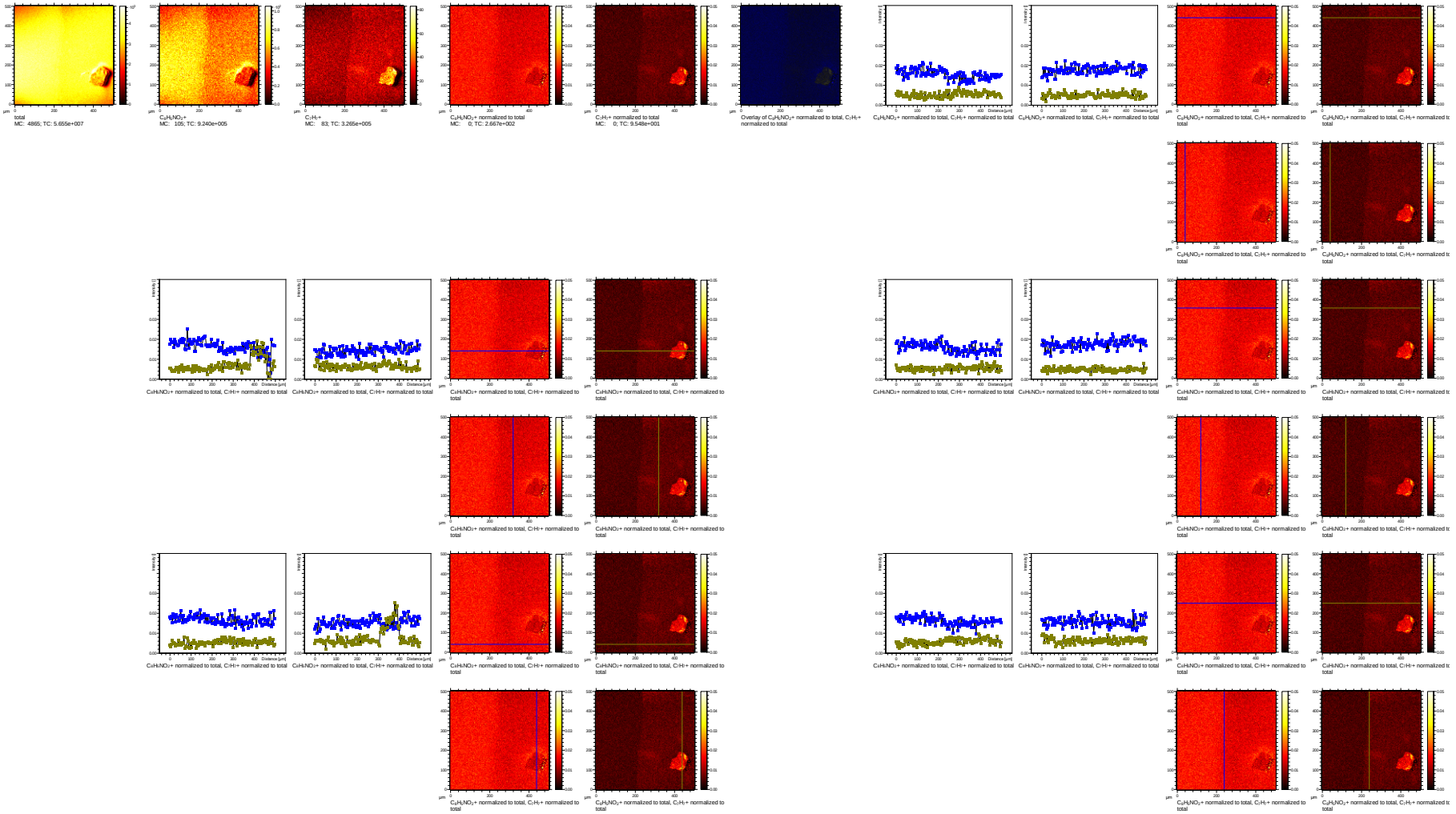

Figure A3.30. *ToF-SIMS results with small area 500x500 µm of sample 48*

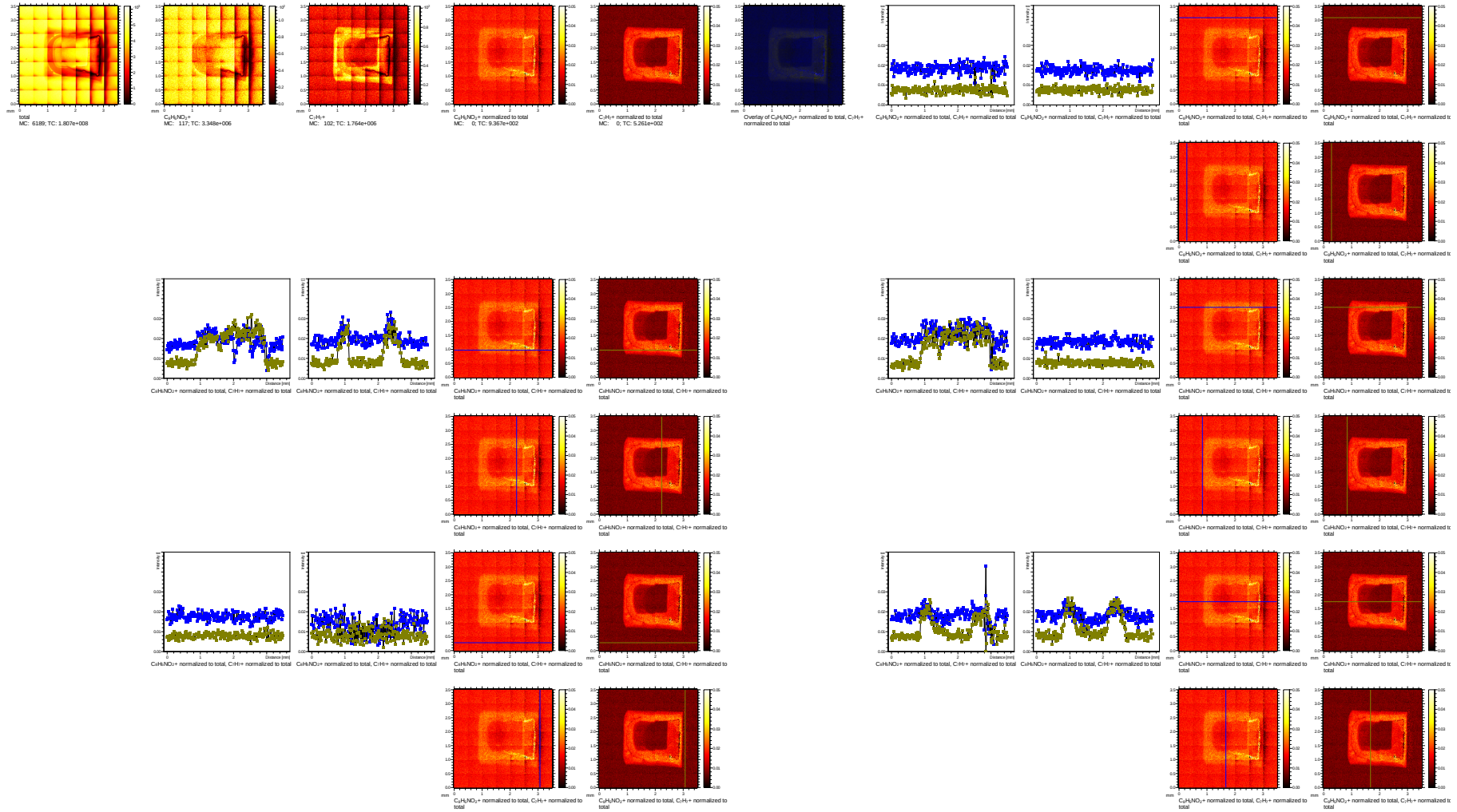

Figure A3.31. *ToF-SIMS results with large area 3.5x3.5 mm of sample 49*

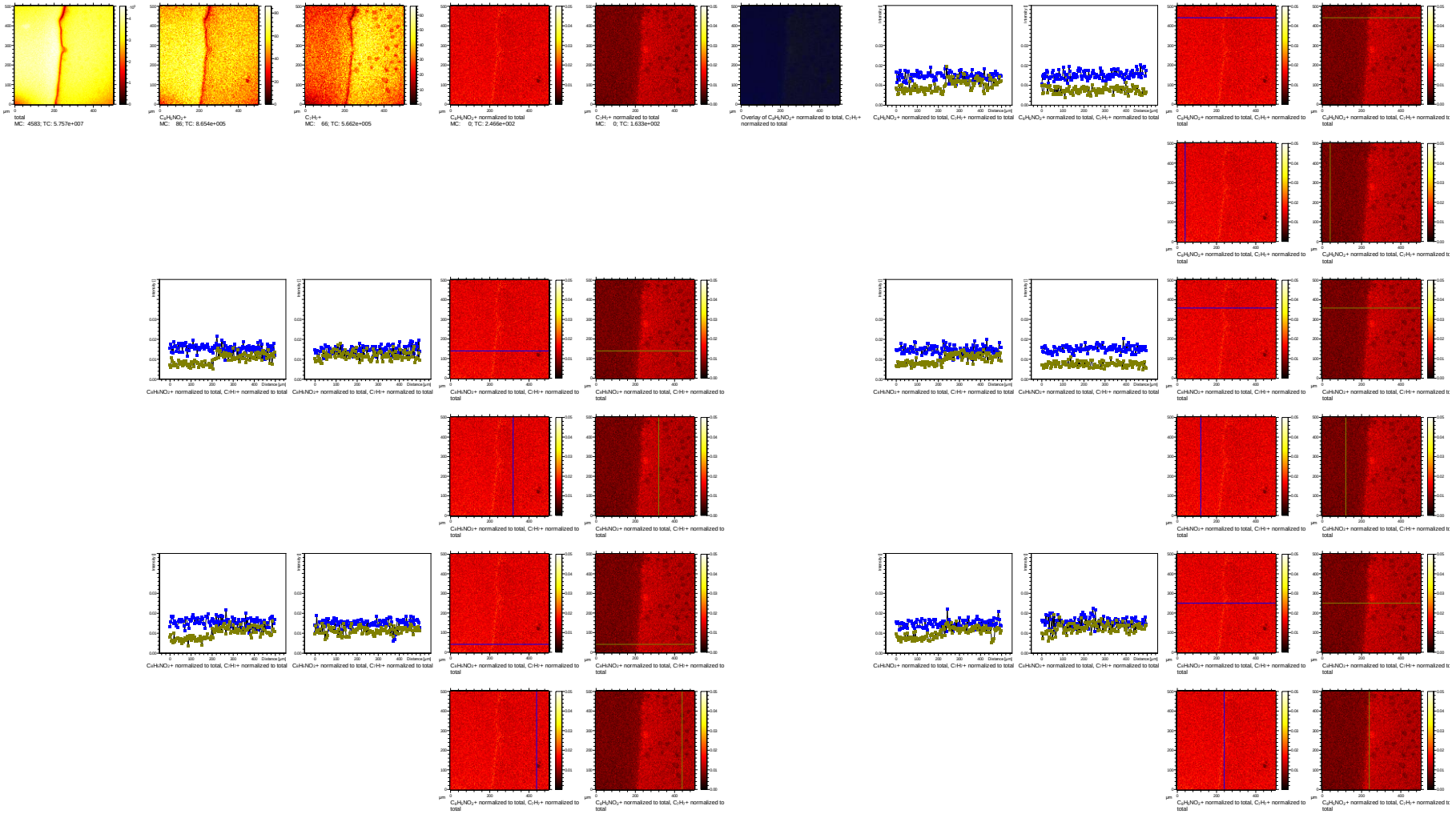

Figure A3.32. *ToF-SIMS results with small area 500x500 µm of sample 49*

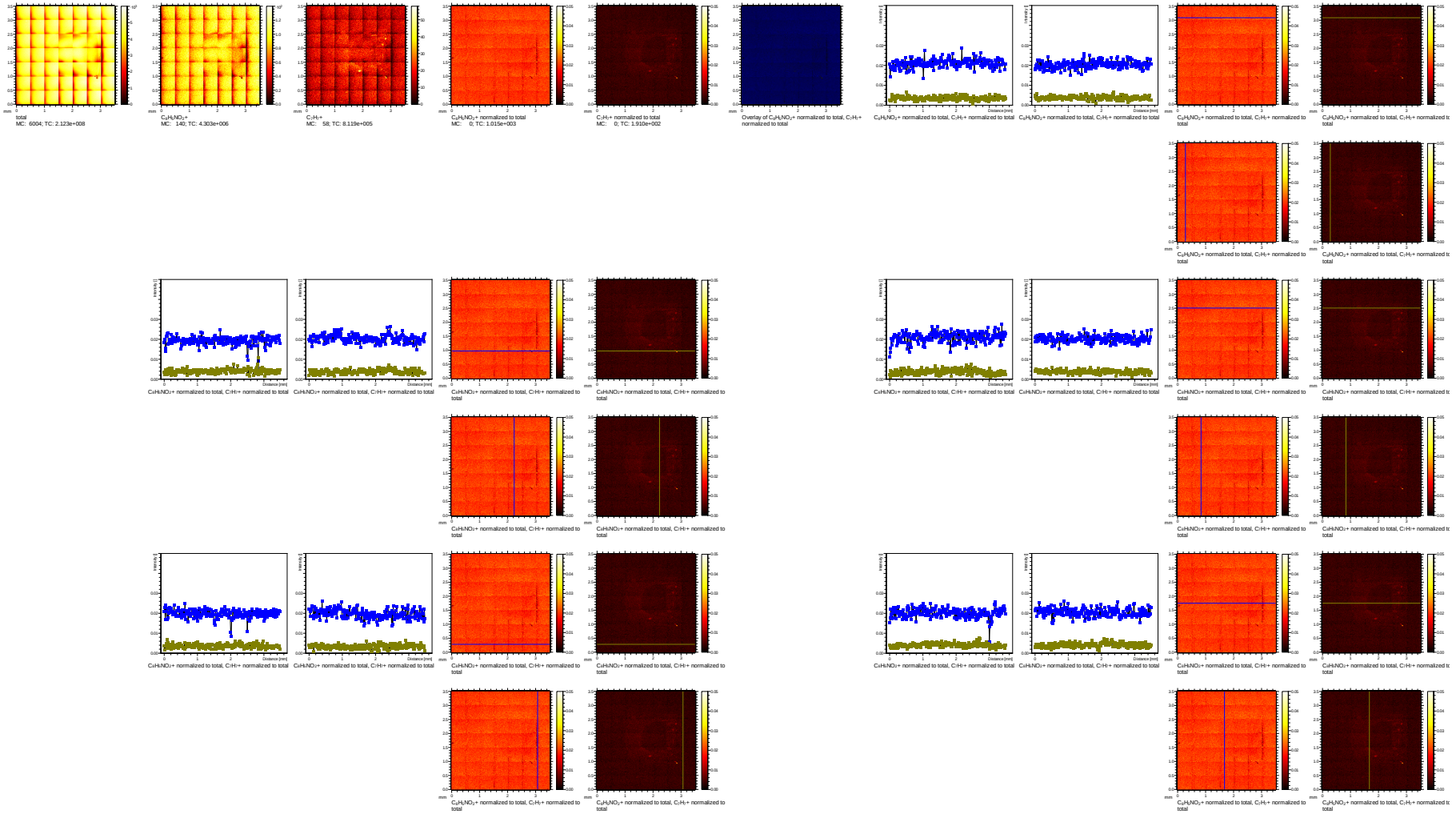

Figure A3.33. *ToF-SIMS results with large area 3.5x3.5 mm of sample 50*

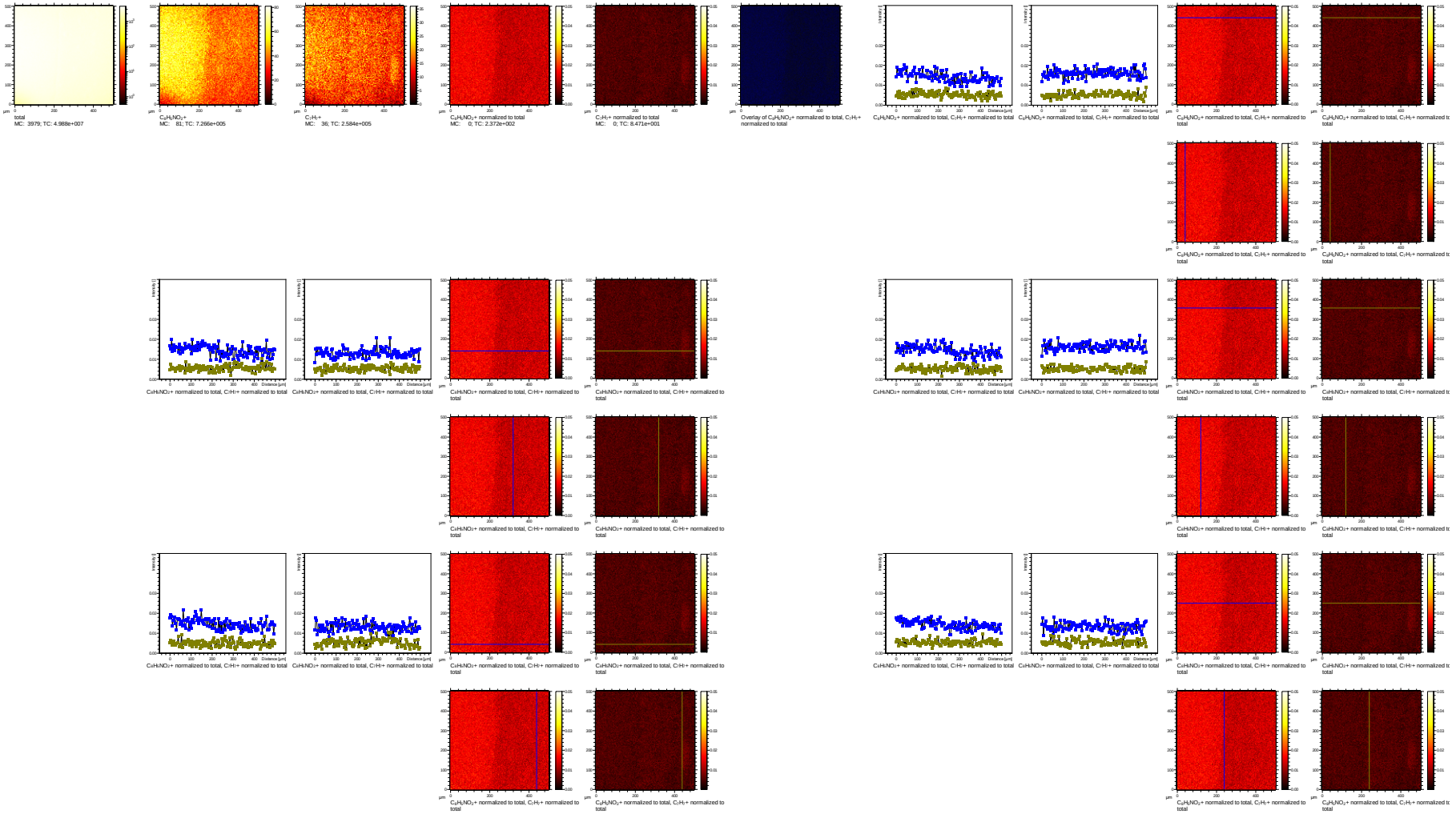

Figure A3.34. *ToF-SIMS results with small area 500x500 µm of sample 50*

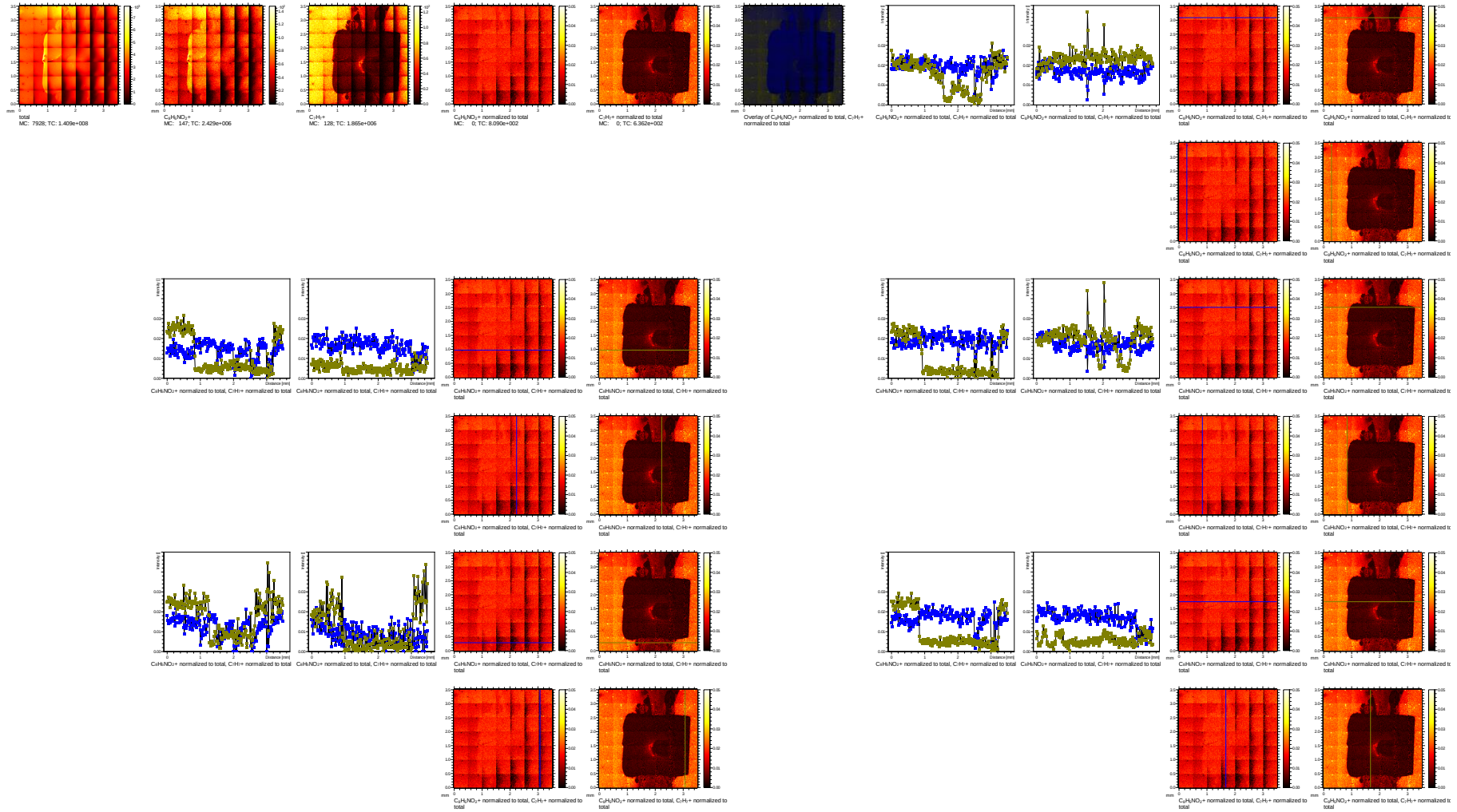

Figure A3.35. *ToF-SIMS results with large area 3.5x3.5 mm of sample 43*

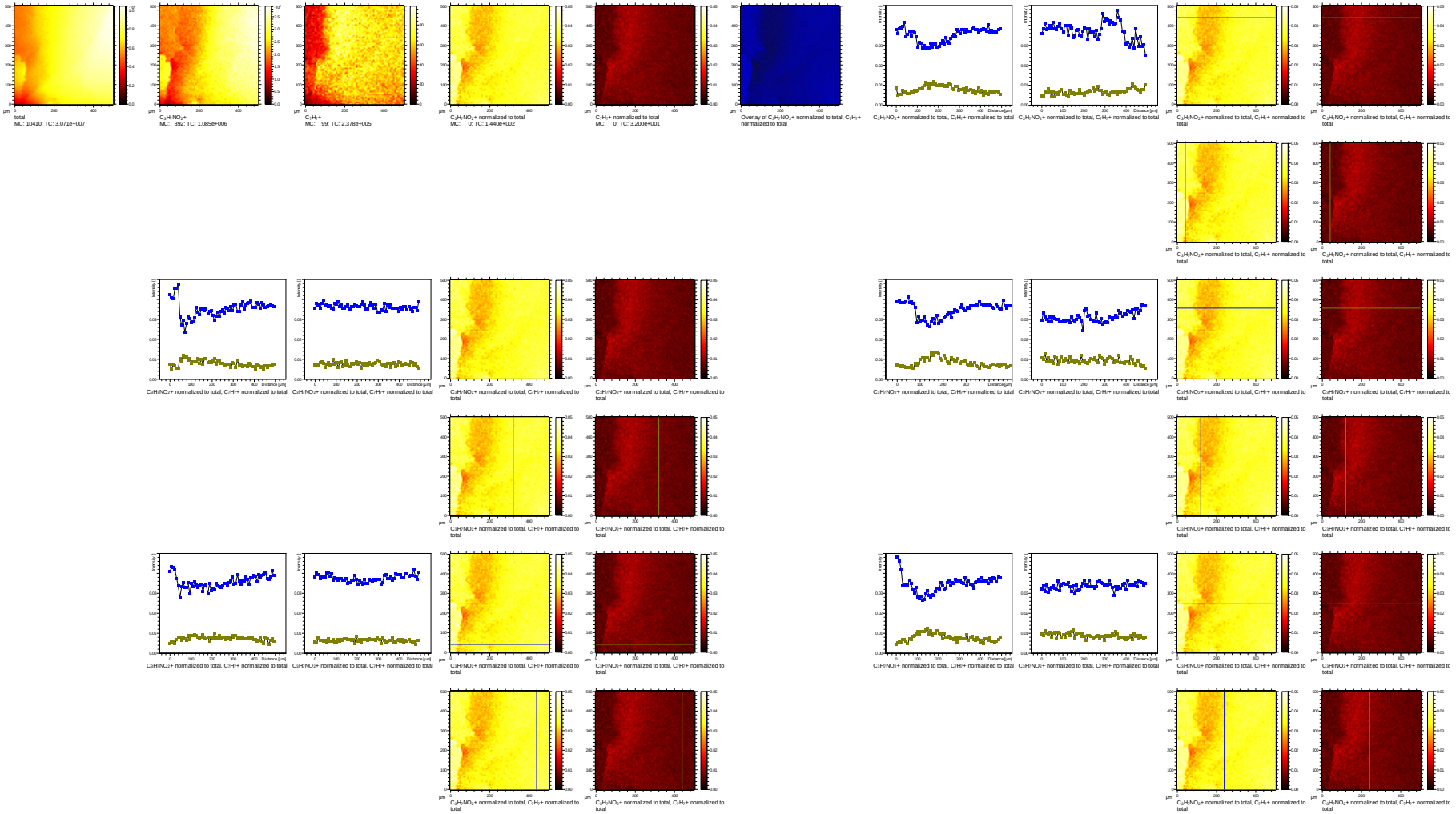

Figure A3.36. *ToF-SIMS results with small area 500x500 µm of sample 43*

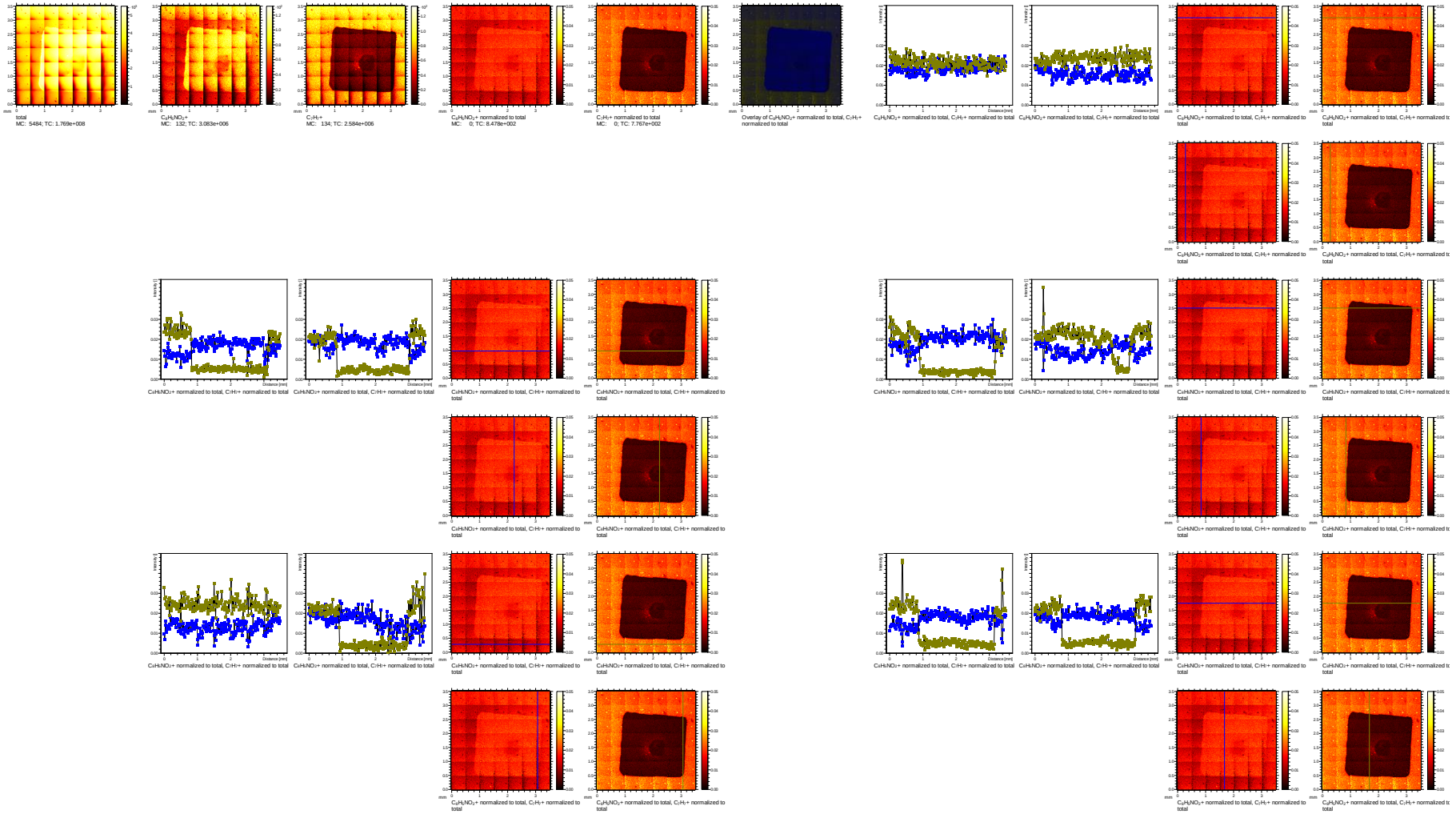

Figure A3.37. *ToF-SIMS results with large area 3.5x3.5 mm of sample 45*

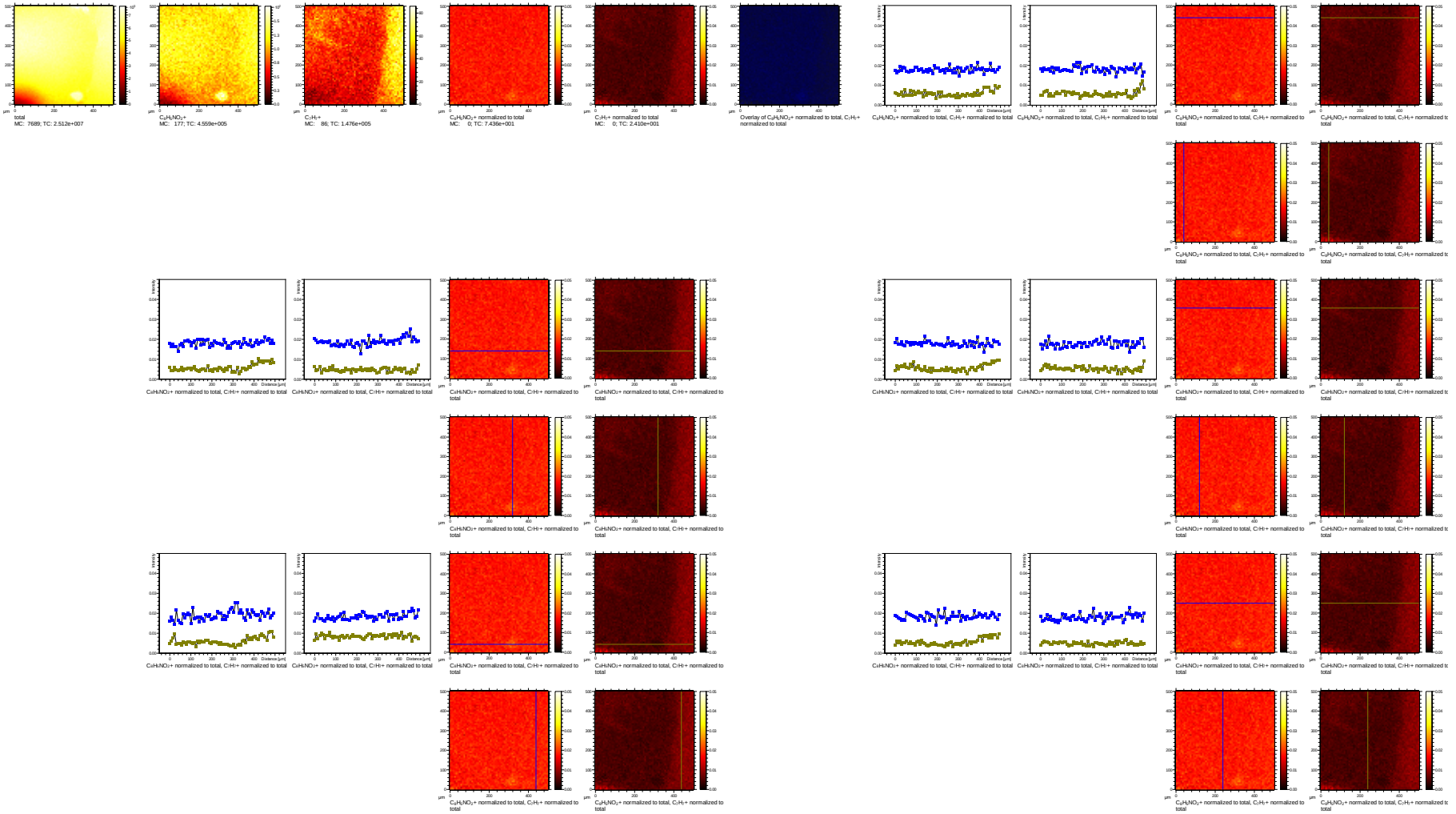

Figure A3.38. *ToF-SIMS results with small area 500x500 µm of sample 45*

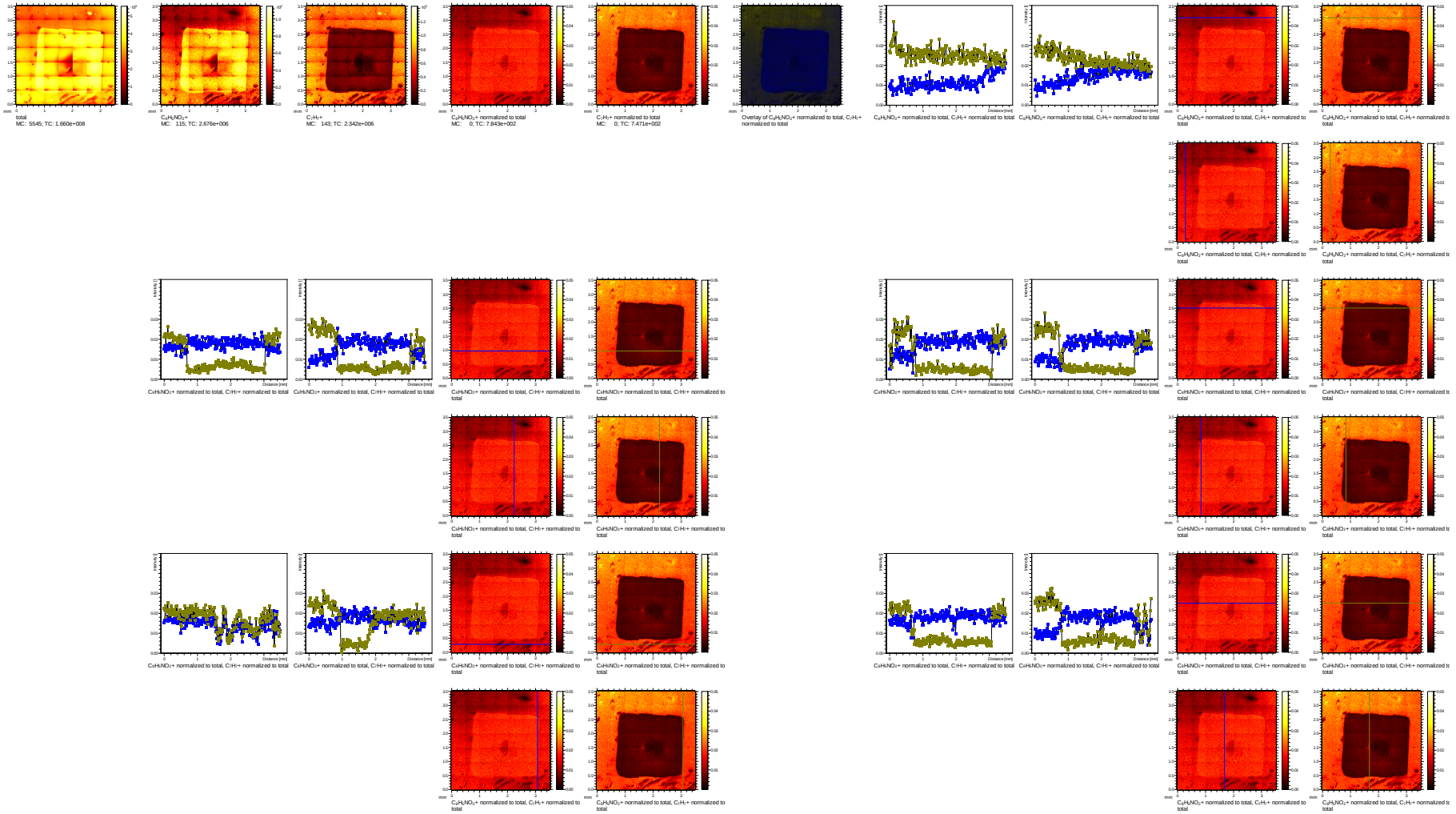

Figure A3.39. *ToF-SIMS results with large area 3.5x3.5 mm of sample 46*

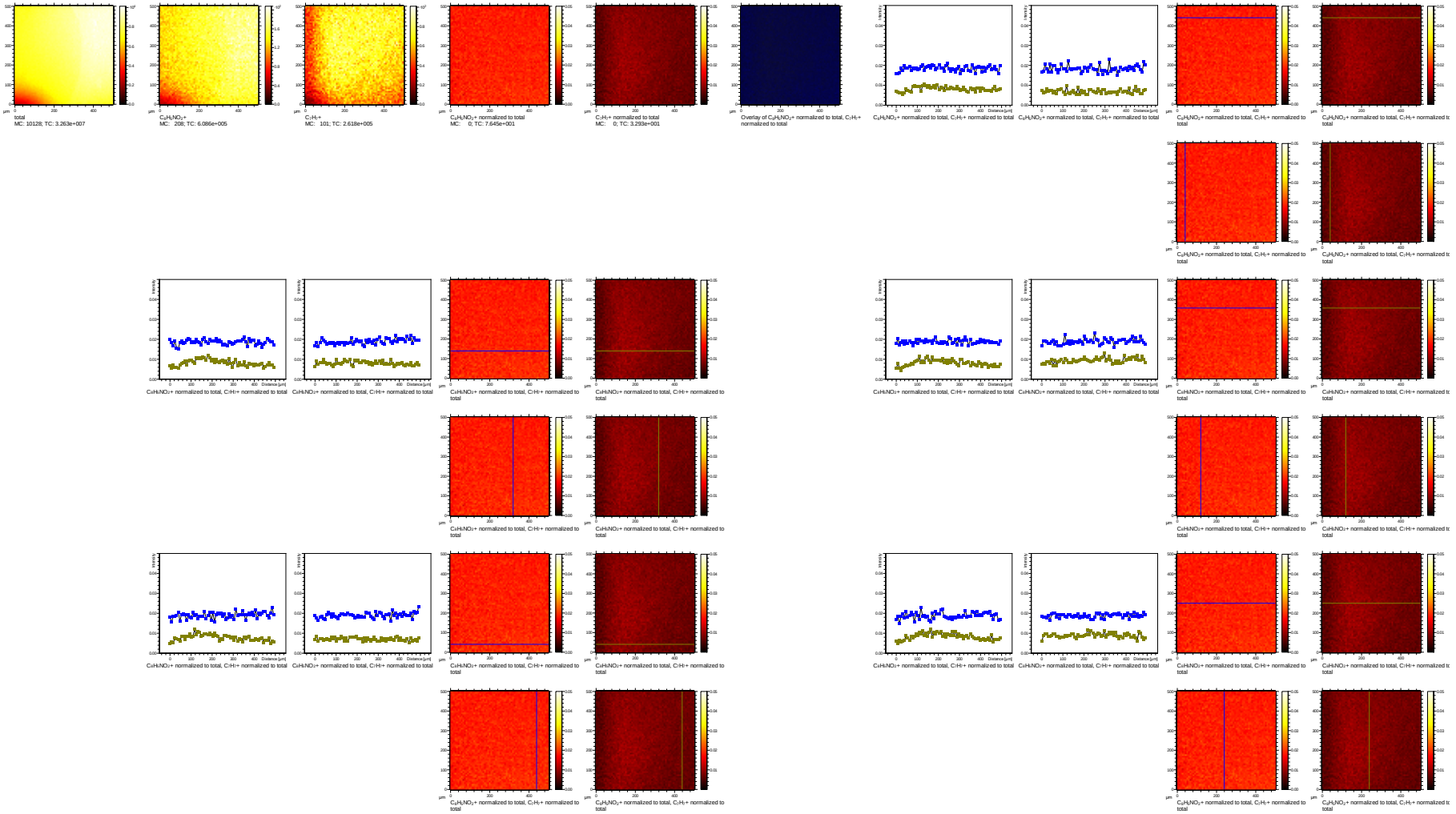

Figure A3.40. *ToF-SIMS results with small area 500x500 µm of sample 46*